Spin susceptibility of two-dimensional electron systems

Inauguraldissertation

zur

Erlangung der Würde eines Doktors der Philosophie

vorgelegt der

Philosophisch-Naturwissenschaftlichen Fakultät

der Universität Basel

von

Robert Andrzej Żak

aus Warschau, Polen

Basel, 2012

creative commons

Namensnennung-Keine kommerzielle Nutzung-Keine Bearbeitung 2.5 Schweiz

---

Sie dürfen:

das Werk vervielfältigen, verbreiten und öffentlich zugänglich machen

Zu den folgenden Bedingungen:

Namensnennung. Sie müssen den Namen des Autors/Rechteinhabers in der von ihm festgelegten Weise nennen (wodurch aber nicht der Eindruck entstehen darf, Sie oder die Nutzung des Werkes durch Sie würden entlohnt).

Keine kommerzielle Nutzung. Dieses Werk darf nicht für kommerzielle Zwecke verwendet werden.

Keine Bearbeitung. Dieses Werk darf nicht bearbeitet oder in anderer Weise verändert werden.

- Im Falle einer Verbreitung müssen Sie anderen die Lizenzbedingungen, unter welche dieses Werk fällt, mitteilen. Am Einfachsten ist es, einen Link auf diese Seite einzubinden.
- Jede der vorgenannten Bedingungen kann aufgehoben werden, sofern Sie die Einwilligung des Rechteinhabers dazu erhalten.
- Diese Lizenz lässt die Urheberpersönlichkeitsrechte unberührt.

Quelle: http://creativecommons.org/licenses/by-nc-nd/2.5/ch/ Datum: 3.4.2009

Genehmigt von der Philosophisch-Naturwissenschaftlichen Fakultät auf Antrag von

Prof. Dr. Daniel Loss

Prof. Dr. Dmitrii Maslov

Basel, den 18. Oktober 2011

Prof. Dr. Martin Spiess
Dekan

Summary

A quantum computer–in contrast to traditional computers based on transistors–is a device that makes direct use of quantum mechanical phenomena, such as superposition and entanglement, to perform computation. One of possible realizations is a so-called spin-qubit quantum computer which uses the intrinsic spin degree of freedom of an electron confined to a quantum dot as a qubit (a unit of quantum information that can be in a linear superposition of the basis states).

Electron spins in semiconductor quantum dots, e.g., in GaAs, are inevitably coupled via hyperfine interaction to the surrounding environment of nuclear spins. This coupling results in decoherence, which is the process leading to the loss of information stored in a qubit. Spontaneous polarization of nuclear spins should suppress decoherence in single-electron spin qubits and ultimately facilitate quantum computing in these systems.

The main focus of this thesis is to study nonanalytic properties of electron spin susceptibility, which was shown to effectively describe the coupling strength between nuclear spins embedded in a two dimensional electron gas, and give detailed insights into the issue of spontaneous polarization of nuclear spins.

In the first part we consider the effect of rescattering of pairs of quasiparticles in the Cooper channel resulting in the strong renormalization of second-order corrections to the spin susceptibility χ in a two-dimensional electron gas (2DEG). We use the Fourier expansion of the scattering potential in the vicinity of the Fermi surface to find that each harmonic becomes renormalized independently. Since some of those harmonics are negative, the first derivative of χ is bound to be negative at small momenta, in contrast to the lowest order perturbation theory result, which predicts a positive slope. We present in detail an effective method to calculate diagrammatically corrections to χ to infinite order.

The second part deals with the effect of the Rashba spin-orbit interaction (SOI) on the nonanalytic behavior of χ for a two-dimensional electron liquid. A long-range interaction via virtual particle-hole pairs between Fermi-liquid quasiparticles leads to

the nonanalytic behavior of χ as a function of the temperature (T), magnetic field ($\mathbf{B}$), and wavenumber ($\tilde{\mathbf{q}}$). Although the SOI breaks the $SU(2)$ symmetry, it does not eliminate nonanalyticity but rather makes it anisotropic: while the linear scaling of χ_{zz} with T and $|\mathbf{B}|$ saturates at the energy scale set by the SOI, that of χ_{xx} ($= \chi_{yy}$) continues through this energy scale, until renormalization of the electron-electron interaction in the Cooper channel becomes important. We show that the Renormalization Group flow in the Cooper channel has a non-trivial fixed point, and study the consequences of this fixed point for the nonanalytic behavior of χ.

In the third part we analyze the ordered state of nuclear spins embedded in an interacting 2DEG with Rashba SOI. Stability of the ferromagnetic nuclear-spin phase is governed by nonanalytic dependences of the electron spin susceptibility χ^{ij} on the momentum ($\tilde{\mathbf{q}}$) and on the SOI coupling constant (α). The uniform ($\tilde{q} = 0$) spin susceptibility is anisotropic (with the out-of-plane component, χ^{zz}, being larger than the in-plane one, χ^{xx}, by a term proportional to $U^2(2k_F)|\alpha|$, where $U(q)$ is the electron-electron interaction). For $\tilde{q} \leq m^*|\alpha|$, corrections to the leading, $U^2(2k_F)|\alpha|$, term scale linearly with $\tilde{q}$ for χ^{xx} and are absent for χ^{zz}. This anisotropy has important consequences for the ferromagnetic nuclear-spin phase: (i) the ordered state–if achieved–is of an Ising type and (ii) the spin-wave dispersion is gapped at $\tilde{q} = 0$. To second order in $U(\tilde{q})$, the dispersion is a decreasing function of $\tilde{q}$, and the anisotropy is not sufficient to stabilize long-range order. However, we show that renormalization in the Cooper channel for $\tilde{q} \ll m^*|\alpha|$ is capable of reversing the sign of the $\tilde{q}$-dependence of χ^{xx} and thus stabilizing the ordered state, if the system is sufficiently close to (but not necessarily in the immediate vicinity of) the Kohn-Luttinger instability.

Contents

Chapter 1

Preface

1.1 Quantum computing

It was in the 1980s, when the idea of exploiting quantum degrees of freedom for information processing was envisioned. The central question at the time was whether and how it was possible to simulate (efficiently) any finite physical system with a man-made machine. Deutsch argued that such a simulation is not possible perfectly within the classical computational framework that had been developed for decades [Deutsch85]. He suggested, together with other researchers such as Feynman [Feynman82, Feynman86], that the universal computing machine should be of quantum nature, i.e., a quantum computer.

Around the same time, developments in two different areas of research and industry took a tremendous influence on the advent of quantum computing. On one hand, it was experimentally confirmed [Aspect82] that Nature indeed does possess some peculiar non-local aspects which were heavily debated since the early days of quantum mechanics [Einstein35]. Schrödinger coined the term *entanglement* [Schrödinger35], comprising the apparent possibility for faraway parties to observe highly correlated measurement results as a consequence of the global and instantaneous collapse of the wave function according to the Copenhagen interpretation of quantum mechanics. The existence of entanglement is crucial for many quantum computations. On the other hand, the booming computer industry led to major progress in semiconductor and laser technology, a prerequisite for the possibility to fabricate, address and manipulate single quantum systems, as needed in a quantum computer.

As the emerging fields of quantum information and nanotechnology inspired and motivated each other in various ways, and are still doing so today more than ever, many interesting results have been obtained so far. While the theories of quantum complexity and entanglement are being established (a process which is far from being complete) and fast quantum algorithms for classically difficult problems have been discovered, the

control and manipulation of single quantum systems is now experimental reality. There are various systems that may be employed as qubits in a quantum computer, i.e., the basic unit of quantum information.

Given a number of practical difficulties in building a quantum computer five most fundamental requirements any proposal for a quantum computer must fulfill in order to work with an arbitrary number of qubits have been listed:

1. A scalable physical system with well characterized qubits.

2. The ability to initialize the state of the qubits to a simple fiducial state.

3. Long relevant decoherence times, much longer than the gate operation time.

4. A "universal" set of quantum gates.

5. A qubit-specific measurement capability.

These are known as the DiVincenzo criteria [DiVincenzo00].

1.1.1 The Loss-DiVincenzo proposal

We now review the spin-qubit proposal for universal scalable quantum computing of Daniel Loss and David DiVincenzo [Loss98]. Here, the physical system representing a qubit is given by the localized spin state of one electron, and the computational basis states $|0\rangle$ and $|1\rangle$ are identified with the two spin states $|\uparrow\rangle$ and $|\downarrow\rangle$, respectively. The considerations discussed in [Loss98] are applicable to electrons confined to any structure, such as, e.g., atoms, defects, or molecules. However, the original proposal focuses on electrons localized in electrically gated semiconductor quantum dots. The relevance of such systems has become clearer in recent years, where remarkable progress in the fabrication and control of single and double GaAs quantum dots has been made (see, e.g., [Hanson07] for a recent experimental review).

Scalability in the proposal of [Loss98] is due to the availability of local gating. Gating operations are realized through the exchange coupling (discussed below), which can be tuned locally with exponential precision. Since neighboring qubits can be coupled and decoupled individually, it is sufficient to study and understand the physics of single and double quantum dots together with the coupling mechanisms to the environment present in particular systems [Coish07]. Undesired interactions between three, four, and more qubits should then not pose any great concern. This is in contrast with proposals that make use of long-ranged interactions (such as dipolar coupling), where scalability might not be easily achieved.

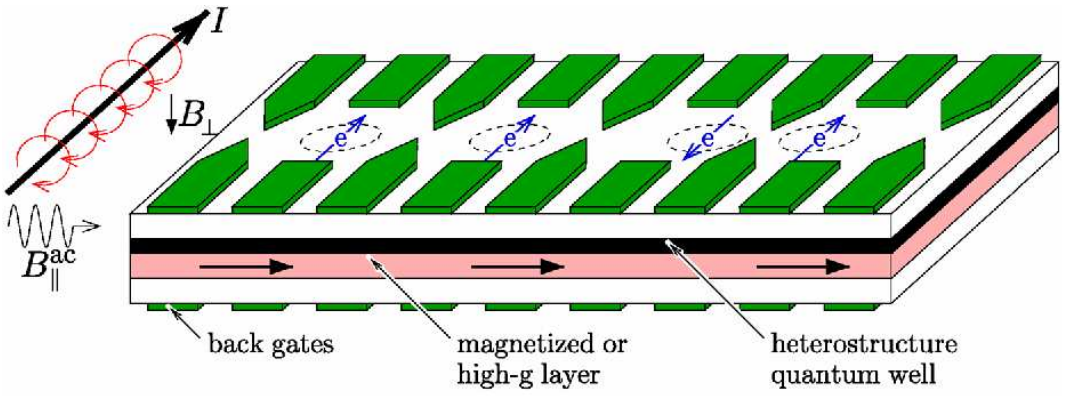

Figure 1.1: An array of quantum dot qubits realized by laterally confining electrons in a two dimensional electron gas formed at the interface of a heterostructure. The confinement is achieved electrostatically by applying voltages to the metallic top gates. Interaction is generally suppressed (as for the two qubits on the left) but may be turned on to realize two-qubit operations by lowering inter-dot gates (as for the two qubits on the right). Single spin rotations may be achieved by dragging electrons down (by changing back gate voltages) to a region where the Zeeman splitting in the presence of the external static magnetic field $B_\perp$ changes due to magnetization or an inhomogeneous g-factor present in that layer. A resonant magnetic ac pulse $B_{||}^{ac}$ can then be used to rotate the spin under consideration, while leaving all other qubits unaffected due to the off-resonant Zeeman splitting (electron spin resonance). All-electrical single spin manipulation may be realized in the presence of SOI by applying ac electric pulses directly via the gates (electric dipole spin resonance).

Figure 1.1 shows part of a possible implementation of a quantum computer. Displayed are four qubits represented by the four single electron spins confined vertically in the heterostructure quantum well and laterally by voltages applied to the top gates. Initialization of the quantum computer could be realized at low temperature T by applying an external magnetic field B satisfying $|g\mu_B B| \gg k_B T$, where g is the g-factor, μ_B is Bohr's magneton, and k_B is the Boltzmann constant. After a sufficiently long time, virtually all spins will have equilibrated to their thermodynamic ground state $|0\rangle = |\uparrow\rangle$. This method for zeroing qubits in a running computation might be too slow to satisfy the 2nd criterion of the last section. Other proposed techniques include initialization through spin-injection from a ferromagnet, as has been performed in bulk semiconductors [Fiederling99, Ohno99], with a spin-polarized current from a spin-filter device [Prinz95, Loss98, DiVincenzo99, Recher00], or by optical pumping [Cortez02, Shabaev03, Gywat04, Bracker05]. The latter method has allowed the preparation of spin states with very high fidelity, in one case as high as 99.8%

[Atatüre06].

The proposal of [Loss98] requires single qubit rotations around a fixed axis in order to implement the CNOT gate (described below). In the original work [Loss98] this is suggested to be accomplished by varying the Zeeman splitting on each dot individually, which was proposed to be done via a site-selective magnetic field (generated by, e.g., a scanning-probe tip) or by controlled hopping of the electron to a nearby auxiliary ferromagnetic dot. Local control over the Zeeman energy may also be achieved through g-factor modulation [Salis01], the inclusion of magnetic layers [Myers05], cf. Figure 1.1, or by modification of the local Overhauser field due to hyperfine couplings [Burkard99]. Arbitrary rotations may be performed via electron spin resonance induced by an externally applied oscillating magnetic field. In this case, however, site-selective tuning of the Zeeman energy is still required in order to bring a specific electron in resonance with the external field, while leaving the other electrons untouched. Alternative all-electrical proposals (i.e., without the need for local control over magnetic fields) in the presence of spin-orbit interaction (SOI) or a static magnetic field gradient have been discussed recently.

Two-qubit nearest-neighbor interaction is controlled in the proposal of [Loss98] by electrical pulsing of a center gate between the two electrons. If the gate voltage is high, the interaction is 'off' since tunneling is suppressed exponentially with the voltage. On the other hand, the coupling can be switched 'on' by lowering the central barrier for a certain switching time τ_s. In this configuration, the interaction of the two spins may be described in terms of the isotropic Heisenberg Hamiltonian

$$H_s(t) = J(t)\mathbf{S}_L \cdot \mathbf{S}_R, \tag{1.1.1}$$

where $J(t) \propto t_0^2(t)/U$ is the time-dependent exchange coupling that is produced by turning on and off the tunneling matrix element $t_0(t)$ via the center gate voltage. U denotes the charging energy of a single dot, and $\mathbf{S}_L$ and $\mathbf{S}_R$ are the spin-$\frac{1}{2}$ operators for the left and right dot, respectively. Equation (1.1.1) is a good description of the double-dot system if the following criteria are satisfied: (i) $\Delta E \gg k_B T$, where T is the temperature and ΔE the level spacing. This means that the temperature cannot provide sufficient energy for transitions to higher-lying orbital states, which can therefore be ignored. (ii) $\tau_s \gg \Delta E/\hbar$, requiring the switching time τ_s to be such that the action of the Hamiltonian is 'adiabatic enough' to prevent transitions to higher orbital levels. (iii) $U > t_0(t)$ for all t in order for the Heisenberg approximation to be accurate. (iv) $\Gamma^{-1} \gg \tau_s$, where Γ^{-1} is the decoherence time. This is basically a restatement of the 3rd DiVincenzo criterion.

The pulsed Hamiltonian Equation (1.1.1) applies a unitary time evolution $U_s(t)$ to the state of the double dot given by $U_s(t) = \exp[-(i/\hbar)\int_0^t J(t')dt'\mathbf{S}_L \cdot \mathbf{S}_R]$. If the constant interaction $J(t) = J_0$ is switched on for a time τ_s such that $\int_0^{\tau_s} J(t)dt/\hbar = J_0\tau_s/\hbar = \pi \mod 2\pi$, then $U_s(\tau_s)$ exchanges the states of the qubits: $U_s(\tau_s)|\mathbf{n}, \mathbf{n}'\rangle = |\mathbf{n}', \mathbf{n}\rangle$. Here, $\mathbf{n}$ and $\mathbf{n}'$ denote real unit vectors and $|\mathbf{n}, \mathbf{n}'\rangle$ is a simultaneous eigenstate of the two

operators $\mathbf{S}_L \cdot \mathbf{n}$ and $\mathbf{S}_R \cdot \mathbf{n}'$. This gate is called SWAP. If the interaction is switched on for the shorter time $\tau_s/2$, then $U_s(\tau_s/2) = U_s(\tau_s)^{1/2}$ performs the so-called 'square-root of swap' denoted by $\sqrt{\text{SWAP}}$. This gate together with single-qubit rotations about a fixed (say, the z-) axis can be used to synthesize the CNOT operation [Loss98]

$$U_{\text{CNOT}} = e^{i(\pi/2)S_L^z} e^{-i(\pi/2)S_R^z} U_s(\tau_s)^{1/2} e^{i\pi S_L^z} U_s(\tau_s)^{1/2}, \tag{1.1.2}$$

or, alternatively, as

$$U_{\text{CNOT}} = e^{i\pi S_L^z} U_s(\tau_s)^{-1/2} e^{-i(\pi/2)S_L^z} U_s(\tau_s) e^{i(\pi/2)S_L^z} U_s(\tau_s)^{1/2}. \tag{1.1.3}$$

The latter representation has the potential advantage that single qubit rotations involve only one spin, in this case the one in the left dot. Writing the CNOT gate as above, it is seen that arbitrary single qubit rotations together with the $\sqrt{\text{SWAP}}$ gate are sufficient for universal quantum computing. Errors during the execution of a $\sqrt{\text{SWAP}}$ gate due to non-adiabatic transitions to higher orbital states [Schliemann10, Requist05], SOI [Bonesteel01, Burkard02, Stepanenko03], and hyperfine coupling to surrounding nuclear spins [Petta05, Coish05, Klauser06, Taylor07] have been studied. Furthermore, realistic systems will include some anisotropic spin terms in the exchange interaction which may cause additional errors. Conversely, this fact might be used to perform universal quantum computing with two-spin encoded qubits, in the absence of single-spin rotations [Bonesteel01, Lidar01, Stepanenko04, Chutia06].

1.2 Relaxation and decoherence in GaAs dots

The requirement of sufficiently long coherence times is perhaps the most challenging aspect for quantum computing architectures in the solid state. It requires a detailed understanding of the different mechanisms that couple the electron's spin to its environment.

1.2.1 Spin-orbit interaction

While fluctuations in the electrical environment do not directly couple to the electron spin, they become relevant for spin decoherence in the presence of SOI. In GaAs two-dimensional electron gas (2DEG) two types of SOI are present. The Dresselhaus SOI originates from the bulk properties of GaAs [Dresselhaus55]. The zinc-blend crystal structure has no center of inversion symmetry and a term of the type $H_D^{3D} \propto p_x(p_y^2 - p_z^2)\sigma_x + p_y(p_z^2 - p_x^2)\sigma_y + p_z(p_x^2 - p_y^2)\sigma_z$ is allowed in three dimensions, where $\mathbf{p}$ is the momentum operator and $\boldsymbol{\sigma}$ are the Pauli matrices. Due to the confining potential along the z-direction, we can substitute the p_z operators with their expectation values. Using $\langle p_z^2 \rangle \neq 0$ and $\langle p_z \rangle = 0$, one obtains

$$H_D = \beta(p_y\sigma_y - p_x\sigma_x). \tag{1.2.1}$$

Smaller terms cubic in $\mathbf{p}$ have been neglected, what is justified by the presence of strong confinement.

The Rashba SOI is due to the asymmetry of the confining potential [Bychkov84b] and can be written in the suggestive form $H_R \propto (\boldsymbol{\mathcal{E}} \times \mathbf{p}) \cdot \boldsymbol{\sigma}$, where $\boldsymbol{\mathcal{E}} = \mathcal{E}\hat{z}$ is an effective electric field along the confining direction:

$$H_R = \alpha(p_x\sigma_y - p_y\sigma_x). \tag{1.2.2}$$

The Rashba and Dresselhaus terms produce an internal magnetic field linear in the electron momentum defined by $\mathbf{B}_{\mathrm{SO}} = -2[(\beta p_x + \alpha p_y)\mathbf{e}_x - (\beta p_y + \alpha p_x)\mathbf{e}_y]/g\mu_B$. If $\beta = 0$, the magnitude of $\mathbf{B}_{\mathrm{SO}}$ is isotropic in $\mathbf{p}$ and the direction is always perpendicular to the velocity. While moving with momentum $\mathbf{p}$, the spin precesses around $\mathbf{B}_{\mathrm{SO}}$ and a full rotation is completed over a distance of order $\lambda_{\mathrm{SO}} = |\hbar/(\alpha m^*)| = 1 - 10$ μm, where m^* is the effective mass. Generally, Rashba and Dresselhaus spin-orbit coupling coexist, their relative strength being determined by the confining potential. This results in the anisotropy of the SOI in the 2DEG plane (e.g., of the spin splitting as function of $\mathbf{p}$). In this case, two distinct spin-orbit lengths can be introduced

$$\lambda_{\pm} = \frac{\hbar}{m^*(\beta \pm \alpha)}. \tag{1.2.3}$$

For GaAs quantum dots, the SOI is usually a small correction that can be treated perturbatively since the size of the dot (typically ~ 100 nm) is much smaller than the SOI lengths $\lambda_{\pm}$. The qualitative effect introduced by the SOI is a small mixing of the spin eigenstates. As a consequence, the perturbed spin eigenstates can be coupled by purely orbital perturbation even if the unperturbed states have orthogonal spin components. Relevant charge fluctuations are produced by lattice phonons, surrounding gates, electron-hole pair excitations, etc. with the phonon bath playing a particularly important role.

1.2.2 Hyperfine interaction

The other mechanism for spin relaxation and decoherence that has proved to be effective in GaAs dots, and ultimately constitutes the most serious limitation of such systems, is due to the nuclear spins bath. All three nuclear species ^{69}Ga, ^{71}Ga, and^{75}As of the host material have spin 3/2 and interact with the electron spin via the Fermi contact hyperfine interaction

$$H_{HF} = \mathbf{S} \cdot \sum_i A_i \mathbf{I}_i, \tag{1.2.4}$$

where A_i and $\mathbf{I}_i$ are the coupling strengths and the nuclear spin operator at site i, respectively. The density of nuclei is $n_0 = 45.6$ nm^{-3} and there are typically $N \sim 10^6$ nuclei in a dot. The strength of the coupling is proportional to the electron density at

site i, and one has $A_i = A|\psi(\mathbf{r}_i)|^2/n_0$, where $\psi(\mathbf{r})$ is the orbital envelope wave function of the electron and $A \approx 90$ μeV.[1]

The study of the hyperfine interaction (1.2.4) represents an intricate problem involving subtle quantum many-body correlations in the nuclear bath and entangled dynamical evolution of the electron's spin and nuclear degrees of freedom. It is useful to present here a qualitative picture based on the expectation value of the Overhauser field $\mathbf{B}_N = \sum_i A_i \mathbf{I}_i / g\mu_B$. This field represents a source of uncertainty for the electron dynamics, since the precise value of $\mathbf{B}_N$ is not known. Due to the fact that the nuclear spin bath is in general a complicated mixture of different nuclear states, the operator $\mathbf{B}_N$ in the direction of the external field $\mathbf{B}$ does not correspond to a well-defined eigenstate, but results in a statistical ensemble of values. These fluctuations have an amplitude of order $B_{N,max}/\sqrt{N} \sim 5$ mT since the maximum value of B_N (with fully polarized nuclear bath) is about 5 T.

Finally, even if it were possible to prepare the nuclei in a specific configuration, e.g., $|\uparrow\uparrow\downarrow\uparrow\ldots\rangle$, the nuclear state would still evolve in time to a statistical ensemble on a time scale t_{nuc}. Although direct internuclear interactions are present (for example, magnetic dipole-dipole interactions between nuclei) the most important contribution to the bath's time evolution is in fact due to the hyperfine coupling itself, causing the back action of the electron spin on the nuclear bath. Estimates of the nuclear bath timescale lead to $t_{\rm nuc} = 10 - 100$ μs or longer at higher values of the external magnetic field $\mathbf{B}$ [Hanson07].

1.3 Dealing with decoherence

Several schemes were proposed to mitigate or even completely lift the decoherence driven by the hyperfine coupling of the electron spin to the nuclear spins bath. One approach is to develop quantum control techniques which effectively lessen or even suppress the nuclear spin coupling to the electron spin [Johnson05, Petta05, Laird06]. Another possibility is to narrow the nuclear spin distribution [Coish04, Klauser06, Stepanenko06] or dynamically polarize the nuclear spins [Burkard99, Khaetskii02, Khaetskii03, Imamoğlu03, Bracker05, Coish04]. What all of the aforementioned methods have in common, is that they aim at reducing nuclear spin fluctuations by external actions.

From the current experimental standpoint these polarization schemes may not seem feasible because polarization of above 99% is required [Coish04] in order to extend the spin decay time by one order of magnitude. This level of polarization is still beyond the reach of experimental techniques with the best result of around 60% polarization achieved so far in quantum dots [Bracker05]. Therefore an alternative mechanism has

[1] This value is a weighted average of the three nuclear species ^{69}Ga, ^{71}Ga, and ^{75}As, which have abundance 0.3, 0.2, and 0.5, respectively. For the three isotopes we have $A = \frac{8\mu_0}{9}\mu_B\mu_I\eta n_0$, where $\mu_I = (2.12,\ 2.56,\ 1.44) \times \mu_N$, while $\eta_{\rm Ga} = 2.7\ 10^3$ and $\eta_{\rm As} = 4.5\ 10^3$ [Petta08].

been recently proposed, namely, the possibility of an intrinsic polarization of nuclear spins at finite but low temperature in the 2DEG confined to the GaAs heterostructure [Simon07].

The main interaction mechanism of nuclear spins embedded in the 2DEG–as shown below–is provided by the Rudermann-Kittel-Kasuya-Yosida (RKKY) interaction [Kittel87], which is mediated by the conduction electrons (the direct dipolar interactions between the nuclear spins proves to be negligible). An intrinsic nuclear spin polarization relies on the existence of a temperature dependent magnetic phase transition, at which a ferromagnetic ordering sets in, thus defining a nuclear spin Curie temperature.

1.3.1 Effective Hamiltonian

A nuclear spin system embedded in a 2DEG can be described by a tight-binding model in which each lattice site contains a single nuclear spin and electrons can hop between neighboring sites. A general Hamiltonian describing such a system is given by

$$H = H_{\mathrm{e-e}} + H_{\mathrm{e-n}} + H_{\mathrm{n-n}} = H_{\mathrm{e-e}} + \frac{1}{2}\sum_{j=1}^{N_l} A_j \mathbf{S}_j \cdot \mathbf{I}_j + \sum_{i,j} v_{ij}^{\alpha\beta} I_i^{\alpha} I_j^{\beta}, \tag{1.3.1}$$

where $H_{\mathrm{e-e}}$ describes electron-electron interactions, $H_{\mathrm{e-n}}$ the hyperfine interaction of electron and nuclear spins, and $H_{\mathrm{n-n}}$ the general dipolar interaction between the nuclear spins; A_j is the hyperfine coupling constant between the electron and the nuclear spin at site $\mathbf{r}_j$ (the total number of lattice sites is denoted by N_l), $\mathbf{S}_j = c_{j\sigma}^{\dagger} \boldsymbol{\tau}_{\sigma\sigma'} c_{j\sigma'}$ is the electron spin operator at site $\mathbf{r}_j$ with $c_{j\sigma}^{\dagger}$ ($c_{j\sigma}$) being a creation (annihilation) operator of an electron at the lattice site $\mathbf{r}_j$ with spin $\sigma = \uparrow, \downarrow$ and $\boldsymbol{\tau}$ representing the Pauli matrices, $\mathbf{I}_j = (I_j^x, I_j^y, I_j^z)$ is a nuclear spin located at the lattice site $\mathbf{r}_j$, and $v_{ij}^{\alpha\beta}$ describes all direct dipolar interaction between nuclear spins. Summation over the spin components $\alpha, \beta = x, y, z$ is implied.

The above Hamiltonian can be further simplified by: (i) noting that the dipolar interaction energy scale $E_{\mathrm{n-n}} \approx 100\ nK$ [Petta08] is the smallest energy scale of the problem and therefore $v_{ij}^{\alpha\beta} \approx 0$; (ii) assuming site-independent antiferromagnetic coupling $A_j = A > 0$; (iii) neglecting any dipolar interaction to other nuclear spins which are not embedded in the 2DEG. The last assumption is important since it allows to focus only on those nuclear spins which lie within the support of the electron envelope wave function (in the growth direction).

An effective RKKY Hamiltonian H_{RKKY} for the nuclear spins in a 2D plane is derived by performing the Schrieffer-Wolff (SW) transformation in order to eliminate terms linear in A (this is appropriate since the nuclear spin dynamics is slow compared to the electron one or, in terms of energy scales, $A \ll E_F$) and subsequently integrating out the electron degrees of freedom. In real space, the resulting Hamiltonian takes the following

form [Simon07, Simon08]

$$H_{\text{eff}} = -\frac{A^2}{8n_s}\sum_{\mathbf{r},\mathbf{r}'}\chi^{ij}(\mathbf{r},\mathbf{r}')I^i(\mathbf{r})I^j(\mathbf{r}') \tag{1.3.2}$$

with

$$\chi^{ij}(\mathbf{r},\mathbf{r}') = -\int_0^{1/T} d\tau \left\langle T_\tau S^i(\mathbf{r},\tau)S^j(\mathbf{r}',0)\right\rangle \tag{1.3.3}$$

being the static electron spin susceptibility (up to a factor μ_B^2).

The outlined derivation makes it clear that the interaction between nuclear spins–described by the 2D static electron spin susceptibility–is mediated by conduction electrons. This interaction is nothing but the standard RKKY interaction [Kittel87], which can be substantially modified by electron-electron interactions as shown later in this thesis.

1.3.2 Electron spin susceptibility

As we have seen in the previous section the magnetic exchange interaction between the nuclear spins is mediated by the electron gas. Therefore, the key quantity governing the magnetic properties of the nuclear spins is the electron spin susceptibility $\chi_s(\mathbf{q})$ in 2D. In the case of non-interacting electrons the static electron spin susceptibility, i.e., the spin susceptibility at vanishing external frequency $\Omega = 0$, is given by

$$\chi_s(q) = -2\int d\omega_k d^2k g(\omega_k,\mathbf{k})g(\omega_k,\mathbf{k}+\mathbf{q}), \tag{1.3.4}$$

where $g(\omega_k,\mathbf{k}) = (i\omega_k - \epsilon_{\mathbf{k}})^{-1}$ is the free electron Green's function, ω_k is a fermionic Matsubara frequency, $\epsilon_{\mathbf{k}}$ is the dispersion relation with $\epsilon_{\mathbf{k}} = k^2/2m^* - \mu$ and μ being the chemical potential. It can be readily shown that $\chi_s(q)$ coincides with the usual density-density (or Lindhard) response function in 2D [Giuliani05] and reads as

$$\chi_s(q) = \chi_0\left(1 - \Theta(q-2k_F)\sqrt{1-4k_F^2/q^2}\right), \tag{1.3.5}$$

where $\chi_0 = m^*/\pi$ and m^* is the effective electron mass in the 2DEG.

The calculation of the static spin susceptibility in an interacting 2DEG has been the subject of intense efforts in the last decade in connection with non-analyticities in the Fermi liquid theory [Belitz97, Hirashima98, Misawa99, Chitov01b, Chitov01a, Chubukov03, Gangadharaiah05, Chubukov05a, Maslov06, Chubukov06, Schwiete06, Aleiner06, Shekhter06a, Shekhter06b]. In particular, the study of nonanalytic behavior of thermodynamic quantities and susceptibilities in electron liquids has attracted recent interest, especially in 2D. Of particular importance for this work is the recent findings by Chubukov and Maslov [Chubukov03] that the static non-uniform spin susceptibility

$\chi_s(q)$ depends *linearly* on the wave vector modulus $q = |\mathbf{q}|$ for $q \ll k_F$ in 2D (while it is q^2 in 3D), with k_F being the Fermi momentum. This non-analyticity arises from the long-range correlations between quasi-particles mediated by virtual particle-hole pairs, despite the fact that electron-electron interactions was assumed to be short-ranged.

The positive slope of the momentum-dependent electron spin susceptibility to second order in electron-electron interaction [Chubukov03] leads to the conclusion that ferromagnetic ordering of nuclear spins is not possible [Simon07, Simon08]. However, given the behavior of the spin susceptibility as a function of temperature, one can reasonably expect that the slope can be reversed (negative) if higher order processes are incorporated.

Indeed, it turns out that the temperature dependence of the electron spin susceptibility $\chi_s(T)$ is rather intricate. On one hand, from perturbative calculations in second order in the short-ranged interaction strength one obtains that $\chi_s(T)$ increases with temperature [Chubukov03, Gangadharaiah05, Chubukov05a, Maslov06, Chubukov06]. The same behavior is reproduced by effective supersymmetric theories [Schwiete06, Aleiner06]. On the other hand, non-perturbative calculations, taking into account renormalization effects, found that $\chi_s(T)$ has a non-monotonic behavior and first decreases with temperature [Shekhter06b, Shekhter06a]. This latter behavior is in agreement with recent experiments on 2DEGs [Prus03].

1.4 Outline

The purpose of this thesis is to study the static electron spin susceptibility beyond second order in electron-electron interaction with a strong focus on the systems with a finite Rashba SOI. The results are directly applied to analyze the stability and nature of the ferromagnetically ordered phase of nuclear spins.

The manuscript is organized as follows: In Chapter 2 we consider the effect of rescattering of pairs of quasiparticles in the Cooper channel resulting in the strong renormalization of second-order corrections to the spin susceptibility χ in a two-dimensional electron system. We use the Fourier expansion of the scattering potential in the vicinity of the Fermi surface to find that each harmonic becomes renormalized independently. Since some of those harmonics are negative, the first derivative of χ is bound to be negative at small momenta, in contrast to the lowest order perturbation theory result, which predicts a positive slope. We present in detail an effective method to calculate diagrammatically corrections to χ to infinite order.

Chapter 3 deals with the effect of the Rashba spin-orbit interaction (SOI) on the nonanalytic behavior of χ for a two-dimensional electron liquid. A long-range interaction via virtual particle-hole pairs between Fermi-liquid quasiparticles leads to the nonanalytic behavior of χ as a function of the temperature (T), magnetic field ($\mathbf{B}$), and

wavenumber ($\tilde{\mathbf{q}}$). Although the SOI breaks the $SU(2)$ symmetry, it does not eliminate nonanalyticity but rather makes it anisotropic: while the linear scaling of χ_{zz} with T and $|\mathbf{B}|$ saturates at the energy scale set by the SOI, that of χ_{xx} ($= \chi_{yy}$) continues through this energy scale, until renormalization of the electron-electron interaction in the Cooper channel becomes important. We show that the Renormalization Group flow in the Cooper channel has a non-trivial fixed point, and study the consequences of this fixed point for the nonanalytic behavior of χ. An immediate consequence of SOI-induced anisotropy in the nonanalytic behavior of χ is a possible instability of a second-order ferromagnetic quantum phase transition with respect to a first-order transition to an XY ferromagnetic state.

In Chapter 4 we analyze the ordered state of nuclear spins embedded in an interacting 2DEG with Rashba SOI. Stability of the ferromagnetic nuclear-spin phase is governed by nonanalytic dependences of the electron spin susceptibility χ^{ij} on the momentum ($\tilde{\mathbf{q}}$) and on the SOI coupling constant (α). The uniform ($\tilde{q} = 0$) spin susceptibility is anisotropic (with the out-of-plane component, χ^{zz}, being larger than the in-plane one, χ^{xx}, by a term proportional to $U^2(2k_F)|\alpha|$, where $U(q)$ is the electron-electron interaction). For $\tilde{q} \leq 2m^*|\alpha|$, corrections to the leading, $U^2(2k_F)|\alpha|$, term scale linearly with $\tilde{q}$ for χ^{xx} and are absent for χ^{zz}. This anisotropy has important consequences for the ferromagnetic nuclear-spin phase: (i) the ordered state–if achieved–is of an Ising type and (ii) the spin-wave dispersion is gapped at $\tilde{q} = 0$. To second order in $U(q)$, the dispersion a decreasing function of $\tilde{q}$, and anisotropy is not sufficient to stabilize long-range order. However, renormalization in the Cooper channel for $\tilde{q} \ll 2m^*|\alpha|$ is capable of reversing the sign of the $\tilde{q}$-dependence of χ^{xx} and thus stabilizing the ordered state. We also show that a combination of the electron-electron and SO interactions leads to a new effect: long-wavelength Friedel oscillations in the spin (but not charge) electron density induced by local magnetic moments. The period of these oscillations is given by the SO length $\pi/m^*|\alpha|$.

More detailed calculations are shifted into the Appendices.

Chapter 2

Momentum dependence of the spin susceptibility in two dimensions: nonanalytic corrections in the Cooper channel

2.1 Introduction

The study of the thermodynamic as well as microscopic properties of Fermi-liquid systems has a long history [Landau57, Landau59, Pines66, Giuliani05], but the interest in nonanalytic corrections to the Fermi-liquid behavior is more recent. The existence of well-defined quasiparticles at the Fermi surface is the basis for the phenomenological description due to Landau [Landau57] and justifies the fact that a system of interacting fermions is similar in many ways to the Fermi gas. The Landau theory of the Fermi liquid is a fundamental paradigm which has been successful in describing properties of ^{3}He, metals, and two-dimensional electronic systems. In particular, the leading temperature dependence of the specific heat or the spin susceptibility (i.e., C_s linear in T and χ_s approaching a constant) is found to be valid experimentally and in microscopic calculations. However, deviations from the ideal Fermi gas behavior exist in the subleading terms.

For example, while the low-temperature dependence of C_s/T for a Fermi gas is a regular expansion in T^2, a correction to C_s/T of the form $T^2 \ln T$ was found in three dimensions [Pethick73, and references therein]. These nonanalytic features are enhanced in two dimensions and, in fact, a correction linear in T is found [Coffey93, Belitz97, Chubukov03]. These effects were observed in ^{3}He, both in the three- [Greywall83] and two-dimensional case [Casey03].

The nonanalytic corrections manifest themselves not only in the temperature depen-

dence. For the special case of the spin susceptibility, it is of particular interest to determine also its dependence on the wave vector $\tilde{q}$. The deviation $\delta\chi_s$ from the $T = \tilde{q} = 0$ value parallels the temperature dependence of the specific heat discussed above: from a second-order calculation in the electron interaction, corrections proportional to $\tilde{q}^2 \ln \tilde{q}$ and $\tilde{q}$ were obtained in three and two dimensions respectively [Belitz97, Hirashima98, Chubukov03]. On the other hand, the dependence on T was found to be $\delta\chi_s \sim T^2$ in three dimensions [Carneiro77, Belitz97] (without any logarithmic factor) and $\delta\chi_s \sim T$ in two dimensions [Hirashima98, Baranov93, Chitov01b, Chitov01a, Chubukov03]. We cite here the final results in the two dimensional case (on which we focus in this Chapter), valid to second order in the interaction potential U_q,

$$\delta\chi_s^{(2)}(T, \tilde{q}) = 2U_{2k_F}^2 F(T, \tilde{q}), \tag{2.1.1}$$

where

$$F(T, 0) = \frac{m^3}{16\pi^3} \frac{k_B T}{E_F} \tag{2.1.2}$$

and

$$F(0, \tilde{q}) \equiv \frac{m^3}{48\pi^4} \frac{v_F \tilde{q}}{E_F}. \tag{2.1.3}$$

Here m is the effective mass, k_F is the Fermi wave vector, $E_F = k_F^2/2m$, and we use $\hbar = 1$ throughout this thesis. Our purpose is to extend this perturbative result to higher order by taking into account the Cooper channel renormalization of the scattering amplitudes.

The extension to higher order of the second-order results has mostly focused on the temperature dependence, both for the specific heat [Chubukov05b, Chubukov05a, Chubukov06, Chubukov07, Aleiner06] and the electron spin susceptibility [Chubukov05b, Shekhter06b, Shekhter06a, Schwiete06]. Recently the spin susceptibility has been measured in a silicon inversion layer as a function of temperature [Prus03]. A strong dependence on T is observed, seemingly incompatible with a T^2 Fermi-liquid correction, and the measurements also reveal that the (positive) value of the spin susceptibility is *decreasing* with temperature, in disagreement with the lowest order result cited above. This discrepancy has stimulated further theoretical investigations in the nonperturbative regime. Possible mechanisms that lead to a negative slope were proposed if strong renormalization effects in the Cooper channel become important [Shekhter06b, Shekhter06a]. These can drastically change the picture given by the lowest order perturbation theory, allowing for a nonmonotonic behavior and, in particular, a negative slope at small temperatures.

The mechanism we consider here to modify the linear $\tilde{q}$ dependence is very much related the one considered in [Shekhter06b]. There it is found that, at $\tilde{q} = 0$ and finite temperature, $U_{2k_F}^2$ in Equation (2.1.1) is substituted by $|\Gamma(\pi)|^2$, where

$$\Gamma(\theta) \equiv \sum_n \Gamma_n e^{in\theta} \tag{2.1.4}$$

is the scattering amplitude in the Cooper channel with θ being the scattering angle ($\theta = \pi$ corresponds to the backscattering process). An additional temperature dependence arises from the renormalization of the Fourier amplitudes

$$\Gamma_n(k_BT) = \frac{U_n}{1 - \frac{mU_n}{2\pi} \ln \frac{k_BT}{\Lambda}}, \tag{2.1.5}$$

where Λ is a large energy scale $\Lambda \sim E_F$ and U_n are the Fourier amplitudes of the interaction potential for scattering in the vicinity of the Fermi surface

$$U(2k_F \sin\theta/2) = \sum_n U_n e^{in\theta}. \tag{2.1.6}$$

A negative slope of $\delta\chi_s$ is possible, for sufficiently small T if one of the amplitudes U_n is negative [Shekhter06b, Kohn65, Chubukov93]. For $(mU_n/2\pi)\ln(k_BT_{KL}/\Lambda) = 1$, the denominator in Equation (2.1.5) diverges what corresponds to the Kohn-Luttinger (KL) instability [Kohn65]. At $T \gtrsim T_{KL}$ the derivative of the spin susceptibility is negative due to the singularity in $\Gamma_n(k_BT)$ and becomes positive far away from T_{KL}.

At $T = 0$ an analogous effect occurs for the momentum dependence. Indeed, it is widely expected that the functional form of the spin susceptibility in terms of k_BT or $v_F\tilde{q}$ is similar. As in the case of a finite temperature, the lowest order expression gains an additional nontrivial dependence on $\tilde{q}$ due to the renormalization of the backscattering amplitude $U_{2k_F}^2$. We obtain

$$\delta\chi_s(\tilde{q}) = 2|\Gamma(\pi)|^2 F(0,\tilde{q}), \tag{2.1.7}$$

where $\Gamma(\pi)$ is given by Equation (2.1.4) and

$$\Gamma_n(v_F\tilde{q}) = \frac{U_n}{1 - \frac{mU_n}{2\pi} \ln \frac{v_F\tilde{q}}{\Lambda}}. \tag{2.1.8}$$

Such result is obtained from renormalization of the interaction in the Cooper channel, while other possible effects are neglected. Moreover, at each perturbative order, only the leading term in the limit of small $\tilde{q}$ is kept. Therefore, corrections to Equation (2.1.7) exist which, for example, would modify the proportionality of $\delta\chi_s$ to $|\Gamma(\pi)|^2$, see [Shekhter06b]. However, in the region $v_F\tilde{q} \gtrsim k_BT_{KL}$, close to the divergence of $\Gamma_n(v_F\tilde{q})$ relative to the most negative U_n, Equation (2.1.7) is expected to give the most important contribution to the spin susceptibility.

The result of Equations (2.1.7) and (2.1.8) could have been perhaps easily anticipated and, in fact, it was suggested already in [Simon08]. The question of the functional dependence of the spin susceptibility on momentum is crucial in light of the ongoing studies on the nuclear spin ferromagnetism [Simon07, Simon08, Galitski03], as the stability of the ferromagnetic phase is governed by the electron spin susceptibility. In this context,

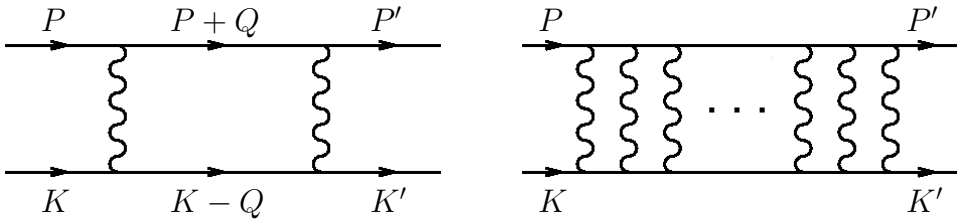

Figure 2.1: The building block (on the left) of any ladder diagram (on the right). Of special interest is the limit of correlated momenta $\mathbf{p} = -\mathbf{k}$, leading to the Cooper instability.

Equations (2.1.7) and (2.1.8) were motivated by a renormalization-group argument. We provide here a complete derivation, based on the standard diagrammatic approach.

This Chapter is organized as follows: in Section 2.2 we discuss the origin of Cooper instability and derive expressions for a general ladder diagram, which is an essential ingredient for the higher order corrections to the spin susceptibility. In Section 2.3 we give a short overview of the lowest order results to understand the origin of the nonanalytic corrections. Based on the results of Section 2.2, we provide an alternative derivation of one of the contributions, which can be easily generalized to higher order. Section 2.4 contains the main finding of this Chapter: the Cooper renormalization of the nonanalytic correction to the spin susceptibility is obtained there. We find an efficient approach to calculate higher order diagrams based on the second-order result. In Section 2.5 the diagrammatic calculation is discussed in relation to the renormalization-group argument of [Simon08]. Section 2.6 contains our concluding remarks. More technical details have been moved to the Appendices A.1-A.4.

2.2 Particle-particle propagator

In this section we consider a generic particle-particle propagator, which includes n interaction lines, as depicted in Figure 2.1. The incoming and outgoing frequencies and momenta are K, P and K', P', respectively, using the relativistic notation $K = (\omega_k, \mathbf{k})$. This particle-particle propagator represents an essential part of the diagrams considered in this Chapter and corresponds to the following expression:

$$\Pi^{(n)}(P, P', K) = (-1)^{n-1} \int_{q_1} \dots \int_{q_{n-1}} U_{|\mathbf{q}_1|} \prod_{i=1}^{n-1} g(K - Q_i) g(P + Q_i) U_{|\mathbf{q}_{i+1} - \mathbf{q}_i|}, \quad (2.2.1)$$

where $\mathbf{q}_n \equiv \mathbf{p}' - \mathbf{p}$ and $\int_{q_i} \equiv (2\pi)^{-3} \int d\Omega_{q_i} d^2 q_i$. The frequencies are along the imaginary axis, i.e., $g(K) = (i\omega_k - \epsilon_{\mathbf{k}})^{-1}$, where $\epsilon_{\mathbf{k}} = k^2/2m - E_F$ with $k = |\mathbf{k}|$.

In particular, we are interested in the case when the sum of incoming frequencies and momenta is small; i.e., $L \equiv K + P \approx 0$. Under this assumption we obtain the following

useful result for which we provide details of the derivation in Appendix A.1:

$$\Pi^{(n)}(L,\theta) = {\sum_{M_1\ldots M_{n-1}}}' \Pi_{M_1}(L)\ldots\Pi_{M_{n-1}}(L)\tilde{U}^n_{M_1\ldots M_{n-1}}(\theta_l,\theta), \tag{2.2.2}$$

where the sum is restricted to $M_i = 0, \pm 2, \pm 4 \ldots$. The angle of $\mathbf{l} = \mathbf{k} + \mathbf{p}$ is from the direction of the incoming momentum $\mathbf{p}$, i.e., $\theta_l \equiv \angle(\mathbf{l}, \mathbf{p})$, while $\theta \equiv \angle(\mathbf{p}, \mathbf{p}')$. In the above formula,

$$\Pi_0(L) = \frac{m}{2\pi} \ln \frac{|\Omega_l| + \sqrt{\Omega_l^2 + v_F^2 l^2}}{\Lambda} \tag{2.2.3}$$

and (M even)

$$\Pi_{M\neq 0}(L) = -\frac{m}{2\pi}\frac{(-1)^{|M|/2}}{|M|}\Big(\frac{1-\sin\phi}{\cos\phi}\Big)^{|M|}, \tag{2.2.4}$$

with $\Lambda \sim E_F$ a high energy cutoff and $\phi \equiv \arctan(|\Omega_l|/v_F l)$. Notice that $\Pi_M(L)$ has no angular (θ_l, θ) dependence, which is only determined by the following quantity:

$$\tilde{U}^n_{M_1\ldots M_{n-1}}(\theta_l,\theta) \equiv \sum_{m,m'} U_m U_{m-M_1}\ldots U_{m-M_1-\ldots-M_{n-1}} e^{im'\theta_l - i\,m\theta}\,\delta_{M_1+M_2+\ldots+M_{n-1},m'} \tag{2.2.5}$$

defined in terms of the amplitudes U_n. Equation (2.1.6) can be used to approximate the interaction potential in Equation (2.2.1) since the relevant contribution originates from the region of external ($p \approx p' \approx k \approx k' \approx k_F$) and internal momenta ($|\mathbf{p} + \mathbf{q}_i| \approx |\mathbf{k} - \mathbf{q}_i| \approx k_F$) close to the Fermi surface. Furthermore, the direction of $\mathbf{l}$ can be equivalently measured from $\mathbf{k}$ without affecting the result since $\theta_l = \angle(\mathbf{l}, \mathbf{k}) + \pi$ and $e^{im'\pi} = 1$ (m' is even).

Notice also that the leading contribution to Equation (2.2.2), in the limit of small Ω_l and l, is determined by the standard logarithmic singularity of $\Pi_0(L)$. However, it will become apparent that this leading contribution is not sufficient to obtain the correct result for the desired (linear-in-$\tilde{q}$) corrections to the response function. The remaining terms, $\Pi_M(L)$, are important because of their nonanalytic form due to the dependence on the ratio $|\Omega_l|/v_F l$.

2.3 Second order calculation

The lowest order nonanalytic correction to the spin susceptibility has been calculated in [Chubukov03] as a sum of four distinct contributions from the diagrams in Figure 4.8,

$$\delta\chi_1^{(2)}(\tilde{q}) = (U_{2k_F}^2 + U_0^2)F(0,\tilde{q}), \tag{2.3.1}$$

$$\delta\chi_3^{(2)}(\tilde{q}) = (U_{2k_F}^2 - U_0^2)F(0,\tilde{q}), \tag{2.3.2}$$

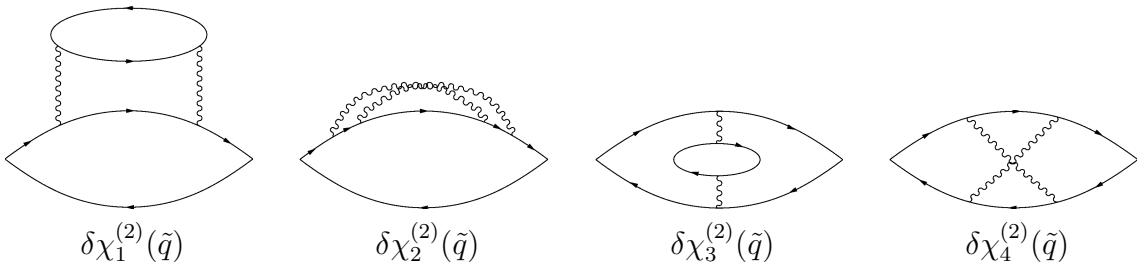

Figure 2.2: The nonvanishing second-order diagrams contributing to the nonanalytic behavior of the electron spin susceptibility.

$$\delta\chi_4^{(2)}(\tilde{q}) = U_0 U_{2k_F} F(0,\tilde{q}), \tag{2.3.3}$$

and $\delta\chi_2^{(2)} = -\delta\chi_4^{(2)}$ such that the final result reads as

$$\delta\chi_s^{(2)}(\tilde{q}) = 2U_{2k_F}^2 F(0,\tilde{q}). \tag{2.3.4}$$

We refer to [Chubukov03] for a thorough discussion of these lowest order results, but we find it useful to reproduce here the result for $\delta\chi_1^{(2)}$. In fact, Equation (2.3.1) has been obtained in [Chubukov03] as a sum of two nonanalytic contributions from the particle-hole bubble at small ($q = 0$) and large ($q = 2k_F$) momentum transfer. These two contributions, proportional to U_0^2 and $U_{2k_F}^2$, respectively, can be directly seen in Equation (2.3.1). However, it is more natural for our purposes to obtain the same result in the particle-particle channel by making use of the propagator discussed in Section 2.2. This approach is more cumbersome but produces these two contributions at the same time. Furthermore, once the origin of the lowest order nonanalytic correction is understood in the particle-particle channel, higher order results are most easily obtained.

We start with the analytic expression of $\delta\chi_1^{(2)}(\tilde{q})$ (see Figure 2.3) in terms of $\Pi^{(2)}$, the $n = 2$ case of Equation (2.2.2);

$$\delta\chi_1^{(2)}(\tilde{q}) = -8\int_k\int_l g^2(K)g(K+\tilde{Q})g(L-K)\Pi^{(2)}(L,0). \tag{2.3.5}$$

It is convenient to define the angle of $\mathbf{k}$ as $\theta_k \equiv \angle(\mathbf{k},\tilde{\mathbf{q}})$, and $\theta_l \equiv \angle(\mathbf{l},\mathbf{k})$. We first perform the integration in d^3k, as explained in Appendix A.2, to obtain

$$\delta\chi_1^{(2)} = -\frac{m}{\pi^4 v_F^2 \tilde{q}^2}\int_0^\infty l dl \int_0^\infty d\Omega_l \int_0^{2\pi} d\theta_l \Pi^{(2)}(L,0) \times\left(1 - \frac{\sqrt{(\Omega_l + iv_F l\cos\theta_l)^2 + (v_F\tilde{q})^2}}{\Omega_l + iv_F l\cos\theta_l}\right). \tag{2.3.6}$$

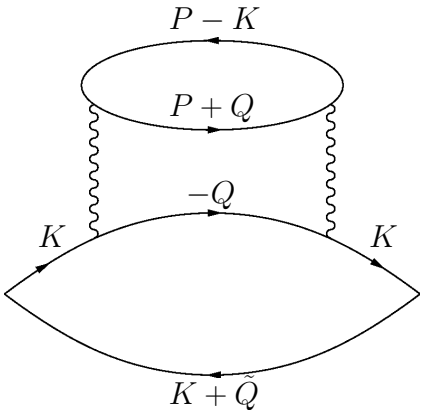

Figure 2.3: Labeling of the $\delta\chi_1^{(2)}$ diagram, as in Equation (2.3.5).

Following the method of [Chubukov03], we rescale the integration variables: $\Omega_l = Rv_F\tilde{q}\sin\phi$, $l = R\tilde{q}\cos\phi$, and $d\Omega_l dl = Rv_F\tilde{q}^2 dRd\phi$. This gives

$$\delta\chi_1^{(2)} = -\frac{m\tilde{q}}{\pi^4 v_F}\int_0^\infty R^2 dR\int_0^{\pi/2} d\phi\int_0^{2\pi} d\theta_l \Pi^{(2)}(R,\phi,\theta_l,0) \times\cos\phi\left(1-\frac{\sqrt{R^2(\sin\phi+i\cos\phi\cos\theta_l)^2+1}}{R(\sin\phi+i\cos\phi\cos\theta_l)}\right). \tag{2.3.7}$$

where, from Equations (2.2.2) and (2.2.5),

$$\Pi^{(2)}(R,\phi,\theta_l,\theta) = {\sum_M}' \tilde{U}_M^2(\theta_l,\theta)\Pi_M(R,\phi) = {\sum_M}'\Pi_M(R,\phi)\sum_m U_m U_{m-M} e^{iM\theta_l - im\theta} \tag{2.3.8}$$

with the primed sum restricted to even values of M.

Now we can see clearly that the linear dependence on $\tilde{q}$ in Equation (2.3.7) can only be modified by the presence of $\Pi^{(2)}$ in the integrand because of

$$\Pi_0(R,\phi) = \frac{m}{2\pi}\ln\frac{v_F\tilde{q}}{\Lambda} + \frac{m}{2\pi}\ln R(1+\sin\phi). \tag{2.3.9}$$

The first logarithmic term is diverging at small $\tilde{q}$ but does not contribute to the final result since it does not depend on θ_l and ϕ. In fact, if we keep only the $\ln v_F\tilde{q}/\Lambda$ contribution, after the change of variable $r = R(\sin\phi + i\cos\phi\cos\theta_l)$ in Equation (2.3.7), we obtain the angular integral $\int_0^{2\pi} d\theta_l \int_0^{\pi/2}\cos\phi(\sin\phi+i\cos\phi\cos\theta_l)^{-3}\,d\phi = 0$ [cf. Equation (A.3.6) for $M=0$]. Details of the calculation are provided in Appendix A.3.

Therefore, only the second term of Equation (2.3.9) is relevant. The integral in Equation (2.3.7) becomes independent of $\tilde{q}$ and gives only a numerical prefactor. The final result is given by Equation (2.3.1), in agreement with [Chubukov03]. In a similar way, the remaining diagrams of Figure 4.8 can be calculated.

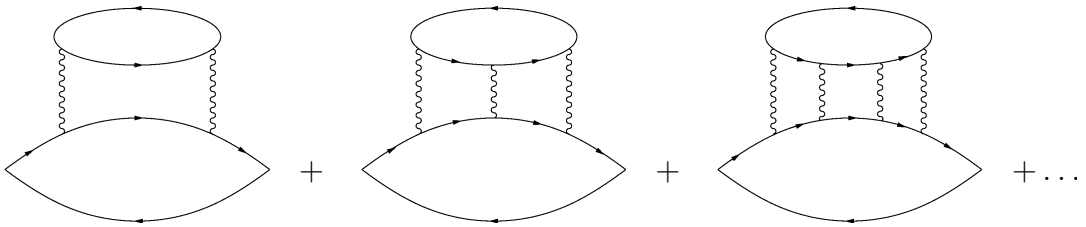

Figure 2.4: The series of diagrams contributing to $\delta\chi_1(\tilde{q})$.

2.4 Higher order diagrams

In this section we aim to find the renormalization of the four diagrams depicted in Figure 4.8 due to higher order contributions in the particle-particle channel. It is well known that the scattering of two electrons with opposite momenta, in the presence of the Fermi sea, leads to the emergence of a logarithmic singularity [Saraga05, Mahan00]. Furthermore, in two dimensions there are just two processes that contribute to $\delta\chi_i^{(2)}(\tilde{q})$, namely, forward- (small momentum transfer, $q = 0$) and back-scattering (large momentum transfer, $q = 2k_F$). This results in the renormalization of the scattering amplitudes appearing in the second-order results (see Section 2.1).

A direct calculation of the particle-particle propagators, depicted in Figure 2.1, shows that for $n+1$ interaction lines, the divergence always appears as the nth power of a logarithm. At each order of the perturbative expansion, we only consider the single diagram which contributes to the nonanalytic correction with the leading logarithmic singularity. This requirement restricts the freedom of adding interaction lines in unfettered manner to the existing second-order diagrams: in order to produce the most divergent logarithmic term, all interaction lines have to build up at most one ladder for $\delta\chi_1$, $\delta\chi_2$, and $\delta\chi_4$, or two ladders for $\delta\chi_3$.

The subset of diagrams generated in this way is not sufficient to obtain the general momentum dependence of the spin susceptibility. However, if one of the harmonics V_n is negative, these diagrams are the only relevant ones in the vicinity of the Kohn-Luttinger instability, $v_F\tilde{q} \gtrsim k_B T_{KL}$. Furthermore, at each order n in the interaction, it suffices to keep the leading contribution in $\tilde{q}$ of the individual diagrams. This turns out to be of order $\tilde{q}\ln^{n-2}\tilde{q}$ because the term proportional to $\ln^{n-1}\tilde{q}$ is suppressed by an additional factor $\tilde{q}^2$. Other perturbative terms, e.g., in the particle-hole channel [Shekhter06a], can be safely neglected as they result in logarithmic factors of lower order.

In the following we discuss explicitly how to insert a ladder diagram into the pre-existing second-order diagrams and show the line of the calculation that has to be carried out.

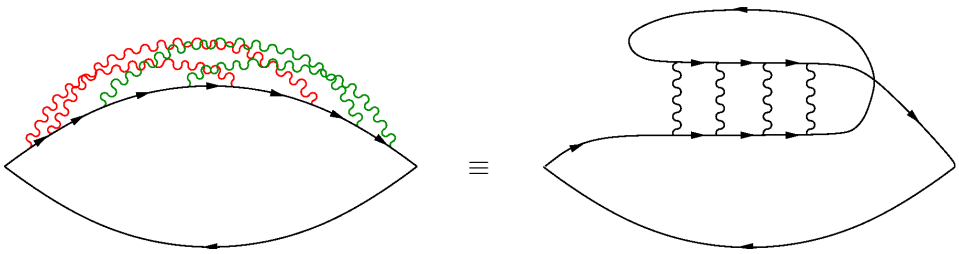

Figure 2.5: An example of diagram contributing to $\delta\chi_2(\tilde{q})$. The maximally crossed diagram (left) is topologically equivalent to its untwisted counterpart (right) in which the particle-particle ladder appears explicitly.

2.4.1 Diagrams 1, 2, and 4

These three diagrams can all be expressed to lowest order in terms of a single particle-particle propagator $\Pi^{(2)}$, which at higher order is substituted by $\Pi^{(n)}$. For the first term we have

$$\delta\chi_1^{(n)}(\tilde{q}) = -8\int_k\int_l g^2(K)g(K+\tilde{Q})g(L-K)\Pi^{(n)}(L), \tag{2.4.1}$$

where the $n=2$ case was calculated in Section 2.3. The corresponding diagrams are, in this case, easily identified and shown in Figure 2.4.

It is slightly more complicated to renormalize $\delta\chi_2^{(2)}$ and $\delta\chi_4^{(2)}$. It requires one to realize that the diagrams depicted in Figure 2.5 are topologically equivalent; i.e., the maximally crossed diagram on the left is equivalent to the untwisted ladder diagram on the right. A similar analysis shows how to lodge the ladder diagram into $\delta\chi_4^{(2)}$, as illustrated in Figure 2.6. The corresponding analytic expressions are:

$$\delta\chi_2^{(n)}(\tilde{q}) = 4\int_k\int_l g^2(K)g(K+\tilde{Q})g(L-K)\Pi^{(n)}(L,\pi), \tag{2.4.2}$$

$$\delta\chi_4^{(n)}(\tilde{q}) = 2\int_k\int_l g(K)g(K+\tilde{Q})g(L-K)g(L-K-\tilde{Q})\Pi^{(n)}(L,\pi). \tag{2.4.3}$$

We show now that the final results can be simply obtained to leading order in $\tilde{q}$ based on the second-order calculation. In fact, we can perform the integration in d^3k and the rescaling of variables as before. For $\delta\chi_1$ we have

$$\delta\chi_1^{(n)} = -\frac{m\tilde{q}}{\pi^4 v_F}\int_0^\infty R^2 dR\int_0^\pi d\theta_l\int_0^{\pi/2}\Pi^{(n)}(R,\phi,\theta_l,0) \times\left(1-\frac{\sqrt{R^2(\sin\phi+i\cos\phi\cos\theta_l)^2+1}}{R(\sin\phi+i\cos\phi\cos\theta_l)}\right)\cos\phi\; d\phi. \tag{2.4.4}$$

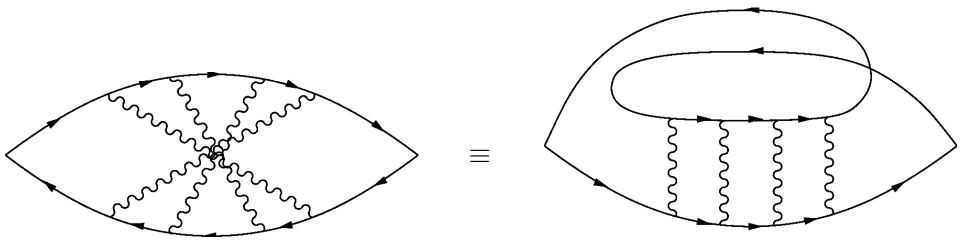

Figure 2.6: A maximally crossed diagram (left) and its untwisted equivalent (right) contributing to $\delta\chi_4(\tilde{q})$.

In the above formula, the $\tilde{q}$ dependence in the integrand is only due to $\Pi^{(n)}$. It is clear that a similar situation occurs for the second and fourth diagrams.

The $\tilde{q}$ dependence of the rescaled Equation (2.2.2) is determined (as in the second order) by the factors $\Pi_0(R,\phi)$. The first term appearing in $\Pi_0(R,\phi)$, see Equation (2.3.9), is large in the small $\tilde{q}$ limit we are interested in. Therefore, we can expand $\Pi^{(n)}$ in powers of $\ln v_F\tilde{q}/\Lambda$ and retain at each perturbative order n only the most divergent nonvanishing contribution. The detailed procedure is explained in Appendix A.4. It is found that the largest contribution from $\Pi^{(n)}$ is of order $(\ln v_F\tilde{q}/\Lambda)^{n-1}$. However, as in the case of the second-order diagram discussed in Section 2.3, this leading term has an analytic dependence on L (in fact, it is a constant), and gives a vanishing contribution to the linear-in-$\tilde{q}$ correction to the spin susceptibility. Therefore, the $(\ln v_F\tilde{q}/\Lambda)^{n-2}$ contribution is relevant here.

A particularly useful expression is obtained upon summation of $\Pi^{(n)}$ to infinite order. In fact, for each diagram, the sum of the relative series involves the particle-particle propagator only. Therefore, $\delta\chi_1$, $\delta\chi_2$, and $\delta\chi_4$ are given by Equations (2.4.1)–(2.4.3) if $\Pi^{(n)}$ is substituted by

$$\Pi^{(\infty)}(L,\theta) = \sum_{n=2}^{\infty} \Pi^{(n)}(L,\theta). \tag{2.4.5}$$

The relevant contribution of $\Pi^{(\infty)}(L,\theta)$, in the rescaled variables, is derived in Appendix A.4. The final result is

$$\Pi^{(\infty)}(R,\phi,\theta_l,\theta) = \sum_{n=2}^{\infty} \Pi^{(n)}(R,\phi,\theta_l,\theta) = {\sum_{M}}' \Pi_M(R,\phi) \sum_{m} \Gamma_m \Gamma_{m-M} e^{iM\theta_l - im\theta} + \ldots, \tag{2.4.6}$$

which should be compared directly to Equation (2.3.8). The only difference is the replacement of U_n with the renormalized amplitudes Γ_n, which depend on $\tilde{q}$ as in Equation (2.1.8).

Hence, it is clear that the final results follow immediately from Equations (2.3.1)–(2.3.3);

$$\delta\chi_1(\tilde{q}) = [\Gamma^2(0) + \Gamma^2(\pi)]F(0,\tilde{q}), \tag{2.4.7}$$

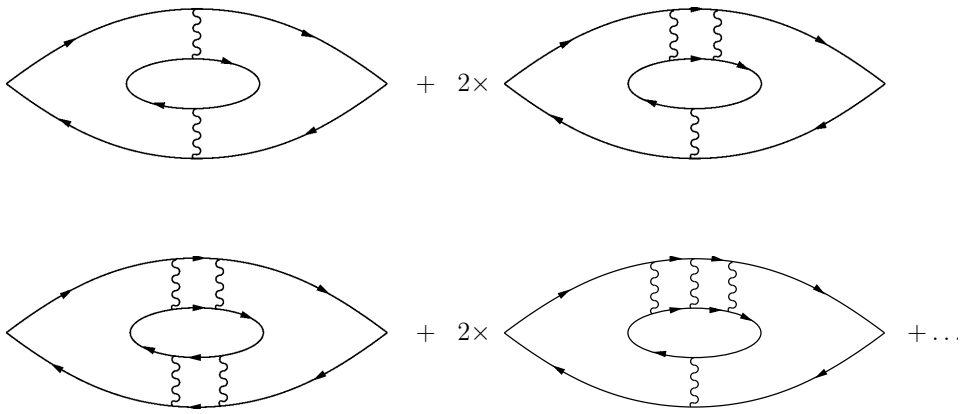

Figure 2.7: The series of diagrams contributing to $\delta\chi_3(\tilde{q})$. At the top, the second- and third-order diagrams. Two equivalent third-order diagrams arise from the addition of a parallel interaction line to either the upper or the lower part of the second-order diagram. At the bottom, three fourth-order diagrams.

$$\delta\chi_4(\tilde{q}) = \Gamma(0)\Gamma(\pi)F(0,\tilde{q}), \tag{2.4.8}$$

and $\delta\chi_2(\tilde{q}) = -\delta\chi_4(\tilde{q})$. We have used notation (2.1.4) while $F(0,\tilde{q})$ is defined in Equation (2.1.3). This explicitly proves what was anticipated in Section 2.1 (and in [Simon08]), i.e., that the renormalization affects only the scattering amplitude. The bare interaction potential is substituted by the dressed one, which incorporates the effect of other electrons on the scattering pair.

2.4.2 Diagram 3

The last diagram $\delta\chi_3^{(2)}$ differs from those already discussed in the sense that it allows for the separate renormalization of either the upper or lower interaction line. This results in the appearance of two equivalent third-order diagrams and three fourth-order diagrams (of which two are equal), and so forth. These lowest order diagrams are shown in Figure 2.7. Accordingly, we define the quantities $\delta\chi_3^{(i,j)}$, where ladders of order i and j are inserted in place of the original interaction lines. In particular, $\delta\chi_3^{(n)} = \sum_{i,j}\delta\chi_3^{(i,j)}\delta_{n,i+j}$ and

$$\delta\chi_3(\tilde{q}) = \sum_{i,j=1}^{\infty}\delta\chi_3^{(i,j)}(\tilde{q}). \tag{2.4.9}$$

The second difference stems from the fact that a finite nonanalytic correction is obtained from the leading terms in the particle-particle ladders of order $(\ln v_F\tilde{q}/\Lambda)^{i-1}$ and $(\ln v_F\tilde{q}/\Lambda)^{j-1}$, respectively. In fact, extracting this leading term from Equation (2.2.2) we obtain

$$\Pi^{(j)}(L,\theta) = \sum_n U_n^j e^{-in\theta}\Big(\frac{m}{2\pi}\ln\frac{v_F\tilde{q}}{\Lambda}\Big)^{j-1} + \dots\ , \tag{2.4.10}$$

and by performing the sum over j we get

$$\sum_{j=1}^{\infty} \Pi^{(j)}(L,\theta) = \Gamma(\theta) + \dots \ . \tag{2.4.11}$$

A similar argument can be repeated for the ith order interaction ladder. Therefore, the bare potential is replaced by renormalized expression (2.1.4) and the final result,

$$\delta\chi_3(\tilde{q}) = [\Gamma^2(\pi) - \Gamma^2(0)]F(0,\tilde{q}), \tag{2.4.12}$$

is immediately obtained from Equation (2.3.2).

2.4.3 Renormalized nonanalytic correction

Combining the results of Section 2.4.1 and 2.4.2, it is clear that the final result has the same form of Equation (2.3.4) if U_{2k_F} is substituted by $\Gamma(\pi)$. The explicit expression reads as

$$\delta\chi_s(\tilde{q}) = \frac{m^3}{24\pi^4}\frac{\tilde{q}}{k_F}\left[\sum_n \frac{U_n(-1)^n}{1-\frac{mU_n}{2\pi}\ln\frac{v_F\tilde{q}}{\Lambda}}\right]^2 . \tag{2.4.13}$$

2.5 Relation to the Renormalization Group approach

As discussed, our calculation was partially motivated by the renormalization group (RG) argument of [Simon08]. In this section, we further substantiate this argument. Starting from Equations (2.3.8) and (2.3.9), one can calculate the second-order correction to the bare vertex $\Pi^{(1)} = \sum_n U_n e^{in\theta}$ given by

$$\Pi^{(2)}(L,\theta) = \frac{m}{2\pi}\ln\frac{v_F\tilde{q}}{\Lambda}\sum_n U_n^2 e^{in\theta} + \dots \ , \tag{2.5.1}$$

where we explicitly extracted the dependence on the upper cutoff Λ. From Equation (2.5.1), we can immediately derive the following RG equations for the scale-dependent couplings $\Gamma_n(s = v_F\tilde{q})$:

$$\frac{d\Gamma_n}{d\ln(s/\Lambda)} = \frac{m}{2\pi}\Gamma_n^2, \tag{2.5.2}$$

as in [Simon08]. This leads to the standard Cooper channel renormalization. A direct derivation of these scaling equations can be found in [Shankar94]. At this lowest order, we obtain an infinite number of independent flow equations, one for each angular momentum n. The integration of these scaling equations directly leads to Equation (2.1.8). These

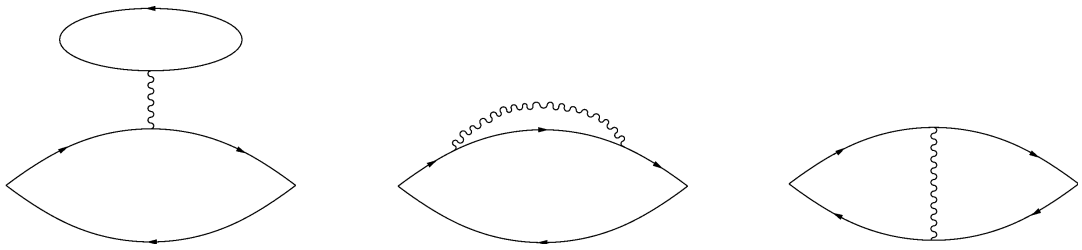

Figure 2.8: First-order diagrams contributing to the spin susceptibility. These are renormalized by the leading logarithmic terms of the higher order diagrams (see Figures 2.4–2.6). However, they do not produce a nonanalytic correction and can be neglected in the limit of small $\tilde{q}$.

flow equations tell us that the couplings Γ_n are marginally relevant in the infrared limit when the bare Γ_n are negative and marginally irrelevant otherwise. Notice that at zero temperature, the running flow parameter s is replaced by the momentum $v_F\tilde{q}$ in the Cooper channel. The idea of the RG is to replace in the perturbative calculations of a momentum-dependent quantity the bare couplings Γ_n by their renormalized values. By doing so, we directly resum an infinite class of (ladder) diagrams.

Let us apply this reasoning now to the susceptibility diagrams and note that the first nonzero contribution to the linear-in-$\tilde{q}$ behavior of $\chi_s(\tilde{q})$ appears in the second order in Γ_n. For the particular example of $\delta\chi_3$, the renormalization procedure has to be carried out independently for the two interaction lines, as illustrated by the series of diagrams in Figure 2.7. For a given order of the interaction ladder in the bottom (top) part of the diagram, one can perform the Cooper channel resummation of the top (bottom) interaction ladders to infinite order, as described in Section 2.4.2 or by using the RG equations. The fact that renormalized amplitudes Γ_n appear in the final results for the remaining diagrams $\delta\chi_{1,2,4}$ is also clear from the RG argument, after insertion of particle-particle ladders as in Figures 2.4–2.6.

Finally, we note that the same series of diagrams that renormalizes the nonanalytic second-order contributions $\delta\chi^{(2)}_{1,2,4}$ also contributes to the renormalization of the first-order diagrams displayed in Figure 2.8 (notice that the first one is actually vanishing because of charge neutrality). As it is clear from the explicit calculation Section 2.4, the highest logarithmic powers, i.e., $\propto (\ln v_F\tilde{q}/\Lambda)^{n-1}$ at order n, renormalize U_m to Γ_m in the final expressions for Figure 2.8. These first-order diagrams have an analytic dependence, at most $\tilde{q}^2$. Therefore, in agreement with the discussion in Section 2.4.1, the largest powers of the logarithms are not important for the linear dependence in $\tilde{q}$ and, in fact, they were already neglected to second order [Chubukov03].

2.6 Summary and discussion

In this Chapter we discussed the renormalization effects in the Cooper channel on the momentum-dependent spin susceptibility. The main result of this Chapter is given by Equation (2.4.13) and shows that each harmonics gets renormalized independently. The derivation of the higher order corrections to the spin susceptibility was based on the second-order result, which we revisited through an independent direct calculation in the particle-particle channel. Taking the angular dependence of the scattering potential explicitly into account, we verified that the main contribution indeed enters through forward- and back-scattering processes. At higher order, we found a simple and efficient way of resumming all the diagrams which contribute to the Cooper renormalization. We identified the leading nonvanishing logarithm in each ladder and used this result in the second-order correction. This method saves a lot of effort and, in fact, makes the calculation possible.

It was argued elsewhere that these renormalization effects might underpin the nonmonotonic behavior of the electron spin susceptibility if the higher negative harmonics override the initially leading positive Fourier components. This would results in the negative slope of the spin susceptibility at small momenta or temperatures [Shekhter06b, Simon08]. Other effects neglected here, as subleading logarithmic terms and nonperturbative contributions beyond the Cooper channel renormalization [Shekhter06a], become relevant far away from the Kohn-Luttinger instability condition, but a systematic treatment in this regime is outside the scope of this work. Our results could be also extended to include material-related issues such as disorder and spin-orbit coupling, which are possibly relevant in actual samples.

We also notice that final expression (2.4.13) parallels the temperature dependence discussed in [Shekhter06b], suggesting that the temperature and momentum dependence are qualitatively similar in two dimensions. This was already observed from the second-order calculation, in which a linear dependence both in $\tilde{q}$ and T is obtained. In our work we find that this correspondence continues to hold in the nonperturbative regime if the Cooper channel contributions are included. This conclusion is nontrivial and, in fact, does not hold for the three-dimensional case.

The last remark, together with the experimental observation of [Prus03], supports the recent prediction that the ferromagnetic ordering of nuclear spins embedded in the two-dimensional electron gas is possible [Simon07, Simon08]. The ferromagnetic phase would be stabilized by the long-range Ruderman-Kittel-Kasuya-Yosida (RKKY) interaction, as determined by the nonanalytic corrections discussed here.

Chapter 3

Spin susceptibility of interacting two-dimensional electron gas in the presence of spin-orbit interaction

3.1 Introduction

The issue of nonanalytic corrections to the Fermi liquid theory has been studied extensively in recent years [Belitz05, Löhneysen07]. The interest to this subject is stimulated by a variety of topics, from intrinsic instabilities of ferromagnetic quantum phase transitions [Belitz05, Löhneysen07, Chubukov04b, Rech06, Maslov06, Maslov09, Conduit09] to enhancement of the indirect exchange interaction between nuclear spins in semiconductor heterostructures with potential applications in quantum computing [Simon08, Simon07, Chesi09]. The origin of the nonanalytic behavior can be traced to an effective long-range interaction of fermions via virtual particle-hole pairs with small energies and with momenta which are either small (compared to the Fermi momentum k_F) or near $2k_F$ [Chubukov06, Chubukov05b]. In 2D, this interaction leads to a linear scaling of χ with a characteristic energy scale E, set by either the temperature T or the magnetic field $|\mathbf{B}|$, or else by the wavenumber of an inhomogeneous magnetic field $|\mathbf{q}|$ (whichever is larger when measured in appropriate units) [Chubukov03, Chubukov04a, Hirashima98, Baranov93, Chitov01b, Chitov01a, Betouras05, Efremov08]. Higher-order scattering processes in the Cooper (particle-particle) channel result in additional logarithmic renormalization of the result: at the lowest energies, $\chi \propto E/\ln^2 E$ [Aleiner06, Shekhter06b, Shekhter06a, Schwiete06, Maslov06, Maslov09, Simon08, Simon07]. The sign of the effect, i.e., whether χ increases or decreases with E, turns out to be nonuniversal, at least in a generic Fermi liquid regime, i.e., away from the ferromagnetic instability: while the second-order perturbation theory predicts that χ increases with E, the sign of the effect may be reversed either due to a proximity to the Kohn-Luttinger

superconducting instability [Shekhter06b, Simon08, Simon07] or higher-order processes in the particle-hole channel [Shekhter06a, Maslov06, Maslov09].

In this Chapter, we explore the effect of the spin-orbit interaction (SOI) on the nonanalytic behavior of the spin susceptibility [Żak10a]. The SOI is important for practically all systems of current interest at low enough energies; at the same time, the nonanalytic behavior is also an inherently low-energy phenomenon. A natural question to ask is: what is the interplay between these two low-energy effects? At first sight, the SOI should regularize nonanalyticities at energy scales below the scale set by this coupling. (For a Rashba-type SOI, the relevant scale is given by the product $|\alpha|k_F$, where α is the coupling constant of the Rashba Hamiltonian; here and in the rest of this thesis, we set $\hbar$ and k_B to unity). Indeed, as we have already mentioned, the origin of the nonanalyticity is the long-range effective interaction originating from the singularities in the particle-hole polarization bubble. If, for instance, the temperature is the largest scale in the problem, these singularities are smeared by the temperature with an ensuing nonanalytic dependence of χ on T. On the other hand, if the Zeeman energy $\mu_B|\mathbf{B}|$ is larger than T, it provides a more efficient mechanism of regularization of the singularities and, as result, χ exhibits a nonanalytic dependence on $|\mathbf{B}|$. The same argument applies also to the $|\tilde{\mathbf{q}}|$ dependence. It is often said that the SOI plays the role of an effective magnetic field, which acts on electron spins. If so, one should expect, for instance, a duality between the T and $|\alpha|k_F$ scalings of χ (by analogy to a duality between T and $\mu_B|\mathbf{B}|$ scalings of χ), i.e., in a system with fixed SOI, the nonanalytic T dependence of χ should saturate at $T \sim |\alpha|k_F$. The main message of this Chapter is that such a duality does not, in fact, exist; more precisely, not all components of the susceptibility tensor exhibit the duality. In particular, the in-plane component of χ, χ_{xx}, continues to scale linearly with T and $\mu_B|\mathbf{B}|$, even if these energies are smaller than $|\alpha|k_F$. On the other hand, the T and $\mu_B|\mathbf{B}|$ dependences of χ_{zz} do saturate at $T \sim |\alpha|k_F$.

The reason for such a behavior is that although the SOI does play a role of the effective magnetic field, this field depends on the electron momentum. To understand the importance of this fact, we consider the Rashba Hamiltonian in the presence of an external magnetic field [Bychkov84b, Bychkov84a], which couples only to the spins of the electrons but not to their orbital degrees of freedom

$$H_R = \frac{k^2}{2m} I + \alpha(\boldsymbol{\sigma} \times \mathbf{k})_z + \frac{g\mu_B \boldsymbol{\sigma}}{2} \cdot \mathbf{B} = \frac{k^2}{2m} I + \frac{g\mu_B \boldsymbol{\sigma}}{2} \cdot [\mathbf{B}_R(\mathbf{k}) + \mathbf{B}], \tag{3.1.1}$$

where α is the SOI, $\mathbf{k}$ is the electron momentum in the plane of a two-dimensional electron gas (2DEG), $\boldsymbol{\sigma}$ is a vector of Pauli matrices, $\mathbf{e}_z$ is a normal to the plane, g is the gyromagnetic ratio, μ_B is the Bohr magneton, and the effective Rashba field, defined as $\mathbf{B}_R = (2\alpha/g\mu_B)(\mathbf{k} \times \mathbf{e}_z)$, is always in the 2DEG plane. The effective Zeeman energy is determined by the total magnetic field $\mathbf{B}_{\text{tot}} = \mathbf{B}_R + \mathbf{B}$ as

$$\bar{\Delta}_{\mathbf{k}} \equiv \frac{g\mu_B |\mathbf{B}_{\text{tot}}|}{2} = \sqrt{\alpha^2 k^2 + 2\alpha (\boldsymbol{\Delta} \times \mathbf{k})_z + \Delta^2}, \tag{3.1.2}$$

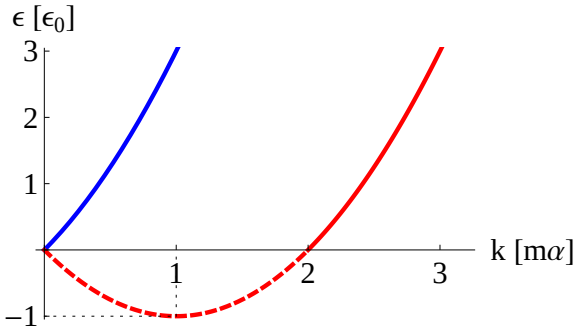

Figure 3.1: Rashba spectrum in zero magnetic field. The energy is measured in units of $\epsilon_0 \equiv m\alpha^2/2$, the momentum is measured in units of $m\alpha$.

where we introduced $\mathbf{\Delta} = g\mu_B\mathbf{B}/2$ for the "Zeeman field", such that Δ is the Zeeman energy of an electron spin in the external magnetic field ($\hbar = 1$) and 2Δ equals to the Zeeman splitting between spin-up and spin-down states. A combined effect of the Rashba and external magnetic fields gives rise to two branches of the electron spectrum (see Figure 3.1) with dispersions

$$\varepsilon_{\mathbf{k}}^{\pm} = \frac{k^2}{2m} \pm \bar{\Delta}_{\mathbf{k}}. \tag{3.1.3}$$

If $\mathbf{B} \parallel \mathbf{e}_z$, the external and effective magnetic fields are perpendicular to each other, as shown in Figure 3.2a, so that the magnitude of the total magnetic field is $|\mathbf{B}_{\text{tot}}| = |\mathbf{B} + \mathbf{B}_R| = \sqrt{B^2 + B_R^2}$. This means that the external and magnetic fields are totally interchangeable, and the T dependence of the spin susceptibility is cut off by the largest of the two scales. However, if the external field is in the plane (and defines the x axis in Figure 3.2b), the magnitude of the total field depends on the angle $\theta_{\mathbf{k}}$ between $\mathbf{k}$ and $\mathbf{B}$. In particular, for a weak external field,

$$\bar{\Delta}_{\mathbf{k}} \approx |\alpha|\, k + \Delta \sin\theta_{\mathbf{k}}. \tag{3.1.4}$$

If the electron-electron interaction is weak, the nonanalytic behavior of the spin susceptibility is due to particle-hole pairs with total momentum near $2k_F$, formed by electron and holes moving in almost opposite directions. In this case, the second term in Equation (3.1.4) is of the opposite sign for electrons and holes. The effective Zeeman energy of the whole pair, formed by fermions from Rashba branches s and s', is

$$\Delta_{\text{pair}} = s\bar{\Delta}_{\mathbf{k}} - s'\bar{\Delta}_{-\mathbf{k}} = (s - s')\,|\alpha|\, k + (s + s')\Delta \sin\theta_{\mathbf{k}}. \tag{3.1.5}$$

Only those pairs which "know" about the external magnetic field –via the second term in Equation (3.1.5)– renormalize the spin susceptibility. According to Equation (3.1.5), such

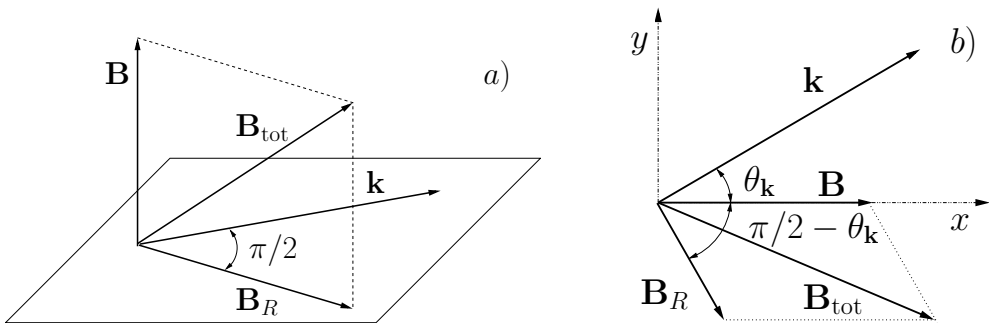

Figure 3.2: Interplay between the external magnetic field $\mathbf{B}$ and effective magnetic field $\mathbf{B}_R$ due to the Rashba SOI. Left: the external field is perpendicular to the plane of motion. Right: the external field is in the plane of motion.

pairs are formed by fermions from the same Rashba branch ($s = s'$). However, since the first term in Equation (3.1.5) vanishes in this case, such pairs do not "know " about the SOI, which means that the Rashba and external magnetic fields are not interchangeable, and the SOI energy scale does not provide a cutoff for the T dependence of χ.

We now briefly summarize the main results. We limit our consideration to the 2D case and to the Rashba SOI, present in any 2D system with broken symmetry with respect to reversal of the normal to the plane. We focus on the dependencies of χ on T, α, and $|B|$, deferring a detailed discussion of the dependence of χ on $|\mathbf{q}|$ to another occasion. Throughout this work, we assume that the spin-orbit and electron-electron interaction, characterized by the coupling constant U, are weak, i.e., $|\alpha|\, k_F \ll E_F$ and $mU \ll 1$. The latter condition implies that only $2k_F$ scattering processes are relevant for the nonanalytic behavior of the spin susceptibility. Accordingly, U is the $2k_F$ Fourier transform of the interaction potential. Renormalization provides another small energy scale at which the product $(mU/2\pi)\ln(\Lambda/T_C)$ (where Λ is an ultraviolet cutoff of the theory) becomes comparable to unity, i.e, $T_C \equiv \Lambda \exp(-2\pi/mU)$. Depending on the ratio of the two small energy scales–$|\alpha|\, k_F$ and T_C–different behaviors are possible.

In Figure 3.3a, we sketch the T dependence of χ_{zz} for the case of $T_C \ll |\alpha|\, k_F$. For $T \gg |\alpha|\, k_F$, χ_{zz} scales linearly with T, in agreement with previous studies; a correction due to the SOI is on the order of $(\alpha k_F/T)^2$ [cf. Equation (3.3.29)]. For $T_C \ll T \ll |\alpha|\, k_F$, χ_{zz} saturates at a value proportional to $|\alpha|$; the correction due to finite T is on the order of $(T/|\alpha|\, k_F)^3$ [cf. Equation (3.3.30)]. For $T \lesssim T_C$, renormalization in the Cooper channel becomes important. In the absence of the SOI, the coupling constant of the electron-electron interaction in the Cooper channel flows to zero as $U/|\ln T|$. Consequently, the T scaling of the spin susceptibility changes to $T/\ln^2 T$ for $T \ll T_C$. In the presence of the SOI, the situation is different. We show that the Renormalization Group (RG) flow of U in this case has a non-trivial fixed point characterized by finite value of the electron-

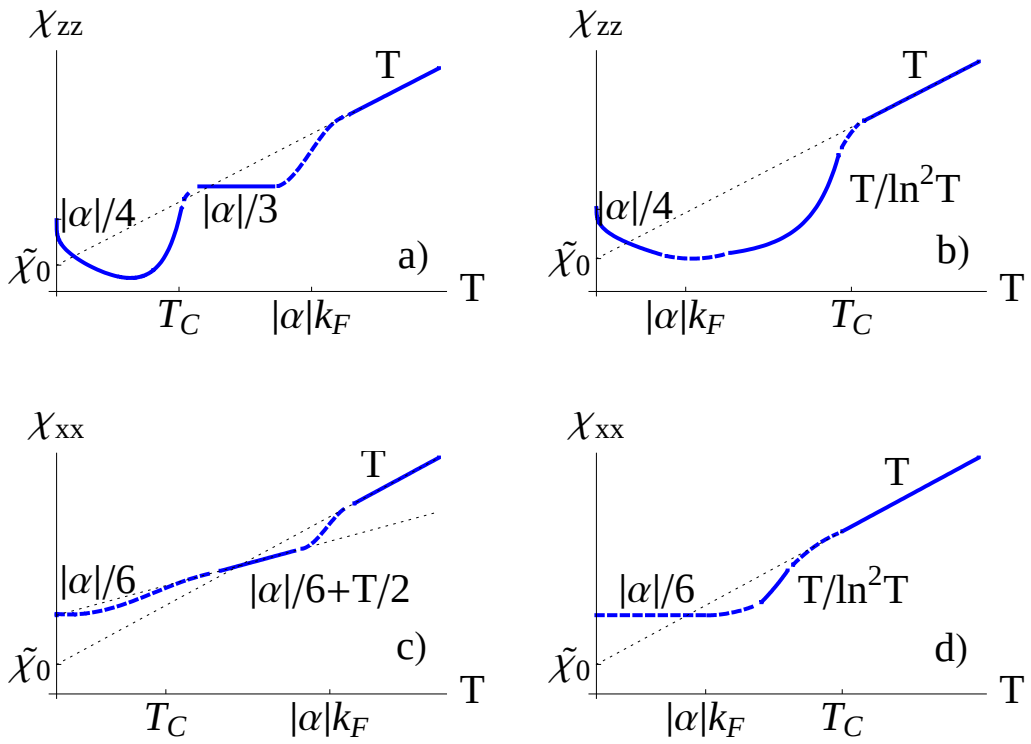

Figure 3.3: A sketch of the temperature dependence of the spin susceptibility for the transverse (top) and in-plane (bottom) magnetic field. Dashed segments in crossovers between various asymptotic regimes do not represent results of actual calculations. The left (right) panel is valid for $T_C \ll |\alpha| k_F$ ($T_C \gg |\alpha| k_F$) where $T_C \equiv \Lambda \exp(-2\pi/mU)$ is the temperature below which renormalization in the Cooper channel becomes significant. The zero temperature limit for interacting electrons, denoted by $\tilde{\chi}_0$, is given by Equation (3.2.8) in the Random Phase Approximation.

electron coupling, which is only numerically smaller than its bare value. In between these two limits, the coupling constant changes non-monotonically with $\ln T$, and so does χ_{zz}. In both high-and low T limits (compared to T_C), however, χ_{zz} is almost T independent, so Cooper renormalization affects the $|\alpha|$ term in χ_{zz}.

The T dependence of χ_{zz} for $T_C \gg |\alpha| k_F$ is sketched in Figure 3.3b. In this case, the crossover between the T and $T/\ln^2 T$ forms occurs first, at $T \sim T_C$, while the $T/\ln^2 T$ form crosses over to $|\alpha|$ at $T \sim |\alpha| k_F$.

We now turn to χ_{xx}. For $T_C \ll |\alpha| k_F$, its T dependence is shown in Figure 3.3c. The high-T behavior is again linear [also with a $(\alpha k_F/T)^2$ correction, cf. Equation (3.3.54)]. For $T_C \ll T \ll |\alpha| k_F$, this behavior changes to $\chi_{xx} \propto |\alpha| k_F/6 + T/2$, which means that χ_{xx} continues to decrease with T with a slope half of that at higher T, see Equation (3.3.55). Finally, for $T \lesssim T_C$, Cooper renormalization leads to the same $|\alpha|$ depen-

dence as for χ_{zz} but with a different prefactor. The behavior of χ_{xx} for $|\alpha|\, k_F \ll T_C$ is shown in Figure 3.3d. Apart from the numbers, this behavior is similar to that of χ_{zz} in that case.

The dependences of χ_{xx} and χ_{zz} on the external magnetic field can be obtained (up to a numerical coefficient) simply by replacing T by Δ in all formulas presented above. In particular, if Cooper renormalization can be ignored, both χ_{xx} and χ_{zz} scale linearly with Δ for $\Delta \gg |\alpha| k_F$ but only χ_{xx} continues to scale with Δ for $\Delta \ll |\alpha| k_F$. A linear scaling of χ_{ii} with Δ implies the presence of a nonanalytic, $|M_i|^3$ term in the free energy, where $\mathbf{M}$ is the magnetization and $i = x, y, z$. Consequently, while the cubic term is isotropic ($F \propto |M|^3$) for larger M (so that the corresponding Zeeman energy is above $|\alpha| k_F$), it is anisotropic at smaller $|M|$: $F \propto |M_x|^3 + |M_y|^3$. A negative cubic term in F implies metamagnetism and an instability of the second-order ferromagnetic quantum phase transition toward a first-order one [Belitz05, Maslov06, Maslov09]. An anisotropic cubic term implies anisotropic metamagnetism, i.e., a phase transition in a finite magnetic field, if it is applied along the plane of motion, but no transition for a perpendicular field, and also that the first-order transition is into an XY rather than Heisenberg ferromagnetic state. This issue is discussed in more detail in Section 4.4.

The rest of this Chapter is organized as follows. In Section 3.2, we formulate the problem and discuss the T dependence of the spin susceptibility for free electrons with Rashba spectrum (more details on this subject are given in Appendix B.1). Section 3.3.1 explains the general strategy of extracting the nonanalytic behavior of χ from the thermodynamic potential in the presence of the SOI. The second-order perturbation theory for the temperature and magnetic-field dependences of the transverse and in-plane susceptibilities is presented in Sections 3.3.2 and 3.3.3, respectively. In Section 3.3.4, we show that, as is also the case in the absence of the SOI, there is no contribution to the nonanalytic behavior of the spin susceptibility from processes with small momentum transfers, including the transfers commensurate with (small) Rashba splitting of the free-electron spectrum (more details on this issue are provided in Appendix B.2). Renormalization of spin susceptibility in the Cooper channel is considered in Section 3.4. An explicit calculation of the third-order Cooper contribution to χ_{zz} is shown in Section 3.4.2. In Section 3.4.3 we derive the RG flow equations for the scattering amplitudes in the absence of the magnetic field; the effect of the finite field on the RG flow is discussed in Appendix B.3. The effect of Cooper-channel renormalization on the nonanalytic behavior of χ_{zz} and χ_{xx} is discussed in Secs. 3.4.3 and 3.4.3, correspondingly. Implications of our results in the context of quantum phase transitions are discussed in Reference 4.4, where we also give our conclusions.

3.2 Free Rashba fermions

In this Section, we set the notations and discuss briefly the properties of Rashba electrons in the absence of the electron-electron interaction. The Hamiltonian describing a two-dimensional electron gas (2DEG) in the presence of a Rashba SOI and an external magnetic field $\mathbf{B}$ is given by Equation (3.1.1).

In the following, we consider two orientations of the magnetic field: transverse ($\mathbf{B} = B\mathbf{e}_z$) and parallel ($\mathbf{B} = B\mathbf{e}_x$) to the 2DEG plane. It is important to emphasize that, when discussing the perpendicular magnetic field, we neglect its orbital effect. Certainly, if the spin susceptibility is measured as a response to an external magnetic field, its orbital and spin effects cannot be separated. However, there are situations when the spin part of χ_{zz} is of primary importance. For example, the Ruderman-Kittel-Kasuya-Yosida (RKKY) interaction between the local moments located in the 2DEG plane arises only from the spin susceptibility of itinerant electrons, because the orbital effect of the dipolar magnetic field of such moments is negligible. In this case, χ_{xx} and χ_{zz} determine the strength of the RKKY interaction between two moments aligned along the x and z axis, respectively. Also, divergences of χ_{zz} and χ_{xx} signal ferromagnetic transitions into states with easy-axis and easy-plane anisotropies, respectively. Since it is this kind of physical situations we are primarily interested in this Chapter, we will ignore the orbital effect of the field from now on.

The Green's function corresponding to the Hamiltonian (3.1.1) is obtained by matrix inversion

$$G_K \equiv \frac{1}{i\omega - H} = \sum_{s=\pm} \Omega_s(\mathbf{k}) g_s(K), \tag{3.2.1}$$

where we use the "relativistic" notation $K \equiv (\omega, \mathbf{k})$ with ω being a fermionic Matsubara frequency, the matrix $\Omega_s(\mathbf{k})$ is defined as

$$\Omega_s(\mathbf{k}) \equiv \frac{1}{2}\left(I + s\zeta\right), \tag{3.2.2a}$$

$$\zeta = \frac{\alpha(k_y\sigma_x - k_x\sigma_y) + \boldsymbol{\sigma}\cdot\boldsymbol{\Delta}}{\bar{\Delta}_{\mathbf{k}}}, \tag{3.2.2b}$$

$g_s(K) = 1/(i\omega - \epsilon_{\mathbf{k}} - s\bar{\Delta}_{\mathbf{k}})$ is the single-electron Green's function, $\epsilon_{\mathbf{k}} \equiv \frac{k^2}{2m} - \mu$, μ is the chemical potential, and $\bar{\Delta}_{\mathbf{k}}$ is given by Equation (3.1.2).

As we have already pointed out in the Introduction, an important difference between the cases of transverse and in-plane magnetic field is the dependence of the effective Zeeman energy [Equation (3.1.2)] on the electron momentum. For the transverse magnetic field, ($\Delta_x = \Delta_y = 0, \Delta_z = \Delta$), the Zeeman energy is isotropic in the momentum space and quadratic in Δ in the weak-field limit: $\bar{\Delta}_{\mathbf{k}} \approx |\alpha|k_F + \Delta^2/2|\alpha|k_F$. Correspondingly, the Fermi surfaces of Rashba branches are concentric circles with slightly (in proportion to Δ^2) different radii. For the in-plane magnetic field, ($\Delta_x = \Delta, \Delta_y = \Delta_z = 0$), the

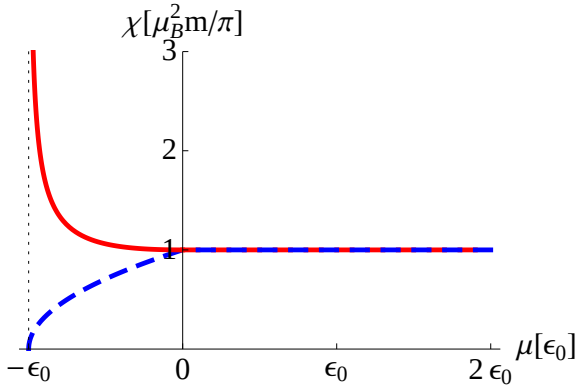

Figure 3.4: Spin susceptibility of free Rashba fermions (in units of $\chi_0 = \mu_B^2 m/\pi$) as a function of the chemical potential μ (in units of $\epsilon_0 = m\alpha^2/2$). Solid (red): $\chi_{xx}^{\{0\}}$; dashed (blue): $\chi_{zz}^{\{0\}}$. Note that $\chi_{xx}^{\{0\}} \neq \chi_{zz}^{\{0\}}$ if only the lowest Rashba branch is occupied ($-\epsilon_0 \leq \mu < 0$) but $\chi_{xx}^{\{0\}} = \chi_{zz}^{\{0\}} = \chi_0$ if both branches are occupied ($\mu > 0$) at $T = 0$.

effective Zeeman energy is anisotropic in the momentum space, cf. Equation (3.1.4). Correspondingly, the Fermi surfaces of Rashba branches are also anisotropic and their centers are shifted by finite momentum, proportional to Δ_x.

We now give a brief summary of results for the susceptibility in the absence of electron-electron interaction, which sets the zeroth order of the perturbation theory (for more details, see Appendix B.1). The in-plane rotational symmetry of the Rashba Hamiltonian guarantees that $\chi_{yy}^{\{0\}} = \chi_{xx}^{\{0\}}$. The static uniform susceptibility (defined in the limit of zero frequency and vanishingly small wavenumber) is still diagonal even in the presence of the SOI: $\chi_{ij}^{\{0\}} = \delta_{ij}\chi_{ii}^{\{0\}}$, although $\chi_{xx}^{\{0\}} = \chi_{yy}^{\{0\}} \neq \chi_{zz}^{\{0\}}$ in general. The susceptibility depends strongly on whether both or only the lower of the two Rashba branches are occupied, see Figure (3.4). In the latter case, the spin response is strongly anisotropic. At $T = 0$,

$$\chi_{zz}^{\{0\}} = \chi_0\sqrt{1+\mu/\epsilon_0} \tag{3.2.3a}$$

$$\chi_{xx}^{\{0\}} = \chi_0\frac{1+\mu/2\epsilon_0}{\sqrt{1+\mu/\epsilon_0}}, \tag{3.2.3b}$$

where $\chi_0 \equiv \mu_B^2 m/\pi$ is the spin susceptibility of 2D electrons in the absence of the SOI, $\epsilon_0 = m\alpha^2/2$ is the depth of the energy minimum of the lower branch and the chemical potential μ is within the range $-\epsilon_0 \leq \mu \leq 0$. The in-plane susceptibility exhibits a 1D-like van Hove singularity at the bottom of the lower branch, i.e., for $\mu \to -\epsilon_0$. On the other hand, if both branches are occupied (which is the case for $\mu > 0$), the spin susceptibility is isotropic and the same as in the absence of the SOI

$$\chi_{zz}^{\{0\}} = \chi_{xx}^{\{0\}} = \chi_0. \tag{3.2.4}$$

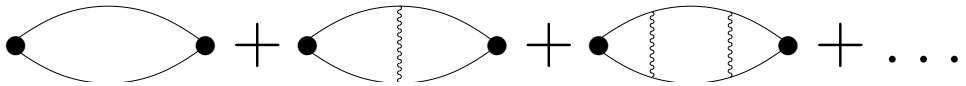

Figure 3.5: The RPA diagrams for the spin susceptibility corresponding to Equation (3.2.7).

This isotropy can be related to a hidden symmetry of the Rashba Hamiltonian manifested by conservation of the square of the electron's velocity operator v [Rashba05]. The eigenvalue of v^2, given by $2\epsilon/m + 2\alpha^2$ with ϵ being the energy, is the same for both branches. The square of the group velocity $v_g^2 = \left(\nabla_{\mathbf{k}}\epsilon_{\mathbf{k}}^{\pm}\right)^2 = 2\epsilon/m + \alpha^2$ also does not depend on the branch index. Therefore, the total density of states

$$\nu(\epsilon) = \frac{1}{2\pi}\frac{k^+ + k^-}{|v_g|} = \frac{m}{\pi}, \tag{3.2.5}$$

where $k^{\pm} = \mp m\alpha + \sqrt{m^2\alpha^2 + 2m\epsilon}$ are the momenta of the $\pm$ branches corresponding to energy ϵ, is the same as without the SOI, if both branches are occupied. One can show also that isotropy of the spin susceptibility is not specific for the Rashba coupling but is there also in the presence of both Rashba and (linear) Dresselhaus interactions [Ashrafi].

As one step beyond the free-electron model, we consider a Stoner-like enhancement of the spin susceptibility by the electron-electron interaction. In the absence of the SOI and for a point-like interaction U, the renormalized spin susceptibility is given by

$$\chi = \frac{\chi_0}{1 - mU/\pi}. \tag{3.2.6}$$

In the presence of the SOI, the ladder series for the susceptibility, shown in Figure 3.5 is given by

$$\begin{aligned}\chi_{ii} =& \chi_{ii}^{\{0\}} + U\mu_B^2 \sum_{K,P} \mathrm{Tr}\left[\sigma_i G(K+Q)G(P+Q)\sigma_i G(P)G(K)\right] \\ &- U^2\mu_B^2 \sum_{K,P,L} \mathrm{Tr}\left[\sigma_i G(K+Q)G(P+Q)G(L+Q)\sigma_i G(L)G(P)G(P)\right] + \dots \end{aligned} \tag{3.2.7}$$

where $Q = (\Omega = 0, \mathbf{q} \to 0)$ and $i = x, z$. Although the traces do look different for χ_{xx} and χ_{zz}, these differences disappear after angular integrations, and the resulting series are the same. As we have shown above, the zero-order susceptibilities are also the same (and equal to χ_0) if both Rashba branches are occupied; hence

$$\chi_{ii} = \mu_B^2\left(\frac{m}{\pi} + \frac{m^2U}{\pi^2} + \frac{m^3U^2}{\pi^3} + \dots\right) = \frac{\chi_0}{1 - mU/\pi}, \tag{3.2.8}$$

which is the same result as in Equation (3.2.6). Therefore, at the mean-field level, the spin susceptibility remains isotropic and independent of the SOI. In the rest of the Chapter, we will show that none of these two features survives beyond the mean-field level: the actual spin susceptibility is anisotropic and both its components do depend on the SOI.

We now come back to the free-electron model and discuss the T dependence of the spin susceptibility. A special feature of a 2DEG in the absence of the SOI is a breakdown of the Sommerfeld expansion at finite T: since the density of states does not depend on the energy, all power-law terms of this expansion vanish, and the resulting T dependence of $\chi^{\{0\}}$ is only exponential. The SOI leads to the energy dependence of the density of states for the individual branches, and one would expect the Sommerfeld expansion to be restored. This is what indeed happens if only the lower branch is occupied. In this case,

$$\chi_{zz}^{\{0\}}(T) = \chi_{zz}^{\{0\}}(0) - \chi_0 \frac{\pi^2}{24} \left(\frac{T}{\epsilon_0}\right)^2 \frac{1}{(1+\mu/\epsilon_0)^{3/2}} \tag{3.2.9a}$$

$$\chi_{xx}^{\{0\}}(T) = \chi_{xx}^{\{0\}}(0) + \chi_0 \frac{\pi^2}{48} \left(\frac{T}{\epsilon_0}\right)^2 \frac{2-\mu/\epsilon_0}{(1+\mu/\epsilon_0)^{5/2}}, \tag{3.2.9b}$$

provided that $T \ll \min\{-\mu, \epsilon_0 + \mu\}$. [Here, $\chi_{zz}^{\{0\}}(0)$ and $\chi_{xx}^{\{0\}}(0)$ are the zero temperature values given by Equations (3.2.3a) and (3.2.3b)]. However, if both branches are occupied, the energy dependent terms in the branch densities of states cancel out, and the resulting dependence is exponential, similar to the case of no SOI, although with different pre-exponential factors:

$$\chi_{zz}^{\{0\}}(T) = \chi_0 \left(1 - \frac{T}{2\epsilon_0} e^{-\mu/T}\right) \tag{3.2.10a}$$

$$\chi_{xx}^{\{0\}}(T) = \chi_0 \left(1 + \frac{T^2}{4\epsilon_0^2}\, e^{-\mu/T}\right) \tag{3.2.10b}$$

for $T \ll \epsilon_0 \ll \mu$, and

$$\chi_{zz}^{\{0\}}(T) = \chi_0 \left[1 - \left(1 - \frac{2\epsilon_0}{3T}\right) e^{-\mu/T}\right] \tag{3.2.11a}$$

$$\chi_{xx}^{\{0\}}(T) = \chi_0 \left[1 - \left(1 - \frac{4\epsilon_0}{3T}\right) e^{-\mu/T}\right] \tag{3.2.11b}$$

for $\epsilon_0 \ll T \ll \mu$. In a similar way, one can show that there are no power-law terms in the dependence of $\chi_{xx}^{\{0\}}$ and $\chi_{zz}^{\{0\}}$ on the external magnetic field.

Notice that $\chi_{xx} \neq \chi_{zz}$ at finite temperature, even if both Rashba subbands are occupied. This suggests that the hidden symmetry of the Rashba Hamiltonian is, in

fact, a rotational symmetry in a $(2+1)$ space with imaginary time being an extra dimension [Rashba]. Finite temperature should then play a role of finite size along the time axis breaking the rotational symmetry.

In what follows, we assume that the SOI is weak, i.e., $|\alpha| \ll v_F$, and thus the energy scales describing SOI are small: $m\alpha^2 \ll |\alpha| k_F \ll \mu$. This condition also means that both Rashba branches are occupied. [Also, from now on we relabel $\mu \to E_F$.] The main result of this section is that, for a weak SO coupling, the T and Δ dependences of χ in the free case are at least exponentially weak and thus cannot mask the power-law dependences arising from the electron-electron interaction, which are discussed in the rest of this Chapter.

3.3 Second order calculation

3.3.1 General strategy

The spin susceptibility tensor χ_{ij} is related to the thermodynamic (grand canonical) potential $\Xi(T, \alpha, \Delta)$ by the following identity

$$\chi_{ij}(T, \alpha) = -\left.\frac{\partial^2 \Xi}{\partial B_i \partial B_j}\right|_{B=0}. \tag{3.3.1}$$

To second order in the electron-electron interaction $U(q)$, there is only one diagram for the thermodynamic potential that gives rise to a nonanalytic behavior: diagram a) in Figure 3.6. The rest of the diagrams in this figure can be shown to be irrelevant (cf. Section 3.3.4). Algebraically, diagram a) in Figure 3.6 reads

$$\delta\Xi^{(2)} \equiv -\frac{1}{4} \sum_Q \sum_K \sum_P U^2_{|\mathbf{k}-\mathbf{p}|} \mathrm{Tr}(G_K G_P) \mathrm{Tr}(G_{K+Q} G_{P+Q}), \tag{3.3.2}$$

where $\sum_Q = (2\pi)^{-2} T \sum_\Omega \int d^2q$, $\sum_K = (2\pi)^{-2} T \sum_\omega \int d^2k$, and we use "relativistic" notation $K \equiv (\omega, \mathbf{k})$ with a fermionic frequency ω and $Q \equiv (\Omega, \mathbf{q})$ with a bosonic frequency Ω.

Evaluation of the first spin trace in Equation (3.3.2) yields

$$\mathrm{Tr}(G_K G_P) = \frac{1}{2} \sum_{ss'} B_{ss'}(\mathbf{k}, \mathbf{p}) g_s(K) g_{s'}(P), \tag{3.3.3}$$

where

$$B_{ss'}(\mathbf{k}, \mathbf{p}) \equiv 1 + ss' \frac{\alpha^2 \mathbf{k} \cdot \mathbf{p} + \alpha \left[\mathbf{\Delta} \times (\mathbf{k} + \mathbf{p})\right]_z + \Delta^2}{\bar{\Delta}_{\mathbf{k}} \bar{\Delta}_{\mathbf{p}}} \tag{3.3.4}$$

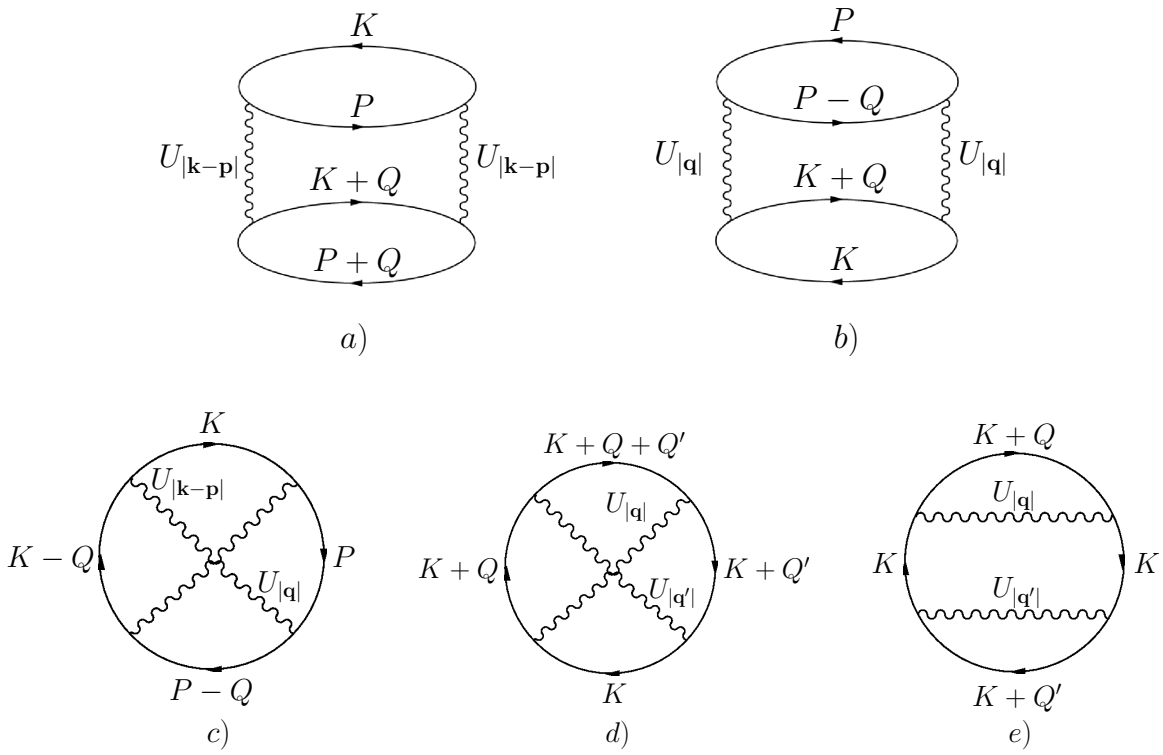

Figure 3.6: Second order diagrams for the thermodynamic potential. A nonanalytic contribution comes only from diagram *a*), where the momenta are arranged in such a way that $\mathbf{k} \approx -\mathbf{p}$ while q is small; therefore, $k \approx p \approx k_F$,and the momentum transfer in each scattering event is close to $|\mathbf{k}-\mathbf{p}| \approx 2k_F$. As is shown in Section 3.3.4, diagrams *b*)-*e*) do not contribute to the nonanalytic behavior of the spin susceptibility.

and $\bar{\Delta}_{\mathbf{k}}$ is given by Equation (3.1.2). The second-order thermodynamic potential then becomes

$$\delta\Xi^{(2)} \equiv -\frac{1}{16}\sum_{Q}\sum_{K}\sum_{P} U^2_{|\mathbf{k}-\mathbf{p}|} B_{s_1 s_3}(\mathbf{k},\mathbf{p}) B_{s_2 s_4}(\mathbf{k}+\mathbf{q},\mathbf{p}+\mathbf{q}) \times g_{s_1}(K) g_{s_2}(P) g_{s_3}(K+Q) g_{s_4}(P+Q). \tag{3.3.5}$$

Equation (3.3.5) describes the interaction among electrons from all Rashba branches via an effective vertex $U_{|\mathbf{k}-\mathbf{p}|}B_{ss'}(\mathbf{k},\mathbf{p})$, which depends not only on the momentum transfer $\mathbf{k}-\mathbf{p}$ but also on the initial momenta $\mathbf{k}$ and $\mathbf{p}$ themselves. This last dependence is due to anisotropy of the Rashba spinors.

It has been shown in [Chubukov03, Maslov06, Maslov09] that, at weak coupling, the main contribution to the nonanalytic part of the spin susceptibility comes from "backscattering" processes, i.e., processes with $\mathbf{p} \approx -\mathbf{k}$ and small q (compared to k_F).

In particular, the second-order contribution is entirely of the backscattering type. The proof given in [Maslov06, Maslov09] applies to any kind of the angular-dependent vertex and, thus, also to vertices in Equation (3.3.5). Therefore, the calculation can be simplified dramatically by putting in $\mathbf{p} = -\mathbf{k}$ and neglecting $\mathbf{q}$ in the effective vertices. The last assumption is justified as long as the typical values of q are determined by the smallest energy of the problem, i.e., $q \sim \max\{T/v_F, m|\alpha|\} \ll k_F$. By the same argument, the magnitudes of $\mathbf{k}$ and $\mathbf{p}$ in the vertices can be replaced by k_F. The bare interaction is then evaluated at $|\mathbf{k} - \mathbf{p}| \approx 2k_F$, and we introduce a coupling constant $U \equiv U_{2k_F}$. Ignoring the angular dependence of $B_{s_i s_j}$ for a moment, Equation (3.3.5) is reduced to a convolution of two particle-hole bubbles, formed by electrons belonging to either the same or different Rashba branches

$$\Pi_{s_i s_j}(Q) = \sum_K g_{s_i}(K) g_{s_j}(K+Q). \tag{3.3.6}$$

By assumption, both components of Q in $\Pi_{s_i s_j}(Q)$, i.e., Ω and q, are small (compared to E_F and k_F, correspondingly). It is important to realize that, despite a two-band nature of the Rashba spectrum, $\Pi_{s_i s_j}(Q)$ has no threshold-like singularities at the momentum $q_0 = 2m\alpha$, separating the Rashba subbands [Pletyukhov06] (for a detailed derivation of this result, see Appendix B.2). Therefore, the nonanalytic behavior of the spin susceptibility comes only from the Landau-damping singularity of the dynamic bubble, as it is also the case in the absence of the SOI.

After the simplifications described above, Equation (3.3.5) becomes

$$\delta\Xi^{(2)} \equiv -\frac{U^2}{16} \sum_Q \sum_K \sum_P B_{s_1 s_3} B_{s_2 s_4} g_{s_1}(K) g_{s_2}(P) g_{s_3}(K+Q) g_{s_4}(P+Q), \tag{3.3.7}$$

where

$$B_{ss'} \equiv B_{ss'}(\mathbf{k}_F, -\mathbf{k}_F) = 1 + ss' \frac{\Delta^2 - \alpha^2 k_F^2}{\bar{\Delta}_{\mathbf{k}_F} \bar{\Delta}_{-\mathbf{k}_F}} \tag{3.3.8}$$

and $\mathbf{k}_F \equiv (\mathbf{k}/k)k_F$. Finally, to obtain the leading T dependence of χ_{ij}, it suffices to replace the fermionic Matsubara sums in Equation (3.3.7) by integrals but keep the bosonic Matsubara sum as it is. The rest of the calculations proceed somewhat differently for the cases of the transverse and in-plane magnetic fields.

3.3.2 Transverse magnetic field

First, we consider a simpler case of the magnetic field transverse to the 2DEG plane: $\mathbf{\Delta} = g\mu_B B \mathbf{e}_z/2$. In this case, the effective Zeeman energy is isotropic in the momentum space; therefore, $\bar{\Delta}_{\mathbf{k}_F} = \bar{\Delta}_{-\mathbf{k}_F}$ and

$$B_{ss'} = 1 + ss' \frac{\Delta^2 - \alpha^2 k_F^2}{\bar{\Delta}^2_{\mathbf{k}_F}} = 1 + ss' \frac{\Delta^2 - \alpha^2 k_F^2}{\Delta^2 + \alpha^2 k_F^2}. \tag{3.3.9}$$

Thereby the integrals over d^3K and d^3P separate, and one obtains

$$\delta\Xi_{zz}^{(2)} = -\frac{U^2}{16}\sum_{s_1\ldots s_4=\pm 1} B_{s_1s_3}B_{s_2s_4}\sum_{Q}\Pi_{s_1s_2}(Q)\Pi_{s_3s_4}(Q), \tag{3.3.10}$$

where $\Pi_{s_is_j}(Q)$ is given by Equation (3.3.6). The single-particle spectrum in the second Green's function in Equation (3.3.6) can be linearized with respect to q as $\epsilon_{\mathbf{k}+\mathbf{q}} \approx \epsilon_{\mathbf{k}} + v_F q\cos\phi_{kq}$ with $\phi_{\mathbf{kq}} \equiv \angle(\mathbf{k},\mathbf{q})$. Since, by assumption, the SOI is small, the effective Zeeman energy in the Green's functions can be replaced by its value at $k = k_F$. Integration over dkk can be then replaced by that over $d\epsilon_{\mathbf{k}}$. The integrals over ω, $\epsilon_{\mathbf{k}}$ and ϕ_{kq} are performed in the same way as in the absence of the SOI, and we arrive at the following expression for the dynamic part of the polarization bubble

$$\Pi_{ss'} = \frac{m}{2\pi}\frac{|\Omega|}{\sqrt{\left[\Omega + i(s'-s)\bar{\Delta}_{\mathbf{k}_F}\right]^2 + (v_Fq)^2}}. \tag{3.3.11}$$

We pause here for a comment. The polarization bubble in Equation (3.3.11) is very similar to the dynamic part of the polarization bubble for spin-up and -down electrons in the presence of the magnetic field but in the absence of the SOI [Maslov06, Maslov09]

$$\Pi_{\uparrow\downarrow}(\Omega,q) = \frac{m}{2\pi}\frac{|\Omega|}{\sqrt{(\Omega - ig\mu_BB)^2 + (v_Fq)^2}}. \tag{3.3.12}$$

As we already mentioned in Section 3.1, the nonanalytic behavior of the spin susceptibility is due to an effective interaction of Fermi-liquid quasiparticles via particle-hole pairs with small energies and momenta near $2k_F$. Our calculation is arranged in such a way that, on a technical level, we deal with pairs with small momenta q. The spectral weight of these pairs is proportional to the polarization bubble, which is singular for small Ω and q. Since finite magnetic field cuts off the singularity in $\Pi_{\uparrow\downarrow}(\Omega,q)$, the nonanalytic dependence of χ on, e.g., temperature, saturates when T becomes comparable to the Zeeman splitting $g\mu_BB$. At lower energies, χ exhibits a nonanalytic dependence on Δ: $\chi \propto |\Delta|$. Likewise, the singularity in Equation (3.3.11) is cut at the effective Zeeman energy $\bar{\Delta}_{\mathbf{k}_F}$, which reduces to the SOI energy scale $|\alpha|k_F$, when the real magnetic field goes to zero. Therefore, one should expect the nonanalytic T dependence of χ_{zz} to be cut by the SOI. Although soft particle-hole pairs can be still generated within a given branch, i.e., for $s = s'$, the entire dependence on the Zeeman energy in this case is eliminated and processes of this type do not affect the spin susceptibility. In the rest of this section, we are going to demonstrate that the SOI indeed plays a role of the magnetic field for χ_{zz}.

For later convenience, we define a new quantity

$$\mathcal{P}_s \equiv \mathcal{P}_s(\Omega,q) = \frac{1}{\sqrt{\left(\Omega - 2is\bar{\Delta}_{\mathbf{k}_F}\right)^2 + v_F^2q^2}} \tag{3.3.13}$$

and sum over the Rashba branches in Equation (3.3.10). The contribution of the set $\{s_1 = s_2 \equiv s, s_3 = s_4 \equiv s'\}$ does not depend on $\bar{\Delta}_{\mathbf{k}_F}$:

$$\sum_{s,s'} B_{ss'}^2 \Pi_{ss}^2 = \left(\frac{m\Omega}{2\pi}\right)^2 \sum_{s,s'} B_{ss'}^2 \mathcal{P}_0^2. \tag{3.3.14}$$

The set $\{s_1 = -s_2 \equiv s, s_3 = -s_4 \equiv s'\}$ gives

$$\sum_{s,s'} B_{ss'} B_{-s,-s'} \Pi_{s,-s} \Pi_{s',-s'} = \left(\frac{m\Omega}{2\pi}\right)^2 \sum_{s,s'} B_{ss'}^2 \mathcal{P}_s \mathcal{P}_{s'}, \tag{3.3.15}$$

where we used that $B_{ss} = B_{-s,-s}$. Finally, the sets $\{s_1 = s_2 \equiv s, s_3 = -s_4 \equiv s'\}$ and $\{s_1 = -s_2 \equiv s, s_3 = s_4 \equiv s'\}$ contribute

$$\sum_{s,s'} (B_{ss'} B_{s,-s'} \Pi_{ss} \Pi_{s',-s'} + B_{ss'} B_{-s,s'} \Pi_{s,-s} \Pi_{s's'}) = 2 \left(\frac{m\Omega}{2\pi}\right)^2 \sum_{ss'} B_{ss'} B_{s,-s'} \mathcal{P}_0 \mathcal{P}_{s'}, \tag{3.3.16}$$

where we relabeled the indices in the second sum ($s \to s'$, $s' \to s$) and used the symmetry property $B_{ss'} = B_{s's}$.

The angular integral contributes a unity, so that

$$\delta\Xi_{zz}^{(2)} = -\left(\frac{mU}{8\pi}\right)^2 T \sum_{\Omega} \Omega^2 \int \frac{dqq}{2\pi} \sum_{ss'} [B_{ss'}^2 (\mathcal{P}_0^2 + \mathcal{P}_s \mathcal{P}_{s'}) + 2 B_{ss'} B_{s,-s'} \mathcal{P}_0 \mathcal{P}_{s'}]. \tag{3.3.17}$$

Now we sum over ss', add and subtract a combination $2(\alpha^4 k_F^4 + 4\alpha^2 k_F^2 \Delta^2 + \Delta^4)\mathcal{P}_0^2$ inside the square brackets, and obtain, after some algebra,

$$\begin{aligned} \delta\Xi_{zz}^{(2)} = &-\left(\frac{mU}{8\pi}\right)^2 T \sum_{\Omega} \Omega^2 \int_0^\infty \frac{dqq}{2\pi} \frac{4}{\bar{\Delta}_{\mathbf{k}_F}^4} [4\bar{\Delta}_{\mathbf{k}_F}^4 \mathcal{P}_0^2 \\ &+ \Delta^4 (\mathcal{P}_+^2 + \mathcal{P}_-^2 - 2\mathcal{P}_0^2) + 4\alpha^2 k_F^2 \Delta^2 \mathcal{P}_0 (\mathcal{P}_+ + \mathcal{P}_- - 2\mathcal{P}_0)], \end{aligned} \tag{3.3.18}$$

where we used that $\int dqq\,(\mathcal{P}_+ \mathcal{P}_- - \mathcal{P}_0^2) = 0$. The first term in the square brackets in Equation (3.3.18) does not depend on the effective field $\bar{\Delta}_{\mathbf{k}_F}$ and, therefore, can be dropped. Integration over q in the remaining terms is performed as

$$\int dqq \mathcal{P}_0 (\mathcal{P}_+ + \mathcal{P}_- - 2\mathcal{P}_0) = \frac{1}{v_F^2} \ln \frac{\Omega^2}{\Omega^2 + \bar{\Delta}_{\mathbf{k}_F}^2}, \tag{3.3.19}$$

$$\int dqq (\mathcal{P}_+^2 + \mathcal{P}_-^2 - 2\mathcal{P}_0^2) = \frac{1}{v_F^2} \ln \frac{\Omega^2}{\Omega^2 + 4\bar{\Delta}_{\mathbf{k}_F}^2}. \tag{3.3.20}$$

Collecting all terms together, we obtain

$$\delta\Xi_{zz}^{(2)} = -\frac{2}{\pi} \left(\frac{mU}{4\pi v_F}\right)^2 \left[\frac{\Delta^4}{4\bar{\Delta}_{\mathbf{k}_F}^4} T \sum_{\Omega} \Omega^2 \ln \frac{\Omega^2}{\Omega^2 + 4\bar{\Delta}_{\mathbf{k}_F}^2} + \frac{\alpha^2 k_F^2 \Delta^2}{\bar{\Delta}_{\mathbf{k}_F}^4} T \sum_{\Omega} \Omega^2 \ln \frac{\Omega^2}{\Omega^2 + \bar{\Delta}_{\mathbf{k}_F}^2}\right]. \tag{3.3.21}$$

The bosonic sum is evaluated by replacing the sum by an integral as follows

$$T\sum_{\Omega} F(\Omega) = \int_{-\infty}^{\infty} \frac{d\Omega}{2\pi} \coth\frac{\Omega}{2T} \mathrm{Im}\left[\lim_{\delta\to 0} F(-i\Omega+\delta)\right] \tag{3.3.22}$$

and using the identity

$$\mathrm{Im}\left[\lim_{\delta\to 0}(-i\Omega+\delta)^2 \ln\frac{(-i\Omega+\delta)^2}{(-i\Omega+\delta)^2+x^2}\right] = \pi\Omega^2 \mathrm{sign}\Omega\Theta(x^2-\Omega^2), \tag{3.3.23}$$

where $\Theta(x)$ stands for the step function.

The thermodynamic potential then becomes

$$\delta\Xi_{zz}^{(2)} = -\frac{2}{\pi}\left(\frac{mU}{4\pi v_F}\right)^2 T^3\left[\frac{\Delta^4}{4\bar{\Delta}_{\mathbf{k}_F}^4}\mathcal{F}\left(\frac{2\bar{\Delta}_{\mathbf{k}_F}}{T}\right) + \frac{\alpha^2 k_F^2\Delta^2}{\bar{\Delta}_{\mathbf{k}_F}^4}\mathcal{F}\left(\frac{\bar{\Delta}_{\mathbf{k}_F}}{T}\right)\right] \tag{3.3.24}$$

with

$$\mathcal{F}(y) = \int_0^y dx x^2 \coth(x/2) = -y^2\left[y + 6\mathrm{Li}_1\left(e^y\right)\right]/3 + 4[\zeta(3) + y\mathrm{Li}_2\left(e^y\right) - \mathrm{Li}_3\left(e^y\right)], \tag{3.3.25}$$

where $\mathrm{Li}_n(z) \equiv \sum_{k=1}^{\infty} z^k/k^n$ is the polylogarithm function and $\zeta(z)$ is the Riemann zeta function. In practice, the integral form of $\mathcal{F}(y)$ is more convenient as it can be easily expanded in the limits of small and large argument. Indeed, for $y \ll 1$, one expands $\coth(x/2)$ as $\coth(x/2) = 2/x + x/6$ and, upon integrating over x in Equation (3.3.25), obtains

$$\mathcal{F}(y) = y^2 + \frac{y^3}{24} + \mathcal{O}\left(y^4\right), \quad \text{for } 0 < y \ll 1. \tag{3.3.26}$$

For $y \gg 1$, one subtracts unity from the integrand and replaces the upper limit in the remaining integral by infinity:

$$\begin{aligned}\mathcal{F}(y) =& \frac{y^3}{3} + \int_0^y dx x^2\left(\coth\frac{x}{2} - 1\right) = \frac{y^3}{3} + \int_0^{\infty} dx x^2\left(\coth\frac{x}{2} - 1\right) \\ &- \int_y^{\infty} dx x^2\left(\coth\frac{x}{2} - 1\right) = \frac{y^3}{3} + 4\zeta(3) + \mathcal{O}\left(e^{-y}\right), \quad \text{for } y \gg 1.\end{aligned} \tag{3.3.27}$$

Temperature dependence of the transverse component

The (linear) spin susceptibility is given by $\chi_{zz} = -\partial^2\Xi/\partial B_z^2|_{B=0}$, which means that only terms proportional to Δ^2 in the thermodynamic potential matter. Therefore, for finite α, the spin susceptibility comes entirely from the second term in the square brackets of Equation (3.3.24), which is proportional to $\alpha^2 k_F^2\Delta^2$. On the other hand, for $\alpha = 0$ the second term vanishes, while $\Delta^4/\bar{\Delta}_{\mathbf{k}_F}^4 = 1$, and the spin susceptibility comes exclusively from the first term: $\delta\Xi_{zz}^{(2)}$ still depends on the magnetic field through $\mathcal{F}(\bar{\Delta}_{\mathbf{k}_F}/T)$, where

the Δ-dependence must be retained; in this case, $\mathcal{F}(\bar{\Delta}_{\mathbf{k}_F}/T)$ is evaluated as shown in [Chubukov03]. Neglecting the first term and differentiating the second one, we obtain the interaction correction to χ_{zz} for $\Delta \to 0$ as

$$\delta\chi_{zz}^{(2)} = 2\chi_0 \left(\frac{mU}{4\pi}\right)^2 \frac{T^3}{\alpha^2 k_F^2 E_F} \mathcal{F}\left(\frac{|\alpha|\, k_F}{T}\right). \tag{3.3.28}$$

For $T \gg |\alpha| k_F$, the asymptotic expansion of $\mathcal{F}$ in Equation (3.3.26) gives

$$\delta\chi_{zz}^{(2)} \approx 2\chi_0 \left(\frac{mU}{4\pi}\right)^2 \left[\frac{T}{E_F} + \frac{1}{24}\frac{\alpha^2 k_F^2}{T E_F} + \dots\right]. \tag{3.3.29}$$

The first term in Equation (3.3.29) coincides with the result of [Chubukov03, Maslov06, Maslov09, Shekhter06b, Schwiete06] obtained in the absence of the SOI, while the second term is a correction due to the finite SOI. In the opposite limit, i.e., for $T \ll |\alpha| k_F$, the asymptotic expansion of $\mathcal{F}$ in Equation (3.3.27) gives

$$\delta\chi_{zz}^{(2)} \approx 2\chi_0 \left(\frac{mU}{4\pi}\right)^2 \left[\frac{|\alpha| k_F}{3E_F} + 4\zeta(3)\frac{T^3}{\alpha^2 k_F^2 E_F} + \dots\right]. \tag{3.3.30}$$

As it was anticipated, the SOI cuts off the nonanalytic T dependence for $T \lesssim |\alpha| k_F$. However, the T dependence is replaced by a nonanalytic $|\alpha|$ dependence on the SOI.

Normalizing Equation (3.3.28) to the leading T dependent term for $\alpha = 0$, i.e., by $\delta\chi_{zz}^{(2)}(T, \alpha = 0) = \chi_0 (mU/4\pi)^2 (T/E_F)$, we express $\delta\chi_{zz}^{(2)}$ via a scaling function of the variable $T/|\alpha| k_F$

$$\frac{\delta\chi_{zz}^{(2)}(T, \alpha)}{\delta\chi_{zz}^{(2)}(T, \alpha = 0)} = \left(\frac{T}{|\alpha| k_F}\right)^2 \mathcal{F}\left(\frac{|\alpha|\, k_F}{T}\right). \tag{3.3.31}$$

The left-hand side of Equation (3.3.31) is plotted in Figure 3.7 along with its high and low T asymptotic forms.

Now we can give a physical interpretation of the above results. Although the electron-electron interaction mixes Rashba branches, the final result in Equation (3.3.28) comes only from a special combination of electron states. Namely, three out of four electron states involved in the scattering process (two for the incoming and two for the outgoing electrons) must belong to the same Rashba branch, while the last one must belong to the opposite branch, as shown in Figure 3.8a. This can be seen from Equation (3.3.18) by considering four terms in the square brackets. The first term, proportional to $\bar{\Delta}_{\mathbf{k}_F}^4$, does not depend on the field upon the cancelation with an overall factor of $\bar{\Delta}_{\mathbf{k}_F}^4$ in the denominator; the second term, proportional to $\alpha^4 k_F^4$, vanishes; the third term is already proportional to Δ^4 and, thus, cannot affect the spin susceptibility for finite α. Therefore, the effect comes exclusively from the last term, proportional to Δ^2, because the product $B_{ss'} B_{s,-s'}$ is equal to $4\Delta^2 (\alpha k_F)^2 / (\alpha^2 k_F^2 + \Delta^2)^2 \approx 4\Delta^2/(\alpha k_F)^2$ for any choice

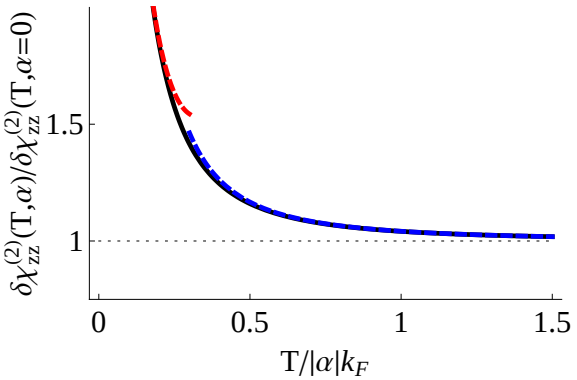

Figure 3.7: (The second-order nonanalytic correction to χ_{zz}, normalized to its value in the absence of the SOI, as a function of $T/|\alpha|k_F$, see Equation (3.3.31). The asymptotic forms, given by Equations (3.3.29) and (3.3.29), are shown by dashed (red and blue) lines.

of s and s'. This term corresponds to the structure $\sum_{ss'} B_{ss'}B_{s,-s'}\Pi_{s,-s}\Pi_{s's'}$ in Equation (3.3.17). The diagrams corresponding to this structure are shown in Figure 3.8a. Pairing electron Green's functions from different bubbles, we always obtain a combination $\sum_K g_\pm(K)\, g_\pm(K+Q)$, which depends neither on the SOI nor on the magnetic field, and a combination $\sum_K g_\pm(K)\, g_\mp(K+Q)$, which depends on both via the effective Zeeman energy $\bar{\Delta}_{\mathbf{k}_F} = \sqrt{\alpha^2 k_F^2 + \Delta^2}$. In the weak-field limit, one needs to keep Δ^2 only in the prefactor. The singularity in the combination $\sum_K g_\pm(K)\, g_\mp(K+Q)$ is then regularized by finite SOI, which is the reason why the nonanalytic T dependence is cut off by the SOI.

Magnetic-field dependence of the transverse component

Now we consider the case of $T \ll \max\{\Delta, |\alpha|k_F\}$ when, to first approximation, one can set $T = 0$. In this case, one can define a non-linear susceptibility $\chi_{zz}(B_z,\alpha) = -\partial^2\Xi_{zz}/\partial B_z^2$ evaluated at finite rather than zero magnetic field. For $T \to 0$, we replace the scaling function $\mathcal{F}$ in Equation (3.3.24) by the first term in its large-argument asymptotic form (3.3.27) to obtain

$$\delta\Xi_{zz}^{(2)} = -\frac{2}{3\pi}\left(\frac{mU}{4\pi v_F}\right)^2 \frac{2\Delta^4 + \alpha^2 k_F^2 \Delta^2}{\sqrt{\Delta^2 + \alpha^2 k_F^2}}. \tag{3.3.32}$$

Differentiating twice with respect to the field, we find

$$\delta\tilde{\chi}_{zz}^{(2)}(B_z,\alpha) = \chi_0 \left(\frac{mU}{4\pi}\right)^2 \frac{|\Delta|}{E_F}\mathcal{G}\left(\frac{|\alpha|k_F}{\Delta}\right), \tag{3.3.33}$$

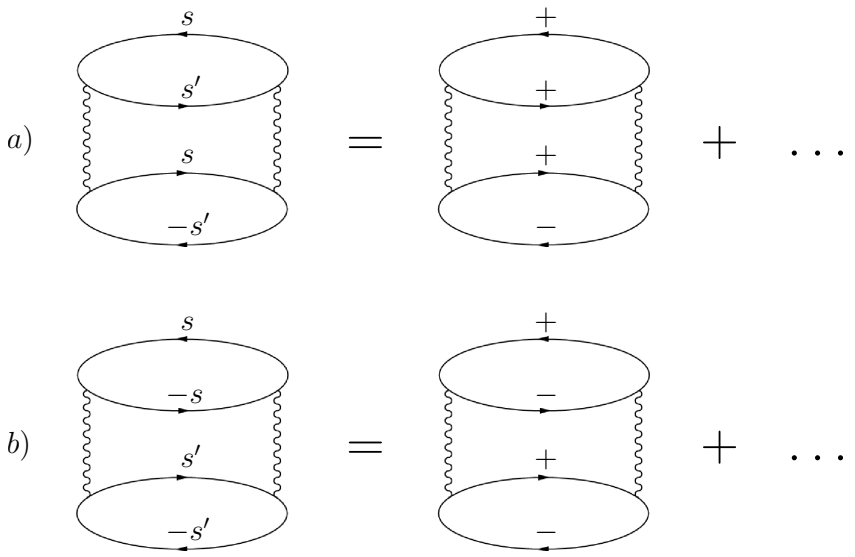

Figure 3.8: Top: Diagrams contributing to nonanalytic behavior of χ_{zz}. There are eight such diagrams with the following choice of Rashba indices: $+++-$, $++-+$, $+-++$, $-+++$, $---+$, $--+-$, $-+--$, and $+---$; one of the them is shown on the right. Bottom: Diagrams contributing to nonanalytic behavior of χ_{xx}. There are four such diagrams with the following choice of Rashba indices: $+-+-$, $+--+$, $-++-$, and $-+-+$; one of them is shown on the right.

where

$$\mathcal{G}(x) = \frac{2x^6 + 23x^4 + 30x^2 + 12}{3(1+x^2)^{5/2}} \tag{3.3.34}$$

has the following asymptotics

$$\mathcal{G}(x \ll 1) = 4 + x^4/6 + \dots, \tag{3.3.35}$$

$$\mathcal{G}(x \gg 1) = (2/3)|x| + 6/|x| + \dots. \tag{3.3.36}$$

For $|\Delta| \gg |\alpha| k_F$, the nonanalytic correction $\tilde{\chi}_{zz}(B_z, \alpha)$ reduces to the result of [Maslov06, Maslov09], obtained in the absence of the SOI, plus a correction term

$$\delta\chi^{(2)}_{zz}(B_z, \alpha) = 4\chi_0 \left(\frac{mU}{4\pi}\right)^2 \left[\frac{|\Delta|}{E_F} + \frac{1}{24}\frac{\alpha^4 k_F^4}{|\Delta|^3 E_F} + \dots\right]. \tag{3.3.37}$$

In the opposite limit of $|\Delta| \ll |\alpha| k_F$, the nonanalytic field dependence is cut off by the SOI

$$\delta\tilde{\chi}^{(2)}_{zz}(B_z, \alpha) = \frac{2}{3}\chi_0 \left(\frac{mU}{4\pi}\right)^2 \left[\frac{|\alpha| k_F}{E_F} + 9\frac{\Delta^2}{|\alpha| k_F E_F} + \dots\right]. \tag{3.3.38}$$

3.3.3 In-plane magnetic field

If the magnetic field is along the x-axis, $\mathbf{\Delta} = \mu_B B \mathbf{e}_x/2$, the effective Zeeman energies, $\bar{\Delta}_{\pm\mathbf{k}_F} \equiv \sqrt{\alpha^2 k_F^2 \pm 2\alpha k_F \sin\theta_{\mathbf{k}} \Delta + \Delta^2}$, depends on the angle $\theta_{\mathbf{k}}$ between $\mathbf{k}$ and the direction of the field, chosen as the x axis. Coming back to Equation (3.3.7), we integrate first over the fermionic frequencies, then over the magnitudes of the fermionic momenta, then over the angle between $\mathbf{p}$ and $\mathbf{q}$, and finally over the angle between $\mathbf{q}$ and $\mathbf{k}$ (at fixed $\mathbf{k}$). This yields

$$\delta\Xi_{xx}^{(2)} = -\frac{U^2}{16} T \sum_{\Omega} \int \frac{d\theta_{\mathbf{k}}}{2\pi} \int \frac{dqq}{2\pi} \sum_{\{s_i\}} B_{s_1 s_3} B_{s_2 s_4} \Pi_{s_1 s_2}^{+\mathbf{k}_F} \Pi_{s_3 s_4}^{-\mathbf{k}_F}, \tag{3.3.39}$$

where

$$\begin{aligned} \Pi_{ss'}^{\pm\mathbf{k}_F} \equiv \Pi_{ss'}^{\pm\mathbf{k}_F}(\Omega, q; \theta_{\mathbf{k}}) &= {\sum_{K}}' g_s^{\pm\mathbf{k}_F}(K) g_{s'}^{\pm\mathbf{k}_F}(K+Q) \\ &= \frac{m}{2\pi} \frac{|\Omega|}{\sqrt{\left[\Omega + i(s'-s)\bar{\Delta}_{\pm\mathbf{k}_F}\right]^2 + v_F^2 q^2}}, \end{aligned} \tag{3.3.40}$$

with $g_s^{\pm\mathbf{k}_F}(K) = 1/(i\omega - \epsilon_{\mathbf{k}} - s\bar{\Delta}_{\pm\mathbf{k}_F})$, and $\sum_K'$ indicates that the integration over $\theta_{\mathbf{k}}$ is excluded. The remaining integration over $\theta_{\mathbf{k}}$ is performed last, after integration over q and summation over Ω.

As in Section 3.3.2, it is convenient to define a new quantity

$$\mathcal{P}_s^{\pm\mathbf{k}_F} \equiv \mathcal{P}_s^{\pm\mathbf{k}_F}(\Omega, q; \theta_{\mathbf{k}}) = \frac{1}{\sqrt{\left(\Omega - 2is\bar{\Delta}_{\pm\mathbf{k}_F}\right)^2 + v_F^2 q^2}}, \tag{3.3.41}$$

and to re-write the thermodynamic potential as

$$\begin{aligned} \delta\Xi_{xx}^{(2)} = -\left(\frac{mU}{8\pi}\right)^2 T \sum_{\Omega} \Omega^2 \int \frac{d\theta_{\mathbf{k}}}{2\pi} \int \frac{dqq}{2\pi} \sum_{ss'} \Big[& B_{ss'} B_{s,-s'} \mathcal{P}_0 (\mathcal{P}_{s'}^{+\mathbf{k}_F} + \mathcal{P}_{s'}^{-\mathbf{k}_F}) \\ & + B_{ss'}^2 (\mathcal{P}_0^2 + \mathcal{P}_s^{+\mathbf{k}_F} \mathcal{P}_{s'}^{-\mathbf{k}_F}) \Big]. \end{aligned} \tag{3.3.42}$$

Subsequently, we sum over s and s', add and subtract $4(\bar{\Delta}_{\mathbf{k}_F}^2 \bar{\Delta}_{-k_F}^2 - 2\alpha^2 k_F^2 \sin 2\theta_{\mathbf{k}}) \mathcal{P}_0^2$ inside the square brackets, and, after some algebraic manipulations, obtain

$$\begin{aligned} \delta\Xi_{xx}^{(2)} = -2\left(\frac{mU}{8\pi}\right)^2 T \sum_{\Omega} \Omega^2 \int \frac{d\theta_{\mathbf{k}}}{2\pi} \int \frac{dqq}{2\pi} \Big[& 8\mathcal{P}_0^2 + a_0 \mathcal{P}_0 \Big(\mathcal{P}_+^{-\mathbf{k}_F} + \mathcal{P}_+^{+\mathbf{k}_F} \\ & + \mathcal{P}_-^{-\mathbf{k}_F} + \mathcal{P}_-^{+\mathbf{k}_F} - 4\mathcal{P}_0 \Big) + a_+ \Big(\mathcal{P}_+^{+\mathbf{k}_F} \mathcal{P}_-^{-\mathbf{k}_F} + \mathcal{P}_+^{-\mathbf{k}_F} \mathcal{P}_-^{+\mathbf{k}_F} \\ & - 2\mathcal{P}_0^2 \Big) + a_- \left(\mathcal{P}_-^{-\mathbf{k}_F} \mathcal{P}_-^{+\mathbf{k}_F} + \mathcal{P}_+^{-\mathbf{k}_F} \mathcal{P}_+^{+\mathbf{k}_F} - 2\mathcal{P}_0^2 \right) \Big], \end{aligned} \tag{3.3.43}$$

where

$$a_0 = \frac{4\alpha^2 k_F^2 \Delta^2 \cos^2\theta_{\mathbf{k}}}{\bar{\Delta}^2_{\mathbf{k}_F}\bar{\Delta}^2_{-\mathbf{k}_F}}, \tag{3.3.44}$$

$$a_\pm = \frac{\alpha^4 k_F^4 + \Delta^4 - 2\alpha^2 k_F^2 \Delta^2 \sin^2\theta_{\mathbf{k}} \pm \bar{\Delta}_{\mathbf{k}_F}\bar{\Delta}_{-\mathbf{k}_F}(\alpha^2 k_F^2 - \Delta^2)}{\bar{\Delta}^2_{\mathbf{k}_F}\bar{\Delta}^2_{-\mathbf{k}_F}}. \tag{3.3.45}$$

The first term in the square brackets in Equation (3.3.43) does not depend on the effective field $\bar{\Delta}_{\pm\mathbf{k}_F}$ and can be dropped. The remaining integrals over q are equal to

$$\int dqq\mathcal{P}_0[\mathcal{P}_+^{-\mathbf{k}_F} + \mathcal{P}_+^{+\mathbf{k}_F} + \mathcal{P}_-^{-\mathbf{k}_F} + \mathcal{P}_-^{+\mathbf{k}_F} - 4\mathcal{P}_0] = \frac{1}{v_F^2}\ln\frac{\Omega^2}{\Omega^2 + \bar{\Delta}^2_{\mathbf{k}_F}} + \frac{1}{v_F^2}\ln\frac{\Omega^2}{\Omega^2 + \bar{\Delta}^2_{-\mathbf{k}_F}}, \tag{3.3.46}$$

$$\int dqq[\mathcal{P}_+^{+\mathbf{k}_F}\mathcal{P}_-^{-\mathbf{k}_F} + \mathcal{P}_+^{-\mathbf{k}_F}\mathcal{P}_-^{+\mathbf{k}_F} - 2\mathcal{P}_0^2] = \frac{1}{v_F^2}\ln\frac{\Omega^2}{\Omega^2 + (\bar{\Delta}_{\mathbf{k}_F} - \bar{\Delta}_{-\mathbf{k}_F})^2}, \tag{3.3.47}$$

and

$$\int dqq[\mathcal{P}_-^{-\mathbf{k}_F}\mathcal{P}_-^{+\mathbf{k}_F} + \mathcal{P}_+^{-\mathbf{k}_F}\mathcal{P}_+^{+\mathbf{k}_F} - 2\mathcal{P}_0^2] = \frac{1}{v_F^2}\ln\frac{\Omega^2}{\Omega^2 + (\bar{\Delta}_{\mathbf{k}_F} + \bar{\Delta}_{-\mathbf{k}_F})^2}. \tag{3.3.48}$$

Evaluating the Matsubara sum in the same way as in Section 3.3.2, we obtain

$$\delta\Xi_{xx}^{(2)} = -2\left(\frac{mU}{8\pi v_F}\right)^2 T^3 \int \frac{d\theta_{\mathbf{k}}}{(2\pi)^2}\Bigg\{a_0\left[\mathcal{F}\left(\frac{\bar{\Delta}_{\mathbf{k}_F}}{T}\right) + \mathcal{F}\left(\frac{\bar{\Delta}_{-\mathbf{k}_F}}{T}\right)\right] + a_+\mathcal{F}\left(\frac{|\bar{\Delta}_{\mathbf{k}_F} - \bar{\Delta}_{-\mathbf{k}_F}|}{T}\right) + a_-\mathcal{F}\left(\frac{\bar{\Delta}_{\mathbf{k}_F} + \bar{\Delta}_{-\mathbf{k}_F}}{T}\right)\Bigg\}, \tag{3.3.49}$$

where the function $\mathcal{F}(x)$ and its asymptotic limits are given by Equations (3.3.25-3.3.27).

The angular integral cannot be performed analytically because the function $\mathcal{F}(y)$ depends in a complicated way on the angle $\theta_{\mathbf{k}}$ through $\bar{\Delta}_{\pm\mathbf{k}_F}$. Therefore, we consider two limiting cases below.

Temperature dependence of the in-plane component

First, we consider the limit of a weak magnetic field: $|\Delta| \ll \max\{|\alpha|k_F, T\}$. The main difference between the cases of in- and transverse orientations of the field is in the term proportional to a_+ in Equation (3.3.49). The argument $\mathcal{F}$ in this term vanishes in the limit of $\Delta \to 0$, whereas the arguments of $\mathcal{F}$ in the rest of the terms reduce to a scaling variable $|\alpha|k_F/T$, as it was also the case for the transverse field. Therefore, the SOI energy scale, $|\alpha|k_F$, and temperature are interchangeable in the rest of the terms, which means that a nonanalytic T dependence arising from these terms is cut off by the SOI

(and vice versa). However, the a_+ term does not depend on α and produces a nonanalytic T dependence which is *not* cut off by the SOI. To see this, we expand prefactors a_0 and $a_\pm$ to leading order in Δ as

$$a_0 = 4\frac{\Delta^2}{\alpha^2 k_F^2}\cos^2\theta_{\mathbf{k}} + \mathcal{O}(\Delta^4), \tag{3.3.50}$$

$$a_+ = 2 - 4\frac{\Delta^2}{\alpha^2 k_F^2}\cos^2\theta_{\mathbf{k}} + \mathcal{O}(\Delta^4), \tag{3.3.51}$$

$$a_- = 2\frac{\Delta^4}{\alpha^4 k_F^4}\cos^4\theta_{\mathbf{k}} + \mathcal{O}(\Delta^6). \tag{3.3.52}$$

The last term in Equation (3.3.49), proportional to a_-, does not contribute to order Δ^2, and we focus on the first two terms. In the term a_0, we replace $\bar{\Delta}_{\pm\mathbf{k}_F} = |\alpha|\, k_F$ in the argument of the $\mathcal{F}$ function. In the a_+ term, we replace $|\bar{\Delta}_{\mathbf{k}_F} - \bar{\Delta}_{-\mathbf{k}_F}| = 2|\Delta \sin\theta_{\mathbf{k}}| + \mathcal{O}(\Delta^2)$, and then expand $\mathcal{F}\left(2|\Delta\sin\theta_{\mathbf{k}}|/T\right) = 4\Delta^2\sin^2\theta_{\mathbf{k}}/T^2$ using Equation (3.3.26). Integrating over $\theta_{\mathbf{k}}$ and differentiating the result twice with respect to B, we obtain

$$\begin{aligned}\delta\chi_{xx}^{(2)}(T,\alpha) &= \chi_0\left(\frac{mU}{4\pi}\right)^2\left[\frac{T^3}{\alpha^2 k_F^2}\mathcal{F}\left(\frac{|\alpha|\, k_F}{T}\right) + \frac{T}{E_F}\right] \\ &= \frac{1}{2}\chi_{zz}^{(2)}(T,\alpha) + \frac{1}{2}\chi_0\left(\frac{mU}{4\pi}\right)^2\frac{T}{E_F},\end{aligned} \tag{3.3.53}$$

where $\chi_{zz}^{(2)}(T,\alpha)$ is the correction to χ_{zz} given by Equation (3.3.28). [Notice a remarkable similarity between Equation (3.3.53) and the relation between χ_{xx} and χ_{zz} in the non-interacting case, Equation (B.1.5).] Equation (3.3.53) is one of the main results of this part. It shows that a nonanalytic T dependence of χ_{xx}, given by the stand-alone T/E_F term survives in the presence of the SOI. Explicitly, the T dependence is

$$\delta\chi_{xx}^{(2)} = 2\chi_0\left(\frac{mU}{4\pi}\right)^2\left[\frac{T}{E_F} + \frac{\alpha^2 k_F^2}{48 T E_F}\right] \tag{3.3.54}$$

for $T \gg |\alpha| k_F$ and

$$\delta\chi_{xx}^{(2)} = 2\chi_0\left(\frac{mU}{4\pi}\right)^2\left[\frac{|\alpha| k_F}{6E_F} + \frac{T}{2E_F} + 2\zeta(3)\frac{T^3}{\alpha^2 k_F^2 E_F}\right] \tag{3.3.55}$$

for $T \ll |\alpha| k_F$.

As it is also the case for the transverse magnetic field, the first term in the second line of Equation (3.3.54) is due to particle-hole pairs formed by electrons from three identical and one different Rashba branches. On the other hand, the linear-in-T term, absent in $\delta\chi_{zz}^{(2)}$, is comes from processes involving electrons from the different Rashba branches in each particle-hole bubble, see Figure 3.8b. Indeed, pairing electrons and holes, which

belong to different Rashba branches and move in the same direction, we obtain particle-hole bubbles $\mathcal{P}_{\pm}^{\pm\mathbf{k}_F}$ [cf. Equation (3.3.43)]. The product of two such bubbles, $\mathcal{P}_{+}^{\pm\mathbf{k}_F}\mathcal{P}_{-}^{\mp\mathbf{k}_F}$, being integrated over q and summed over Ω, depends on the difference of the Zeeman energies $|\bar{\Delta}_{\mathbf{k}_F} - \bar{\Delta}_{-\mathbf{k}_F}|$. Since $\sin\theta_{\mathbf{k}}$ is odd upon $\mathbf{k} \to -\mathbf{k}$, this difference is finite and proportional to $|\Delta|$ for $\Delta \to 0$ but does not depend on α. This is a mechanism by which one gets an $\mathcal{O}(\Delta^2)$ contribution to the thermodynamic potential and, therefore, a T dependent contribution to χ_{xx}, which does not involve the SOI.

Magnetic-field dependence of the in-plane component

Now we analyze the non-linear in-plane susceptibility $\chi_{xx}(B_x, \alpha) = -\partial^2\Xi_{xx}/\partial B_x^2$ at $T = 0$. Replacing $\mathcal{F}$ in Equation (3.3.49) by its large-argument asymptotics from Equation (3.3.27), we obtain

$$\delta\Xi_{xx}^{(2)} = -\frac{2}{3}\left(\frac{mU}{8\pi v_F}\right)^2 \int \frac{d\phi_{kx}}{(2\pi)^2}\Big\{a_0\left[\bar{\Delta}_{\mathbf{k}_F}^3 + \bar{\Delta}_{-\mathbf{k}_F}^3\right] + a_+|\bar{\Delta}_{\mathbf{k}_F} - \bar{\Delta}_{-\mathbf{k}_F}|^3 + a_-\left[\bar{\Delta}_{\mathbf{k}_F} + \bar{\Delta}_{-\mathbf{k}_F}\right]^3\Big\}. \tag{3.3.56}$$

The angular integral can now be solved explicitly in the limiting cases of $|\Delta| \ll |\alpha|k_F$ and $|\Delta| \gg |\alpha|k_F$. Since our primary interest is just to see whether a nonanalytic field-dependence survives in the presence of the SOI, we will consider only the weak-field case: $|\Delta| \ll |\alpha|k_F$. The a_- term in Equation (3.3.56) can then be dropped, while the a_0 and a_+ ones yield

$$\delta\chi_{xx}^{(2)}(B_x, \alpha) = \frac{1}{3}\chi_0\left(\frac{mU}{4\pi}\right)^2\left[\frac{|\alpha|\,k_F}{E_F} + \frac{16}{\pi}\frac{|\Delta|}{E_F}\right]. \tag{3.3.57}$$

The first term in Equation (4.1.10) is just half of the first term in $\delta\chi_{zz}^{(2)}$ [cf. Equation (3.3.38)]. However, the second term represents a nonanalytic dependence on the field which is not cut off by the SOI.

3.3.4 Remaining diagrams

Besides the diagrams considered so far, there are other second order diagrams, which – in principle – could contribute to the spin susceptibility. These diagrams are depicted in Figure 3.6*b-e*. In the absence of the SOI, these diagrams are irrelevant because the electron-electron interaction conserves spin. This means that the spins of electrons in each of the bubbles in, e.g, diagram *b*) are the same and, therefore, the Zeeman energies, entering the Green's functions, can be absorbed into the chemical potential. The same argument also goes for the other two diagrams. In the presence of the SOI, this argument does not work because spin is not a good quantum number and the interaction mixes states from all Rashba branches with different Zeeman energies. However, one can show

that the net result is the same as without the SOI: diagrams in Figure 3.6*b*-*e* do not contribute to the nonanalytic behavior of the spin susceptibility. This is what we are going to show in this section.

We begin with diagram *b*), which is a small momentum-transfer counterpart of diagram in *a*):

$$\delta\Xi_b^{(2)} = -U_0^2 T \sum_Q \left[\mathrm{Tr}\Pi(Q)\right]^2, \tag{3.3.58}$$

where

$$\Pi(Q) = \frac{1}{2}\sum_K G(K)G(K+Q) = \frac{1}{2}\sum_{s,t=\pm1} \Omega_s\Omega_t \sum_K g_s(K)\, g_t(K+Q) \tag{3.3.59}$$

is the full (summed over Rashba branches) polarization bubble, and both the space- and time-like components of $Q \equiv (\Omega, \mathbf{q})$ are small. As it is also the case in the absence of the SOI, the small-Q bubble does not depend on the magnetic field. Indeed, noticing that the matrix ζ in Equation (3.2.2a) has the following properties

$$\zeta^2 = I \text{ and } \mathrm{Tr}\zeta = 0, \tag{3.3.60}$$

it is easy to show that

$$\Omega_s\Omega_t = \frac{1}{4}\left[(1+st)I + (s+t)\,\zeta\right]. \tag{3.3.61}$$

Consequently, $\Omega_+\Omega_+ = \Omega_-\Omega_- = I/2$ and $\Omega_+\Omega_- = \Omega_-\Omega_+ = 0$. Therefore, electrons from different branches do not contribute to $\Pi(Q)$, while the Zeeman energies in the contributions from the same branch can be absorbed into the chemical potential. As a result, the dynamic part of the bubble depends neither on the field nor on the SOI (as long as a weak dependence of the Fermi velocity for a given branch on α is neglected):

$$\Pi(Q) = I\frac{m}{2\pi}\frac{|\Omega|}{\sqrt{\Omega^2 + v_F^2 q^2}}. \tag{3.3.62}$$

Therefore diagram *b*) does not contribute to the spin susceptibility. We remind the reader that, since there are no threshold-like singularities in the static polarization bubble (see discussion in Section 4.2), the Landau-damping singularity in Equation (3.3.62) is the only singularity which may have contributed to a nonanalytic behavior of the spin susceptibility. However, as we have just demonstrated, Landau damping is not effective in diagrams with small momentum transfers.

Similarly, diagram *c*) with two crossed interaction lines, one of which carries a small momentum and the other one carries a momentum near $2k_F$, is expressed via a small Q bubble as

$$\delta\Xi_c^{(2)} = -U_0 U_{2k_F} \sum_Q \mathrm{Tr}\left[\Pi^2(Q)\right] \tag{3.3.63}$$

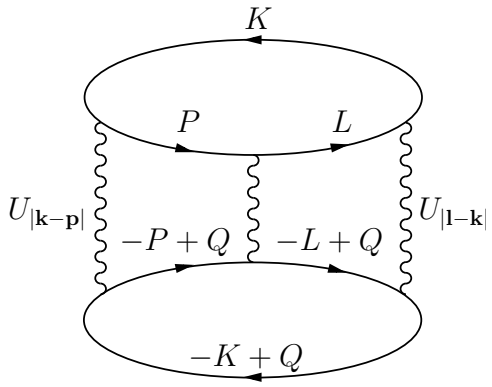

Figure 3.9: The third-order Cooper-channel diagram for the thermodynamic potential.

and, therefore, does not depend on the magnetic field. Diagram d), with both interaction lines carrying small momenta, contains a trace of four Green's functions

$$\begin{aligned}\delta\Xi_d^{(2)} =& -\frac{U_0^2}{4}\sum_{Q,Q',K}\mathrm{Tr}\left[G\left(K\right)G(K+Q)G(K+Q+Q')G(K+Q')\right]\\ =& -\frac{U_0^2}{4}\sum_{Q,Q',K}\sum_{p,r,s,t=\pm}\mathrm{Tr}\left[\Omega_p\Omega_r\Omega_s\Omega_t\right]\\ &\times g_p\left(K\right)g_r\left(K+Q\right)g_s\left(K+Q+Q'\right)g_t\left(K+Q'\right),\end{aligned} \tag{3.3.64}$$

where Q and Q' are small, so that dependence of Ω_l on either of the bosonic momenta can be neglected. Using again the properties of the projection operator from Equation (3.3.60), we find that

$$\begin{aligned}\mathrm{Tr}\left[\Omega_p\Omega_r\Omega_s\Omega_t\right] =& \frac{1}{16}\mathrm{Tr}\big\{\left[(1+pr)\left(1+st\right)+(p+r)(s+t)\right]I\\ &+\left[(1+pr)\left(s+t\right)+\left(1+st\right)\left(p+r\right)\right]\zeta\big\}\\ =& \frac{1}{8}\left[(1+pr)\left(1+st\right)+(p+r)(s+t)\right].\end{aligned} \tag{3.3.65}$$

This expression vanishes if at least one of the indices from the set $\{p,r,s,t\}$ is different from the others. Therefore, only electrons from the same branch contribute to $\delta\Xi_d^{(2)}$, the Zeeman energy can again be absorbed into the chemical potential, and $\delta\Xi_d^{(2)}$ does not depend on the magnetic field.

Finally, the last diagram, $\delta\Xi_e^{(2)}$ corresponds to the first-order self-energy inserted twice into the zeroth order thermodynamic potential. Such an insertion only shifts the chemical potential and, for a q dependent U, gives a regular correction to the electron effective mass but does not produce any nonanalytic behavior.

3.4 Cooper-channel renormalization

3.4.1 General remarks

The second-order nonanalytic contribution to the spin susceptibility comes from "backscattering" processes in which two fermions moving in almost opposite directions experience almost complete backscattering. Because the total momentum of two fermions is small, the backscattering process is a special case of the interaction in the Cooper (particle-particle) channel. Higher order processes in this channel lead to logarithmic renormalization of the second-order result [Chubukov05a, Chubukov06, Maslov06, Maslov09, Chubukov07, Aleiner06, Shekhter06b, Shekhter06a, Schwiete06, Simon08, Simon07, Chesi09]. For a weak interaction, considered throughout this Chapter, this is the leading higher-order effect. In the absence of the SOI, resummation of all orders in the Cooper channel leads to the following scaling form of the spin susceptibility

$$\delta\chi \propto \frac{E}{\ln^2(E/\Lambda)}, \tag{3.4.1}$$

where Λ is the ultraviolet cutoff and $E \equiv \max\{T, |\Delta|\}$ is small enough so that $mU|\ln(E/\Lambda)| \gg 1$. As we see, both the linear-in-E term, which occurs already at second order, and its logarithmic renormalization contain the same energy scale. The reason for this symmetry is very simple: an arbitrary order Cooper diagram for the thermodynamic potential contains two bubbles joined by a ladder. The spin susceptibility is determined only by diagrams with opposite fermion spins in each of the bubbles. Therefore, all Cooper bubbles in such diagrams are formed by fermions with opposite spins, so that the logarithmic singularity of the bubble is cut off at the largest of the two energy scales, i.e, temperature or Zeeman energy. At zero incoming momentum and frequency, the Cooper bubble is

$$\Pi_C^{\uparrow\downarrow} = \frac{m}{2\pi}\ln\frac{\Lambda}{\max\{T,\Delta\}}, \tag{3.4.2}$$

hence the symmetry of the result with respect to interchanging T and Δ follows immediately. It will be shown in this section that this symmetry does not hold in the presence of the SOI. The reason is that the Rashba branches are not the states with definite spins, and diagrams with Cooper bubbles formed by electrons from the same branches also contribute to the spin susceptibility. Although a Cooper bubble formed by electrons from branches s and s'

$$\Pi_C^{s,s'} = T\sum_\omega \frac{m}{2\pi}\int\frac{d\theta_{\mathbf{p}}}{2\pi}\int d\epsilon_p g_s(\omega,\mathbf{p})g_{s'}(-\omega,-\mathbf{p}) = \frac{m}{2\pi}\ln\frac{\Lambda}{\max\left\{T,|s-s'|\,\bar{\Delta}_{\mathbf{k}_F}\right\}} \tag{3.4.3}$$

looks similar to that in the absence of the SOI, Equation (3.4.2), its diagonal element Π_C^{ss} depends only on T even if $T \ll \bar{\Delta}_{\mathbf{k}_F}$. Therefore, for $\Delta = 0$, the Cooper logarithm in

Equation (3.4.1) will depend only on T in the limit of $T \to 0$ while the energy E in the numerator may be given either by T or by $|\alpha|k_F$. [1]

3.4.2 Third-order Cooper channel contribution to the transverse part

Is this section, we obtain the third-order Cooper channel contribution to χ_{zz}. This calculation will help to understand the general strategy employed later, in Secs. 3.4.3 and 3.4.3, in resumming Cooper diagrams to all orders.

The third-order Cooper diagram for the thermodynamic potential, depicted in Figure 3.9, is given by

$$\delta\Xi^{(3)}_{zz} = \frac{U^3}{6}\sum_{K,P,L,Q}\mathrm{Tr}(G_K G_P G_L)\mathrm{Tr}(G_{-K+Q}G_{-P+Q}G_{-L+Q}). \tag{3.4.4}$$

First, we evaluate the traces $\mathrm{Tr}(G_K G_P G_L) = \sum_{rst}\mathcal{B}_{rst}g_r(K)g_s(P)g_t(L)$ with the coefficients

$$\begin{aligned}\mathcal{B}_{rst} \equiv&\mathrm{Tr}[\Omega_r(\mathbf{k})\Omega_s(\mathbf{p})\Omega_t(\mathbf{l})] = \frac{1}{4\bar{\Delta}_{\mathbf{k}}\bar{\Delta}_{\mathbf{p}}\bar{\Delta}_{\mathbf{l}}}[\bar{\Delta}_{\mathbf{k}}\bar{\Delta}_{\mathbf{p}}\bar{\Delta}_{\mathbf{l}} + irst\alpha^2\Delta(\mathbf{k}\times\mathbf{p}+\mathbf{p}\times\mathbf{l}+\mathbf{l}\times\mathbf{k})_z\\ &+ rs(\alpha^2\mathbf{k}\cdot\mathbf{p}+\Delta^2)\bar{\Delta}_{\mathbf{l}} + rt(\alpha^2\mathbf{k}\cdot\mathbf{l}+\Delta^2)\bar{\Delta}_{\mathbf{p}} + st(\alpha^2\mathbf{l}\cdot\mathbf{p}+\Delta^2)\bar{\Delta}_{\mathbf{k}}].\end{aligned} \tag{3.4.5}$$

Since $\mathbf{q}$ is small and $\mathcal{B}_{rst}$ is an even function of the fermionic momenta,

$$\mathrm{Tr}\left[\Omega_{r'}(-\mathbf{k}+\mathbf{q})\Omega_{s'}(-\mathbf{p}+\mathbf{q})\Omega_{t'}(-\mathbf{l}+\mathbf{q})\right] \approx \mathrm{Tr}\left[\Omega_{r'}(-\mathbf{k})\Omega_{s'}(-\mathbf{p})\Omega_{t'}(-\mathbf{l})\right] = \mathcal{B}_{r's't'}, \tag{3.4.6}$$

[1] In fact, the particle-hole propagator in Equation (3.4.3) has to be evaluated at finite Ω and q, since only such a diagram is an actual building block of the free energy. In that case one obtains

$$\Pi_C^{s,s'} = T\sum_{\omega}\frac{m}{2\pi}\int\frac{d\theta_{\mathbf{p}}}{2\pi}\int d\epsilon_p g_s(\omega,\mathbf{p})g_{s'}(-\omega+\Omega,-\mathbf{p}+\mathbf{q}) = \frac{m}{2\pi}\ln\frac{\Lambda}{\max\left\{T, |s-s'|\,\bar{\Delta}_{\mathbf{k}_F}, \sqrt{v_F^2q^2+\Omega^2}\right\}}$$

and even if the SOI drops out for $s = s'$, the logarithm still depends on T and $\sqrt{v_F^2q^2+\Omega^2} \sim |\alpha|k_F$. Since $T \ll |\alpha|k_F$, we conclude that $\Pi_C^{s,s}$ depends on the logarithm of Ω, v_Fq rather than the temperature. It can be shown that $\Pi_C^{s,s} \propto \ln\sqrt{v_F^2q^2+\Omega^2}$ does not lead to the logarithmic renormalization of the second order $|\alpha|k_F$ result and, thus, $\Pi_C^{s,s}$ can be neglected compared to $\Pi_C^{s,-s} \propto \ln(\Lambda/|\alpha|k_F)$. Therefore the renormalization of the second order free energy (and so, the spin susceptibility) is due to the SOI and not temperature.

For this reason the results of Section 3.4 and Appendix B.3 that rely on the assumption $\Omega = v_Fq = 0$ are erroneous. In order to correct them one could rederive the RG equations with a proper selection of the Rashba indices, for example

$$-\frac{d}{dL}U_{s_1s_2;s_3s_4}(L) = \sum_s U_{s_1s_2;s-s}(L)U_{s-s;s_3s_4}(L)$$

instead of Equation (3.4.24a). This approach, however, leads to a result that still disagrees with the linear response calculation beyond second order [Żak]. The reason for the discrepancy remains an open question and is beyond the scope of this work.

and the thermodynamic potential becomes

$$\delta\Xi_{zz}^{(3)} = \frac{U^3}{6}\sum_{K,P,L,Q}\sum_{rst}\sum_{r's't'}\mathcal{B}_{rst}\mathcal{B}_{r's't'}g_r(K)g_{r'}(-K+Q)g_s(P)g_{s'}(-P+Q)g_t(l)g_{t'}(-L+Q). \tag{3.4.7}$$

Each pair of the Green's functions with opposite momenta forms a Cooper bubble, which depends logarithmically on the largest of the two energy scales–temperature or the effective Zeeman energy, see Equation (3.4.3). The third-order contribution contains one such logarithmic factor which can be extracted from any of the three Cooper bubbles; this gives an overall factor of three:

$$\delta\Xi_{zz}^{(3)} = \frac{U^3}{2}\sum_{K,P,Q}\sum_{rst}\sum_{r's't'}\int\frac{d\theta_{\mathbf{kl}}}{2\pi}\mathcal{B}_{rst}\mathcal{B}_{r's't'}\Pi_C^{t,t'}g_r(K)g_{r'}(-K+Q)g_s(P)g_{s'}(-P+Q), \tag{3.4.8}$$

where $\theta_{\mathbf{kl}} \equiv \angle(\mathbf{k},\mathbf{l})$. With this procedure, the third-order diagram reduces effectively to the second-order one, but with a new set of coefficients. Since we already know that the nonanalytic part of the second-order diagram comes from processes with $\mathbf{k} \approx -\mathbf{p}$, the coefficient $\mathcal{B}_{rst}$ (and its primed counterpart) simplify significantly because $\mathbf{k}\times\mathbf{p} = \mathbf{0}$ and $\mathbf{p}\times\mathbf{l} = \mathbf{l}\times\mathbf{k}$. Integrating over $\theta_{\mathbf{kl}}$, we obtain

$$\begin{aligned}\mathcal{A}_{rstr's't'} \equiv \int\frac{d\theta_{\mathbf{kl}}}{2\pi}\mathcal{B}_{rst}\mathcal{B}_{r's't'} = \frac{1}{16\bar{\Delta}_{\mathbf{k}_F}^6}\Big\{ &-2rstr's't'\alpha^4k_F^4\Delta^2 + \frac{1}{2}(rtr't' + sts't' \\ &- rts't' - r't'st)\alpha^4k_F^4\bar{\Delta}_{\mathbf{k}_F}^2 + \bar{\Delta}_{\mathbf{k}_F}^2[\bar{\Delta}_{\mathbf{k}_F}^2 + (rs+rt+st)\Delta^2 - rs\alpha^2k_F^2] \\ &\times[\bar{\Delta}_{\mathbf{k}_F}^2 + (r's'+r't'+s't')\Delta^2 - r's'\alpha^2k_F^2]\Big\},\end{aligned} \tag{3.4.9}$$

and

$$\delta\Xi_{zz}^{(3)} = \frac{U^3}{2}\sum_{rst}\sum_{r's't'}\mathcal{A}_{rstr's't'}\Pi_C^{t,t'}\sum_{K,P,Q}g_r(K)g_{r'}(-K+Q)g_s(P)g_{s'}(-P+Q). \tag{3.4.10}$$

The convolution of two Cooper bubbles in Equation (3.4.10) can be re-written via a convolution of two particle-hole bubbles by relabeling $Q \to Q+K+P$:

$$\begin{aligned}&\sum_{K,P,Q}g_r(K)g_{r'}(-K+Q)g_s(P)g_{s'}(-P+Q) \\ &\quad= \sum_Q\sum_K g_r(K)g_{s'}(K+Q)\sum_P g_s(P)g_{r'}(P+Q)\sum_Q\Pi_{rs'}(Q)\Pi_{sr'}(Q),\end{aligned} \tag{3.4.11}$$

where $\Pi_{s,s'}(Q)$ is a particle-hole bubble defined in Equation (3.3.6). Summing over the Rashba indices, integrating over the momentum, and assuming that the Zeeman energy

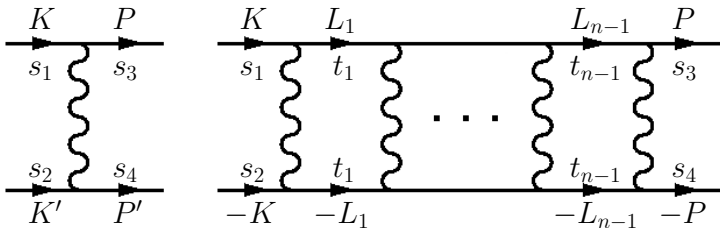

Figure 3.10: Left: the effective scattering amplitude $\Gamma^{(1)}_{s_1 s_2; s_3 s_4}(\mathbf{k}, \mathbf{k}'; \mathbf{p}, \mathbf{p}')$ in the chiral basis. Right: a generic n-th order ladder diagram in the Cooper channel, $\Gamma^{(n)}_{s_1 s_2; s_3 s_4}(\mathbf{k}, -\mathbf{k}; \mathbf{p}, -\mathbf{p})$.

is the smallest energy in the problem, i.e., that $\Delta \ll \max\{T, |\alpha|\, k_F\}$, we find

$$\delta\Xi^{(3)}_{zz} = -\frac{1}{2\pi v_F^2}\left(\frac{mU}{4\pi}\right)^3 \frac{\Delta^2 T^3}{\alpha^2 k_F^2}\Bigg\{ \left[12\mathcal{F}\left(\frac{|\alpha| k_F}{T}\right) - \mathcal{F}\left(\frac{2|\alpha| k_F}{T}\right)\right] \ln\frac{T}{\Lambda} + \left[4\mathcal{F}\left(\frac{|\alpha| k_F}{T}\right) + \mathcal{F}\left(\frac{2|\alpha| k_F}{T}\right)\right] \ln\frac{\max\{T, |\alpha| k_F\}}{\Lambda}\Bigg\} \tag{3.4.12}$$

with $\mathcal{F}(y)$ given by Equation (3.3.25).

The asymptotic behavior of χ_{zz} for $T \gg |\alpha| k_F$ is computed from Equation (3.4.12)

$$\delta\chi^{(3)}_{zz} = 8\chi_0 \left(\frac{mU}{4\pi}\right)^3 \frac{T}{E_F} \ln\frac{T}{\Lambda} \tag{3.4.13}$$

and, as to be expected, $\delta\chi^{(3)}_{zz}$ scales as $T \ln T$.

In the opposite limit of $T \ll |\alpha| k_F$,

$$\delta\chi^{(3)}_{zz} = \frac{2}{3}\chi_0 \left(\frac{mU}{4\pi}\right)^3 \frac{|\alpha| k_F}{E_F}\left(\ln\frac{T}{\Lambda} + 3\ln\frac{|\alpha| k_F}{\Lambda}\right) \approx \frac{2}{3}\chi_0 \left(\frac{mU}{4\pi}\right)^3 \frac{|\alpha| k_F}{E_F} \ln\frac{T}{\Lambda}, \tag{3.4.14}$$

since $|\ln(T/\Lambda)| \gg |\ln(|\alpha| k_F/\Lambda)|$. As it was advertised in Section 3.4.1, the $T \ln T$ scaling at high temperatures is replaced by the $|\alpha| \ln T$ scaling at low temperatures which implies that the energy scales $|\alpha| k_F$ and T are not interchangeable.

3.4.3 Resummation of all Cooper channel diagrams

Scattering amplitude in the chiral basis

It is more convenient to resum the Cooper ladder diagrams in the chiral basis, in which the Green's functions are diagonal. Introducing Rashba spinors $|\mathbf{k}, s\rangle$, we re-write the number-density operator as

$$\rho_{\mathbf{q}} = \sum_{\mathbf{k}} \sum_{s_1, s_2} \langle \mathbf{k} + \mathbf{q}, s_2 | \mathbf{k}, s_1 \rangle c^\dagger_{\mathbf{k}+\mathbf{q}, s_2} c_{\mathbf{k}, s_1}, \tag{3.4.15}$$

so that the Hamiltonian of the four-fermion interaction becomes

$$H_{\text{int}} = \frac{1}{2}\sum_{\mathbf{q}} U_{|\mathbf{q}|}\rho_{\mathbf{q}}\rho_{-\mathbf{q}} = \frac{1}{2}\sum_{\mathbf{p},\mathbf{p}',\mathbf{k},\mathbf{k}'}\sum_{\{s_i\}} \Gamma^{(1)}_{s_1s_2;s_3s_4}(\mathbf{k},\mathbf{k}';\mathbf{p},\mathbf{p}')c^\dagger_{\mathbf{p}',s_4}c^\dagger_{\mathbf{p},s_3}c_{\mathbf{k},s_1}c_{\mathbf{k}',s_2}, \quad (3.4.16)$$

where the effective scattering amplitude is defined by (cf. Figure 3.10)

$$\Gamma^{(1)}_{s_1s_2;s_3s_4}(\mathbf{k},\mathbf{k}';\mathbf{p},\mathbf{p}') = U_{|\mathbf{k}-\mathbf{p}|}\langle \mathbf{p},s_3|\mathbf{k},s_1\rangle\langle \mathbf{p}',s_4|\mathbf{k}',s_2\rangle. \quad (3.4.17)$$

In the absence of the magnetic field,

$$|\mathbf{k},s\rangle = \frac{1}{\sqrt{2}}\begin{pmatrix} -ise^{-i\theta_{\mathbf{k}}} \\ 1 \end{pmatrix}, \quad (3.4.18)$$

where $\theta_{\mathbf{k}} \equiv \angle(\mathbf{k},x)$, and Equation (3.4.17) gives [Gor'kov01]

$$\Gamma^{(1)}_{s_1s_2;s_3s_4}(\mathbf{k},\mathbf{k}';\mathbf{p},\mathbf{p}') = \frac{1}{4}U_{|\mathbf{k}-\mathbf{p}|}\left[1+s_1s_3e^{i(\theta_{\mathbf{p}}-\theta_{\mathbf{k}})}\right]\left[1+s_2s_4e^{i(\theta_{\mathbf{p}'}-\theta_{\mathbf{k}'})}\right]. \quad (3.4.19)$$

In order to resum the ladder diagrams for the thermodynamic potential to infinite order, we consider a skeleton diagram depicted in Figure 3.11, which is obtained from the second-order diagram –shown in Figure 3.6a– by replacing the bare interaction $U(\mathbf{q})$ with the dressed scattering amplitudes: $\Gamma_{s_1s_2;s_3s_4}(\mathbf{k},-\mathbf{k}+\mathbf{q};\mathbf{p},-\mathbf{p}+\mathbf{q})$ and its time reversed counterpart. The dressed amplitudes contain infinite sums of the Cooper ladder diagrams shown in Figure 3.10. We will be interested in the limit of vanishingly small magnetic fields and temperatures smaller than the SOI energy scale: $\Delta \ll T \ll |\alpha|k_F$. In this limit, the largest contribution to the ladder diagrams comes from the internal Cooper bubbles formed by electrons from the same Rashba subbands. Each "rung" of this ladder contributes a large Cooper logarithm $L \equiv (m/2\pi)\ln(\Lambda/T)$, which depends only on the temperature, and one has to select the diagrams with a maximum number of L factors.

Renormalization Group for scattering amplitudes

Resummation of Cooper diagrams is performed most conveniently via the Renormalization Group (RG) procedure [Chesi09]. In the Cooper channel, the bare amplitude is given by Equation (3.4.19) with $\mathbf{p}' = -\mathbf{p}$ and $\mathbf{k}' = -\mathbf{k}$ or, equivalently, $\theta_{\mathbf{k}'} = \theta_{\mathbf{k}} + \pi$ and $\theta_{\mathbf{p}'} = \theta_{\mathbf{p}} + \pi$:

$$\Gamma^{(1)}_{s_1s_2;s_3s_4}(\mathbf{k},-\mathbf{k};\mathbf{p},-\mathbf{p}) = U^{(1)}_{s_1s_2;s_3s_4}V^{(1)}_{s_1s_2;s_3s_4}e^{i(\theta_{\mathbf{p}}-\theta_{\mathbf{k}})} + W^{(1)}_{s_1s_2;s_3s_4}e^{2i(\theta_{\mathbf{p}}-\theta_{\mathbf{k}})}, \quad (3.4.20)$$

where the three terms correspond to orbital momenta $\ell = 0,1,2$, respectively. The bare values of partial amplitudes are given by

$$U^{(1)}_{s_1s_2;s_3s_4} = U/4, \quad (3.4.21a)$$
$$V^{(1)}_{s_1s_2;s_3s_4} = (U/4)(s_1s_3 + s_2s_4), \quad (3.4.21b)$$
$$W^{(1)}_{s_1s_2;s_3s_4} = (U/4)s_1s_2s_3s_4. \quad (3.4.21c)$$

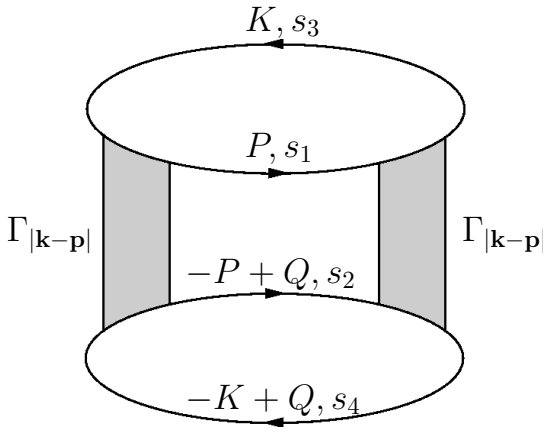

Figure 3.11: A skeleton diagram for the thermodynamic potential Ξ.

Consider now a ladder diagram consisting of n interaction lines and $2(n-1)$ internal fermionic lines, as shown in Figure 3.10. As we have already pointed out, in the limit $T \ll |\alpha| k_F$, the dominant logarithmic-in-T contribution originates from those Cooper bubbles which are formed by electrons from the same Rashba branch. Therefore, the n-th order Cooper ladder can be written iteratively as

$$\Gamma^{(n)}_{s_1 s_2; s_4 s_3}(\mathbf{k}, -\mathbf{k}; \mathbf{p}, -\mathbf{p}) = -L \int_{\theta_\mathbf{l}} \sum_s \Gamma^{(n-1)}_{s_1 s_2; s s}(\mathbf{k}, -\mathbf{k}; \mathbf{l}, -\mathbf{l}) \Gamma^{(1)}_{s s; s_3 s_4}(\mathbf{l}, -\mathbf{l}; \mathbf{p}, -\mathbf{p}) \quad (3.4.22)$$

where $n \geq 2$. Since only "charge-neutral" terms of the type $e^{i(\theta_\mathbf{p} - \theta_\mathbf{l})} e^{i(\theta_\mathbf{l} - \theta_\mathbf{k})}$ survive upon averaging over $\theta_\mathbf{l}$, different partial harmonics are renormalized independently of each other, i.e., we have the following group property:

$$\Gamma^{(n)}_{s_1 s_2; s_3 s_4}(\mathbf{k}, -\mathbf{k}; \mathbf{p}, -\mathbf{p}) = (-L)^{n-1} [U^{(n)}_{s_1 s_2; s_3 s_4} + V^{(n)}_{s_1 s_2; s_3 s_4} e^{i(\theta_\mathbf{p} - \theta_\mathbf{k})} + W^{(n)}_{s_1 s_2; s_3 s_4} e^{2i(\theta_\mathbf{p} - \theta_\mathbf{k})}]. \quad (3.4.23)$$

Differentiating Equation (3.4.22) for $n = 2$ with respect to L we obtain three decoupled one-loop RG flow equations

$$-\frac{d}{dL} U_{s_1 s_2; s_3 s_4}(L) = \sum_s U_{s_1 s_2; s s}(L) U_{s s; s_3 s_4}(L), \quad (3.4.24a)$$

$$-\frac{d}{dL} V_{s_1 s_2; s_3 s_4}(L) = \sum_s V_{s_1 s_2; s s}(L) V_{s s; s_3 s_4}(L), \quad (3.4.24b)$$

$$-\frac{d}{dL} W_{s_1 s_2; s_3 s_4}(L) = \sum_s W_{s_1 s_2; s s}(L) W_{s s; s_3 s_4}(L) \quad (3.4.24c)$$

with initial conditions specified by $U_{s_1 s_2; s_3 s_4}(0) = U^{(1)}_{s_1 s_2; s_3 s_4}$, $V_{s_1 s_2; s_3 s_4}(0) = V^{(1)}_{s_1 s_2; s_3 s_4}$, and $V_{s_1 s_2; s_3 s_4}(0) = V^{(1)}_{s_1 s_2; s_3 s_4}$.

Solving this system of RG equations and substituting the results into the backscattering amplitude,

$$\Gamma_{s_1s_2;s_3s_4}(\mathbf{k},-\mathbf{k};-\mathbf{k},\mathbf{k}) = U_{s_1s_2;s_3s_4}(L) - V_{s_1s_2;s_3s_4}(L) + W_{s_1s_2;s_3s_4}(L) \tag{3.4.25}$$

which is a special case of the Cooper amplitude for $\mathbf{p} = -\mathbf{k}$, we obtain

$$\Gamma_{ss;\pm s\pm s}(\mathbf{k},-\mathbf{k};-\mathbf{k},\mathbf{k}) = \frac{U}{2+UL} \mp \frac{U}{2(1+UL)}, \tag{3.4.26}$$

$$\Gamma_{s-s;\mp s\pm s}(\mathbf{k},-\mathbf{k};-\mathbf{k},\mathbf{k}) = \frac{U}{2+UL} \pm \frac{U}{2}, \tag{3.4.27}$$

$$\Gamma_{\sigma(\pm\mp;\mp\mp)}(\mathbf{k},-\mathbf{k};-\mathbf{k},\mathbf{k}) = 0, \tag{3.4.28}$$

where $\sigma(s_1s_2;s_3s_4) \equiv \{(s_1s_2;s_3s_4),\ (s_2,s_3;s_4s_1),\ (s_3,s_4;s_1s_2),\ (s_4,s_1;s_2,s_3)\}$ stands for all cyclic permutations of indices.

We see that the RG flow described by Equations (3.4.24a-3.4.24c) has a non-trivial solution: whereas the amplitudes in Equations (3.4.26) and (3.4.28) flow to zero in the limit of $L \to \infty$, the amplitudes in Equation (3.4.27) approach RG-invariant values of $\pm U/2$. This behavior is in a striking contrast to what one finds in the absence of the SOI, when the repulsive interaction is renormalized to zero in the Cooper channel. Notice that we consider only the energy scales below the SOI energy, while the conventional behavior is recovered at energies above the SOI scale.

The scattering amplitudes can be also derived by iterating Equation (3.4.22) directly. Examining a few first orders, one recognizes the pattern for the n-th order partial amplitudes to be

$$\Gamma^{(n)}_{ss;\pm s\pm s}(\mathbf{k},-\mathbf{k};-\mathbf{k},\mathbf{k}) = U^n(-L)^{n-1}\frac{1\mp 2^{n-1}}{2^n}, \tag{3.4.29}$$

$$\Gamma^{(n)}_{s-s;\mp s\mp s}(\mathbf{k},-\mathbf{k};-\mathbf{k},\mathbf{k}) = U^n(-L)^n\left(\frac{1}{2^n} \pm \frac{1}{2}\delta_{n,1}\right), \tag{3.4.30}$$

$$\Gamma^{(n)}_{\sigma(\pm\mp;\mp\mp)}(\mathbf{k},-\mathbf{k};-\mathbf{k},\mathbf{k}) = 0. \tag{3.4.31}$$

Summing these amplitudes over n, one reproduces the RG result.

Renormalization of the transverse component

The infinite-order result for the thermodynamic potential is obtained by replacing the bare contact interaction U by its "dressed" counterpart Γ in the second-order skeleton diagram Figure 3.11

$$\delta\Xi_{zz} = -\frac{1}{4}\sum_{Q}\sum_{\{s_i\}}\Gamma_{s_1s_4;s_3s_2}(\mathbf{k},-\mathbf{k};-\mathbf{k},\mathbf{k})\Gamma_{s_3s_2;s_1s_4}(-\mathbf{k},\mathbf{k};\mathbf{k},-\mathbf{k})\Pi_{s_1s_2}\Pi_{s_3s_4} \tag{3.4.32}$$

with $\Gamma_{s_3s_4;s_1s_2}(-\mathbf{k},\mathbf{k};\mathbf{k},-\mathbf{k}) = \Gamma_{s_1s_2;s_3s_4}(\mathbf{k},-\mathbf{k};-\mathbf{k},\mathbf{k})$.

Now, we derive the asymptotic form of $\delta\chi_{zz}$ valid in the limit of strong Cooper renormalization, i.e., for $UL \gg 1$. In this limit, the only non-vanishing scattering amplitude is given by Equation (3.4.27). Replacing the full Γ by its RG-invariant asymptotic limit $\Gamma_{s-s;\mp s\pm s}(\mathbf{k},-\mathbf{k};-\mathbf{k},\mathbf{k}) = \pm U/2$, we obtain

$$\delta\Xi_{zz} = -\frac{U^2}{16} T \sum_{\Omega} \int \frac{qdq}{2\pi} \left[(\Pi_{+-}^2 + \Pi_{-+}^2 - 2\Pi_0^2) + 4\Pi_0^2 \right] \tag{3.4.33}$$

In contrast to the perturbation theory, where the magnetic-field dependence of the thermodynamic potential was provided by the vertices while the polarization bubbles supplied the dependence on the temperature and on the SOI, the vertices in the non-perturbative result (3.4.33) depend neither on the field nor on the SOI. Therefore, the dependences of Ξ on all three parameters (B, T, and α) must come from the polarization bubbles. The integral over q along with the sum over the Matsubara frequency Ω have already been performed in Section 4.2. Note that the last term in square brackets (proportional to Π_0^2) does not depend on the magnetic field and thus can be dropped. The final result reads

$$\delta\Xi_{zz} = -\frac{T^3}{8\pi v_F^2} \left(\frac{mU}{2\pi}\right)^2 \mathcal{F}\left(\frac{2\bar{\Delta}_{\mathbf{k}_F}}{T}\right) \tag{3.4.34}$$

so that

$$\delta\chi_{zz} = \frac{\chi_0}{2} \left(\frac{mU}{4\pi}\right)^2 \frac{|\alpha| k_F}{E_F}, \tag{3.4.35}$$

where use was made of the expansion

$$\frac{\partial^2}{\partial\Delta^2} \mathcal{F}\left(\frac{2\bar{\Delta}_{\mathbf{k}_F}}{T}\right) \approx \frac{2}{|\alpha| k_F T} \mathcal{F}'\left(\frac{2|\alpha| k_F}{T}\right) \tag{3.4.36}$$

and made use of the asymptotic form (3.3.27) of the function $\mathcal{F}$ to find that $\mathcal{F}'(x) \approx x^2$ for $x \gg 1$. Comparing the non-perturbative and second-order results for χ_{zz}, given by Equations (3.4.35) and (3.3.30), respectively, we see that the only effect of Cooper renormalization is a change in the numerical coefficient of the nonanalytic part of χ_{zz}. This is a consequence of a non-trivial fixed point in the Cooper channel which corresponds to finite rather than vanishing Coulomb repulsion.

The temperature dependence of χ_{zz} can be also found for an arbitrary value of the Cooper renormalization parameter UL. Deferring the details to Appendix B.3.1, we present here only the final result

$$\begin{aligned} \delta\chi_{zz} \;=\; & \chi_0 \frac{2|\alpha| k_F}{E_F} \left(\frac{mU}{4\pi}\right)^2 \left[\left(\frac{1}{2+UL} - \frac{1}{2}\right)^2 + \frac{1}{3}\left(\frac{1}{2(1+UL)} + \frac{1}{2+UL}\right)^2 \right. \\ & \left. + \frac{4}{3}\left(\frac{1}{2(1+UL)} - \frac{2}{(2+UL)^2} + \frac{2}{2+UL}\right)\left(\frac{1}{2+UL} - \frac{1}{2}\right) \right]. \end{aligned} \tag{3.4.37}$$

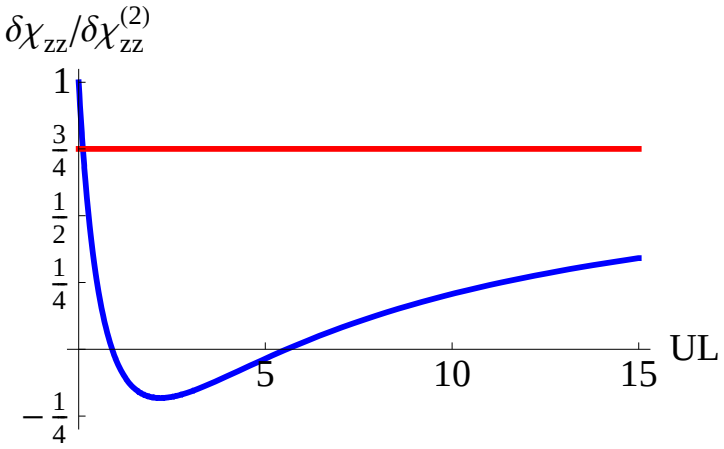

Figure 3.12: Nonanalytic part of χ_{zz}, normalized by the second-order result (3.3.30), as a function of the Cooper-channel renormalization parameter $UL = (mU/2\pi)\ln(\Lambda/T)$. The horizontal line marks the low-temperature limit.

In the limit of strong renormalization in the Cooper channel, i.e., for $UL \gg 1$, only the first term survives the logarithmic suppression, and Equation (3.4.37) reduces to Equation (3.4.35). In the absence of Cooper renormalization, i.e., for $L = 0$, Equation (3.4.37) reduces to the second-order result (3.3.30). In between these two limits, $\delta\chi_{zz}$ is a non-monotonic function of UL: as shown in Figure 3.12, $\delta\chi_{zz}$ exhibits a (shallow) minimum at $UL \approx 2.1$. In a wide interval of UL ($0.9 \leq UL \leq 5.6$), the sign of $\delta\chi_{zz}$ is opposite (negative) to that in either of the high- and low-temperature limits. It is also seen from this plot that the low-T asymptotic value (marked by a straight line) is reached only at very large ($\gtrsim 100$) values of UL.

Renormalization of the in-plane component

The second-order result for the in-plane magnetic field is renormalized in a similar way with two exceptions. First, because the Zeeman energy is anisotropic in this case – the effective magnetic field $\bar{\Delta}_{\pm\mathbf{k}_F}(\theta_{\mathbf{l}}) \equiv \sqrt{\alpha^2 k_F^2 \pm 2\alpha k_F \Delta \sin\theta_{\mathbf{l}} + \Delta^2}$ depends on the direction of the electron momentum $\mathbf{l}$ with respect to the field $\theta_{\mathbf{l}} \equiv \angle(\mathbf{l}, \mathbf{B})$– integration in the "rungs" of the Cooper ladder can be performed only over the fermionic frequency and the magnitude of the electron momenta (or, equivalently, the variable $\epsilon_{\mathbf{l}}$). Consequently, the elementary building block of the ladder

$$L(\theta_{\mathbf{l}}) = T\sum_{\omega}\frac{m}{2\pi}\int d\epsilon_{\mathbf{l}} g_t(\omega,\mathbf{l})g_{t'}(-\omega,-\mathbf{l}) = \frac{m}{2\pi}\ln\frac{\Lambda}{\max\left\{T, \left|t\bar{\Delta}_{\mathbf{k}_F}(\theta_{\mathbf{l}}) - t'\bar{\Delta}_{-\mathbf{k}_F}(\theta_{\mathbf{l}})\right|\right\}} \tag{3.4.38}$$

depends on $\theta_{\mathbf{l}}$.

In principle, the dependence of L on the angle $\theta_{\mathbf{l}}$ should be taken into account when averaging over $\theta_{\mathbf{l}}$. However, in the limit of $\Delta \ll T \ll |\alpha| k_F$, the angle-dependent term under the logarithm can be approximated as $\left|t\bar{\Delta}_{k_F}(\theta_{\mathbf{l}}) - t'\bar{\Delta}_{-k_F}(\theta_{\mathbf{l}})\right| \approx |t - t'|\,|\alpha| k_F$ and, as it was also the case for χ_{zz}, $L = (m/2\pi)\ln(\Lambda/T)$ provided that $t = t'$.

Second, the particle-hole bubbles also depend on the direction of the electron momentum, hence, the infinite-order result for the thermodynamic potential is found again by replacing the bare interaction U in the second-order diagram by $\Gamma_{s_1 s_2; s_3 s_4}(\theta_{\mathbf{k}})$ and retaining the angular dependence of the bubbles.

The RG equations for the in-plane magnetic field are considerably more complicated. The main difference is that even the RG-invariant terms depend on the magnetic field. A detailed discussion of Cooper renormalization of the scattering amplitudes and spin susceptibility for this case is given in Appendices B.3.2 and B.3.2, respectively. Below, we only show the final result for the renormalized spin susceptibility

$$\delta\chi_{xx} = \frac{\chi_0}{3}\left(\frac{mU}{4\pi}\right)^2 \frac{|\alpha| k_F}{E_F} + \mathcal{O}\left(\frac{T}{\ln T}\right). \tag{3.4.39}$$

The T-independent term is the same as without the Cooper renormalization [cf. (3.3.55)]. The linear-in-T term however is suppressed by at least a factor of $1/\ln T$, similar to the case of no SOI, where it is suppressed by a $\ln^2 T$ factor.

3.5 Summary and discussion

We have considered a two-dimensional electron liquid in the presence of the Rashba spin-orbit interaction (SOI). The main result of this Chapter is that the combined effect of the electro-electron and spin-orbit interactions breaks isotropy of the spin response, whereas either of these two mechanisms does not. Namely, nonanalytic behavior of the spin susceptibility, as manifested by its temperature–and magnetic-field dependences, studied in this Chapter, is different for different components of the susceptibility tensor: whereas the nonanalytic behavior of χ_{zz} is cut off at the energy scale associated with the SOI (given by $|\alpha| k_F$ for the Rashba SOI), that of χ_{xx} (and $\chi_{yy} = \chi_{xx}$) continues through the SOI energy scale. The reason for this difference is the dependence of the SOI-induced magnetic field on the electron momentum. If the external magnetic field is perpendicular to the plane of motion, its effect is simply dual to that of the SOI-field: the T dependence of χ_{zz} is cut by whichever of the two fields is larger. If the external field is in the plane of motion, it is always possible to form a virtual particle-hole pair, which mediates the long-range interaction between quasiparticles, from the states belonging to the same Rashba branch. The energy of such a pair depends on the external but not on the effective field, so that the SOI effectively drops out of the result. We have also studied a non-perturbative renormalization of the spin susceptibility in

the Cooper channel of the electron-electron interaction. It turns out the RG flow of scattering amplitudes is highly non-trivial. As a result, the spin susceptibility exhibits a non-monotonic dependence on the Cooper-channel renormalization parameter ($\ln T$) and eventually saturates as a temperature-independent value, proportional to the SOI coupling $|\alpha|$.

Notably, all the results of this Chapter are readily applicable to the systems with large Dresselhaus SOI and negligible Rashba SOI. In this case the Rashba spin-orbit coupling should be simply replaced by the Dresselhaus spin-orbit coupling.

Now we would like to discuss possible implications of these results for (in)stability of a second-order ferromagnetic quantum critical point (QCP). This phenomenon depends crucially on the sign of the nonanalytic correction. In this regard, we should point out that we limited our analysis to the simplest possible model, which does not involve the Kohn-Luttinger superconducting instability and higher-order processes in the particle-hole channel. Therefore, the sign of our nonanalytic correction is "anomalous", i.e., the spin susceptibility increases with the corresponding energy scale. As in the absence of the SOI, however, either of these two effects (Kohn-Luttinger and particle-hole) can reverse the sign of nonanalyticity. Therefore, it is instructive to consider consequences of both signs.

In the absence of the SOI, a nonanalyticity of the anomalous sign renders a second-order ferromagnetic QCP unstable with respect to either a first-order phase transition or a transition into a spiral state [Maslov06, Maslov09, Conduit09]. This result was previously believed to be relevant only to systems with a $SU(2)$ symmetry of electron spins; in particular it was shown in [Chubukov04b, Rech06] that there is no nonanalyticity in χ for a model case of the Ising-like exchange interaction between electrons. We have shown here that broken (by the SOI) $SU(2)$ symmetry is not sufficient for eliminating a nonanalyticity in the in-plane component of the spin susceptibility (χ_{xx}). Based on our results for the magnetic-field dependence of χ_{zz} and χ_{xx} [cf. Equations (3.3.38) and (4.1.10)], we can construct a model form for the free energy as a function of the magnetization M. The most interesting case for us is the one in which the Zeeman energy due to spontaneous magnetization, $\sim M/m\mu_B$ is larger than the SOI energy scale $|\alpha|k_F$, so that $\chi_{xx} \neq \chi_{zz}$. Ignoring Cooper-channel renormalization, we can write the free energy as

$$F = aM^2 - b\left(|M_x|^3 + |M_y|^3\right) + M^4, \tag{3.5.1}$$

where $M = \left(M_x^2 + M_y^2 + M_z^2\right)^{1/2}$ and the coefficient of the quartic term was absorbed into the overall scale of F, which is irrelevant for our discussion. An important difference of this free energy, compared to the case of no SOI, is easy-plane anisotropy of the nonanalytic, cubic term. In the absence of the cubic term ($b = 0$), a second-order quantum phase transitions occurs when $a = 0$; in the paramagnetic phase, a is positive but small near the QCP. Since χ is isotropic at the mean-field level [cf. Equation (3.2.8)],

the regular, M^2 and M^4 terms in Equation (3.5.1) are isotropic as well. If $b > 0$ (which corresponds to the anomalous sign of nonanalyticity), the cubic term leads to a minimum of F at finite M; when the minimum value of F reaches zero, the states with zero and finite magnetization become degenerate, and a first-order phase transition occurs. The first-order critical point is specified by the following equations

$$\frac{\partial F}{\partial M_z} = 0, \ \frac{\partial F}{\partial M_x} = 0, \ \frac{\partial F}{\partial M_y} = 0, \text{ and } F = 0. \tag{3.5.2}$$

For $a > 0$, the only root of the first equation is $M_z = 0$, i.e., there is no net magnetization in the z direction. Substituting $M_z = 0$ into the remaining equations and employing in-plane symmetry ($M_x = M_y$), we find that the first-order phase transition occurs at $a = b^2/8$. The broken-symmetry state is an XY ferromagnet with spontaneous in-plane magnetization $M_x^{\{c\}} = M_y^{\{c\}} = b/4$. The first-order transition to an XY ferromagnet occurs if the Zeeman energy, corresponding to a jump of the magnetization at the critical point, is larger than the SOI energy, i.e., $M_x^{\{c\}}/m\mu_B \gg |\alpha|k_F$. In the opposite case, the SOI is irrelevant, and the first-order transition is to a Heisenberg ferromagnet.

If the nonanalyticity is of the "normal" sign ($b < 0$), the transition remains second order and occurs at $a = 0$. However, the critical indices are different for the in-plane and transverse magnetization: in the broken-symmetry phase ($a < 0$), $M_x = M_y \propto (-a)$ while $M_z \propto (-a)^{1/2}$. Since $|a| \ll 1$, the resulting state is an Ising-like ferromagnet with $M_z \gg M_x = M_y$.

A detailed study of the $|\tilde{\mathbf{q}}|$ dependence of χ in the presence of the SOI is a subject of Chapter 4.

Chapter 4

Ferromagnetic order of nuclear spins coupled to conduction electrons: a combined effect of electron-electron and spin-orbit interactions

4.1 Introduction

Spontaneous nuclear spin polarization in semiconductor heterostructures at finite but low temperatures has recently attracted a considerable attention both on the theoretical [Simon07, Simon08, Chesi09, Żak10a] and experimental [Clark10] sides. Apart from a fundamental interest in the new type of a ferromagnetic phase transition, the interest is also motivated by an expectation that spontaneous polarization of nuclear spins should suppress decoherence in single-electron spin qubits caused by the hyperfine interaction with the surrounding nuclear spins [Simon07, Simon08], and ultimately facilitate quantum computing with single-electron spins [Loss98, Żak10b].

Improvements in experimental techniques have lead to extending the longitudinal spin relaxation times in semiconductor quantum dots (QDs) to as long as 1s [Kroutvar04, Elzerman04, Amasha08]. The decoherence time in single electron GaAs QDs has been reported to exceed 1μs in experiments using spin-echo techniques at magnetic fields below 100mT [Petta06, Koppens08], whereas a dephasing time of GaAs electron-spin qubits coupled to a nuclear bath has lately been measured to be above 200μs [Bluhm04]. Still, even state-of-the-art dynamical nuclear polarization methods [Burkard99, Khaetskii02, Khaetskii03, Coish04, Bracker05] allow for merely up to 60% polarization of nuclear spins [Bracker05], whereas polarization of above 99% is required in order to extend the electron spin decay time only by one order of magnitude[Coish04]. Full magnetization of nuclear spins by virtue of a ferromagnetic nuclear spin phase tran-

sition (FNSPT), if achieved in practice, promises a drastic improvement over other decoherence reduction techniques.

The main mechanism of the interaction between nuclear spins in the presence of conduction electrons is the Ruderman-Kittel-Kasuya-Yosida (RKKY) interaction [Kittel87]. The effective Hamiltonian of the RKKY interaction between on-site nuclear spins of magnitude I

$$H_{\mathrm{RKKY}} = -\frac{1}{2}\sum_{\mathbf{r},\mathbf{r}'} J^{ij}(\mathbf{r},\mathbf{r}')I^i(\mathbf{r})I^j(\mathbf{r}'), \tag{4.1.1}$$

is parameterized by an effective exchange coupling

$$J^{ij}(\mathbf{r},\mathbf{r}') = \frac{A^2}{4n_s^2}\chi^{ij}(\mathbf{r},\mathbf{r}'), \tag{4.1.2}$$

where A is the hyperfine coupling constant, n_s is the number density of nuclear spins, and

$$\chi^{ij}(\mathbf{r},\mathbf{r}') = -\int_0^{1/T} d\tau \langle T_\tau S^i(\mathbf{r},\tau)\, S^j(\mathbf{r}',0)\rangle \tag{4.1.3}$$

is the (static) correlation function of electron spins. [Hereafter, we will refer to $\chi^{ij}(\mathbf{r},\mathbf{r}')$– and to its momentum-space Fourier transform–as to "spin susceptibility", although it is to be understood that this quantity differs from the thermodynamic susceptibility, defined as a correlation function of electron magnetization, by a factor of μ_B^2, where μ_B is the Bohr magneton.] It is worth emphasizing that $\chi^{ij}(\mathbf{r},\mathbf{r}')$ contains all the effects of the electron-electron interaction [Simon07, Simon08]–this circumstance has two important consequences for the RKKY coupling. First, the electron-electron interaction increases the uniform spin susceptibility which should lead to an enhancement of the critical temperature of the FNSPT, at least at the mean-field level. Second, stability of the nuclear-spin ferromagnetic order is controlled by the long-wavelength behavior of the magnon dispersion $\omega(\tilde{\mathbf{q}})$ which, in its turn, is determined by $\chi^{ij}(\tilde{\mathbf{q}})$ at $\tilde{q} \to 0$. In a spin-isotropic and translationally invariant system,

$$\omega(\tilde{q}) = \frac{A^2}{4n_s} I[\chi(0) - \chi(\tilde{q})], \tag{4.1.4}$$

with $\chi^{ij} = \delta_{ij}\chi$, while the magnetization is given by

$$M(T) = \mu_N I\left[n_s - \int_{\tilde{\mathbf{q}}\in \mathrm{BZ}} \frac{d^D\tilde{q}}{(2\pi)^D}\frac{1}{e^{\omega(\tilde{q})/T}-1}\right], \tag{4.1.5}$$

where μ_N is the nuclear-spin magneton (we set $k_B = \hbar = 1$ throughout this work). The second term in Equation (4.1.5) describes a reduction in the magnetization due to thermally excited magnons. In a free two-dimensional electron gas (2DEG), $\chi(\tilde{q})$ is constant for $\tilde{q} \le 2k_F$, and thus the magnon contribution to $M(T)$ diverges in the

$\tilde{q} \to 0$ limit, which means that long-range order (LRO) is unstable. However, residual interactions among the Fermi-liquid quasiparticles lead to a non-analytic behavior of the spin-susceptibility: for $\tilde{q} \ll k_F$, $\chi(\tilde{q}) = \chi(0) + C\tilde{q}$, where both the magnitude and the *sign* of C depend on the strength of the electron-electron interaction [Chubukov03, Rech06]. In two opposite limits-at weak-coupling and near the Stoner instability[1]–the prefactor C is positive which, according to Equations (4.1.4) and (4.1.5), means that LRO is unstable. However, C is negative (and thus the integral in Equation (4.1.5) is convergent) near a Kohn-Luttinger superconducting instability [Shekhter06b, Chesi09]; also, in a generic Fermi liquid with neither strong nor weak interactions C is likely to be negative due to higher-order scattering processes in the particle-hole channel [Maslov06, Maslov09, Shekhter06a].[2]

The spin-wave–theory argument presented above is supported by the analysis of the RKKY kernel in real space. A linear-in-$\tilde{q}$ term in $\chi(\tilde{q})$ corresponds to a dipole-dipole–like., $1/r^3$ term in $\chi(r)$ (see Section 4.3). If $C > 0$, the dipole-dipole interaction is repulsive, and the ferromagnetic ground state is unstable; vice versa, if $C < 0$, the dipole-dipole attraction stabilizes the ferromagnetic state.

It is worth noting here that even finiteness of the magnon contribution to the magnetization does not guarantee the existence of LRO. Although the Mermin-Wagner theorem [Mermin66] in its original formulation is valid only for sufficiently short-range forces and thus not applicable to the RKKY interaction, it has recently been proven [Loss11] that magnetic LRO is impossible even for the RKKY interaction in $D \leq 2$. From the practical point of view, however, the absence of LRO in 2D is not really detrimental for suppression of nuclear-spin induced decoherence. Indeed, nuclear spins need to be ordered within the size of the electron qubit (a double QD system formed by gating a 2DEG) as well as its immediate surrounding such that there is no flow of magnetization. Since fluctuations grow only as a logarithm of the system size in 2D, it is always possible to achieve a quasi-LRO at low enough temperatures and on a scale smaller that the thermal correlation length. In addition, spin-orbit interaction (SOI)–which is the main subject of this thesis, see below–makes a long-range order possible even in 2D [Loss11].

The electron spin susceptibility in Equation (4.1.4) was assumed to be at zero temperature. First, since the nuclear spin temperature is finite, the system as a whole is not in equilibrium. However, a time scale associated with 'equilibration' is sufficiently

[1] In a quantum-critical region near the Stoner instability, the $\tilde{q}$ term in the spin susceptibility transforms into a $\tilde{q}^{3/2}$ one, cf. [Rech06].

[2] Strictly speaking, the non-analytic behavior of χ in the generic FL regime was analyzed as a function of the temperature [Maslov06, Maslov09, Shekhter06a] and of the magnetic field [Maslov06, Maslov09] rather than as a function of $\tilde{q}$. However, in all cases studied so far the non-analytic dependence of $\chi(\tilde{q}, H, T)$ has always been found to be symmetric in all variables, i.e., $\chi(\tilde{q}, H, T) = \chi(0, 0, 0) + \max\{C_{\tilde{q}}\tilde{q}, C_H H, C_T T\}$, with $C_{\tilde{q},H,T}$ being of the same sign. It is likely that the same also holds true in the generic FL regime.

long to assume that there is no energy transfer from the nuclear- to electron-spin system. Second, if the electron temperature is finite, the linear $\tilde{q}$ scaling of $\chi(\tilde{q})$ is cut off at the momentum of order $T/v_F \equiv 1/L_T$. For $\tilde{q} \ll 1/L_T$, $\chi(T,\tilde{q}) \propto T + \mathcal{O}\left(v_F^2\tilde{q}^2/T\right)$ such that $\omega(\tilde{q}) \propto \tilde{q}^2$ and, according to Equation (4.1.5), spin waves would destroy LRO. However, at low enough temperatures the thermal length L_T is much larger than a typical size of the electron qubit L_Q. (For example, $L_T \sim 1$mm at $T \sim 1$mK.) Therefore, $\tilde{q} \gtrsim 1/L_Q \gg 1/L_T = T/v_F$ and, indeed, the electron temperature can be assumed to be zero.

In practically all nuclear-spin systems of current interest, such as GaAs or carbon-13 nanotubes, spin-orbit interaction (SOI) plays a vital role. The main focus of this thesis is the combined effect of the electron-electron and SO interactions on the spin susceptibility of 2DEG and, in particular, on its $\tilde{q}$ dependence, and thus on the existence/stability of the nuclear-spin ferromagnetic order.

The interplay between the electron-electron and SOIs is of crucial importance here. Although the SOI breaks spin-rotational invariance and thus may be expected to result in an anisotropic spin response, this does not happen for the Rashba and Dresselhaus SOIs alone: the spin susceptibility of *free* electrons is isotropic [up to $\exp(-E_F/T)$ terms] as long as both spin-orbit–split subbands remain occupied [Żak10a]. The electron-electron interaction breaks isotropy, which can be proven within a Fermi-liquid formalism generalized for systems with SOI [Ashrafi]. Specific models adhere to this general statement. In particular, $\chi^{zz} > \chi^{xx} = \chi^{yy}$ for a dense electron gas with the Coulomb interaction [Chesi07].

In this thesis, we analyze the $\tilde{q}$ dependence of the spin susceptibility in the presence of the SOI. The natural momentum-space scale introduced by a (weak) Rashba SOI with coupling constant α ($|\alpha| \ll v_F$) is the difference of the Fermi momenta in two Rashba subbands:

$$q_\alpha \equiv 2m^*|\alpha|, \tag{4.1.6}$$

where m^* is the band mass of 2DEG. Accordingly, the dependence of χ^{ij} on $\tilde{q}$ is different for $\tilde{q}$ above and below q_α; in the latter case, it is also different for the out-of-plane and in-plane components. To second order in electron-electron interaction with potential $U(q)$, the out-of-plane component is independent of $\tilde{q}$ for $\tilde{q} \le q_\alpha$:

$$\delta\chi^{zz}(\tilde{q},\alpha) = 2\chi_0 u_{2k_F}^2 \frac{|\alpha|k_F}{3E_F}. \tag{4.1.7a}$$

On the other hand, the in-plane component scales linearly with $\tilde{q}$ even for $\tilde{q} \le q_\alpha$:

$$\begin{aligned} \delta\chi^{xx}(\tilde{q},\alpha) &= \delta\chi^{yy}(\tilde{q},\alpha) \\ &= \chi_0 u_{2k_F}^2 \left[\frac{|\alpha|k_F}{3E_F} + \frac{4}{9\pi}\frac{v_F\tilde{q}}{E_F}\right], \end{aligned} \tag{4.1.7b}$$

In Equations (4.1.7a,4.1.7b), $u_q \equiv m^*U(q)/4\pi$, k_F is the Fermi momentum, $E_F = k_F^2/2m^*$ is the Fermi energy, $\chi_0 = m^*/\pi$ is the spin susceptibility of a free 2DEG,

and $\delta\chi^{ij}$ denotes a nonanalytic part of χ^{ij}. For $q_\alpha \ll \tilde{q} \ll k_F$, the spin susceptibility goes back to the result of [Chubukov03] valid in the absence of the SOI:

$$\delta\chi^{ij}(\tilde{q}, \alpha = 0) = \delta_{ij}\frac{2}{3\pi}\chi_0 u_{2k_F}^2 \frac{v_F\tilde{q}}{E_F}. \tag{4.1.8}$$

Note that the subleading term in $\tilde{q}$ in Eq. (4.1.7b) differs by a factor of 2/3 from the leading term in $\tilde{q}$ in Eq. (4.1.8). There is no contradiction, however, because Eqs. (4.1.8) and (4.1.7b) correspond to the regions of $q \leq q_\alpha$ and $q \gg q_\alpha$, correspondingly.

Equations (4.1.7a) and (4.1.7b) show that the uniform spin susceptibility is anisotropic: $\delta\chi^{zz}(0, \alpha) = 2\delta\chi^{xx}(0, \alpha)$. This implies that the RKKY coupling is stronger if nuclear spins are aligned along the normal to the 2DEG plane, and thus the nuclear-spin order is of the Ising type. In general, a 2D Heisenberg system with anisotropic exchange interaction is expected to have a finite-temperature phase transition [Caride83a, Caride83b, Kaufman84]. In an anisotropic case, the dispersion of the out-of-plane spin-wave mode [Ashcroft76, Simon08] is given by

$$\omega(\tilde{q}) = \frac{A^2}{4n_s} I[\chi^{zz}(0) - \chi^{xx}(\tilde{q})], \tag{4.1.9}$$

with $\tilde{\mathbf{q}} \perp \hat{\mathbf{z}}$. Ising-like anisotropy implies a finite gap in the magnon spectrum. In our case, however, the situation is complicated by the positive slope of the linear $\tilde{q}$ dependence of the second-order result for $\chi^{xx}(q)$, which–according to Equation (4.1.9)–translates into $\omega(\tilde{q})$ *decreasing* with $\tilde{q}$. Combining the asymptotic forms of χ^{ij} from Equations (4.1.7a,4.1.7b), and (4.1.8) together, as shown in Figure 4.1, we see that $\omega(\tilde{q})$ is necessarily negative in the interval $q_\alpha \ll \tilde{q} \ll k_F$, and thus LRO is unstable. Therefore, anisotropy alone is not sufficient to ensure the stability of LRO: in order to reverse the sign of the $\tilde{q}$ dependence, one also needs to invoke other mechanisms, arising from higher orders in the electron-electron interaction. We show that at least one of these mechanisms–renormalization in the Cooper channel–is still operational even for $\tilde{q} \ll q_\alpha$ and capable of reversing the sign of the $\tilde{q}$-dependence is the system is close to (but not necessarily in the immediate vicinity of) the Kohn-Luttinger instability.

We note that the dependences of $\delta\chi^{ij}$ on $\tilde{q}$ in the presence of the SOI is similar to the dependences on the temperature and magnetic field, [Żak10a] presented below for

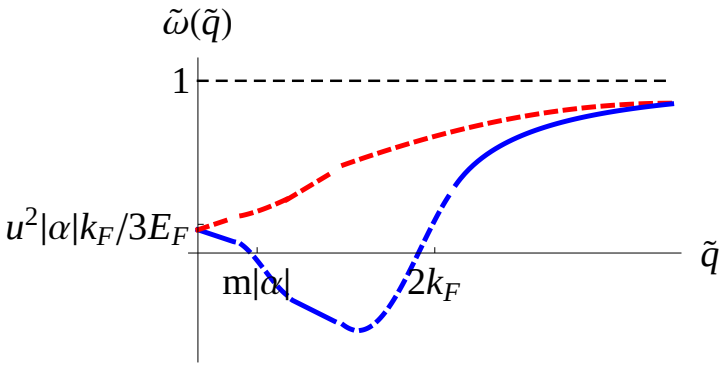

Figure 4.1: (color online): A normalized dispersion of the out-of-plane spin-wave mode $\tilde{\omega}(\tilde{q}) = \omega(\tilde{q})/[A^2 I\chi_0/4n_s]$ as a function of the momentum. To second order in interaction (lower curve) $\omega(\tilde{q})$ is necessarily negative for $m|\alpha| \ll \tilde{q} \ll k_F$, and thus LRO is unstable. Solid parts of the curves corresponds to actual calculations; dashed parts are interpolations between various asymptotic regimes. Renormalization effects in the Cooper channel reverse the slope of $\omega(\tilde{q})$ (upper curve) and stabilize LRO.

completeness:

$$\begin{aligned}
\delta\chi^{zz}(T,\alpha) &= 2\chi_0 u_{2k_F}^2 \left[\frac{|\alpha|k_F}{3E_F} + \mathcal{O}\left(T^3\right)\right] \\
\delta\chi^{zz}(B_z,\alpha) &= 2\chi_0 u_{2k_F}^2 \left[\frac{|\alpha|\,k_F}{3E_F} + \mathcal{O}\left(\Delta_z^2\right)\right] \\
\delta\chi^{xx}(T,\alpha) &= \chi_0 u_{2k_F}^2 \left[\frac{|\alpha|k_F}{3E_F} + \frac{T}{E_F} + \mathcal{O}\left(T^3\right)\right] \\
\delta\chi^{xx}(B_x,\alpha) &= \chi_0 u_{2k_F}^2 \left[\frac{|\alpha|\,k_F}{3E_F} + \frac{16}{3\pi}\frac{|\Delta_x|}{E_F}\right]
\end{aligned} \tag{4.1.10}$$

Here, $\Delta_i = g\mu_B B_i/2$ and $T, \Delta_i \ll |\alpha|k_F$. As Equations (4.1.7a,4.1.7b) and (4.1.10) demonstrate, while nonanalytic scaling of $\delta\chi^{zz}$ with all three variables ($\tilde{q}$, T, B) is cut off by the scale introduced by SOI, scaling of $\delta\chi^{zz}$ continues below the SOI scale. This difference was shown in [Żak10a] to arise from the differences in the dependence of the energies of particle-hole pairs with zero total momentum on the magnetic field: while the energy of such a pair depends on the SO energy for $\mathbf{B}||\hat{\mathbf{z}}$, this energy drops out for $\mathbf{B} \perp \hat{\mathbf{z}}$.

In addition to modifying the behavior of χ^{ij} for $\tilde{q} \leq q_\alpha$, SOI leads to a new type of the Kohn anomaly arising due to interband transitions: a nonanalyticity of $\chi^{ij}(\tilde{q},\alpha)$ at $\tilde{q} = q_\alpha$. The nonanalyticity is stronger in χ^{zz} than in χ^{xx}: $\delta\chi^{zz}(\tilde{q} \approx q_\alpha) \propto (\tilde{q} - q_\alpha)^{3/2}\,\Theta(\tilde{q} - q_\alpha)$ while $\delta\chi^{xx}(\tilde{q} \approx q_\alpha) \propto (\tilde{q} - q_\alpha)^{5/2}\,\Theta(\tilde{q} - q_\alpha)$, where $\Theta(x)$ is the step-function. Consequently, the real-space RKKY interaction exhibits long-wavelength oscillations $\chi^{zz}(r) \propto \cos(q_\alpha r)/r^3$ and $\chi^{xx}(r) \propto \sin(q_\alpha r)/r^4$, in addition to conventional

Friedel oscillations behaving as $\sin(2k_F r)/r^2$. It is worth noting that the long-wavelength Friedel oscillations occur only in the presence of *both* electron-electron and SO interactions.

This Chapter is organized as follows. In Section 4.2 we derive perturbatively the electron spin susceptibility of interacting 2DEG with the SOI as a function of momentum; in particular, Sections 4.2.1–4.2.4 outline the derivation of all relevant second-order diagrams, Section 4.2.5 is devoted to Cooper renormalization of the second order result, and in Section 4.2.6 we show that, in contrast to the spin susceptibility, the charge susceptibility is analytic at small $\tilde{q}$ (as it is also the case in the absence of SOI) . In Section 4.3, we derive the real-space form the of the RKKY interaction and show that it exhibits long-wavelength oscillations with period given by the SO length $2\pi/q_\alpha$. Details of the calculations are delegated to Appendices C.1-C.4. In particular, the free energy in the presence of the SOI is derived beyond the Random Phase Approximation in Appendix C.4. The summary and discussion of the main results are provided in Section 4.4.

4.2 Spin susceptibility of interacting electron gas

Dynamics of a free electron in a two-dimensional electron gas (2DEG) in the presence of the Rashba spin-orbit interaction (SOI) with a coupling strength α is described by the following Hamiltonian

$$H = \frac{p^2}{2m^*} + \alpha(p_x\sigma^y - p_y\sigma^x), \tag{4.2.1}$$

where $\mathbf{p} = (p_x, p_y)$ is the electron momentum of an electron, and $\boldsymbol{\sigma}$ is a vector of Pauli matrices. The interaction between electrons will be treated perturbatively. For this purpose, we introduce a Green's function

$$G(P) = \frac{1}{i\omega_p - H - E_F} = \sum_s \Omega_s(\mathbf{p}) g_s(P) \tag{4.2.2}$$

with

$$\Omega_s(\mathbf{p}) = \frac{1}{2}\left[1 + \frac{s}{p}(p_y\sigma^x - p_x\sigma^y)\right] \tag{4.2.3}$$

and

$$g_s(P) = \frac{1}{i\omega_p - \epsilon_{\mathbf{p}} - s\alpha p}, \tag{4.2.4}$$

where $P \equiv (\omega_p, \mathbf{p})$ with ω_p being a fermionic Matsubara frequency, $\epsilon_{\mathbf{p}} = p^2/2m^* - E_F$, and $s = \pm 1$ is a Rashba index.

The nonanalytic part of a spin susceptibility tensor to second order in electron-electron interaction is given by seven linear response diagrams depicted in Figs. 4.2-4.7. Due to symmetry of the Rashba SOI, $\chi^{ij}(\tilde{\mathbf{q}}) = \chi^{ii}(\tilde{q})\delta_{ij}$ and $\chi^{xx} = \chi^{yy} \neq \chi^{zz}$.

In the following subsections, we calculate all diagrams that contribute to non-analytic behavior of the out-of-plane, χ^{zz}, and in-plane, $\chi^{xx} = \chi^{yy}$, components of the spin susceptibility tensor for small external moment ($\tilde{q} \ll k_F$) and at $T = 0$. In the absence of SOI, the non-analytic contributions to the spin susceptibility from individual diagrams are determined by "backscattering" or "Cooper-channel" processes [Chubukov03, Maslov06, Maslov09], in which two fermions with initial momenta $\mathbf{k}$ and $\mathbf{p}$ move in almost opposite directions, such that $\mathbf{k} \approx -\mathbf{p}$. Backscattering processes are further subdivided into those with small momentum transfer, such that $(\mathbf{k}, -\mathbf{k}) \to (\mathbf{k}, -\mathbf{k})$, and those with momentum transfers near $2k_F$, such that $(\mathbf{k}, -\mathbf{k}) \to (-\mathbf{k}, \mathbf{k})$. In the net result, all $q = 0$ contributions cancel out and only $2k_F$ contributions survive. We will show that this also the case in the presence of the SOI. In what follows, all "$q = 0$ diagrams" are to be understood as the $q = 0$ channel of the backscattering process.

4.2.1 Diagram 1

General formulation

The first diagram is a self-energy insertion into the free-electron spin susceptibility, see Figure 4.2. There are two contributions to the nonanalytic behavior: (i) from the region of small momentum transfers, i.e., $q \ll k_F$,

$$\begin{aligned}\chi^{ij}_{1,q=0}(\tilde{q}) =& 2U^2(0)\int_Q\int_K\int_P \mathrm{Tr}[G(P)G(P+Q)] \\ &\times \mathrm{Tr}[G(K+\tilde{Q})\sigma^i G(K)G(K+Q)G(K)\sigma^j] \end{aligned} \tag{4.2.5a}$$

and (ii) from the region of momentum transfers close to $2k_F$, i.e., $|\mathbf{k}-\mathbf{p}| \approx 2k_F$ and $q \ll k_F$,

$$\begin{aligned}\chi^{ij}_{1,q=2k_F}(\tilde{q}) =& 2U^2(2k_F)\int_Q\int_K\int_P \mathrm{Tr}[G(K+Q)G(P+Q)] \\ &\times \mathrm{Tr}[G(K+\tilde{Q})\sigma^i G(K)G(P)G(K)\sigma^j]. \end{aligned} \tag{4.2.5b}$$

Here, $K \equiv (\omega_k, \mathbf{k})$ and $\int_K \equiv (2\pi)^{-3}\int d\omega_k d^2k$ (and the same for other momenta). The time component of $\tilde{Q} = (\tilde{\Omega}, \tilde{\mathbf{q}})$ is equal to zero throughout this thesis. Since the calculation is performed at $T = 0$, there is no difference between the fermionic and bosonic Matsubara frequencies. A factor of 2 appears because the self-energy can be inserted either into the upper or the lower arm of the free-electron susceptibility. As subsequent analysis will show, a typical value of the momentum transfer q is on the order of either the external momentum $\tilde{q}$ or the "Rashba momentum" q_α [cf. Equation (4.1.6)], whichever is larger. In both cases, $q \ll k_F$ while the momenta of both fermions are near k_F, thus we neglect $\mathbf{q}$ in the angular dependencies of the Rashba vertices: $\Omega_s(\mathbf{k}+\mathbf{q}) \approx \Omega_s(\mathbf{k}+\tilde{\mathbf{q}}) \approx \Omega_s(\mathbf{k}) = [1+s(\sin\theta_{k\tilde{q}}\sigma^x - \cos\theta_{k\tilde{q}}\sigma^y)]/2$ with $\theta_{ab} \equiv \angle(\mathbf{a}, \mathbf{b})$.

[The origin of the $\hat{\mathbf{x}}$-axis is arbitrary and can be chosen along $\tilde{\mathbf{q}}$.] Also, we impose the backscattering correlation between the fermionic momenta: $\mathbf{k} = -\mathbf{p}$ in the $2k_F$-part of the diagram. With these simplifications, we obtain

$$\chi^{ij}_{1,q=0}(\tilde{q}) = 2U^2(0)\int\frac{d\Omega}{2\pi}\int\frac{d\theta_{k\tilde{q}}}{2\pi}\int\frac{qdq}{2\pi}a^{ij}_{lmnr}b_{st}I_{lmnr}(\Omega,\theta_{k\tilde{q}},q,\tilde{q})\Pi_{st}(\Omega,q), \tag{4.2.6a}$$

$$\chi^{ij}_{1,q=2k_F}(\tilde{q}) = 2U^2(2k_F)\int\frac{d\Omega}{2\pi}\int\frac{d\theta_{k\tilde{q}}}{2\pi}\int\frac{qdq}{2\pi}\tilde{a}^{ij}_{lmsr}\tilde{b}_{nt}I_{lmnr}(\Omega,\theta_{k\tilde{q}},q,\tilde{q})\Pi_{st}(\Omega,q), \tag{4.2.6b}$$

where summation over the Rashba indices is implied,

$$a^{ij}_{lmnr} \equiv \mathrm{Tr}[\Omega_l(\mathbf{k})\sigma^i\Omega_m(\mathbf{k})\Omega_n(\mathbf{k})\Omega_r(\mathbf{k})\sigma^j], \tag{4.2.7a}$$

$$b_{st} \equiv \mathrm{Tr}[\Omega_s(\mathbf{p})\Omega_t(\mathbf{p})] = (1+st)/2, \tag{4.2.7b}$$

$$\tilde{a}^{ij}_{lmsr} \equiv \mathrm{Tr}[\Omega_l(\mathbf{k})\sigma^i\Omega_m(\mathbf{k})\Omega_s(-\mathbf{k})\Omega_r(\mathbf{k})\sigma^j], \tag{4.2.7c}$$

$$\tilde{b}_{nt} \equiv \mathrm{Tr}[\Omega_n(-\mathbf{p})\Omega_t(\mathbf{p})] = (1-nt)/2 \tag{4.2.7d}$$

$$\begin{aligned} I_{lmnr}(\Omega,\theta_{k\tilde{q}},q,\tilde{q}) \equiv &\int\frac{d\theta_{kq}}{2\pi}\int\frac{d\omega_k}{2\pi}\int\frac{d\epsilon_k}{2\pi} \\ &\times g_l(\omega_k,\mathbf{k}+\tilde{\mathbf{q}})g_m(\omega_k,\mathbf{k})g_n(\omega_k+\Omega,\mathbf{k}+\mathbf{q})g_r(\omega_k,\mathbf{k}) \end{aligned} \tag{4.2.7e}$$

and, finally, the partial components of the particle-hole bubble are given by

$$\begin{aligned} \Pi_{st}(\Omega,q) \equiv &\int\frac{d\theta_{pq}}{2\pi}\int\frac{d\omega_p}{2\pi}\int\frac{d\epsilon_{\mathbf{p}}}{2\pi}g_s(\omega_p,\mathbf{p})g_t(\omega_p+\Omega,\mathbf{p}+\mathbf{q}) \\ =&\frac{m}{2\pi}\frac{1}{\sqrt{v_F^2q^2+(\Omega+i(t-s)\alpha k_F)^2}}. \end{aligned} \tag{4.2.7f}$$

For the derivation of the particle-hole bubble, see 3.3.2. Calculation of other common integrals is presented in Appendix C.1.

The main difference between the out-of-plane and in-plane components is in the structure of the "quaternion", defined by Equation (4.2.7e) and calculated explicitly in Appendix C.1 [cf. Equation (C.1.3)]. The dependence of I_{lmnr} on the external momentum $\tilde{q}$ enters only in a combination with the SOI coupling as $v_F\tilde{q}\cos\theta_{k\tilde{q}} + (s-s')\alpha k_F$, where $s, s' \in \{l, m, n, r\}$. Combinations of indices l, m, n, r are determined by the spin vertices $\sigma^{i,j}$ and are, therefore, different for the out-of-plane and in-plane components. The out-of-plane component contains only such combinations $\{l, m, n, r\}$ for which the coefficient $s - s'$ is finite. Therefore, the SOI energy scale is always present and, for $\tilde{q} \ll q_\alpha$, one can expand in $\tilde{q}/q_\alpha$. The leading term in this expansion is proportional to $|\alpha|$ but any finite-order correction in $\tilde{q}/q_\alpha$ vanishes. In fact, one can calculate the entire dependence of χ_1^{zz}

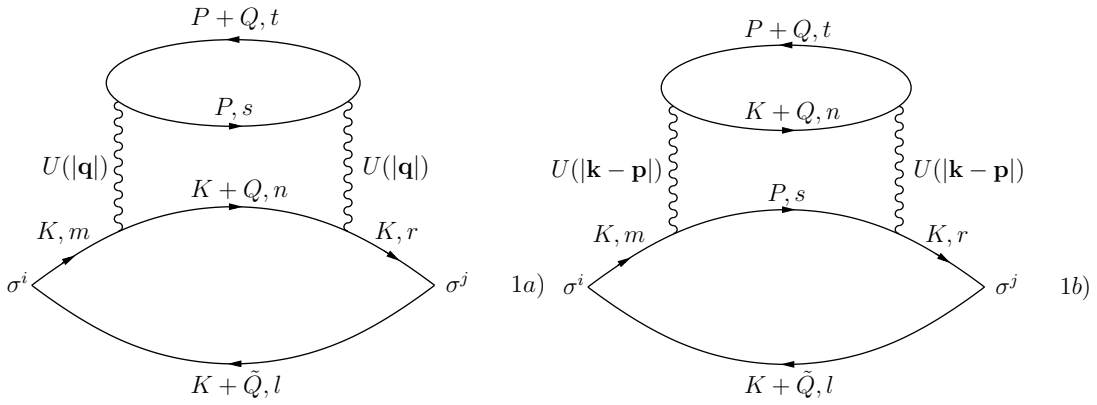

Figure 4.2: Diagram 1. Left: small-momentum transfer part. Right: $2k_F$-momentum transfer part. K, s denotes a fermion from Rashba subband $s = \pm 1$ with "four-momentum" $K = (\omega_k, \mathbf{k})$.

on $\tilde{q}$ (what is done in Appendix C.2) and show that χ_1^{zz} is indeed independent of $\tilde{q}$ for $\tilde{q} \leq q_\alpha$ (and similar for the remaining diagrams). On the other hand, some quaternions, entering the in-plane component, have $s = s'$ and thus do not contain the SOI, which means that one cannot expand in $\tilde{q}/q_\alpha$ anymore. These quaternions provide linear-in-$\tilde{q}$ dependence of χ_1^{xx} even for $\tilde{q} \leq q_\alpha$, where the slope of this dependence is 2/3 of that in the absence of the SOI. This is the origin of the difference in the $\tilde{q}$ dependencies of χ^{zz} and χ^{xx}, as presented by Equations (4.1.7a) and (4.1.7b).

The evaluation of the out-of-plane and in-plane part of diagram 1 is a subject of the next two subsections.

Diagram 1: out-of-plane component

We begin with the out-of-plane component of the spin susceptibility, in which case $a^{zz}_{lmnr} = [1 + mr + n(m + r) - l(m + n + r + mnr)]/8$ and $\tilde{a}^{zz}_{lmsr} = [1 + mr - s(m + r) + l(s - m - r + mrs)]/8$. Summation over the Rashba indices yields

$$\chi^{zz}_{1,q=0} = 4U^2(0) \int \frac{d\Omega}{2\pi} \int \frac{d\theta_{k\tilde{q}}}{2\pi} \int \frac{qdq}{2\pi} (I_{+---} + I_{-+++})\Pi_0, \tag{4.2.8a}$$

and

$$\chi^{zz}_{1,q=2k_F} = 2U^2(2k_F) \int \frac{d\Omega}{2\pi} \int \frac{d\theta_{k\tilde{q}}}{2\pi} \int \frac{qdq}{2\pi} [(I_{+---} + I_{-+++})\Pi_0 + I_{+-+-}\Pi_{+-} + I_{-+-+}\Pi_{-+}], \tag{4.2.8b}$$

where $\Pi_0 = \Pi_{++} = \Pi_{--}$.

As we explained in Section 4.2.1, the quaternions in Equations (4.2.8a) and (4.2.8b) contain $\tilde{q}$ only in combination with q_α. Therefore, for $q \ll q_\alpha$, the leading term is obtained by simply setting $\tilde{q} = 0$, upon which the remaining integrals can be readily calculated. The results are given by Equations (C.1.7) and (C.1.8), so that

$$\chi^{zz}_{1,q=0} = u_0^2 \chi_0 \frac{|\alpha| k_F}{3E_F} \tag{4.2.9a}$$

and

$$\chi^{zz}_{1,q=2k_F} = u^2_{2k_F} \chi_0 \frac{|\alpha| k_F}{3E_F}. \tag{4.2.9b}$$

In fact, it is shown in Appendix C.2 that Equations (4.2.9a) and (4.2.9b) hold for any $q \leq q_\alpha$ rather than only for $\tilde{q} = 0$.

Diagram 1: in-plane component

The in-plane component of the spin susceptibility differs substantially from its out-of-plane counterpart due the angular dependence of the traces a^{ij}_{lmnr} and $\tilde{a}^{ij}_{lmsr}$ which, for the in-plane case, read as

$$\begin{aligned} a^{xx}_{lmnr} &= \tfrac{1}{8}\left[1 + mr + n(m+r) - l(m+n+r+mnr)\cos 2\theta_k\right] \\ \tilde{a}^{xx}_{lmsr} &= \tfrac{1}{8}\left[1 + mr - s(m+r) + l(s-m-r+mrs)\cos 2\theta_k\right]. \end{aligned}$$

(For the sake of convenience, we choose the x axis to be perpendicular to $\tilde{\mathbf{q}}$ when calculating all diagrams for χ^{xx}.) Summing over the Rashba indices, one arrives at

$$\begin{aligned} \chi^{xx}_{1,q=0} =& 4U^2(0) \int \frac{d\Omega}{2\pi} \int \frac{d\theta_{k\tilde{q}}}{2\pi} \int \frac{q dq}{2\pi} \\ & \times [\sin^2\theta_{k\tilde{q}} (I_{+---} + I_{-+++})\Pi_0 \\ & + \cos^2\theta_{k\tilde{q}} (I_{++++} + I_{----})\Pi_0] \end{aligned} \tag{4.2.10a}$$

and

$$\begin{aligned} \chi^{xx}_{1,q=2k_F} =& 2U^2(2k_F) \int \frac{d\Omega}{2\pi} \int \frac{d\theta_{k\tilde{q}}}{2\pi} \int \frac{q dq}{2\pi} \\ & \times [\sin^2\theta_{k\tilde{q}} (I_{+---} + I_{-+++})\Pi_0 \\ & + \cos^2\theta_{k\tilde{q}} (I_{++++} + I_{----})\Pi_0 \\ & + \sin^2\theta_{k\tilde{q}} (I_{+-+-}\Pi_{+-} + I_{-+-+}\Pi_{-+}) \\ & + \cos^2\theta_{k\tilde{q}} (I_{++-+}\Pi_{-+} + I_{--+-}\Pi_{+-})]. \end{aligned} \tag{4.2.10b}$$

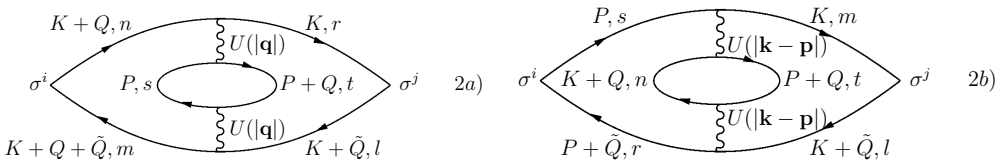

Figure 4.3: Diagram 2. Left: small-momentum transfer part. Right: $2k_F$-momentum transfer part.

Details of the calculation are given in Appendix. C.1.2; here we present only the results in the interval $\tilde{q} \leq q_\alpha$:

$$\begin{aligned} \chi^{xx}_{1,q=0} &= \frac{1}{2}\chi^{zz}_{1,q=0} + u_0^2\chi_0\frac{2}{9\pi}\frac{v_F\tilde{q}}{E_F} \\ &= u_0^2\chi_0\left(\frac{|\alpha|k_F}{6E_F} + \frac{2}{9\pi}\frac{v_F\tilde{q}}{E_F}\right) \qquad (4.2.11a) \\ \chi^{xx}_{1,q=2k_F} &= \frac{1}{2}\chi^{zz}_{1,q=2k_F} + u_{2k_F}^2\chi_0\frac{2}{9\pi}\frac{v_F\tilde{q}}{E_F} \\ &= u_{2k_F}^2\chi_0\left(\frac{|\alpha|k_F}{6E_F} + \frac{2}{9\pi}\frac{v_F\tilde{q}}{E_F}\right). \qquad (4.2.11b) \end{aligned}$$

Notice that the linear-in-$\tilde{q}$ dependence survives in the in-plane component of the spin susceptibility even for $\tilde{q} \leq q_\alpha$. Similar behavior was found in [Żak10a] for the temperature dependence of the uniform spin susceptibility in the presence of the SOI.

4.2.2 Diagram 2

Diagram 2, shown in Figure 4.3, is a vertex correction to the spin susceptibility. As in the previous case, there are two regions of momentum transfers relevant for the non-analytic behavior of the spin susceptibility: the $q = 0$ region, where

$$\begin{aligned} \chi^{ij}_{2,q=0} =& U^2(0)\int_Q\int_K\int_P \mathrm{Tr}[G(P)G(P+Q)] \\ &\times \mathrm{Tr}[G(K+\tilde{Q})G(K+Q+\tilde{Q})\sigma^i G(K+Q)G(K)\sigma^j], \qquad (4.2.12a) \end{aligned}$$

and the $2k_F$-region, where

$$\begin{aligned} \chi^{ij}_{2,q=2k_F} =& U^2(2k_F)\int_Q\int_K\int_P \mathrm{Tr}[G(K+Q)G(P+Q)] \\ &\times \mathrm{Tr}[G(K+\tilde{Q})G(P+\tilde{Q})\sigma^i G(P)G(K)\sigma^j]. \qquad (4.2.12b) \end{aligned}$$

Explicitly,

$$\begin{aligned} \chi^{ij}_{2,q=0} =& U^2(0)\int\frac{d\Omega}{2\pi}\int\frac{d\theta_{k\tilde{q}}}{2\pi}\int\frac{qdq}{2\pi}c^{ij}_{lmnr}b_{st} \\ &\times J_{lmnr}(\Omega,\theta_{k\tilde{q}},q,\tilde{q})\Pi_{st}(\Omega,q), \qquad (4.2.13a) \end{aligned}$$

$$\chi^{ij}_{2,q=2k_F} = U^2(2k_F)\int\frac{d\Omega}{2\pi}\int\frac{d\theta_{k\tilde{q}}}{2\pi}\int\frac{qdq}{2\pi}\tilde{c}^{ij}_{lrsm}\tilde{b}_{nt} \times I_{lmn}(\Omega,\theta_{k\tilde{q}},q,\tilde{q})I_{rst}(\Omega,\theta_{k\tilde{q}},q,-\tilde{q}), \tag{4.2.13b}$$

where

$$c^{ij}_{lmnr} \equiv \mathrm{Tr}[\Omega_l(\mathbf{k})\Omega_m(\mathbf{k})\sigma^i\Omega_n(\mathbf{k})\Omega_r(\mathbf{k})\sigma^j], \tag{4.2.14a}$$

$$\tilde{c}^{ij}_{lrsm} \equiv \mathrm{Tr}[\Omega_l(\mathbf{k})\Omega_r(-\mathbf{k})\sigma^i\Omega_s(-\mathbf{k})\Omega_m(\mathbf{k})\sigma^j], \tag{4.2.14b}$$

$$J_{lmnr}(\Omega,\theta_{k\tilde{q}},q,\tilde{q}) \equiv \int\frac{d\theta_{kq}}{2\pi}\int\frac{d\omega_p}{2\pi}\int\frac{d\epsilon_k}{2\pi} \times g_l(\omega_k+\Omega,\mathbf{k}+\mathbf{q})g_m(\omega_k+\Omega,\mathbf{k}+\mathbf{q}+\tilde{\mathbf{q}}) \times g_n(\omega_k+\Omega,\mathbf{k}+\mathbf{q})g_r(\omega_k,\mathbf{k}), \tag{4.2.14c}$$

$$I_{lmn}(\Omega,\theta_{k\tilde{q}},q,\tilde{q}) \equiv \int\frac{d\theta_{kq}}{2\pi}\int\frac{d\omega_p}{2\pi}\int\frac{d\epsilon_k}{2\pi} \times g_l(\omega_k,\mathbf{k}+\tilde{\mathbf{q}})g_m(\omega_k,\mathbf{k})g_n(\omega_k+\Omega,\mathbf{k}+\mathbf{q}), \tag{4.2.14d}$$

As before, summation over the Rashba is implied. Integrals (4.2.14c) and (4.2.14d) are derived in Appendix C.1.

Traces entering the $q = 0$ part of the out-of-plane and in-plane components are evaluated as

$$\begin{aligned} c^{zz}_{lmnr} &= \frac{1+nr-m(n+r)+l(m-n-r+mnr)}{8}, \\ c^{xx}_{lmnr} &= \frac{(1+lm)(1+nr)+(l+m)(n+r)\cos 2\theta_{k\tilde{q}}}{8}. \end{aligned} \tag{4.2.15}$$

Summing over the Rashba indices and using the symmetry properties of I_{lmnr} and J_{lmnr}, it can be shown that the $q = 0$ parts of diagrams 1 and 2 cancel each other

$$\chi^{ij}_{2,q=0} = -\chi^{ij}_{1,q=0}, \tag{4.2.16}$$

which is also the case in the absence of the SOI [Chubukov03]. Therefore, we only need to calculate the $2k_F$-part of diagram 2.

Diagram 2: out-of-plane component

Summation over the Rashba indices with the coefficient $\tilde{c}^{zz}_{lrsm} = [1+mr-s(m+r)+l(s-r-m+mrs)]/8$ for the out-of-plane part gives

$$\chi^{zz}_{2,q=2k_F} = U^2(2k_F)\int\frac{d\Omega}{2\pi}\int\frac{d\theta_{k\tilde{q}}}{2\pi}\int\frac{qdq}{2\pi} \times [I_{+-+}(\Omega,\theta_{k\tilde{q}},q,\tilde{q})I_{-+-}(\Omega,\theta_{k\tilde{q}},q,-\tilde{q}) + I_{+--}(\Omega,\theta_{k\tilde{q}},q,\tilde{q})I_{-++}(\Omega,\theta_{k\tilde{q}},q,-\tilde{q}) + (\tilde{q}\to-\tilde{q})], \tag{4.2.17}$$

where $(\tilde{q} \to -\tilde{q})$ stands for the preceding terms with an opposite sign of momentum. Integrating over $\mathbf{q}$ and Ω at $\tilde{q} = 0$, yields [cf. Equation (C.1.9)],

$$\chi^{zz}_{2,q=2k_F} = u^2_{2k_F}\chi_0 \frac{|\alpha|k_F}{3E_F}. \tag{4.2.18}$$

Again, an exact calculation at finite $\tilde{q}$ proves that this results holds for any $\tilde{q} \leq q_\alpha$.

Diagram 2: in-plane component

The in-plane component comes with a Rashba coefficient $\tilde{c}^{zz}_{lmsr} = [(1-lr)(1-ms)(l-r)(m-s)\cos 2\theta_{k\tilde{q}}]/8$, such that

$$\begin{aligned}
\chi^{xx}_{2,q=2k_F} &= U^2(2k_F)\int\frac{d\Omega}{2\pi}\int\frac{d\theta_{k\tilde{q}}}{2\pi}\int\frac{qdq}{2\pi} \\
&\times \{\sin^2\theta_{k\tilde{q}}[I_{+-+}(\Omega,\theta_{k\tilde{q}},q,\tilde{q})I_{-+-}(\Omega,\theta_{k\tilde{q}},q,-\tilde{q}) \\
&+ I_{+--}(\Omega,\theta_{k\tilde{q}},q,\tilde{q})I_{-++}(\Omega,\theta_{k\tilde{q}},q,-\tilde{q})] \\
&+ \cos^2\theta_{k\tilde{q}}[I_{+++}(\Omega,\theta_{k\tilde{q}},q,\tilde{q})I_{---}(\Omega,\theta_{k\tilde{q}},q,-\tilde{q}) \\
&+ I_{++-}(\Omega,\theta_{k\tilde{q}},q,\tilde{q})I_{--+}(\Omega,\theta_{k\tilde{q}},q,-\tilde{q})] \\
&+ (\tilde{q}\to-\tilde{q})\}.
\end{aligned} \tag{4.2.19}$$

The first part, proportional to $\sin^2\theta_{k\tilde{q}}$, contains the SOI coupling α. In this part, $\tilde{q}$ can be set to zero, and the resulting linear-in-$|\alpha|$ part equals half of that for the out-of-plane component due to the integral over $\sin^2\theta_{k\tilde{q}}$. On the other hand, in the term proportional to $\cos^2\theta_{k\tilde{q}}$, the dependence on $|\alpha|$ drops out upon integration over q, and the final result for $\tilde{q} \leq q_\alpha$ reads as [cf. see Equation (C.1.12)]

$$\begin{aligned}
\chi^{xx}_{2,q=2k_F} &= \frac{1}{2}\chi^{zz}_{2,q=2k_F} + u^2_{2k_F}\chi_0\frac{2}{9\pi}\frac{v_F\tilde{q}}{E_F} \\
&= u^2_{2k_F}\chi_0\left(\frac{|\alpha|k_F}{6E_F} + \frac{2}{9\pi}\frac{v_F\tilde{q}}{E_F}\right).
\end{aligned} \tag{4.2.20}$$

4.2.3 Diagrams 3 and 4

We now turn to "Aslamazov-Larkin" diagrams, Figure 4.4, which represent interaction via fluctuational particle-hole pairs. Without SOI, these diagrams are identically equal to zero because the spin vertices are averaged independently and thus vanish. With SOI, this argument does not hold because the Green's functions now also contain Pauli matrices and, in general, diagrams 3 and 4 do not vanish identically. Nevertheless, we show here the non-analytic parts of diagrams 2 and 3 are still equal to zero.

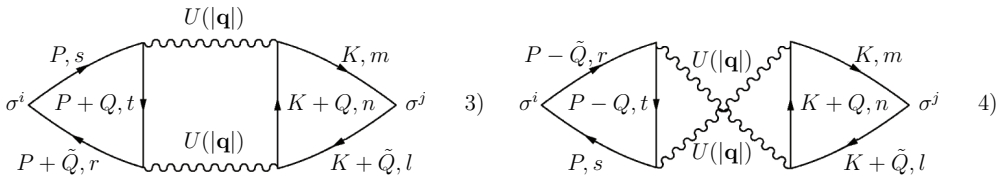

Figure 4.4: Left: diagram 3. Right: diagram 4. The momentum transfer q in both diagrams can be either small or close to $2k_F$.

Diagrams 3 and 4 correspond to the following analytical expressions:

$$\chi_3^{ij} = \int_Q \int_K \int_P U^2(|\mathbf{q}|)\mathrm{Tr}[G(P-\tilde{Q})G(P-Q)G(P)\sigma^i] \times \mathrm{Tr}[G(K+\tilde{Q})G(K+Q)G(K)\sigma^j], \tag{4.2.21a}$$

$$\chi_3^{ij} = \int_Q \int_K \int_P U^2(|\mathbf{q}|)\mathrm{Tr}[G(P)G(P+Q)G(P+\tilde{Q})\sigma^i] \times \mathrm{Tr}[G(K+\tilde{Q})G(K+Q)G(K)\sigma^j]. \tag{4.2.21b}$$

Note that the second trace is the same in both diagrams. In what follows, we prove that

$$\chi_3^{ij} = \chi_4^{ij} = 0 \tag{4.2.22}$$

for both small and large momentum transfer q.

Diagrams 3 and 4: out-of-plane components

The out-of-plane case is straightforward. Evaluating the second traces in Equations (4.2.21a) and (4.2.21b), one finds that they vanish:

$$d^z_{lnm} \equiv \mathrm{Tr}[\Omega_l(\mathbf{k})\Omega_n(\mathbf{k})\Omega_m(\mathbf{k})\sigma^z] = 0, \tag{4.2.23}$$

for the $q = 0$ case, and

$$\tilde{d}^z_{lnm} \equiv \mathrm{Tr}[\Omega_l(\mathbf{k})\Omega_n(-\mathbf{k})\Omega_m(\mathbf{k})\sigma^z] = 0, \tag{4.2.24}$$

for the $q = 2k_F$ case. Therefore, $\chi_3^{zz} = \chi_4^{zz} = 0$.

Diagrams 3 and 4: in-plane components

For the in-plane part of the spin susceptibility, the proof is more complicated as the traces do not vanish on their own. To calculate the $q = 0$ part, we need the following two objects

$$\begin{aligned} d^x_{lnm} &\equiv \mathrm{Tr}[\Omega_l(\mathbf{k})\Omega_n(\mathbf{k})\Omega_m(\mathbf{k})\sigma^x] \\ &= \cos\theta_{k\tilde{q}}(l+m+n+lmn)/4 \end{aligned} \tag{4.2.25}$$

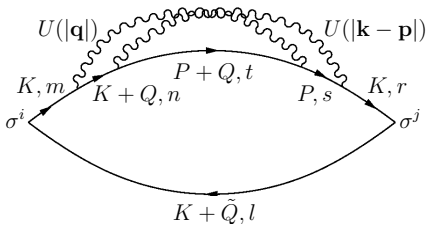

Figure 4.5: Diagram 5. The momentum transfer q is close to zero and $|\mathbf{k}-\mathbf{p}| = 2k_F$.

and

$$\begin{aligned} I'_{lmn}(\Omega,\theta_{k\tilde{q}},q,\tilde{q}) \equiv \frac{m^*}{2\pi}\int d\omega_k \int d\epsilon_k g_l(\omega_k,\mathbf{k}+\tilde{\mathbf{q}}) \\ \times g_m(\omega_k,\mathbf{k}) g_n(\omega_k+\Omega,\mathbf{k}+\mathbf{q}) \\ = \frac{im^*\Omega}{i\Omega - v_F q\cos\theta_{kq} + v_F\tilde{q}\cos\theta_{k\tilde{q}} + (l-n)\alpha k_F} \\ \times \frac{1}{i\Omega - v_F q\cos\theta_{kq} + (m-n)\alpha k_F}. \end{aligned} \tag{4.2.26}$$

The prime over I denotes that integration over the angle θ_{kq} is not yet performed as compared to $I_{lmn}(\Omega,\theta_{k\tilde{q}},q,\tilde{q})$ defined by Equation (4.2.14d).

Summing over the Rashba indices, one finds

$$\sum_{lmn} d^x_{lnm} I'_{lmn}(\Omega,\theta_{k\tilde{q}},q,\tilde{q}) = 0 \tag{4.2.27}$$

and, therefore, the in-plane component at small momentum transfer vanishes.

The trace for the $q = 2k_F$ case turns out to be the same as for the $q = 0$ one

$$\tilde{d}^x_{lnm} \equiv \mathrm{Tr}[\Omega_l(\mathbf{k})\Omega_n(-\mathbf{k})\Omega_m(\mathbf{k})\sigma^x] = d^x_{lnm}. \tag{4.2.28}$$

However, in order to see the vanishing of the $2k_F$ part, the integral over ϵ_k has to be evaluated explicitly with $q = 2k_F$, i.e.,

$$\begin{aligned} I''_{lmn}(\Omega,\theta_{k\tilde{q}},q=2k_F,\tilde{q}) = \frac{m^*}{2\pi}\int d\epsilon_k g_l(\omega_k,\mathbf{k}+\tilde{\mathbf{q}}) g_m(\omega_k,\mathbf{k}) g_n(\omega_k+\Omega,\mathbf{k}+\mathbf{q}) \\ = \frac{im^*[1-\Theta(\omega_k)-\Theta(\omega_k+\Omega)]}{[i(2\omega_k+\Omega) - v_F\tilde{q}\cos\theta_{k\tilde{q}} - v_F q - 2v_F k_F\cos\theta_{kq} - (m+n)\alpha k_F][i(2\omega_k+\Omega) - v_F q - 2v_F k_F\cos\theta_{kq} -} \end{aligned} \tag{4.2.29}$$

where we used an expansion of $\epsilon_{\mathbf{k}+\mathbf{q}}$ around $q = 2k_F$: $\epsilon_{\mathbf{k}+\mathbf{q}} \approx -\epsilon_k + v_F(q-2k_F) + 2v_F k_F\cos\theta_{kq}$. Summing over the Rashba indices, we obtain

$$\sum_{lmn} \tilde{d}^x_{lnm} I''_{lmn}(q \approx 2k_F,\tilde{q}) = 0 \tag{4.2.30}$$

and, therefore, the $2k_F$ part of the in-plane components of diagrams 3 and 4 is also equal to zero.

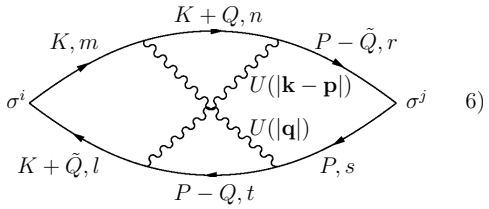

6)

Figure 4.6: Diagram 6. The momentum transfer q is close to zero and $|\mathbf{k}-\mathbf{p}| = 2k_F$.

4.2.4 Remaining diagrams and the final result for the spin susceptibility

The remaining diagrams can be expressed in terms of the diagrams we have already calculated.

Diagram 5 in Figure 4.5 reads as

$$\begin{aligned}\chi_5^{ij} =& -4U(0)U(2k_F)\int_Q\int_K\int_P \mathrm{Tr}[G(K+\tilde{Q})\sigma^i G(K)\\ &\times G(K+Q)G(P+Q)G(P)G(K)\sigma^j]\\ =& -4U(0)U(2k_F)\int\frac{d\Omega}{2\pi}\int\frac{d\theta_{k\tilde{q}}}{2\pi}\int\frac{qdq}{2\pi}f^{ij}_{lmntsr}I_{lmnr}\Pi_{st}\end{aligned} \tag{4.2.31}$$

with

$$\begin{aligned}f^{ij}_{lmntsr} \equiv& \mathrm{Tr}[\Omega_l(\mathbf{k})\sigma^i\Omega_m(\mathbf{k})\Omega_n(\mathbf{k})\\ &\times\Omega_t(-\mathbf{k})\Omega_s(-\mathbf{k})\Omega_r(\mathbf{k})\sigma^j]\end{aligned} \tag{4.2.32}$$

and $q \ll |\mathbf{k}-\mathbf{p}| = 2k_F$. A factor of 4 appears because the "sunrise" self-energy can be inserted into either the lower or the upper arm of the bubble while each of the interaction line can carry momentum of either $q = 0$ or $q = 2k_F$. A minus sign is due to an odd number of fermionic loops. Upon summation over the Rashba indices, we obtain

$$\frac{\chi_5^{ij}}{U(0)U(2k_F)} = -\frac{\chi^{ij}_{1,q=0}}{U^2(0)}. \tag{4.2.33}$$

Diagrams 6 and 7*b* in Figs. 4.6 and 4.7, correspondingly, are related as well. Explicitly, diagram 6 reads as

$$\begin{aligned}\chi_6^{ij} =& -2U(0)U(2k_F)\int_Q\int_K\int_P \mathrm{Tr}[G(K+\tilde{Q})\sigma^i G(K)\\ &\times G(K+Q)G(P-\tilde{Q})\sigma^j G(P)G(P-Q)]\\ =& -2U(0)U(2k_F)\int\frac{d\Omega}{2\pi}\int\frac{d\theta_{k\tilde{q}}}{2\pi}\int\frac{qdq}{2\pi}g^{ij}_{lmnrst}\\ &\times I_{lmn}(\Omega,\theta_{k\tilde{q}},q,\tilde{q})I_{rst}(-\Omega,\theta_{k\tilde{q}},-q,\tilde{q})\end{aligned} \tag{4.2.34}$$

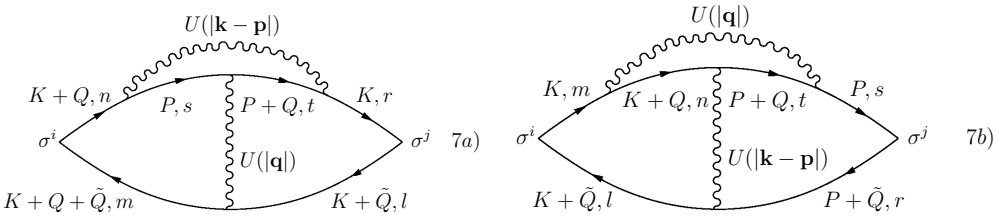

Figure 4.7: Diagram $5a$ (left figure) and diagram $5b$ (right figure). The transferred momenta are $q =$ and $|\mathbf{k}-\mathbf{p}| = 2k_F$.

with

$$g^{ij}_{lmntsr} \equiv \mathrm{Tr}[\Omega_l(\mathbf{k})\sigma^i\Omega_m(\mathbf{k})\Omega_n(\mathbf{k}) \times \Omega_r(-\mathbf{k})\sigma^j\Omega_s(-\mathbf{k})\Omega_t(-\mathbf{k})]. \tag{4.2.35}$$

On the other hand, for diagram $7b$ we obtain

$$\begin{aligned}\chi^{ij}_{7b} =& -2U(0)U(2k_F)\int_Q\int_K\int_P \mathrm{Tr}[G(K+\tilde{Q})\sigma^i G(K) \\ &\times G(K+Q)G(P+Q)G(P)\sigma^j G(P+\tilde{Q})] \\ =& -2U(0)U(2k_F)\int\frac{d\Omega}{2\pi}\int\frac{d\theta_{k\tilde{q}}}{2\pi}\int\frac{qdq}{2\pi}\tilde{h}^{ij}_{lmntsr} \\ &\times I_{lmn}(\Omega,\theta_{k\tilde{q}},q,\tilde{q})I_{rst}(\Omega,\theta_{k\tilde{q}},q,-\tilde{q})\end{aligned} \tag{4.2.36}$$

with

$$\tilde{h}^{ij}_{lmntsr} \equiv \mathrm{Tr}[\Omega_l(\mathbf{k})\sigma^i\Omega_m(\mathbf{k})\Omega_n(\mathbf{k}) \times \Omega_t(-\mathbf{k})\Omega_s(-\mathbf{k})\sigma^j\Omega_r(-\mathbf{k})]. \tag{4.2.37}$$

In both cases, $q \ll |\mathbf{k}-\mathbf{p}| = 2k_F$. Using the symmetry property$I_{rst}(-\Omega,\theta_{k\tilde{q}},-q,-\tilde{q}) = -I_{-r-s-t}(\Omega,\theta_{k\tilde{q}},q,\tilde{q})$ in χ^{ij}_4, summing over the Rashba indices, and noticing that $I_{+++}(\Omega,\theta_{k\tilde{q}},q,\tilde{q}) = I_{---}(\Omega,\theta_{k\tilde{q}},q,\tilde{q})$, we arrive at

$$\chi^{ij}_6 = \chi^{ij}_{7b}. \tag{4.2.38}$$

Finally, diagram $7a$ shown in Figure 4.7 is related to diagram 2 at small momentum transfer. Indeed,

$$\begin{aligned}\chi^{ij}_{7a} =& -2U(0)U(2k_F)\int_Q\int_K\int_P \mathrm{Tr}[G(K+Q+\tilde{Q})\sigma^i G(K+Q) \\ &\times G(P)G(P+Q)G(K)\sigma^j G(K+\tilde{Q})] \\ =& -2U(0)U(2k_F)\int\frac{d\Omega}{2\pi}\int\frac{d\theta_{k\tilde{q}}}{2\pi}\int\frac{qdq}{2\pi}h^{ij}_{lmnstr}J_{lmnr}\Pi_{st}\end{aligned} \tag{4.2.39}$$

with

$$h^{ij}_{lmnstr} \equiv \mathrm{Tr}[\Omega_l(\mathbf{k})\Omega_m(\mathbf{k})\sigma^i\Omega_n(\mathbf{k}) \times \Omega_s(-\mathbf{k})\Omega_t(-\mathbf{k})\Omega_r(\mathbf{k})\sigma^j], \tag{4.2.40}$$

where again $q \ll |\mathbf{k}-\mathbf{p}| = 2k_F$. After summation over the Rashba indices, this diagram proves related to the small-momentum part of diagram 2 as

$$\frac{\chi^{ij}_{5a}}{U(0)U(2k_F)} = -\frac{\chi^{ij}_{2,q=0}}{U^2(0)}. \tag{4.2.41}$$

The results of this section along with Equation (4.2.16) show that the sum of all diagrams proportional to $U(0)U(2k_F)$ cancel each other

$$\chi^{ij}_5 + \chi^{ij}_6 + \chi^{ij}_{7a} + \chi^{ij}_{7b} = 0. \tag{4.2.42}$$

Therefore, as in the absence of SOI, the non-analytic part of the spin susceptibility is determined only by the Kohn anomaly at $q = 2k_F$.

Summing up the contributions from diagrams $1-3$, we obtain the results presented in Equations (4.1.7a) and (4.1.7b).

4.2.5 Cooper-channel renormalization to higher orders in the electron-electron interaction

An important question is how the second-order results, obtained earlier in this Section, are modified by higher-order effects. In the absence of SOI, the most important effect–at least within the weak-coupling approach– is logarithmic renormalization of the second-order result by to the interaction in the Cooper channel. As it was shown in [Chesi09], this effect reverses the sign of the $\tilde{q}$ dependence due to proximity to the Kohn-Luttinger superconducting instability; the sign reversal occurs at $\tilde{q} = e^2 T_{KL}/v_F \approx 7.4 T_{KL}/v_F$, where T_{KL} is the Kohn-Luttinger critical temperature. For momenta below the SO scale (q_α), χ^{zz} ceases to depend on $\tilde{q}$ but χ^{xx} still scales linearly with $\tilde{q}$. What is necessary to understand now is whether the linear-in-$\tilde{q}$ term in χ^{xx} renormalized in the Cooper channel. The answer to this question is quite natural. The $|\alpha|$- and $\tilde{q}$ terms in the second-order result for χ^{xx} [Equation (4.1.7b)] come from different parts of diagram: the $|\alpha|$ term comes from $\tilde{q}$ independent part and vice versa. Starting from the third order and beyond, these two terms acquire logarithmic renormalizations but the main logarithm of these renormalizations contains only one energy scale. In other words, the $|\alpha|$ term is renormalized via $\ln|\alpha|$ while the $\tilde{q}$ is renormalized via $\ln\tilde{q}$. For example, the third-order result for the $2k_F$ part of diagram 1 (Figure 4.2) reads as (for simplicity, we assume here a contact interaction with $U(q) = \mathrm{const}$)

$$\chi^{xx}_{1,q=2k_F} = -u^3 \frac{2\chi_0}{3}\left[\frac{|\alpha|k_F}{E_F}\ln\frac{\Lambda}{|\alpha|k_F} + \frac{2}{3\pi}\frac{v_F\tilde{q}}{E_F}\ln\frac{\Lambda}{v_F\tilde{q}}\right], \tag{4.2.43}$$

where $u = m^*U/4\pi$ and Λ is the ultraviolet cutoff. Details of this calculation are given in Appendix C.3. It is clear already from this result the logarithmic renormalization of the $\tilde{q}$ term in χ^{xx} remains operational even for $\tilde{q} < q_\alpha$, with consequences similar to those in [Chesi09].

4.2.6 Charge susceptibility

In the absence of SOI, non-analytic behavior as a function of external parameters–$\tilde{q}$, T, H–is present only in the spin but not charge susceptibility [Belitz97, Chitov01b, Chubukov03]. An interesting question is whether the charge susceptibility also becomes non-analytic in the presence of SOI. We answer this question in the negative: the charge susceptibility remains analytic. To show this, we consider all seven diagrams replacing both spin vertices by unities. The calculation goes along the same lines as before, thereby we only list the results for specific diagrams; for $\tilde{q} \ll q_\alpha$,

$$\begin{aligned}
\delta\chi_1^c &= -\delta\chi_4^c = \frac{\chi_0}{3\pi}\left(u_0^2 + u_{2k_F}^2\right)\frac{v_F\tilde{q}}{E_F}, \\
\delta\chi_2^c &= -\delta\chi_3^c = \frac{\chi_0}{3\pi}\left(u_{2k_F}^2 - u_0^2\right)\frac{v_F\tilde{q}}{E_F}, \\
\delta\chi_5^c &= -\delta\chi_6^c = -\frac{\chi_0}{3\pi}u_0 u_{2k_F}\frac{v_F\tilde{q}}{E_F},
\end{aligned} \tag{4.2.44}$$

whereas $\chi_7^c = 0$ on its own ($\chi_{7a}^c = -\chi_{7b}^c$). First, we immediately notice that SOI drops out from every diagram even in the limit $\tilde{q} \ll q_\alpha$. Second, the sum of the non-analytic parts of all the charge susceptibility diagrams is zero, $\delta\chi^c = 0$, as in the case of no SOI.

4.3 RKKY interaction in real space

A nonanalytic behavior of the spin susceptibility in the momentum space leads to a power-law decrease of the RKKY interaction with distance. In this Section, we discuss the relation between various nonanalyticities in $\chi^{ij}(q)$ and the real-space behavior of the RKKY interaction. We show that, in addition to conventional $2k_F$ Friedel oscillations, a combination of the electron-electron and SO interactions lead to a new effect: long-range Friedel-like oscillations with the period given by the SO length.

4.3.1 No spin-orbit interaction

First, we discuss the case of no SOI, when the spin susceptibility is isotropic: $\chi^{ij}(\tilde{q}) = \delta_{ij}\chi(\tilde{q})$. For free electrons, the only non-analyticity in $\chi_0(\tilde{q})$ is the Kohn anomaly at $\tilde{q} = 2k_F$, which translates into Friedel oscillations of the RKKY kernel; in 2D, and for

$k_F r \gg 1$ [Żak10a],

$$\chi_0(r) = \frac{\chi_0}{2\pi} \frac{\sin(2k_F r)}{r^2}. \tag{4.3.1}$$

One effect of the electron-electron interaction is a logarithmic amplification of the Kohn anomaly (which also becomes symmetric about the $\tilde{q} = 2k_F$ point): $\chi(\tilde{q} \approx 2k_F) \propto \sqrt{|\tilde{q} - 2k_F|} \ln|\tilde{q} - 2k_F|$ [Khalil02]. Consequently, $\chi(r)$ is also enhanced by logarithmic factor compared to the free-electron case: $\chi(r) \propto \sin(2k_F r) \ln(k_F r)/r^2$.

Another effect is related to the nonanalyticity at small $\tilde{q}$: $\chi(\tilde{q}) = \chi_0 + C\tilde{q}$ [Chubukov03]. To second order in the electron-electron interaction [cf. Equation (4.1.8)],

$$C_2 = \frac{4\chi_0}{3\pi k_F} u_{2k_F}^2; \tag{4.3.2}$$

however, as we explained in Section 4.1, both the magnitude and sign of C can changed due to higher-order effects. (Cooper channel renormalization leads also to multiplicative $\ln\tilde{q}$ corrections to the linear-in-$\tilde{q}$ term; those correspond to multiplicative $\ln r$ renormalization of the real-space result and are ignored here.)

In 2D, $\chi(r)$ is related to $\chi(\tilde{q})$ via

$$\chi(r) = \frac{1}{2\pi} \int_0^\infty d\tilde{q}\tilde{q}\chi(\tilde{q}) J_0(\tilde{q}r). \tag{4.3.3}$$

Power-counting suggests that the $\tilde{q}$ term in $\chi(\tilde{q})$ translates into a dipole-dipole–like, $1/r^3$ term in $\chi(r)$. To see if this indeed the case, we calculate the integral

$$A = \int_0^\Lambda d\tilde{q}\tilde{q}^2 J_0(\tilde{q}r) \tag{4.3.4}$$

with an arbitrary cutoff Λ, and search for a universal, Λ-independent term in the result. If such a term exists, it corresponds to a long-range component of the RKKY interaction. Using an identity $xJ_0(x) = \frac{d}{dx}(xJ_1(x))$ and integrating by parts, we obtain

$$A = \frac{1}{r^3}\left[(\Lambda r)^2 J_1(\Lambda r) - \int_0^{\Lambda r} dx x J_1(x)\right] = \frac{1}{r^3}\left[(\Lambda r)^2 J_1(\Lambda r) - \frac{\pi\Lambda r}{2}\{J_1(\Lambda r)\mathbf{H}_0(\Lambda r) - J_0(\Lambda r)\mathbf{H}_1(\Lambda r)\}\right], \tag{4.3.5}$$

where $\mathbf{H}_\nu(x)$ is the Struve function. The asymptotic expansion of the last term in the preceding equation indeed contains a universal term

$$\frac{\pi\Lambda r}{2}\{J_1(\Lambda r)\mathbf{H}_0(\Lambda r) - J_0(\Lambda r)\mathbf{H}_1(\Lambda r)\}\big|_{\Lambda r\to\infty} = 1 + \ldots \tag{4.3.6}$$

where $\ldots$ stands for non-universal terms. A corresponding term in $\chi(r)$ reads

$$\chi(r) = -\frac{C}{2\pi r^3}. \tag{4.3.7}$$

As a check, we also calculate the Fourier transform of the $\tilde{q}$-independent term in χ^{ij}. The corresponding integral

$$\tilde{A} = \int_0^\Lambda d\tilde{q}\tilde{q}J_0(\tilde{q}r) = \frac{\Lambda}{r}J_1(\Lambda r). \tag{4.3.8}$$

does not contain a Λ-independent term and, therefore, a constant term in $\chi(\tilde{q})$ does not produce a long-range component of the RKKY interaction, which is indeed the case for free electrons.

Equation (4.3.7) describes a dipole-dipole–like part of the RKKY interaction that falls off faster than Friedel oscillations but is not oscillatory. Incidentally, it is the same behavior as that of a screened Coulomb potential in 2D, which also has a $\tilde{q}$ nonanalyticity at small $\tilde{q}$ [Ando82].

In a translationally invariant system, $H_{\mathrm{RKKY}} = -\frac{A^2}{8n_s^2}\sum_{\mathbf{r},\mathbf{r}'}\chi(r-r')I^i_{\mathbf{r}}I^j_{\mathbf{r}'}$. Therefore, if $C > 0$, i.e., $\chi(\tilde{q})$ increases with $\tilde{q}$, the dipole-dipole interaction is repulsive for parallel nuclear spins and attractive for antiparallel ones. Since the $1/r^3$ behavior sets in only at large distances, the resulting phase is a helimagnet rather than an antiferromagnet. Vice versa, if $C < 0$, the dipole-dipole interaction is attractive for parallel spins. This corresponds precisely to the conclusions drawn from the spin-wave theory: a stable FM phase requires that $\omega(\tilde{q}) > 0$, which is the case if $C < 0$.

4.3.2 With spin-orbit interaction

4.3.3 Free electrons

In a free electron system, the SOI splits the Fermi surface into two surfaces corresponding to two branches of the Rashba spectrum with opposite helicities. Consequently, both components of the spin susceptibility in the momentum space have two Kohn anomalies located at momenta $2k_F^{\pm} = 2k_F \mp q_\alpha$ with $q_\alpha = 2m^*|\alpha|$. To see this explicitly, we evaluate the diagonal components of $\chi^{ij}(\tilde{q})$ for $\tilde{q} \approx 2k_F$

$$\chi_0^{ii}(\tilde{q}) = -\sum_{s,t}\int_K \left|\langle \mathbf{k},\mathbf{s}|\sigma^i|\mathbf{k}+\tilde{\mathbf{q}},t\rangle\right|^2 g_t(\omega,\mathbf{k}+\tilde{\mathbf{q}})\, g_s(\omega,\mathbf{k}). \tag{4.3.9}$$

For $\tilde{q} \approx 2k_F$, the matrix elements of the spin operators in the helical basis reduce to

$$|\langle \mathbf{k}+\tilde{\mathbf{q}},t|\sigma^x|\mathbf{k},\mathbf{s}\rangle|^2 = |\langle \mathbf{k}+\tilde{\mathbf{q}},t|\sigma^z|\mathbf{k},\mathbf{s}\rangle|^2 = \frac{1}{2}(1+st). \tag{4.3.10}$$

Therefore, $\chi^{ii}(\tilde{q})$ contains only contributions from intraband transitions

$$\begin{aligned}\chi_0^{xx}(\tilde{q}) &= \chi^{zz}(\tilde{q}) = -\int_K g_+(\omega,\mathbf{k}+\tilde{\mathbf{q}})\, g_+(\omega,\mathbf{k}) \\ &\quad -\int_K g_-(\omega,\mathbf{k}+\tilde{\mathbf{q}})\, g_-(\omega,\mathbf{k}).\end{aligned} \tag{4.3.11}$$

Each of the two terms in Equation (4.3.11) has its own Kohn anomaly at $\tilde{q} = 2k_F^s$, $s = \pm$. In real space, this corresponds to beating of Friedel oscillations with a period $2\pi/q_\alpha$.

This behavior needs to be contrasted with that of Friedel oscillations in the charge susceptibility, where–to leading order in α–the Kohn anomaly is present only at twice the Fermi momenta in the absence of SOI [Pletyukhov06]. Consequently, the period of Friedel oscillations is the same as in the absence of SOI. (Beating occurs in the presence of both Rashba and Dresselhaus interactions [Badalyan10]. This is so because, for $\tilde{q}$ near $2k_F$, the matrix element entering $\chi^c(\tilde{q})$ reduces to

$$|\langle \mathbf{k}+\tilde{\mathbf{q}}, t|\mathbf{k}, \mathbf{s}\rangle|^2 = \frac{1}{2}(1 - st),$$

which implies that χ^c contains only contributions from interband transitions:

$$\chi_0^c(\tilde{q}) = -2\int_K g_+(\omega, \mathbf{k}+\tilde{\mathbf{q}})\, g_-(\omega, \mathbf{k}). \tag{4.3.12}$$

The Kohn anomaly in χ_0^c corresponds to the nesting condition $\epsilon^+_{\mathbf{k}+\tilde{\mathbf{q}}} = -\epsilon^-_{\mathbf{k}}$, which is satisfied only for $\tilde{q} = 2k_F$.

Interacting electrons

The electron-electron interaction is expected to affect the $2k_F$-Kohn anomalies in χ^{xx} and χ^{zz} in a way similar to that in the absence of SOI. However, a combination of the electron-electron and SO interaction leads to a new effect: a Kohn anomaly at the momentum $q_\alpha \ll 2k_F$. Consequently, the RKKY interaction contains a component which oscillates with a long period given by the SO length $\lambda_{SO} = 2\pi/q_\alpha$ rather than the half of the Fermi wavelength.

To second order in the electron-electron interaction, the full dependence of the electron spin susceptibility on the momentum is shown in Appendix C.2 to be given by

$$\begin{aligned}\delta\chi^{xx}(\tilde{q}) =& \frac{2C_2\tilde{q}}{3} + \frac{C_2\tilde{q}}{2}\,\mathrm{Re}\left[\frac{1}{3}\sqrt{1-\left(\frac{q_\alpha}{\tilde{q}}\right)^2}\left(2+\left(\frac{q_\alpha}{\tilde{q}}\right)^2\right)\right.\\ &\left. + \frac{q_\alpha}{\tilde{q}}\arcsin\frac{q_\alpha}{\tilde{q}}\right], \end{aligned}\tag{4.3.13a}$$

$$\delta\chi^{zz}(\tilde{q}) = C_2\tilde{q}\,\mathrm{Re}\left[\sqrt{1-\left(\frac{q_\alpha}{\tilde{q}}\right)^2} + \frac{q_\alpha}{\tilde{q}}\arcsin\frac{q_\alpha}{\tilde{q}}\right]. \tag{4.3.13b}$$

Equations (4.3.13a) and (4.3.13b) are valid for an arbitrary value of the ratio $\tilde{q}/q_\alpha$ (but for $\tilde{q} \ll k_F$). For $\tilde{q} \gg q_\alpha$, both $\delta\chi^{xx}$ and $\delta\chi^{zz}$ scale as $\tilde{q}$. For $\tilde{q} \ll q_\alpha$, $\delta\chi^{xx}$ continues to scale as $\tilde{q}$ (but with a smaller slope compared to the opposite case), while $\delta\chi^{zz}$ is $\tilde{q}$

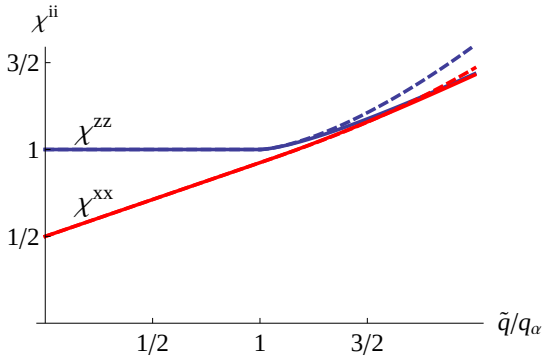

Figure 4.8: (color online) The nonanalytic part of the electron spin susceptibility in units of $(2/3\pi)u^2_{2k_F}(|\alpha|/v_F)\chi_0$ as a function of the momentum in units of $q_\alpha = 2m^*|\alpha|$. $i = x, z$. Solid: exact results (4.3.13a) and (4.3.13b). Dashed: approximate results (4.3.14a) and (4.3.14b) valid near the singularity at $q = q_\alpha$.

independent. The crossover between the two regimes is not continuous, however: certain derivatives of both $\delta\chi^{xx}$ and $\delta\chi^{zz}$ diverge at $\tilde{q} = q_\alpha$. Expanding around the singularity at $\tilde{q} = q_\alpha$, one finds

$$\delta\chi^{xx} = \frac{2C_2\tilde{q}}{3} + \frac{\tilde{C}_2}{2}\Big[\Theta(q_\alpha - \tilde{q}) + \Theta(\tilde{q} - q_\alpha)\Big(1 + \frac{2b}{5}\Big(\frac{\tilde{q}}{q_\alpha} - 1\Big)^{5/2}\Big)\Big], \tag{4.3.14a}$$

$$\delta\chi^{zz} = \tilde{C}_2\Big[\Theta(q_\alpha - \tilde{q}) + \Theta(\tilde{q} - q_\alpha)\Big(1 + b\Big(\frac{\tilde{q}}{q_\alpha} - 1\Big)^{3/2}\Big)\Big], \tag{4.3.14b}$$

where $\Theta(x)$ is the step-function, $\tilde{C}_2 = \pi C_2 q_\alpha/2$ and $b = 4\sqrt{2}/3\pi$. The $\tilde{q}$ dependencies of $\delta\chi^{xx}$ and $\delta\chi^{zz}$ are shown in Figure 4.8.

The singularity is stronger in $\delta\chi^{zz} \propto (\tilde{q} - q_\alpha)^{3/2}$ whose second derivative diverges at $\tilde{q} = q_\alpha$, whereas it is only third derivative of $\delta\chi^{xx} \propto (\tilde{q} - q_\alpha)^{5/2}$ that diverges at this point. Both divergences are weaker than the free-electron Kohn anomaly $\chi \propto (\tilde{q} - 2k_F)^{1/2}$.

We now derive the real-space form of the RRKY interaction, starting from $\chi^{zz}(r)$. Substituting Equation (4.3.14b) into Equation (4.3.3) and noting that only the part proportional to $(\tilde{q}/q_\alpha - 1)^{3/2}$ contributes, we arrive at the following integral

$$\chi^{zz}(r) = \frac{\tilde{C}_2 b}{2\pi}\int_{q_\alpha}^{\Lambda} d\tilde{q}\tilde{q}J_0(\tilde{q}r)\left(\frac{\tilde{q}}{q_\alpha} - 1\right)^{3/2}, \tag{4.3.15}$$

where Λ is an arbitrarily chosen cutoff which does affect the long-range behavior of $\chi^{zz}(r)$. Replacing $J_0(x)$ by its large-x asymptotic form and $\tilde{q}$ by q_α in all non-singular

and non-oscillatory parts of the integrand, we simplify the previous expression to

$$\chi^{zz}(r) = \frac{\tilde{C}_2 b}{2\pi}\sqrt{\frac{2q_\alpha}{\pi r}}\int_0^\Lambda d\tilde{q}\left(\frac{\tilde{q}}{q_\alpha}\right)^{3/2}\cos\left((\tilde{q}+q_\alpha)r-\frac{\pi}{4}\right). \tag{4.3.16}$$

Integrating by parts twice and dropping the high-energy contribution, we arrive at an integral that converges at the upper limit. The final results reads

$$\chi^{zz}(r) = -\chi_0\frac{2}{3\pi^2}\frac{u_{2k_F}^2}{k_F}\frac{\cos(q_\alpha r)}{r^3}. \tag{4.3.17}$$

Equation (4.3.17) describes long-wavelength Friedel-like oscillations which fall off with r faster than the usual $2k_F$ oscillations. Notice that Equation (4.3.17), while valid formally only for $q_\alpha r \gg 1$, reproduces correctly the dipole-dipole term [Equation (4.3.7) with $C = C_2$] in the opposite limit of $q_\alpha r \ll 1$. Therefore, Equation (4.3.17) can be used an extrapolation formula applicable for any value of $q_\alpha r$.

In addition to the Kohn anomaly at $\tilde{q} = q_\alpha$, the in-plane component also contains a non-oscillatory but nonanalytic term, proportional to $\tilde{q}$. As it was also the case in the absence of SOI, this term translates into a dipole-dipole part of the RKKY interaction. Analysis of Section 4.3 fully applies here: we just need to replace the prefactor C in Equation (4.3.7) by $2C_2/3$, where C_2 is defined by Equation (4.3.2). The role of the cutoff Λ in Equation (4.3.4) is now being played by q_α, therefore, $C \to 2C_2/3$ for $r \gg q_\alpha^{-1}$. For $r \ll q_\alpha^{-1}$, the prefactor is the same as in the absence of SOI. Summarizing, the dipole-dipole part of the in-plane RKKY interaction is

$$\chi^{xx}_{\mathrm{d-d}}(r) = -\frac{2}{3\pi^2}u_{2k_F}^2\chi_0 \times \begin{cases} 1/r^3, \text{ for } q_\alpha r \ll 1 \\ 2/3r^3, \text{ for } q_\alpha r \gg 1 \end{cases} \tag{4.3.18}$$

The oscillatory part of $\chi^{xx}(r)$ is obtained by the same method as for $\chi^{zz}(r)$; one only needs to integrate by parts three times in order to obtain a convergent integral. Consequently, $\chi^{xx}(r)$ falls off with r as $1/r^4$. The r-dependence of $\chi^{xx}(r)$, resulting from the SOI, is given by a sum of the non-oscillatory and oscillatory parts

$$\chi^{xx}(r) = \chi^{xx}_{\mathrm{d-d}}(r) + \chi_0\frac{1}{3\pi^2}\frac{u_{2k_F}^2}{q_\alpha k_F}\frac{\sin(q_\alpha r)}{r^4}. \tag{4.3.19}$$

Finally, the conventional, $2k_F$ Friedel oscillations should be added to Equations (4.3.17) and (4.3.19) to get a complete r dependence. The dipole-dipole part and long-wavelength Friedel oscillations fall off faster then conventional Friedel oscillations. In order to extract the long-wavelength part from the data, one needs to average the measured $\chi^{ij}(r)$ over many Fermi wavelengths. Recently, $2k_F$ oscillations in the RKKY interaction between magnetic adatoms on metallic surfaces have been observed directly via scanning tunneling microscopy [Zhou10]. Hopefully, improvements in spatial resolution would allow for

an experimental verification of our prediction for the long-wavelength component of the RKKY interaction.

As a final remark, we showed in Section 4.2.6 that the charge susceptibility does not exhibit small-q nonanalyticities. This result also implies that the long-wavelength oscillations are absent in the charge susceptibility; therefore, Friedel oscillations produced by non-magnetic impurities contains only a conventional, $2k_F$ component.

4.4 Summary and discussion

We have studied the nonanalytic behavior of the electron spin susceptibility of a two-dimensional electron gas (2DEG) with SOI as a function of momentum $\tilde{q} = |\tilde{\mathbf{q}}|$ in the context of a ferromagnetic nuclear-spin phase transition (FNSPT). Similarly to the dependence on temperature and magnetic-field [Żak10a], the combined effect of the electro-electron and spin-orbit interactions affects two distinct components of the spin susceptibility tensor differently. For $\tilde{q} \leq 2m^*|\alpha|$, where m^* is the effective electron mass and α is the spin-orbit coupling, the out-of-plane component of the spin susceptibility, $\chi^{zz}(\tilde{q}, \alpha)$, does not depend on momentum (in other words, momentum-dependence is cut off by the SOI), [cf. Equation (4.1.7a)], whereas its in-plane counterparts, $\chi^{xx}(\tilde{q}, \alpha) = \chi^{yy}(\tilde{q}, \alpha)$, scale linearly with $\tilde{q}$ even below the energy scale given by the SOI [cf. Equation (4.1.7b)]. Notably, both results are exact for $\tilde{q} \leq 2m^*|\alpha|$.

Beyond second order in electron-electron interaction renormalization effects in the Cooper channel, being the most relevant channel in the weak coupling regime, start to play a dominant role. As we have shown in Section 4.2.5 the leading linear-in-$|\alpha|$ term becomes renormalized by $\ln|\alpha|$, while the subleading linear-in-$\tilde{q}$ term acquires additional $\ln\tilde{q}$ dependence. This behavior is a natural consequence of the separation of energy scales in each of the diagrams and suggests that, in general, $\chi^{(n)}(\{E_i\}) \propto U^n \sum_i E_i \ln^{n-2} E_i$, where E_i stands for a generic energy scale (in our case $E_i = \{|\alpha|k_F, v_F\tilde{q}\}$ but temperature or the magnetic field could be included as well).

Our analysis of the spin susceptibility gives important insights into the nature of a FNSPT. First, the SOI-induced anisotropy of the spin susceptibility implies that the ordered phase is of an Ising type with nuclear spins aligned along the z-axis since $\chi^{zz} > \chi^{xx}$. Second, the ferromagnetic phase cannot be stable as long as the higher-order effects of the electron-electron interaction are not taken into account. In this Chapter, we focused only on one type of those effects, i.e., renormalization in the Cooper channel. Without Cooper renormalization, the slope of the magnon dispersion is negative, even though the magnon spectrum is gapped at zero-momentum, cf. Figure 4.1. This implies that spin-wave excitations destroy the ferromagnetic order. Only inclusion of higher-order processes in the Cooper channel, similarly to the mechanism proposed in [Chesi09], leads to the reversal of the slope of the spin susceptibility in the (not necessarily imme-

diate) vicinity of the Kohn-Luttinger instability, and allows for the spin-wave dispersion to become positive at all values of the momentum. This ensures stability of the ordered phase at sufficiently low temperatures [Simon07, Simon08].

We have also shown that a combination of the electron-electron and SO interactions leads to a new effect: a Kohn anomaly at the momentum splitting of the two Rashba subbands. Consequently, the real-space RKKY interaction has a long-wavelength component with a period determined by the SO rather than the Fermi wavelength.

Another issue is whether the SOI modifies the behavior of the charge susceptibility which is known to be analytic in the absence of the SOI [Belitz97, Chitov01b, Chubukov03]. As our calculation shows, the answer to this question is negative.

One more comment on the spin and charge susceptibilities is in order: despite the fact that we considered only the Rashba SOI, all our results are applicable to systems where the Dresselhaus SOI with coupling strength β takes place of Rashba SOI, i.e., $\beta \neq 0$, $\alpha = 0$; in this case, the Rashba SOI should be simply replaced by the Dresselhaus SOI ($\alpha \to \beta$).

Finally, we analyzed the nonanalytic dependence of the free energy, $\mathcal{F}$, in the presence of the SOI and at zero temperature beyond the Random Phase Approximation (RPA). This analysis is important in the context of interacting helical Fermi liquids that have recently attracted considerable attention [Agarwal11, Chesi11b, Chesi11a]. In contrast to the RPA result [Chesi11b], which predicts that the free energy scales with α as $\alpha^4 \ln|\alpha|$, our result shows that the renormalization is stronger, namely, $\mathcal{F} \propto U^2|\alpha|^3\mathcal{C}(U\ln|\alpha|)$, where $\mathcal{C}(x \to 1) \sim x^2$ and $\mathcal{C}(x \to \infty) \sim 1/x^2$.

Appendix **A**

Appendix to 'Momentum dependence of the spin susceptibility in two dimensions: nonanalytic corrections in the Cooper channel'

A.1 Derivation of ladder diagrams

To calculate the ladder diagram given by Equation (2.2.1) we begin from the simultaneous change of all Q_i variables, $Q_i \to -Q_i - P$, and expand the scattering potential into its Fourier components given by Equation (2.1.6). Thus,

$$\Pi^{(n)}(P,P',K) = \sum_{m_1 \ldots m_n} (-1)^{n-1+m_1-m_n} U_{m_1} \ldots U_{m_n} e^{-im_1\theta_p + im_n\theta_{p'}} \times \prod_{i=1}^{n-1} \int_{q_i} g(-Q_i) g(Q_i + L) e^{i(m_i - m_{i+1})\theta_{q_i}}, \tag{A.1.1}$$

where $L \equiv K + P$. We first evaluate the factors $\Pi_M(L) \equiv -\int_q g(-Q)G(Q+L)e^{iM\theta_q}$ appearing in the above formula. To this end, we integrate over the frequency Ω_q and linearize the spectrum around the Fermi surface, $\epsilon_{\mathbf{q}+\mathbf{l}} \approx \epsilon_{\mathbf{q}} + v_F l \cos\theta_q$. This requires that θ_q, and all the angles in Equation (A.1.1), are defined from the direction of $\mathbf{l}$. We also use $\epsilon = \epsilon_{\mathbf{q}}$ as integration variable, which gives

$$\Pi_M(L) = -\frac{m}{(2\pi)^2} \int_0^{2\pi} d\theta_q e^{iM\theta_q} \int d\epsilon \, \frac{\Theta(\epsilon + v_F l \cos\theta_q) - \Theta(-\epsilon)}{2\epsilon + v_F l \cos\theta_q - i\Omega_l}. \tag{A.1.2}$$

The unit step functions, $\Theta(\epsilon + v_F l\cos\theta_q)$ and $\Theta(-\epsilon)$, determine the integration range in ϵ, which is $-v_F l\cos\theta_q$ to Λ and $-\Lambda$ to 0, respectively, with Λ being the high energy cutoff. The energy integration yields

$$\Pi_M(L) = \frac{m}{(2\pi)^2}\int_0^{2\pi} d\theta_q\ \frac{e^{iM\theta}}{2}\left(i\pi\mathrm{sign}\Omega_l - \ln\frac{-2\Lambda}{+v_F l\cos\theta_q + i\Omega_l} - \ln\frac{2\Lambda}{v_F l\cos\theta_q - i\Omega_l}\right), \tag{A.1.3}$$

with the sign term coming from the lower limit of the second integration, $\ln(-2\Lambda - i\Omega_l) = \ln 2\Lambda - i\pi\mathrm{sign}\Omega_l$.

If we change variables in the integral over the first logarithm, $\theta_q \to \theta_q + \pi$, we make it identical to the second one, except for the multiplicative term $(-1)^M$ originating from $e^{iM(\theta_q+\pi)}$. Therefore, we find that

$$\Pi_M(L) = \frac{m}{(2\pi)^2}\int_0^{2\pi} d\theta_q\ e^{iM\theta_q}\left[\frac{i\pi}{2}\mathrm{sign}\Omega_l + \ln\frac{-i\Omega_l}{\Lambda} + \ln\left(1 + i\frac{v_F l}{\Omega_l}\cos\theta_q\right)\right], \tag{A.1.4}$$

where M is even and the factor of 2 in front of Λ has been absorbed into the cutoff. Writing the second logarithm as a series, $\ln(1+x) = -\sum_{n=1}^{\infty}(-1)^n x^n/n$, we can easily integrate term by term.

The $M = 0$ contribution is

$$\begin{aligned}\Pi_0(L) =& \frac{m}{(2\pi)^2}\int_0^{2\pi} d\theta_q\left[\ln\frac{|\Omega_l|}{\Lambda} - \sum_{n=1}^{\infty}\frac{1}{n}\Big(\frac{-iv_F l}{\Omega_l}\cos\theta_q\Big)^n\right]\\ =& \frac{m}{2\pi}\left[\ln\frac{|\Omega_l|}{\Lambda} - {\sum_{n\geq 2}}'\frac{1}{n}\binom{n}{\frac{n}{2}}\Big(\frac{-iv_F l}{2\Omega_l}\Big)^n\right],\end{aligned} \tag{A.1.5}$$

where n is even in the primed sum. The summation of the series gives Equation (2.2.3) shown in the main text.

For $M \neq 0$ (M even) we get

$$\begin{aligned}\Pi_M(L) &= -\frac{m}{(2\pi)^2}\int_0^{2\pi} d\theta_q e^{iM\theta_q}\sum_n\frac{1}{n}\Big(\frac{-iv_F l}{\Omega_l}\cos\theta_q\Big)^n\\ &= -\frac{m}{2\pi}{\sum_{n\geq|M|}}'\frac{1}{n}\binom{n}{\frac{n-|M|}{2}}\Big(\frac{-iv_F l}{2\Omega_l}\Big)^n.\end{aligned} \tag{A.1.6}$$

Upon summation over even values of n, Equation (2.2.4) in the main text is obtained. We now consider Equation (A.1.1), and to simplify the notation we introduce summation indexes $M_{n-i} \equiv m_i - m_{i+1}$ (for $i = 1, 2, \ldots n-1$) and $m \equiv -m_n$. We also introduce $m' = m_1 - m_n = \sum_i M_i$, which is even. We express the angles from the direction of $\mathbf{p}$, i.e., $\theta_p \to -\theta_l$ and $\theta_{p'} \to \theta - \theta_l$. Finally, we obtain

$$\Pi^{(n)}(L,\theta) = {\sum_{m',M_1\ldots M_{n-1}}}' U_{-m}U_{M_1-m}\ldots U_{M_1+\ldots M_{n-1}-m}e^{im'\theta_l - im\theta}\Pi_{M_1}(L)\ldots\Pi_{M_{n-1}}(L), \tag{A.1.7}$$

which can be written as in Equation (2.2.2) using definition (2.2.5). The special case of $\Pi^{(2)}$ is given by Equation (2.3.8) and can be directly used for the derivation of RG equations in Section 2.5.

A.2 Green's functions integration of n-th order diagram 1

We consider here the integration of the Green's functions appearing explicitly in Equations (2.3.5) and (2.4.1);

$$A \equiv -\int \frac{d^2k}{(2\pi)^2} \lim_{\epsilon_{\mathbf{k}'}\to\epsilon_{\mathbf{k}}} \int \frac{d\omega_k}{2\pi} \frac{1}{(\omega_k + i\epsilon_{\mathbf{k}})(\omega_k + i\epsilon_{\mathbf{k}'})(\omega_k + i\epsilon_{\mathbf{k}+\tilde{\mathbf{q}}})(\omega_k - \Omega_l - i\epsilon_{\mathbf{k}-\mathbf{l}})}. \tag{A.2.1}$$

The integration over ω_k can be performed with the method of residues (we choose the lower half-plane contour);

$$\begin{aligned} A = im \int \frac{d\theta_k d\epsilon_{\mathbf{k}}}{(2\pi)^2} \lim_{\epsilon_{\mathbf{k}'}\to\epsilon_{\mathbf{k}}} \Bigg[& \frac{\Theta(\epsilon_{\mathbf{k}})}{(\epsilon_{\mathbf{k}'} - \epsilon_{\mathbf{k}})(\epsilon_{\mathbf{k}+\tilde{\mathbf{q}}} - \epsilon_{\mathbf{k}})(\Omega_l + i\epsilon_{\mathbf{k}} + i\epsilon_{\mathbf{k}-\mathbf{l}})} \\ & + \frac{\Theta(\epsilon_{\mathbf{k}'})}{(\epsilon_{\mathbf{k}} - \epsilon_{\mathbf{k}'})(\epsilon_{\mathbf{k}+\tilde{\mathbf{q}}} - \epsilon_{\mathbf{k}'})(\Omega_l + i\epsilon_{\mathbf{k}'} + i\epsilon_{\mathbf{k}-\mathbf{l}})} \\ & + \frac{\Theta(\epsilon_{\mathbf{k}+\tilde{\mathbf{q}}})}{(\epsilon_{\mathbf{k}} - \epsilon_{\mathbf{k}+\tilde{\mathbf{q}}})(\epsilon_{\mathbf{k}'} - \epsilon_{\mathbf{k}+\tilde{\mathbf{q}}})(\Omega_l + i\epsilon_{\mathbf{k}+\tilde{\mathbf{q}}} + i\epsilon_{\mathbf{k}-\mathbf{l}})} \\ & + \frac{\Theta(-\epsilon_{\mathbf{k}-\mathbf{l}})}{(\Omega_l + i\epsilon_{\mathbf{k}} + i\epsilon_{\mathbf{k}-\mathbf{l}})(\Omega_l + i\epsilon_{\mathbf{k}'} + i\epsilon_{\mathbf{k}-\mathbf{l}})(\Omega_l + i\epsilon_{\mathbf{k}+\tilde{\mathbf{q}}} + i\epsilon_{\mathbf{k}-\mathbf{l}})} \Bigg]. \end{aligned} \tag{A.2.2}$$

Since the sum of all residues of the integrand in Equation (A.2.1) in the entire complex plane is zero, we can subtract the same quantity $\Theta(\epsilon_{\mathbf{k}})$ from each numerator in Equation (A.2.2) without affecting the result. This cancels the first term and, using $\lim_{\epsilon_{\mathbf{k}'}\to\epsilon_{\mathbf{k}}}[\Theta(\epsilon_{\mathbf{k}'}) - \Theta(\epsilon_{\mathbf{k}})]/[\epsilon_{\mathbf{k}'} - \epsilon_{\mathbf{k}}] = \delta(\epsilon_{\mathbf{k}})$, we obtain

$$\begin{aligned} A = A_1 + A_2 + A_3 = im \int \frac{d\theta_k d\epsilon_{\mathbf{k}}}{(2\pi)^2} \Bigg[& \frac{i\delta(\epsilon_{\mathbf{k}})}{(\epsilon_{\mathbf{k}} - \epsilon_{\mathbf{k}+\tilde{\mathbf{q}}})(\Omega_l + i\epsilon_{\mathbf{k}} + i\epsilon_{\mathbf{k}-\mathbf{l}})} \\ & + \frac{\Theta(\epsilon_{\mathbf{k}+\tilde{\mathbf{q}}}) - \Theta(\epsilon_{\mathbf{k}})}{(\epsilon_{\mathbf{k}} - \epsilon_{\mathbf{k}+\tilde{\mathbf{q}}})^2(\Omega_l + i\epsilon_{\mathbf{k}+\tilde{\mathbf{q}}} + i\epsilon_{\mathbf{k}-\mathbf{l}})} + \frac{\Theta(-\epsilon_{\mathbf{k}-\mathbf{l}}) - \Theta(\epsilon_{\mathbf{k}})}{(\Omega_l + i\epsilon_{\mathbf{k}} + i\epsilon_{\mathbf{k}-\mathbf{l}})^2(\Omega_l + i\epsilon_{\mathbf{k}+\tilde{\mathbf{q}}} + i\epsilon_{\mathbf{k}-\mathbf{l}})} \Bigg]. \end{aligned} \tag{A.2.3}$$

We can now perform the integration in $d\epsilon_{\mathbf{k}}$. To this end we linearize the energy spectrum near the Fermi surface, $\epsilon_{\mathbf{k}+\tilde{\mathbf{q}}} \approx \epsilon_{\mathbf{k}} + v_F\tilde{q}\cos\theta_k$ and $\epsilon_{\mathbf{k}-\mathbf{l}} \approx \epsilon_{\mathbf{k}} - v_F l\cos\theta_l$, which

is a good approximation since $\tilde{q}, l \ll k_F$. We also define $\zeta \equiv \Omega_l - iv_F l\cos\theta_l$ (and the complex conjugate $\bar{\zeta} \equiv \Omega_l + iv_F l\cos\theta_l$). The first two integrals are vanishing,

$$A_1 = \frac{m}{(2\pi)^2}\int_0^{2\pi} d\theta_k \frac{1}{\zeta v_F \tilde{q}\cos\theta_k} = 0 \tag{A.2.4}$$

and

$$A_2 = \frac{m}{8\pi^2}\int_0^{2\pi} \frac{d\theta_k}{(v_F\tilde{q}\cos\theta_k)^2}\ln\left(\frac{\zeta + iv_F\tilde{q}\cos\theta_k}{\zeta - iv_F\tilde{q}\cos\theta_k}\right) = 0, \tag{A.2.5}$$

since the integrands are odd with respect to $\cos\theta_k$.

For the remaining term we make use of the indefinite integral,

$$\int \frac{d\epsilon}{(2i\epsilon + z_1)^2(2i\epsilon + z_2)} = \frac{z_1 - z_2 + (z_1 + 2i\epsilon)\ln\left(\frac{z_2+2i\epsilon}{z_1+2i\epsilon}\right)}{2i(z_1 - z_2)^2(2i\epsilon + z_1)}, \tag{A.2.6}$$

which tends to zero for $\epsilon \to \pm\infty$, and hence only the integration limits at 0 and $v_F l\cos\theta_l$ contribute;

$$A = \frac{m}{8\pi^2}\int_0^{2\pi} d\theta_k \Bigg\{ \frac{1}{(v_F\tilde{q}\cos\theta_k)^2}\Bigg[\ln\left(\frac{\bar{\zeta}}{\bar{\zeta} + iv_F\tilde{q}\cos\theta_k}\right) + \ln\left(\frac{\zeta}{\zeta + iv_F\tilde{q}\cos\theta_k}\right)\Bigg] + \frac{2i\Omega_l}{|\zeta|^2 v_F\tilde{q}\cos\theta_k}\Bigg\}. \tag{A.2.7}$$

The last term vanishes and the final integration in $d\theta_k$ can be done using

$$\int_0^{2\pi} \frac{\ln\left(\frac{z}{z+ia\cos\theta}\right)}{a^2\cos^2\theta}\, d\theta = \frac{2\pi}{a^2}\Big(1 - \mathrm{sign}(\mathrm{Re}z)\frac{\sqrt{z^2+a^2}}{z}\Big), \tag{A.2.8}$$

which yields

$$= \frac{m}{4\pi(v_F\tilde{q})^2}\Bigg[2 - \frac{\sqrt{(\Omega_l + iv_F l\cos\theta_l)^2 + (v_F\tilde{q})^2}}{\Omega_l + iv_F l\cos\theta_l}\mathrm{sign}\,\Omega_l - \frac{\sqrt{(\Omega_l - iv_F l\cos\theta_l)^2 + (v_F\tilde{q})^2}}{\Omega_l - iv_F l\cos\theta_l}\mathrm{sign}\,\Omega_l\Bigg]. \tag{A.2.9}$$

Notice that A is even in Ω_l. Furthermore, the last two terms give the same contribution upon integration $\int_0^{2\pi} d\theta_l$, and therefore Equation (2.3.6) is obtained.

A.3 Second order calculation of diagram 1

In this appendix we consider the explicit evaluation of Equation (2.3.7). It receives contributions from all possible values of M appearing in $\Pi^{(2)}$ [see Equation (2.3.8)]. We

consider first $M = 0$ for which Equation (2.3.9) is useful. With the change of variables $r = R(\sin\phi + i\cos\phi\cos\theta_l)$ we obtain

$$\delta\chi^{(2)}_{1,0} = -\frac{m^2\tilde{q}}{2\pi^5 v_F}\tilde{U}_0^2 \int_0^{\pi/2} d\phi\cos\phi \int_0^{2\pi} d\theta_l \int_0^{r_{max}(\phi,\theta_l)} dr r^2 \times\Big(1-\frac{\sqrt{r^2+1}}{r}\Big)\frac{\ln\left(\frac{1+\sin\phi}{\sin\phi+i\cos\phi\cos\theta_l}\right)+\ln\left(\frac{v_F\tilde{q}r}{\Lambda}\right)}{(\sin\phi+i\cos\phi\cos\theta_l)^3}, \tag{A.3.1}$$

where $r_{max} = (\Lambda/v_F\tilde{q})(\sin\phi + i\cos\phi\cos\theta_l)$. Note, that it is necessary to introduce the upper cutoff in the integral over r, which is formally divergent. However, this upper limit turns out to be irrelevant for the nonanalytic correction.

We start from the first contribution in the above equation, where the r integration gives

$$\tilde{q}\int_0^{r_{max}} dr r^2\Big(1-\frac{\sqrt{r^2+1}}{r}\Big) = \frac{\tilde{q}}{3}[r_{max}^3 - (1+r_{max}^2)^{3/2}+1] \approx \frac{\Lambda}{v_F}(\sin\phi + i\cos\phi\cos\theta_l) + \frac{\tilde{q}}{3}. \tag{A.3.2}$$

The term proportional to Λ, as in [Chubukov03], is the dominant contribution to the spin susceptibility. However, it does not depend on $\tilde{q}$ and therefore is uninteresting for us. The term proportional to $\tilde{q}$, from the lower integration limit, is the desired nonanalytic correction to the spin susceptibility and does not depend on ϕ and θ_l. Therefore, the angular integration can be performed using[1]

$$\int_0^{\pi/2} d\phi\cos\phi\int_0^{2\pi} d\theta_l \frac{\ln\left(\frac{1+\sin\phi}{\sin\phi+i\cos\phi\cos\theta_l}\right)}{(\sin\phi+i\cos\phi\cos\theta_l)^3} = -\frac{\pi}{2}. \tag{A.3.3}$$

The same analysis can be applied to the second term of Equation (A.3.1), which contains $\ln(v_F\tilde{q}r/\Lambda)$. The integration in r gives a constant from the lower limit and the remaining angular integrations yield zero, as discussed in the main text.

Hence, the final result is

$$\delta\chi^{(2)}_{1,0}(\tilde{q}) = \frac{m^2}{12\pi^4 v_F}\tilde{q}\sum_n U_n^2. \tag{A.3.4}$$

We now aim to calculate terms with $M \neq 0$. By making use of Equation (2.2.4) for $\Pi_M(R,\phi)$ and substituting again $r \equiv R(\sin\phi + i\cos\phi\cos\theta_l)$ we obtain

$$\delta\chi^{(2)}_{1,M} = \frac{m^2\tilde{q}}{2|M|\pi^5 v_F}\sum_n U_{M-n}U_n \int_0^{\pi/2} d\phi\int_0^{2\pi} d\theta_l\int_0^{r_{max}} dr r^2 \times\Big(1-\frac{\sqrt{r^2+1}}{r}\Big)\Big(\frac{1-\sin\phi}{i\cos\phi}\Big)^{|M|}\frac{\cos\phi\, e^{-iM\theta_l}}{(\sin\phi+i\cos\phi\cos\theta_l)^3}. \tag{A.3.5}$$

[1]This result has been obtained by accurate numerical integration.

The integral over r can be performed as before. The integration over θ_l yields

$$\int_0^{2\pi} d\theta_l \frac{e^{-iM\theta_l}}{(\sin\phi + i\cos\phi\cos\theta_l)^3} = \pi(M^2+3|M|\sin\phi+3\sin^2\phi-1)\Big(\frac{1-\sin\phi}{i\cos\phi}\Big)^{|M|}, \quad \text{(A.3.6)}$$

which can be obtained by standard contour integration in the complex plane ($z = e^{-i\theta_l}$). Finally,

$$\begin{aligned}\delta\chi^{(2)}_{1,M} =& \frac{m^2\tilde{q}}{6|M|\pi^4 v_F}\sum_n U_{M-n}U_n \int_0^{\pi/2} d\phi\cos\phi\Big(\frac{1-\sin\phi}{\cos\phi}\Big)^{2|M|} \\ &\times (M^2+3|M|\sin\phi+3\sin^2\phi-1) = \frac{m^2\tilde{q}}{12\pi^4 v_F}\sum_n U_{M-n}U_n, \end{aligned} \quad \text{(A.3.7)}$$

since the last integration gives a factor of $|M|/2$. Thus, the total second order correction is

$$\delta\chi^{(2)}_1(\tilde{q}) = \frac{m^2}{24\pi^4}\frac{\tilde{q}}{v_F}{\sum_M}' \sum_n 2U_{M-n}U_n. \quad \text{(A.3.8)}$$

Rewriting the double sum as $\sum_{m,n} U_m U_n + \sum_{m,n}(-1)^{m+n}U_m U_n$, we recover the two contributions as in Equation (2.3.1).

A.4 Small momentum limit of n-th order particle-particle propagator

We expand $\Pi^{(n)}$ [see Equation (2.2.2)] in powers of $\Pi_0(R,\phi)$ as follows

$$\Pi^{(n)}(R,\phi,\theta_l,\theta) \approx \tilde{U}^n_{00\ldots0}\Pi_0^{n-1} + {\sum_{M\neq0}}'\Big(\tilde{U}^n_{M0\ldots0} + \ldots \tilde{U}^n_{00\ldots M}\Big)\Pi_M\Pi_0^{n-2} + \ldots\ . \quad \text{(A.4.1)}$$

The expression of $\Pi_0(R,\phi)$ is given by Equation (2.3.9). Therefore, the leading contribution in the above equation at small $\tilde{q}$ is from the first term since $\Pi_0^{n-1} \propto (\ln v_F\tilde{q}/\Lambda)^{n-1}$. However, the leading order does not contribute to the nonanalytic correction. Neglecting such constant terms, we can write the relevant subleading contribution in the following way:

$$\begin{aligned}[\Pi_0(R,\phi)]^{n-1} =& (n-1)\Big(\frac{m}{2\pi}\ln\frac{v_F\tilde{q}}{\Lambda}\Big)^{n-2}\frac{m}{2\pi}\ln R(1+\sin\phi) + \ldots \\ =& (n-1)\Big(\frac{m}{2\pi}\ln\frac{v_F\tilde{q}}{\Lambda}\Big)^{n-2}\Pi_0(R,\phi) + \ldots\ . \end{aligned} \quad \text{(A.4.2)}$$

Furthermore, by using $\Pi_0^{n-2} \propto (\ln v_F\tilde{q}/\Lambda)^{n-2}$, we can simplify Equation (A.4.1) to the following form:

$$\Pi^{(n)}(R,\phi,\theta_l,\theta) = \Big(\frac{m}{2\pi}\ln\frac{v_F\tilde{q}}{\Lambda}\Big)^{n-2}{\sum_M}'\Big(\tilde{U}^n_{M0\ldots0} + \tilde{U}^n_{0M\ldots0} + \ldots \tilde{U}^n_{00\ldots M}\Big)\Pi_M + \ldots\ . \quad \text{(A.4.3)}$$

By making use of Equation (2.2.5) we have

$$\tilde{U}^n_{M0\ldots0} + \tilde{U}^n_{0M\ldots0} + \ldots \tilde{U}^n_{00\ldots M} = \sum_k \sum_{j=1}^{n-1} U_k^{n-j} U^j_{k-M} e^{iM\theta_l - ik\theta} \tag{A.4.4}$$

and therefore Equation (A.4.3) is written explicitly as

$$\begin{aligned}\Pi^{(n)}(R,\phi,\theta_l,\theta) =& {\sum_M}' \Pi_M(R,\phi) \sum_k U_k U_{k-M} e^{iM\theta_l - ik\theta} \\ &\times \sum_{j,j'=0}^{\infty} \delta_{j+j',n-2} \left(\frac{mU_k}{2\pi} \ln \frac{v_F \tilde{q}}{\Lambda}\right)^j \left(\frac{mU_{k-M}}{2\pi} \ln \frac{v_F \tilde{q}}{\Lambda}\right)^{j'} + \ldots \ .\end{aligned} \tag{A.4.5}$$

We can now sum previous expression (A.4.5) over the index $n \geq 2$, which removes the constraint $j + j' = n - 2$. Hence, the last double summation factorizes in the product of two geometric series, that can be evaluated explicitly, and we obtain Equation (2.4.6).

Appendix **B**

Appendix to 'Spin susceptibility of interacting two-dimensional electron gas in the presence of spin-orbit interaction'

B.1 Temperature dependence for free Rashba fermions

In this Appendix, we consider the temperature dependence of the spin susceptibility of free 2D electrons in the presence of the Rashba SOI. The transverse and parallel spin susceptibilities, $\chi_{zz}^{\{0\}}$ and $\chi_{xx}^{\{0\}}$, are given by

$$\chi_{zz}^{\{0\}} = -\sum_{K} \mathrm{Tr}\left[G\left(K\right)\sigma_z G\left(K'\right)\sigma_z\right] \tag{B.1.1}$$

$$\chi_{xx}^{\{0\}} = -\sum_{K} \mathrm{Tr}\left[G\left(K\right)\sigma_x G\left(K'\right)\sigma_x\right], \tag{B.1.2}$$

where $K = (\omega, \mathbf{k})$ and $K' = (\omega, \mathbf{k}+\mathbf{q})$ with $q \to 0$. Evaluating the traces, we obtain for $\chi_{zz}^{\{0\}}$

$$\chi_{zz}^{\{0\}} = -T\sum_{\omega}\int \frac{d^2k}{(2\pi)^2}\sum_{s,t}\frac{1}{2}(1-st)g_s(\omega,\mathbf{k})g_t(\omega,\mathbf{k}) = -2T\sum_{\omega}\int\frac{dkk}{2\pi}g_+(\omega,\mathbf{k})g_-(\omega,\mathbf{k}), \tag{B.1.3}$$

where we took advantage of the isotropy of $g_\pm(\omega,\mathbf{k})$ and put $q=0$, because the poles in the Green's functions of different branches reside on opposite sides of the real axis. We see that $\chi_{zz}^{\{0\}}$ is determined only by inter-subband transitions. Similarly, we obtain

for $\chi_{xx}^{\{0\}}$

$$\chi_{xx}^{\{0\}} = -T\sum_{\omega}\int\frac{d^2k}{(2\pi)^2}\sum_{s,t}\frac{1}{2}\left[1-st\cos(2\theta_{\mathbf{k}})\right]g_s(\omega,\mathbf{k})g_t(\omega,\mathbf{k}+\mathbf{q})|_{q\to 0}. \tag{B.1.4}$$

Since $\cos\theta_{\mathbf{k}}$ averages to zero, $\chi_{xx}^{\{0\}}$ can be written as

$$\chi_{xx}^{\{0\}} = \frac{1}{2}\chi_{zz}^{\{0\}} + \frac{1}{2}\delta\chi_{xx}^{\{0\}}, \tag{B.1.5}$$

where

$$\delta\chi_{xx}^{\{0\}} \equiv -T\sum_{\omega}\int\frac{d^2k}{(2\pi)^2}[g_+(\omega,\mathbf{k})g_+(\omega,\mathbf{k}+\mathbf{q}) + g_-(\omega,\mathbf{k})g_-(\omega,\mathbf{k}+\mathbf{q})]|_{q\to 0} \tag{B.1.6}$$

is the contribution from intra-subband transitions, absent in $\chi_{zz}^{\{0\}}$.

Let us evaluate $\chi_{zz}^{\{0\}}$ first. Performing the fermionic Matsubara sum, we obtain

$$\begin{aligned}\chi_{zz}^{\{0\}} =& -2\int_0^\infty\frac{kdk}{2\pi}\,T\sum_{\omega}\frac{1}{2\alpha k}\left(\frac{1}{i\omega-\epsilon_{\mathbf{k}}-\alpha k}-\frac{1}{i\omega-\epsilon_k+\alpha k}\right)\\ =&\frac{1}{2\pi\alpha}\int_0^\infty dk[n_F(\epsilon_{\mathbf{k}}-\alpha k)-n_F(\epsilon_{\mathbf{k}}+\alpha k)]\end{aligned} \tag{B.1.7}$$

with a Fermi function $n_F(\epsilon) = \left[e^{(\epsilon-\mu)/T}+1\right]^{-1}$ and $\epsilon_{\mathbf{k}} = k^2/2m-\mu$. Changing variables in the first integral to $\epsilon_{\mathbf{k}}-\alpha k = \epsilon_- - \mu$, we find two roots: $k_-^{(1)} = m\alpha - \sqrt{(m\alpha)^2+2m\epsilon_-}$, valid for $-\epsilon_0 < \epsilon_- < 0$ with $dk_-^{(1)}/d\epsilon_- < 0$, and $k_-^{(2)} = m\alpha + \sqrt{(m\alpha)^2+2m\epsilon_-}$, valid for $\epsilon_- > 0$ with $dk_-^{(2)}/d\epsilon_- > 0$, where $\epsilon_0 \equiv m\alpha^2/2$. Similarly, we change variables in the second integral to $\epsilon_{\mathbf{k}}+\alpha k = \epsilon_+ - \mu$ and obtain only one positive root $k_+ = -m\alpha + \sqrt{(m\alpha)^2+2m\epsilon_+}$, valid for $\epsilon_+ > 0$ with $dk_+/d\epsilon_+ > 0$. Notice that the absolute values of the (inverse) group velocities are the same for both branches: $|dk_-^{(1,2)}/d\epsilon_-| = |dk_+/d\epsilon_+| = m[(m\alpha)^2+2m\epsilon_\pm]^{-1/2}$. Therefore,

$$\begin{aligned}\chi_{zz}^{\{0\}} =&\frac{1}{2\pi\alpha}\left(\int_{-\epsilon_0}^0 d\epsilon\left|\frac{dk_-^{(1)}}{d\epsilon}\right| + \int_0^\infty d\epsilon\left|\frac{dk_-^{(2)}}{d\epsilon}\right| - \int_0^\infty d\epsilon\left|\frac{dk_+}{d\epsilon}\right|\right)n_F(\epsilon)\\ =&\frac{m}{2\pi\alpha}\int_{-\epsilon_0}^0 d\epsilon\frac{n_F(\epsilon)}{\sqrt{(m\alpha)^2+2m\epsilon}},\end{aligned} \tag{B.1.8}$$

where we dropped the index on the integration variable ϵ. Notably, the high energy contributions from the two Rashba branches cancel each other for any value of the chemical potential and the spin susceptibility is determined exclusively by the bottom part of the lower Rashba branch. Integration by parts yields

$$\chi_{zz}^{\{0\}} = \chi_0\left(n_F(0) - \int_{-\epsilon_0}^0 d\epsilon\sqrt{1+\frac{\epsilon}{\epsilon_0}}\frac{\partial n_F(\epsilon)}{\partial\epsilon}\right), \tag{B.1.9}$$

where $n_F(0) = [e^{-\mu/T}+1]^{-1}$. In order to evaluate this integral, it is convenient to consider three limiting cases.

For $T \ll \epsilon_0 \ll \mu$, i.e., when both Rashba subbands are occupied and the temperature is lower than the minimum of the lower subband, we approximate $n_F(0) \approx 1 - e^{-\mu/T}$, $-T\partial n_F(\epsilon)/\partial\epsilon \approx e^{(\epsilon-\mu)/T}$, and $\sqrt{1+\epsilon/\epsilon_0} \approx 1 + \epsilon/2\epsilon_0$, so that

$$\chi_{zz}^{\{0\}} = \chi_0 \left[(1 - e^{-\mu/T}) + \frac{1}{T} e^{-\mu/T} \int_0^\infty d\epsilon \left(1 - \frac{\epsilon}{2\epsilon_0}\right) e^{-\epsilon/T} \right] = \chi_0 \left(1 - \frac{T}{2\epsilon_0} e^{-\mu/T}\right). \tag{B.1.10}$$

At $T = 0$, $\chi_{zz}^{\{0\}} = \chi_0$.

For $\epsilon_0 \ll T \ll \mu$, i.e., when again both Rashba subbands are occupied but the temperature is higher than the minimum of the lower subband, we keep the same approximations for $n_F(0)$ and $-T\partial n_F(\epsilon)/\partial\epsilon$ but neglect the ϵ dependence of the Fermi function in the integrand:

$$\begin{aligned} -\int_{-\epsilon_0}^{\{0\}} d\epsilon \sqrt{1+\frac{\epsilon}{\epsilon_0}} \frac{\partial n_F(\epsilon)}{\partial\epsilon} &\approx \frac{1}{T} e^{-\mu/T} \int_0^{\epsilon_0} d\epsilon \sqrt{1+\frac{\epsilon}{\epsilon_0}}\, e^{-\epsilon/T} \\ &\approx \frac{1}{T} e^{-\mu/T} \int_0^{\epsilon_0} d\epsilon \sqrt{1+\frac{\epsilon}{\epsilon_0}} = \frac{2\epsilon_0}{3T} e^{-\mu/T}. \end{aligned} \tag{B.1.11}$$

Thus,

$$\chi_{zz}^{\{0\}} = \chi_0 \left[1 - \left(1 - \frac{2\epsilon_0}{3T}\right) e^{-\mu/T} \right]. \tag{B.1.12}$$

Finally, for $\mu < 0$, i.e., when only the lower Rashba subband is occupied, the first term in Equation (B.1.9) gives only an exponentially weak temperature dependence, while the Sommerfeld expansion of the second term generates a T^2 contribution because the density of states depends on ϵ:

$$\chi_{zz}^{\{0\}} = \chi_0 \left[\sqrt{1-|\mu|/\epsilon_0} - \frac{\pi^2}{24} \left(\frac{T}{\epsilon_0}\right)^2 \frac{1}{(1-|\mu|/\epsilon_0)^{3/2}} \right] \tag{B.1.13}$$

At zero temperature, $\chi_{zz}^{\{0\}} = \chi_0 \sqrt{1-|\mu|/\epsilon_0}$ vanishes at the bottom of the lower subband.

We now calculate $\delta\chi_{xx}^{\{0\}}$ given by Equation (B.1.6), which can be written as

$$\delta\chi_{xx}^{\{0\}} = -\int_0^\infty \frac{dkk}{2\pi} \left(\frac{\partial n_F(\epsilon_-)}{\partial\epsilon_-} + \frac{\partial n_F(\epsilon_+)}{\partial\epsilon_+} \right). \tag{B.1.14}$$

The change of variables is straightforward in the second integral, since the equation $\epsilon_+ - \mu = \epsilon_{\mathbf{k}} + \alpha k$ has only one positive root k_+ and the density of states is given by

$$\nu_+(\epsilon) = \frac{k_+}{2\pi}\frac{dk_+}{d\epsilon} = \frac{m}{2\pi} \frac{\sqrt{1+\epsilon/\epsilon_0} - 1}{\sqrt{1+\epsilon/\epsilon_0}} \tag{B.1.15}$$

with $\epsilon_0 \equiv m\alpha^2/2$. In the first integral more care must be taken: for $\epsilon > 0$, we have $k_-^{(2)} = m\alpha + \sqrt{(m\alpha)^2 + 2m\epsilon}$ and the density of states is given by

$$\nu_-^{>}(\epsilon) = \frac{k_-^{(2)}}{2\pi}\frac{dk_-^{(2)}}{d\epsilon} = \frac{m}{2\pi}\frac{\sqrt{1+\epsilon/\epsilon_0}+1}{\sqrt{1+\epsilon/\epsilon_0}}; \tag{B.1.16}$$

however, for $-\epsilon_0 < \epsilon < 0$ both roots enter the density of states

$$\nu_-^{<}(\epsilon) = \int_0^\infty \frac{kdk}{2\pi}\delta(\epsilon-\epsilon_-) = \frac{1}{2\pi}\left(k_-^{(1)}\left|\frac{dk_-^{(1)}}{d\epsilon_-}\right| + k_-^{(2)}\left|\frac{dk_-^{(2)}}{d\epsilon_-}\right|\right) = \frac{m}{\pi}\frac{1}{\sqrt{1+\epsilon/\epsilon_0}}. \tag{B.1.17}$$

Summing up the contributions from all energies, we find

$$\begin{aligned}\delta\chi_{xx}^{\{0\}} &= \left(\int_{-\epsilon_0}^0 d\epsilon\nu_-^{<}(\epsilon) + \int_0^\infty d\epsilon\nu_-^{>}(\epsilon) + \int_0^\infty d\epsilon\nu_+(\epsilon)\right)\left(-\frac{\partial n_F(\epsilon)}{\partial\epsilon}\right)\\ &= \int_{-\epsilon_0}^0 d\epsilon\nu_-^{<}(\epsilon)\left(-\frac{\partial n_F(\epsilon)}{\partial\epsilon}\right) + \chi_0 n_F(0),\end{aligned} \tag{B.1.18}$$

where the second and third integrals are easily evaluated because ϵ drops out of the sum $\nu_+ + \nu_-^{>} = m/\pi$. Combining the above result with Equations (B.1.2) and (B.1.8), we get

$$\chi_{xx}^{\{0\}} = \chi_0\left(n_F(0) - \int_{-\epsilon_0}^0 d\epsilon\frac{1+\epsilon/2\epsilon_0}{\sqrt{1+\epsilon/\epsilon_0}}\frac{\partial n_F(\epsilon)}{\partial\epsilon}\right). \tag{B.1.19}$$

For $T \ll \epsilon_0 \ll \mu$, we approximate $n_F(0) \approx 1 - e^{-\mu/T}$ and $-T\partial n_F(\epsilon)/\partial\epsilon = e^{(\epsilon-\mu)/T}(e^{(\epsilon-\mu)/T}+1)^{-2} \approx e^{(\epsilon-\mu)/T}$ as before, and expand $(1+\epsilon/2\epsilon_0)/\sqrt{1+\epsilon/\epsilon_0} \approx 1 + \epsilon^2/8\epsilon_0^2$, so that

$$\chi_{xx}^{\{0\}} = \chi_0\left[n_F(0) + \frac{1}{T}e^{-\mu/T}\int_0^\infty d\epsilon\left(1+\frac{\epsilon^2}{8\epsilon_0^2}\right)e^{-\epsilon/T}\right] = \chi_0\left(1+\frac{T^2}{4\epsilon_0^2}e^{-\mu/T}\right). \tag{B.1.20}$$

For $\epsilon_0 \ll T \ll \mu$, we keep the same approximations for the Fermi function but, as it was also the case for $\chi_{zz}^{\{0\}}$, neglect the ϵ dependence of the Fermi function in the integrand

$$\begin{aligned}\int_{-\epsilon_0}^0 d\epsilon\frac{1+\epsilon/2\epsilon_0}{\sqrt{1+\epsilon/\epsilon_0}}\frac{\partial n_F(\epsilon)}{\partial\epsilon} &\approx \frac{1}{T}e^{-\mu/T}\int_0^{\epsilon_0} d\epsilon\frac{1-\epsilon/2\epsilon_0}{\sqrt{1-\epsilon/\epsilon_0}}e^{-\epsilon/T}\\ &\approx \frac{1}{T}e^{-\mu/T}\int_0^{\epsilon_0} d\epsilon\frac{1-\epsilon/2\epsilon_0}{\sqrt{1-\epsilon/\epsilon_0}} = \frac{4\epsilon_0}{3T}e^{-\mu/T}.\end{aligned} \tag{B.1.21}$$

Thus,

$$\chi_{xx}^{\{0\}} = \chi_0\left[1-\left(1-\frac{4\epsilon_0}{3T}\right)e^{-\mu/T}\right]. \tag{B.1.22}$$

Finally, for $\mu < 0$, the Sommerfeld expansion of the second term in Equation (B.1.19) yields

$$\chi_{xx}^{\{0\}} = \chi_0\left[\frac{1-|\mu|/2\epsilon_0}{(1-|\mu|/\epsilon_0)^{1/2}} + \frac{\pi^2}{48}\left(\frac{T}{\epsilon_0}\right)^2\frac{2+|\mu|/\epsilon_0}{(1-|\mu|/\epsilon_0)^{5/2}}\right] \tag{B.1.23}$$

for $T \ll \min\{|\mu|, \epsilon_0 - |\mu|\}$. At zero temperature, $\chi_{xx}^{\{0\}} = \chi_0\left(1-|\mu|/2\epsilon_0\right)/\left(1-|\mu|/\epsilon_0\right)^{1/2}$ diverges at the bottom of the lower subband.

B.2 Absence of a $q_0 \equiv 2m\alpha$ singularity in a static particle-hole propagator

In Secs. 4.2 and 3.3.4, we argued that there is no contribution to the nonanalytic behavior of the spin susceptibility from the region of small bosonic momenta, $q \ll k_F$. This statement contradicts [Chen99], where it was argued that, in the presence of the SOI, a static particle-hole bubble has a square-root singularity at $q = q_0 \equiv 2m\alpha$ (in addition to the Kohn anomaly which is also modified by the SOI). For a weak SOI, q_0 is much smaller than k_F and thus the region of small q may also contribute to the nonanalytic behavior. Later on, however, [Pletyukhov06, Pletyukhov07] showed that there is no singularity at $q = q_0$. According to [Pletyukhov06], the reason is related to a subtlety in approaching the static limit of a dynamic bubble. While we agree with the authors of n PhysRevB.74.045307 in that there are no small-q singularities in the bubble, we find that a cancelation of singular terms occurs in the calculation of a purely static bubble. The same result was obtained in an unpublished work [Mishchenko]. For the sake of completeness, we present our derivation in this Appendix.

Evaluating the spin trace, we obtain for the static polarization bubble

$$\Pi(q) \equiv \sum_K \mathrm{Tr}[G_{\omega,\mathbf{k}+\mathbf{q}} G_{\omega,\mathbf{k}}] = \frac{1}{2}\sum_K \sum_{s,t} \left[1 + st\cos(\varphi_{\mathbf{k}+\mathbf{q}} - \varphi_{\mathbf{k}})\right] g_s(\omega, \mathbf{k}+\mathbf{q}) g_t(\omega, \mathbf{k}), \tag{B.2.1}$$

where, as before, $K = (\omega, \mathbf{k})$, $\varphi_{\mathbf{k}+\mathbf{q}} \equiv \angle(\mathbf{k}+\mathbf{q}, \mathbf{e}_x)$ and $\varphi_{\mathbf{k}} \equiv \angle(\mathbf{k}, \mathbf{e}_x)$. We divide $\Pi(q)$ into intra- and intersubband contributions as

$$\Pi(q) = \Pi_{++}(q) + \Pi_{--}(q) + \Pi_{\pm}(q), \tag{B.2.2}$$

where

$$\Pi_{\pm\pm}(q) \equiv \frac{1}{2}\sum_K [1 + \cos(\varphi_{\mathbf{k}+\mathbf{q}} - \varphi_{\mathbf{k}})] g_{\pm}(\omega, \mathbf{k}+\mathbf{q}) g_{\pm}(\omega, \mathbf{k}), \tag{B.2.3a}$$

$$\begin{aligned} \Pi_{\pm}(q) &\equiv \frac{1}{2}\sum_K [1 - \cos(\varphi_{\mathbf{k}+\mathbf{q}} - \varphi_{\mathbf{k}})][g_+(\omega, \mathbf{k}+\mathbf{q}) g_-(\omega, \mathbf{k}) + g_-(\omega, \mathbf{k}+\mathbf{q}) g_+(\omega, \mathbf{k})] \\ &= \sum_K [1 - \cos(\varphi_{\mathbf{k}+\mathbf{q}} - \varphi_{\mathbf{k}})] g_+(\omega, \mathbf{k}+\mathbf{q}) g_-(\omega, \mathbf{k}). \end{aligned} \tag{B.2.3b}$$

In the last line, we employed obvious symmetries of the Green's function.

First, we focus on the intersubband part, $\Pi_{\pm}(q)$. Summation over the Matsubara frequency yields

$$T\sum_{\omega} g_+(\mathbf{p},\omega) g_-(\mathbf{k},\omega) = \frac{n_F(\epsilon^+_{\mathbf{p}}) - n_F(\epsilon^-_{\mathbf{k}})}{\epsilon^+_{\mathbf{p}} - \epsilon^-_{\mathbf{k}}}, \tag{B.2.4}$$

where $\mathbf{p} = \mathbf{k} + \mathbf{q}$, $\epsilon^{\pm}_{\mathbf{k}} = \epsilon_{\mathbf{k}} \pm \alpha k$ and, as before, $\epsilon_{\mathbf{k}} = k^2/2m - E_F$. Introducing additional integration over the momentum $\mathbf{p}$, as it was done in [Chen99], Equation (B.2.3b) can be

re-written as

$$\Pi_{\pm}(q) = \frac{2}{(2\pi)^2}\int_0^{2\pi} d\theta \int_0^{\infty} dk k \int_0^{\infty} dp p\, \delta(p^2 - |\mathbf{k}+\mathbf{q}|^2) \times \left(1 - \frac{\mathbf{k}\cdot(\mathbf{k}+\mathbf{q})}{kp}\right) \frac{n_F(\epsilon_{\mathbf{p}}^{+}) - n_F(\epsilon_{\mathbf{k}}^{-})}{\epsilon_{\mathbf{p}}^{+} - \epsilon_{\mathbf{k}}^{-}}, \tag{B.2.5}$$

where $\theta = \angle(\mathbf{k}, \mathbf{q})$. Integration over θ yields

$$\int_0^{2\pi} d\theta \delta(p^2 - k^2 - q^2 - 2kq\cos\theta)\left(1 - \frac{k^2 + kq\cos\theta}{kp}\right) = \frac{1}{kp}\frac{q^2 - (k-p)^2}{\sqrt{(k+q)^2 - p^2}\sqrt{p^2 - (k-q)^2}}, \tag{B.2.6}$$

which imposes a constraint on the range of integration over p, i.e., $|k-q| < p < k+q$. Since we assume that $q \ll k \approx p \approx k_F$, Equation (B.2.6) can be simplified to

$$\frac{\sqrt{q^2 - (k-p)^2}}{2k_F^3}, \tag{B.2.7}$$

and $\Pi_{\pm}(q)$ becomes

$$\Pi_{\pm}(q) = \frac{1}{4\pi^2 k_F^3}\int_0^{\infty} dk k \int_{|k-q|}^{k+q} dp p \sqrt{q^2 - (k-p)^2}\, \frac{n_F(\epsilon_{\mathbf{p}}^{+}) - n_F(\epsilon_{\mathbf{k}}^{-})}{\epsilon_{\mathbf{p}}^{+} - \epsilon_{\mathbf{k}}^{-}}. \tag{B.2.8}$$

For a weak SOI ($m|\alpha| \ll k_F$) , $\epsilon_{\mathbf{k}}^{\pm} \approx \epsilon_{\mathbf{k}} \pm \alpha k_F$. Switching from integration over k and p to integration over $\epsilon_{\mathbf{k}}$ and $\epsilon_{\mathbf{p}}$, we find

$$\Pi_{\pm}(q) = \frac{1}{4\pi^2 v_F^3 k_F}\int_{-\infty}^{\infty} d\epsilon_{\mathbf{k}} \int_{\epsilon_{\mathbf{k}} - v_F q}^{\epsilon_{\mathbf{k}} + v_F q} d\epsilon_{\mathbf{p}} \times \sqrt{(v_F q)^2 - (\epsilon_{\mathbf{k}} - \epsilon_{\mathbf{p}})^2}\frac{n_F(\epsilon_{\mathbf{p}} + \alpha k_F) - n_F(\epsilon_{\mathbf{k}} - \alpha k_F)}{\epsilon_{\mathbf{p}} - \epsilon_{\mathbf{k}} + 2\alpha k_F}. \tag{B.2.9}$$

Shifting the integration variables as $\epsilon_{\mathbf{p}} \to \epsilon_{\mathbf{p}} - \alpha k_F$, $\epsilon_{\mathbf{k}} \to \epsilon_{\mathbf{k}} + \alpha k_F$, we eliminate the dependence of the Fermi functions on αk_F. Assuming also that $T = 0$, we obtain

$$\Pi_{\pm}(q) = \frac{1}{4\pi^2 v_F^3 k_F}\int_{-\infty}^{\infty} d\epsilon_{\mathbf{k}} \int_{\epsilon_{\mathbf{k}} + 2\alpha k_F - v_F q}^{\epsilon_{\mathbf{k}} + 2\alpha k_F + v_F q} d\epsilon_{\mathbf{p}} \times \sqrt{(v_F q)^2 - (\epsilon_{\mathbf{p}} - \epsilon_{\mathbf{k}} - 2\alpha k_F)^2}\, \frac{\Theta(-\epsilon_{\mathbf{p}}) - \Theta(-\epsilon_{\mathbf{k}})}{\epsilon_{\mathbf{p}} - \epsilon_{\mathbf{k}}}, \tag{B.2.10}$$

where $\Theta(x)$ is the step function. Notice that the integrand is finite only if $\epsilon_{\mathbf{k}}\epsilon_{\mathbf{p}} < 0$, which imposes further constraints on the integration range.

We will now prove that $\Pi_\pm(q)$ given by Equation (B.2.10) is continuous at $q = q_0$. To this end, it is convenient to consider the cases of $q < q_0$ and $q > q_0$. Combining all the constraints together, we find that $\Pi_\pm$ for $q < q_0$ can be written as

$$\Pi_\pm^<(q) \equiv \Pi_\pm(q < q_0) = -\frac{1}{4\pi^2 v_F^3 k_F}\Bigg(\int_{-v_F q - 2\alpha k_F}^{v_F q - 2\alpha k_F} d\epsilon_{\mathbf{k}} \int_0^{\epsilon_{\mathbf{k}} + 2\alpha k_F + v_F q} d\epsilon_{\mathbf{p}} + \int_{v_F q - 2\alpha k_F}^{0} d\epsilon_{\mathbf{k}} \int_{\epsilon_{\mathbf{k}} + 2\alpha k_F - v_F q}^{\epsilon_{\mathbf{k}} + 2\alpha k_F + v_F q} d\epsilon_{\mathbf{p}} \Bigg) \frac{\sqrt{(v_F q)^2 - (\epsilon_{\mathbf{p}} - \epsilon_{\mathbf{k}} - 2\alpha k_F)^2}}{\epsilon_{\mathbf{p}} - \epsilon_{\mathbf{k}}}, \quad \text{(B.2.11)}$$

Reversing the sign of $\epsilon_{\mathbf{k}}$, absorbing $\epsilon_{\mathbf{k}}$ into $\epsilon_{\mathbf{p}}$, and defining the dimensionless variables $x = \epsilon_{\mathbf{k}}/v_F q$ and $y = \epsilon_{\mathbf{p}}/v_F q$, we obtain

$$\Pi_\pm^<(q) = -\frac{q^2}{4\pi^2 v_F k_F}\left(\int_{\beta-1}^{\beta+1} dx \int_x^{\beta+1} dy + \int_0^{\beta-1} dx \int_{\beta-1}^{\beta+1} dy \right) \frac{\sqrt{1-(y-\beta)^2}}{y}, \quad \text{(B.2.12)}$$

where $\beta \equiv q_0/q > 1$. Next, we switch the order of integration in the first term, so that the integrals over x can be readily evaluated

$$\begin{aligned} \Pi_\pm^<(q) &= -\frac{q^2}{4\pi^2 v_F k_F} \int_{\beta-1}^{\beta+1} dy \left(\int_{\beta-1}^{y} dx + \int_0^{\beta-1} dx \right) \frac{\sqrt{1-(y-\beta)^2}}{y} \\ &= -\frac{q^2}{4\pi^2 v_F k_F} \int_{\beta-1}^{\beta+1} dy \sqrt{1-(y-\beta)^2} = -\frac{m}{2\pi}\left(\frac{q}{2k_F}\right)^2. \end{aligned} \quad \text{(B.2.13)}$$

For $q > q_0$, we have

$$\Pi_\pm^>(q) \equiv \Pi_\pm(q > q_0) = \frac{1}{4\pi^2 v_F^3 k_F}\Bigg(\int_0^{v_F q - 2\alpha k_F} d\epsilon_{\mathbf{k}} \int_{\epsilon_{\mathbf{k}} + 2\alpha k_F - v_F q}^{0} d\epsilon_{\mathbf{p}} - \int_{-v_F q - 2\alpha k_F}^{0} d\epsilon_{\mathbf{k}} \int_0^{\epsilon_{\mathbf{k}} + 2\alpha k_F + v_F q} d\epsilon_{\mathbf{p}} \Bigg) \frac{\sqrt{(v_F q)^2 - (\epsilon_{\mathbf{p}} - \epsilon_{\mathbf{k}} - 2\alpha k_F)^2}}{\epsilon_{\mathbf{p}} - \epsilon_{\mathbf{k}}}. \quad \text{(B.2.14)}$$

Manipulations similar to those for the previous case yield

$$\Pi_\pm^>(q) = -\frac{q^2}{4\pi^2 v_F k_F}\Bigg(\int_0^{1-\beta} dx \int_x^{1-\beta} dy \frac{\sqrt{1-(y+\beta)^2}}{y} + \int_0^{1+\beta} dx \int_x^{1+\beta} dy \frac{\sqrt{1-(y-\beta)^2}}{y} \Bigg) \quad \text{(B.2.15)}$$

with $\beta = q_0/q < 1$. Interchanging the order of integrations over x and y, we find

$$\Pi_\pm(q > 2m\alpha) = -\frac{q^2}{4\pi^2 v_F k_F}\Bigg(\int_0^{1-\beta} dy \sqrt{1-(y+\beta)^2} + \int_0^{1+\beta} dy \sqrt{1-(y-\beta)^2} \Bigg) = -\frac{m}{2\pi}\left(\frac{q}{2k_F}\right)^2. \quad \text{(B.2.16)}$$

Since $\Pi_{\pm}^{<}(q = q_0 - 0^+) = \Pi_{\pm}^{>}(q = q_0 + 0^+)$, the function $\Pi_{\pm}(q) = -(m/2\pi)(q/2k_F)^2$ is continuous at $q = q_0$ and, thus, there is no singularity in the static particle-hole response function. In addition, $\Pi_{\pm}(q)$ does not depend on the SOI. However, since there is no q^2 term in the 2D bubble for $q \leq 2k_F$ in the absence of the SOI, the q^2 term must be canceled out by similar terms in $\Pi_{++}(q)$ and $\Pi_{--}(q)$, which is what we will show below.

Having proven that $\Pi_{\pm}(q)$ is an analytic function of q, we can re-derive its q dependence simply by expanding the combination $\varphi_{\mathbf{k}+\mathbf{q}} - \varphi_{\mathbf{k}}$ in Equation (B.2.3b) for $q \ll k_F$ as $\varphi_{\mathbf{k}+\mathbf{q}} - \varphi_{\mathbf{k}} \approx (q/k_F)\sin\varphi_{\mathbf{kq}}$, where $\varphi_{\mathbf{kq}} \equiv \angle(\mathbf{k}, \mathbf{q})$; then $1 - \cos(\varphi_{\mathbf{k}+\mathbf{q}} - \varphi_{\mathbf{k}}) \approx (q/k_F)^2 \sin^2(\varphi_{\mathbf{kq}})/2$. Since we already have a factor of q^2 up front, the Green's functions in Equation (B.2.3b) can be evaluated at $q = 0$. Accordingly, Equation (B.2.3b) becomes

$$\Pi_{\pm}(q) = \frac{1}{2}\left(\frac{q}{k_F}\right)^2 \sum_K \sin^2\varphi_{\mathbf{kq}} g_+(\mathbf{k},\omega) g_-(\mathbf{k},\omega) = \frac{m}{2\pi}\left(\frac{q}{2k_F}\right)^2 \int d\epsilon_{\mathbf{k}} \frac{n_F(\epsilon_{\mathbf{k}}^+) - n_F(\epsilon_{\mathbf{k}}^-)}{\epsilon_{\mathbf{k}}^+ - \epsilon_{\mathbf{k}}^-}$$
$$= -\frac{m}{2\pi}\left(\frac{q}{2k_F}\right)^2 \int_{-\alpha k_F}^{\alpha k_F} d\epsilon_{\mathbf{k}} \frac{1}{2\alpha k_F} = -\frac{m}{2\pi}\left(\frac{q}{2k_F}\right)^2. \tag{B.2.17}$$

Expanding Equation (B.2.3a) for the intraband contribution to the bubble also to second order in q, we obtain

$$\Pi_{\pm\pm}(Q) = \sum_K g_{\pm}(\mathbf{k}+\mathbf{q},\omega) g_{\pm}(\mathbf{k},\omega)|_{\mathbf{q}\to 0}$$
$$- \frac{1}{4}\left(\frac{q}{k_F}\right)^2 \sum_K \sin^2\varphi_{\mathbf{kq}} g_{\pm}(\mathbf{k}+\mathbf{q},\omega) g_{\pm}(\mathbf{k},\omega)|_{q\to 0} = -\frac{m}{2\pi} + \frac{m}{4\pi}\left(\frac{q}{2k_F}\right)^2, \tag{B.2.18}$$

since

$$\sum_K g_{\pm}(\mathbf{k}+\mathbf{q},\omega) g_{\pm}(\mathbf{k},\omega)|_{\mathbf{q}\to 0} = -m \int \frac{d\epsilon_{\mathbf{k}}}{2\pi} \frac{\Theta(\epsilon_{\mathbf{k}+\mathbf{q}}^{\pm}) - \Theta(\epsilon_{\mathbf{k}}^{\pm})}{\epsilon_{\mathbf{k}+\mathbf{q}}^{\pm} - \epsilon_{\mathbf{k}}^{\pm}}\Big|_{q\to 0}$$
$$= -m \int \frac{d\epsilon_{\mathbf{k}}}{2\pi} \delta(\epsilon_{\mathbf{k}} \pm |\alpha| k_F) = -\frac{m}{2\pi}. \tag{B.2.19}$$

Thereby the total bubble (B.2.2)

$$\Pi(q) = -\frac{m}{\pi} \tag{B.2.20}$$

is independent of q for $q \ll 2k_F$.

B.3 Renormalization of scattering amplitudes in a finite magnetic field

In this Appendix, we present the derivation of the RG flow equations for the scattering amplitudes in the Cooper channel in the presence of the magnetic field. These amplitudes

are then used to find the non-perturbative results for the spin susceptibility. Since the amplitudes are renormalized quite differently for the field applied perpendicularly and parallel to the 2DEG plane, we will treat these two cases separately.

B.3.1 Transverse magnetic field

Renormalization Group flow of scattering amplitudes

If the magnetic field is transverse to the 2DEG plane, $\mathbf{B} = B\mathbf{e}_z$, the eigenvectors of the Hamiltonian (3.1.1) read

$$|\mathbf{k}, s\rangle = \frac{1}{\sqrt{N_s(k)}} \begin{pmatrix} (\Delta - s\bar{\Delta}_{\mathbf{k}})ie^{-i\theta_{\mathbf{k}}}/\alpha k \\ 1 \end{pmatrix}, \tag{B.3.1}$$

where $N_s(k) = 2 + 2\Delta(\Delta - s\bar{\Delta}_{\mathbf{k}})/(\alpha k)^2$ is the normalization factor and, as before, $\bar{\Delta}_{\mathbf{k}} \equiv (\Delta^2 + \alpha^2 k^2)^{-1/2}$ is the effective Zeeman energy. Since, by assumption, $|\alpha| k_F \ll E_F$, we approximate $\bar{\Delta}_{\mathbf{k}}$ by $\bar{\Delta}_{\mathbf{k}_F}$. Substituting the above eigenvectors into Equation (3.4.17), we find the scattering amplitude

$$\begin{aligned} \Gamma^{(1)}_{s_1 s_2; s_4 s_3}(\mathbf{k}, \mathbf{k}'; \mathbf{p}, \mathbf{p}') = U &\left(\prod_{i=1}^{4} \frac{1}{\sqrt{2 + \frac{2\Delta(\Delta - s_i \bar{\Delta}_{\mathbf{k}_F})}{\alpha^2 k_F^2}}} \right) \\ &\times \left[1 + \frac{1}{\alpha^2 k_F^2} (\Delta - s_1 \bar{\Delta}_{\mathbf{k}_F})(\Delta - s_3 \bar{\Delta}_{\mathbf{k}_F}) e^{i(\theta_{\mathbf{p}} - \theta_{\mathbf{k}})} \right] \\ &\times \left[1 + \frac{1}{\alpha^2 k_F^2} (\Delta - s_2 \bar{\Delta}_{\mathbf{k}_F})(\Delta - s_4 \bar{\Delta}_{k_F}) e^{i(\theta_{\mathbf{p}'} - \theta_{\mathbf{k}'})} \right]. \end{aligned} \tag{B.3.2}$$

To find the spin susceptibility, we need to know the scattering amplitude to second order in the magnetic field. Expanding Equation (B.3.2) to second order in $\delta \equiv \Delta/|\alpha| k_F$ (note that $s_i^2 = 1$ and $s_i^3 = s_i$) and projecting the amplitude onto the Cooper channel, where the momenta are correlated in such a way that $\mathbf{k}' = -\mathbf{k}$ and $\mathbf{p}' = -\mathbf{p}$ or, equivalently, $\theta_{\mathbf{k}'} = \theta_{\mathbf{k}} + \pi$ and $\theta_{\mathbf{p}'} = \theta_{\mathbf{p}} + \pi$, we obtain

$$\Gamma^{(1)}_{s_1 s_2; s_3 s_4}(\mathbf{k}, -\mathbf{k}; \mathbf{p}, -\mathbf{p}) = U_{s_1 s_2; s_3 s_4} + V_{s_1 s_2; s_3 s_4} e^{i(\theta_{\mathbf{p}} - \theta_{\mathbf{k}})} + W_{s_1 s_2; s_3 s_4} e^{2i(\theta_{\mathbf{p}} - \theta_{\mathbf{k}})}, \tag{B.3.3}$$

where we introduced partial amplitudes

$$U_{s_1 s_2; s_3 s_4} = \frac{U}{4} + \frac{U}{8}(s_1 + s_2 + s_3 + s_4)\delta + \frac{U}{16}(s_1 s_2 + s_1 s_3 + s_1 s_4 + s_2 s_3 + s_2 s_4 + s_3 s_4 - 2)\delta^2 + \mathcal{O}(\delta^3), \tag{B.3.4}$$

$$\begin{aligned} V_{s_1 s_2; s_3 s_4} = &\frac{U}{4}(s_1 s_3 + s_2 s_4) + \frac{U}{8}(s_1 s_2 s_3 + s_1 s_2 s_4 + s_1 s_3 s_4 + s_2 s_3 s_4 - s_1 - s_2 - s_3 - s_4)\delta \\ &+ \frac{U}{8}(1 - s_1 s_2 - s_2 s_3 - s_3 s_4 - s_1 s_4 - s_1 s_3 - s_2 s_4 + s_1 s_2 s_3 s_4)\delta^2 + \mathcal{O}(\delta^3), \end{aligned} \tag{B.3.5}$$

$$W_{s_1s_2;s_3s_4} = \frac{U}{4}s_1s_2s_3s_4 - \frac{U}{8}(s_1s_2s_3 + s_1s_2s_4 + s_1s_3s_4 + s_2s_3s_4)\delta + \frac{U}{16}(s_1s_2 + s_1s_3 + s_1s_4 + s_2s_3 + s_2s_4 + s_3s_4 - 2s_1s_2s_3s_4)\delta^2 + \mathcal{O}(\delta^3). \tag{B.3.6}$$

For $\delta = 0$, the partial amplitudes reduce back to Equations (3.4.21a-3.4.21c). The RG flow equations for the partial amplitudes are the same as in the absence of the magnetic field and are given by Equations (3.4.24a)–(3.4.24c) with initial conditions (B.3.4)–(B.3.6). Since the differential equations for U, V, and Λ are identical, for the sake of argument we select the first one, copied below for the reader's convenience,

$$-\frac{d}{dL}U_{s_1s_2;s_3s_4}(L) = \sum_s U_{s_1s_2;ss}(L)U_{ss;s_3s_4}(L) \tag{B.3.7}$$

and introduce the following ansatz

$$U_{s_1s_2;s_3s_4}(L) = \frac{U_{s_1s_2;s_3s_4}(0) + a_{s_1s_2;s_3s_4}L}{1 + bL}, \tag{B.3.8}$$

which satisfies the initial condition. Substituting this formula into the differential equation for U and multiplying the result by $(1 + bL)^2$, we obtain an algebraic equation for $a_{s_1s_2;s_3s_4}$ and b

$$bU_{s_1s_2;s_3s_4}(0) - a_{s_1s_2;s_3s_4} + \sum_s (U_{s_1s_2;ss}(0) + a_{s_1s_2;ss}L)(U_{ss;s_3s_4}(0) + a_{ss;s_3s_4}L) = 0. \tag{B.3.9}$$

Grouping coefficients of a polynomial in L, we obtain the following set of equations

$$bU_{s_1s_2;s_3s_4}(0) - a_{s_1s_2;s_3s_4} + \sum_s U_{s_1s_2;ss}(0)U_{ss;s_3s_4}(0) = 0, \tag{B.3.10}$$

$$\sum_s [U_{s_1s_2;ss}(0)a_{ss;s_3s_4} + a_{s_1s_2;ss}U_{ss;s_3s_4}(0)] = 0, \tag{B.3.11}$$

$$\sum_s a_{s_1s_2;ss}a_{ss;s_3s_4} = 0, \tag{B.3.12}$$

which are not independent. Thereby, we choose two out of three equations, namely, Equation (B.3.10) and Equation (B.3.12) with the $s_1 = s_2 = s_3 = s_4 = 1$ combination of the Rashba indices, so that there are 17 equations for 17 unknown variables: $a_{s_1s_2;s_3s_4}$ and b. The final solutions are listed below

$$U_{\pm\pm;\pm\pm}(L) = \frac{U}{4}\frac{(1 \pm \delta)^2}{1 + (1 + \delta^2)UL/2}, \tag{B.3.13}$$

$$U_{ss;-s-s}(L) = U_{s-s;-ss}(L) = U_{s-s;s-s}(L) = \frac{U}{4}\frac{1 - \delta^2}{1 + (1 + \delta^2)UL/2}, \tag{B.3.14}$$

$$U_{\sigma(\pm\mp;\mp\pm)}(L) = \frac{U}{4}\frac{1 \mp \delta - \delta^2/2}{1 + (1 + \delta^2)UL/2}. \tag{B.3.15}$$

The same procedure is repeated to derive the V- and Λ-amplitudes listed below

$$V_{ss;ss}(L) = \frac{U}{2}\frac{1-\delta^2}{1+(1-\delta^2)UL}, \tag{B.3.16}$$

$$V_{ss;-s-s}(L) = -\frac{U}{2}\frac{1-\delta^2}{1+(1-\delta^2)UL}, \tag{B.3.17}$$

$$V_{s-s;-ss}(L) = -\frac{U}{2}(1-\delta^2) - \frac{U}{2}\frac{\delta^2 UL}{1+(1-\delta^2)UL}, \tag{B.3.18}$$

$$V_{s-s;s-s}(L) = \frac{U}{2}(1+\delta^2) - \frac{U}{2}\frac{\delta^2 UL}{1+(1-\delta^2)UL}, \tag{B.3.19}$$

$$V_{\sigma(\pm\mp;\mp\mp)}(L) = \pm\frac{U}{2}\frac{\delta}{1+(1-\delta^2)UL} \tag{B.3.20}$$

and

$$W_{\pm\pm;\pm\pm}(L) = \frac{U}{4}\frac{(1\mp\delta)^2}{1+(1+\delta^2)UL/2}, \tag{B.3.21}$$

$$W_{ss;-s-s}(L) = W_{s-s;-ss}(L) = W_{s-s;s-s}(L) = \frac{U}{4}\frac{1-\delta^2}{1+(1+\delta^2)UL/2}, \tag{B.3.22}$$

$$W_{\sigma(\pm\mp;\mp\mp)}(L) = -\frac{U}{4}\frac{1\pm\delta-\delta^2/2}{1+(1+\delta^2)UL/2}. \tag{B.3.23}$$

Summing up all the contributions to the backscattering amplitude, obtained from the Cooper amplitude for a special choice of the momenta $\mathbf{p} = -\mathbf{k}$, i.e., for $\theta_{\mathbf{p}} - \theta_{\mathbf{k}} = \pi$, we obtain

$$\Gamma_{s_1s_2;s_3s_4}(\mathbf{k},-\mathbf{k};-\mathbf{k},\mathbf{k}) = U_{s_1s_2;s_3s_4}(L) - V_{s_1s_2;s_3s_4}(L) + W_{s_1s_2;s_3s_4}(L). \tag{B.3.24}$$

To second order in the field, the backscattering amplitudes read

$$\Gamma_{ss;ss}(\mathbf{k},-\mathbf{k};-\mathbf{k},\mathbf{k}) = \left(\frac{U}{2+UL} - \frac{U}{2(1+UL)}\right) + \left(\frac{U}{2(1+UL)^2} + \frac{2U}{(2+UL)^2}\right)\delta^2, \tag{B.3.25a}$$

$$\Gamma_{ss;-s-s}(\mathbf{k},-\mathbf{k};-\mathbf{k},\mathbf{k}) = \left(\frac{U}{2+UL} + \frac{U}{2(1+UL)}\right) \tag{B.3.25b}$$

$$- \left(\frac{U}{2(1+UL)^2} - \frac{2U}{(2+UL)^2} + \frac{2U}{2+UL}\right)\delta^2, \tag{B.3.25c}$$

$$\Gamma_{s-s;-ss}(\mathbf{k},-\mathbf{k};-\mathbf{k},\mathbf{k}) = \left(\frac{U}{2+UL} + \frac{U}{2}\right) - \left(\frac{U}{2(1+UL)} - \frac{2U}{(2+UL)^2} + \frac{2U}{2+UL}\right)\delta^2, \tag{B.3.25d}$$

$$\Gamma_{s-s;s-s}(\mathbf{k},-\mathbf{k};-\mathbf{k},\mathbf{k}) = \left(\frac{U}{2+UL} - \frac{U}{2}\right) - \left(\frac{U}{2(1+UL)} - \frac{2U}{(2+UL)^2} + \frac{2U}{2+UL}\right)\delta^2, \tag{B.3.25e}$$

$$\Gamma_{\sigma(\pm\mp;\mp\mp)}(\mathbf{k},-\mathbf{k};-\mathbf{k},\mathbf{k}) = \mp\left(\frac{U}{2(1+UL)} + \frac{U}{2+UL}\right)\delta. \tag{B.3.25f}$$

For $\delta = 0$, we reproduce Equations (3.4.26-3.4.28). In the limit of strong renormalization in the Cooper channel, i.e., for $UL \to \infty$, the field-dependent terms in Equations (B.3.25a-B.3.25f) vanish. *A posteriori*, this explains why we could obtain the renormalized result (3.4.35) for χ_{zz} in the main text using only the zero-field amplitudes.

Renormalization of the transverse component

As in Section 3.4.3, the thermodynamic potential in the presence of Cooper renormalization is obtained by substituting the renormalized scattering amplitudes (B.3.25a-B.3.25f) into Equation (3.4.32)

$$\delta\Xi_{zz} = -\frac{1}{2}T\sum_{\Omega}\int\frac{qdq}{2\pi}\Bigg[\frac{1}{2}\left(\frac{U}{2+UL}-\frac{U}{2}\right)^2(\Pi_{+-}^2+\Pi_{-+}^2-2\Pi_0^2)+(\Pi_{+-}\Pi_{-+}-\Pi_0^2)$$
$$\times\left(\frac{U}{2+UL}+\frac{U}{2(1+UL)}\right)^2-\frac{U^2(16+32UL+22U^2L^2+6U^2L^3+U^4L^4)}{4(1+UL)^2(2+UL)^2}\Pi_0^2\Bigg] \tag{B.3.26a}$$
$$-\frac{\Delta^2}{\alpha^2k_F^2}T\sum_{\Omega}\int\frac{qdq}{2\pi}\Bigg[\left(\frac{U}{2(1+UL)}+\frac{U}{2+UL}\right)^2\Pi_0(\Pi_{+-}+\Pi_{-+}-2\Pi_0)$$
$$+\frac{1}{2}\left(\frac{U}{2(1+UL)}-\frac{2U}{(2+UL)^2}+\frac{2U}{2+UL}\right)\left(\frac{U}{2+UL}-\frac{U}{2}\right)(\Pi_{+-}^2+\Pi_{-+}^2-2\Pi_0^2) \tag{B.3.26b}$$
$$-\left(\frac{U}{2(1+UL)^2}-\frac{2U}{(2+UL)^2}+\frac{2U}{2+UL}\right)\left(\frac{U}{2+UL}+\frac{U}{2(1+UL)}\right)(\Pi_{+-}\Pi_{-+}-\Pi_0^2)$$
$$-\frac{U^4L^2(12+18UL+7U^2L^2)}{2(1+UL)^2(2+UL)^3}\Pi_0^2\Bigg]. \tag{B.3.26c}$$

The first part of $\delta\Xi_{zz}$ (B.3.26a) came from the field-independent terms in the scattering amplitudes. This part depends on the magnetic field through the combinations of the polarization bubbles. The second part (B.3.26c) already contains a field-dependent prefactor (Δ^2) resulting from the field-dependent terms in the scattering amplitudes. Therefore, the polarization bubbles in this part can be evaluated in zero field. The integrals over q along with the summation over the Matsubara frequency Ω have already been performed in Section 4.2. Note that in each square bracket the last term (proportional to Π_0^2) depends neither on the field nor on the SOI. In fact, it can be shown [Chubukov05b, Chubukov05a] that this formally divergent contribution has a cubic dependence on temperature, $T\sum_\Omega\int qdq\Pi_0^2 \propto T^3$, thus it adds a higher order correction

and can be dropped. The final result reads

$$\begin{aligned}\delta\Xi_{zz} = &-\frac{T^3}{8\pi v_F^2}\left(\frac{mU}{2\pi}\right)^2\left[\left(\frac{1}{2+UL}-\frac{1}{2}\right)^2\mathcal{F}\left(\frac{2\sqrt{\alpha^2k_F^2+\Delta^2}}{T}\right)\right]\\ &-\frac{\Delta^2}{\alpha^2k_F^2}\frac{T^3}{2\pi v_F^2}\left(\frac{mU}{2\pi}\right)^2\left[\left(\frac{1}{2(1+UL)}+\frac{1}{2+UL}\right)^2\mathcal{F}\left(\frac{|\alpha|k_F}{T}\right)\right.\\ &\left.+\frac{1}{2}\left(\frac{1}{2(1+UL)}-\frac{2}{(2+UL)^2}+\frac{2}{2+UL}\right)\left(\frac{1}{2+UL}-\frac{1}{2}\right)\mathcal{F}\left(\frac{2|\alpha|k_F}{T}\right)\right].\end{aligned} \tag{B.3.27}$$

The spin susceptibility is obtained by expanding Equation (B.3.27) further to order Δ^2. We also need to recall that our treatment of Cooper renormalization is only valid for $T \ll |\alpha|k_F$, because we kept only the T- but not α-dependent Cooper logarithms (see the discussion at the end of Section 3.4.3). Therefore, the function $\mathcal{F}$ and its derivative should be replaced by their large-argument forms, Equation (3.3.27). Doing so, we obtain the final result for the nonanalytic part of the χ_{zz}, presented in Equation (3.4.37) in the main text.

B.3.2 In-plane magnetic field

Renormalization Group flow of scattering amplitudes

For the in-plane magnetic field, $\mathbf{B} = B\mathbf{e}_x$, the RG flow of the scattering amplitudes is more cumbersome because the eigenvectors of Hamiltonian (3.1.1) depend in a complicated way on the angle between the magnetic field and the electron momentum

$$\mid \mathbf{k}, s\rangle = \frac{1}{\sqrt{2}}\begin{pmatrix} s\bar{\Delta}_{\mathbf{k}}/(\Delta - ie^{i\theta_{\mathbf{k}}}\alpha k) \\ 1 \end{pmatrix}, \tag{B.3.28}$$

where $\bar{\Delta}_{\mathbf{k}} \equiv (\Delta^2 + 2\alpha k\Delta\sin\theta_{\mathbf{k}} + \alpha^2k^2)^{-1/2}$ is the effective Zeeman energy. For that reason, the (double) Fourier series of the scattering amplitude (3.4.17) in the angles $\theta_{\mathbf{k}}$ and $\theta_{\mathbf{p}}$ contains infinitely many harmonics:

$$\Gamma^{(1)}_{s_1s_2;s_3s_4}(\mathbf{k},-\mathbf{k};\mathbf{p},-\mathbf{p}) = \sum_{m,n=-\infty}^{\infty}\Gamma^{(1)\{m,n\}}_{s_1s_2;s_3s_4}e^{im\theta_{\mathbf{p}}}e^{in\theta_{\mathbf{k}}}, \tag{B.3.29}$$

To second order in the field, however, the number of nonvanishing harmonics is limited to 15. Indeed, expanding the eigenvector (B.3.28) to second order in $\delta \equiv \Delta/|\alpha|k_F$ as

$$\mid \mathbf{k}, s\rangle = \frac{1}{\sqrt{2}}\begin{pmatrix} sie^{-i\theta_{\mathbf{k}}}[1 - i\cos\theta_{\mathbf{k}}\delta - (\cos^2\theta_{\mathbf{k}} - i\sin 2\theta_{\mathbf{k}})\delta^2/2] \\ 1 \end{pmatrix} + \mathcal{O}(\delta^3) \tag{B.3.30}$$

and substituting Equation (B.3.30) into the scattering amplitude (3.4.17) with $\mathbf{k}' = -\mathbf{k}$ and $\mathbf{p}' = -\mathbf{p}$, we obtain

$$\begin{aligned}\Gamma^{(1)}_{s_1s_2;s_3s_4}(\mathbf{k},-\mathbf{k};\mathbf{p},-\mathbf{p}) &= U_{s_1s_2;s_3s_4} + V_{s_1s_2;s_3s_4}e^{i\theta_\mathbf{p}}e^{-i\theta_\mathbf{k}} + W_{s_1s_2;s_3s_4}e^{2i\theta_\mathbf{p}}e^{-2i\theta_\mathbf{k}} \\ &+ A_{s_1s_2;s_3s_4}e^{i\theta_\mathbf{p}}e^{i\theta_\mathbf{k}} + B_{s_1s_2;s_3s_4}e^{-i\theta_\mathbf{p}}e^{-i\theta_\mathbf{k}} + F_{s_1s_2;s_3s_4}e^{2i\theta_\mathbf{p}}e^{-i\theta_\mathbf{k}} \\ &+ G_{s_1s_2;s_3s_4}e^{i\theta_\mathbf{p}}e^{-2i\theta_\mathbf{k}} + H_{s_1s_2;s_3s_4}e^{i\theta_\mathbf{p}} + J_{s_1s_2;s_3s_4}e^{-i\theta_\mathbf{k}} \\ &+ L_{s_1s_2;s_3s_4}e^{2i\theta_\mathbf{p}} + M_{s_1s_2;s_3s_4}e^{-2i\theta_\mathbf{k}} + P_{s_1s_2;s_3s_4}e^{3i\theta_\mathbf{p}}e^{-i\theta_\mathbf{k}} \\ &+ Q_{s_1s_2;s_3s_4}e^{i\theta_\mathbf{p}}e^{-3i\theta_\mathbf{k}} + R_{s_1s_2;s_3s_4}e^{4i\theta_\mathbf{p}}e^{-2i\theta_\mathbf{k}} + S_{s_1s_2;s_3s_4}e^{2i\theta_\mathbf{p}}e^{-4i\theta_\mathbf{k}} + \mathcal{O}(\delta^3). \qquad \text{(B.3.31)}\end{aligned}$$

Here,

$$U_{s_1s_2;s_3s_4} = \Gamma^{(1)\{0,0\}}_{s_1s_2;s_3s_4} = (U/16)[4 + (s_1s_3 + s_2s_4)\delta^2], \qquad \text{(B.3.32)}$$
$$V_{s_1s_2;s_3s_4} = \Gamma^{(1)\{1,-1\}}_{s_1s_2;s_3s_4} = (U/8)(s_1s_3 + s_2s_4)(2 - \delta^2), \qquad \text{(B.3.33)}$$
$$W_{s_1s_2;s_3s_4} = \Gamma^{(1)\{2,-2\}}_{s_1s_2;s_3s_4} = (U/16)[4s_1s_2s_3s_4 + (s_1s_3 + s_2s_4)\delta^2], \qquad \text{(B.3.34)}$$
$$A_{s_1s_2;s_3s_4} = \Gamma^{(1)\{1,1\}}_{s_1s_2;s_3s_4} = (U/32)(s_1s_3 + s_2s_4)\delta^2, \qquad \text{(B.3.35)}$$
$$B_{s_1s_2;s_3s_4} = \Gamma^{(1)\{-1,-1\}}_{s_1s_2;s_3s_4} = A_{s_1s_2;s_3s_4}, \qquad \text{(B.3.36)}$$
$$F_{s_1s_2;s_3s_4} = \Gamma^{(1)\{2,-1\}}_{s_1s_2;s_3s_4} = (U/8)i(s_1s_3 - s_2s_4)\delta, \qquad \text{(B.3.37)}$$
$$G_{s_1s_2;s_3s_4} = \Gamma^{(1)\{1,-2\}}_{s_1s_2;s_3s_4} = -F_{s_1s_2;s_3s_4}, \qquad \text{(B.3.38)}$$
$$H_{s_1s_2;s_3s_4} = \Gamma^{(1)\{1,0\}}_{s_1s_2;s_3s_4} = -F_{s_1s_2;s_3s_4}, \qquad \text{(B.3.39)}$$
$$J_{s_1s_2;s_3s_4} = \Gamma^{(1)\{0,-1\}}_{s_1s_2;s_3s_4} = F_{s_1s_2;s_3s_4}, \qquad \text{(B.3.40)}$$
$$L_{s_1s_2;s_3s_4} = \Gamma^{(1)\{2,0\}}_{s_1s_2;s_3s_4} = (U/16)(s_1s_3 + s_2s_4 + 2s_1s_2s_3s_4)\delta^2, \qquad \text{(B.3.41)}$$
$$M_{s_1s_2;s_3s_4} = \Gamma^{(1)\{0,-2\}}_{s_1s_2;s_3s_4} = L_{s_1s_2;s_3s_4}, \qquad \text{(B.3.42)}$$
$$P_{s_1s_2;s_3s_4} = \Gamma^{(1)\{3,-1\}}_{s_1s_2;s_3s_4} = -3A_{s_1s_2;s_3s_4}, \qquad \text{(B.3.43)}$$
$$Q_{s_1s_2;s_3s_4} = \Gamma^{(1)\{1,-3\}}_{s_1s_2;s_3s_4} = P_{s_1s_2;s_3s_4}, \qquad \text{(B.3.44)}$$
$$R_{s_1s_2;s_3s_4} = \Gamma^{(1)\{4,-2\}}_{s_1s_2;s_3s_4} = -(U/8)s_1s_2s_3s_4\delta^2, \qquad \text{(B.3.45)}$$
$$S_{s_1s_2;s_3s_4} = \Gamma^{(1)\{2,-4\}}_{s_1s_2;s_3s_4} = R_{s_1s_2;s_3s_4}. \qquad \text{(B.3.46)}$$

The second-order amplitude is derived from Equation (3.4.22) with $n = 2$

$$\begin{aligned}\Gamma^{(2)}_{s_1s_2;s_4s_3}(\mathbf{k},-\mathbf{k};\mathbf{p},-\mathbf{p}) &= -L\sum_s\{U_{s_1s_2;ss}U_{ss;s_3s_4} + H_{s_1s_2;ss}J_{ss;s_3s_4} + [V_{s_1s_2;ss}V_{ss;s_3s_4} \\ &+ F_{s_1s_2;ss}G_{ss;s_3s_4} + J_{s_1s_2;ss}H_{ss;s_3s_4}]e^{i\theta_\mathbf{p}}e^{-i\theta_\mathbf{k}} + [W_{s_1s_2;ss}W_{ss;s_3s_4} + G_{s_1s_2;ss}F_{ss;s_3s_4}] \\ &\times e^{2i\theta_\mathbf{p}}e^{-2i\theta_\mathbf{k}} + A_{s_1s_2;ss}V_{ss;s_3s_4}e^{i\theta_\mathbf{p}}e^{i\theta_\mathbf{k}} + V_{s_1s_2;ss}B_{ss;s_3s_4}e^{-i\theta_\mathbf{p}}e^{-i\theta_\mathbf{k}} + [V_{s_1s_2;ss}F_{ss;s_3s_4} \\ &+ F_{s_1s_2;ss}W_{ss;s_3s_4}]e^{2i\theta_\mathbf{p}}e^{-i\theta_\mathbf{k}} + [W_{s_1s_2;ss}G_{ss;s_3s_4} + G_{s_1s_2;ss}V_{ss;s_3s_4}]e^{i\theta_\mathbf{p}}e^{-2i\theta_\mathbf{k}} \\ &+ [H_{s_1s_2;ss}V_{ss;s_3s_4} + U_{s_1s_2;ss}H_{ss;s_3s_4}]e^{i\theta_\mathbf{p}} + [V_{s_1s_2;ss}J_{ss;s_3s_4} + J_{s_1s_2;ss}U_{ss;s_3s_4}]e^{-i\theta_\mathbf{k}} \\ &+ [H_{s_1s_2;ss}F_{ss;s_3s_4} + U_{s_1s_2;ss}L_{ss;s_3s_4} + L_{s_1s_2;ss}W_{ss;s_3s_4}]e^{2i\theta_\mathbf{p}} + [W_{s_1s_2;ss}M_{ss;s_3s_4} \\ &+ G_{s_1s_2;ss}J_{ss;s_3s_4} + M_{s_1s_2;ss}U_{ss;s_3s_4}]e^{-2i\theta_\mathbf{k}} + V_{s_1s_2;ss}P_{ss;s_3s_4}e^{3i\theta_\mathbf{p}}e^{-i\theta_\mathbf{k}} + Q_{s_1s_2;ss}V_{ss;s_3s_4} \\ &\times e^{i\theta_\mathbf{p}}e^{-3i\theta_\mathbf{k}} + W_{s_1s_2;ss}R_{ss;s_3s_4}e^{4i\theta_\mathbf{p}}e^{-2i\theta_\mathbf{k}} + S_{s_1s_2;ss}W_{ss;s_3s_4}e^{2i\theta_\mathbf{p}}e^{-4i\theta_\mathbf{k}}\} + \mathcal{O}(\delta^3), \qquad \text{(B.3.47)}\end{aligned}$$

where $L = (m/2\pi)\ln(\Lambda/T)$. The second-order amplitude contains the same combinations of the harmonics $e^{im\theta_{\mathbf{p}}}$ and $e^{in\theta_{\mathbf{k}}}$ as the first-order amplitude, which proves the group property. The RG flow equations are obtained by replacing the left-hand side of Equation (B.3.47) by the bare amplitude, letting the coefficients $U \dots S$ to depend on L, and differentiating with respect to L:

$$-\frac{d}{dL}U_{s_1s_2;s_3s_4}(L) = U_{s_1s_2;ss}(L)U_{ss;s_3s_4}(L) + H_{s_1s_2;ss}(L)J_{ss;s_3s_4}(L), \tag{B.3.48}$$

$$-\frac{d}{dL}V_{s_1s_2;s_3s_4}(L) = V_{s_1s_2;ss}(L)V_{ss;s_3s_4}(L) + F_{s_1s_2;ss}(L)G_{ss;s_3s_4}(L) + J_{s_1s_2;ss}(L)H_{ss;s_3s_4}(L), \tag{B.3.49}$$

$$-\frac{d}{dL}W_{s_1s_2;s_3s_4}(L) = W_{s_1s_2;ss}(L)W_{ss;s_3s_4}(L) + G_{s_1s_2;ss}(L)F_{ss;s_3s_4}(L), \tag{B.3.50}$$

$$-\frac{d}{dL}A_{s_1s_2;s_3s_4}(L) = A_{s_1s_2;ss}(L)V_{ss;s_3s_4}(L), \tag{B.3.51}$$

$$-\frac{d}{dL}B_{s_1s_2;s_3s_4}(L) = V_{s_1s_2;ss}(L)B_{ss;s_3s_4}(L), \tag{B.3.52}$$

$$-\frac{d}{dL}F_{s_1s_2;s_3s_4}(L) = V_{s_1s_2;ss}(L)F_{ss;s_3s_4}(L) + F_{s_1s_2;ss}(L)W_{ss;s_3s_4}(L), \tag{B.3.53}$$

$$-\frac{d}{dL}G_{s_1s_2;s_3s_4}(L) = W_{s_1s_2;ss}(L)G_{ss;s_3s_4}(L) + G_{s_1s_2;ss}(L)V_{ss;s_3s_4}(L), \tag{B.3.54}$$

$$-\frac{d}{dL}H_{s_1s_2;s_3s_4}(L) = H_{s_1s_2;ss}(L)V_{ss;s_3s_4}(L) + U_{s_1s_2;ss}(L)H_{ss;s_3s_4}(L), \tag{B.3.55}$$

$$-\frac{d}{dL}J_{s_1s_2;s_3s_4}(L) = V_{s_1s_2;ss}(L)J_{ss;s_3s_4}(L) + J_{s_1s_2;ss}(L)U_{ss;s_3s_4}(L), \tag{B.3.56}$$

$$-\frac{d}{dL}L_{s_1s_2;s_3s_4}(L) = H_{s_1s_2;ss}(L)F_{ss;s_3s_4}(L) + U_{s_1s_2;ss}(L)L_{ss;s_3s_4}(L) + L_{s_1s_2;ss}(L)W_{ss;s_3s_4}(L), \tag{B.3.57}$$

$$-\frac{d}{dL}M_{s_1s_2;s_3s_4}(L) = W_{s_1s_2;ss}(L)M_{ss;s_3s_4}(L) + G_{s_1s_2;ss}(L)J_{ss;s_3s_4}(L) + M_{s_1s_2;ss}(L)U_{ss;s_3s_4}(L), \tag{B.3.58}$$

$$-\frac{d}{dL}P_{s_1s_2;s_3s_4}(L) = V_{s_1s_2;ss}(L)P_{ss;s_3s_4}(L), \tag{B.3.59}$$

$$-\frac{d}{dL}Q_{s_1s_2;s_3s_4}(L) = Q_{s_1s_2;ss}(L)V_{ss;s_3s_4}(L), \tag{B.3.60}$$

$$-\frac{d}{dL}R_{s_1s_2;s_3s_4}(L) = W_{s_1s_2;ss}(L)R_{ss;s_3s_4}(L), \tag{B.3.61}$$

$$-\frac{d}{dL}S_{s_1s_2;s_3s_4}(L) = S_{s_1s_2;ss}(L)W_{ss;s_3s_4}(L), \tag{B.3.62}$$

where summation over the repeated index s is implied. The initial conditions are given by $X_{s_1,s_2;s_3,s_4}(0) = X_{s_1,s_2;s_3,s_4}$ with $X = U \dots S$. Since it is very difficult to solve this system of differential equations analytically, a new approach is required. In what follows, we will determine $U(L), \dots, S(L)$ for a few lowest orders in the "RG time" L and then

make a guess for a form of an arbitrary-order term. The RG equations will then provide a necessary check as to whether our guess, based on the perturbative calculation, gives a correct answer.

A few lowest order amplitudes can be derived perturbatively from Equation (3.4.22), copied here for the reader's convenience

$$\Gamma^{(j)}_{s_1s_2;s_4s_3}(\mathbf{k},-\mathbf{k};\mathbf{p},-\mathbf{p})(L) = -L\sum_s \int_0^{2\pi} \frac{d\theta_l}{2\pi}\Gamma^{(j-1)}_{s_1s_2;ss}(\mathbf{k},-\mathbf{k};\mathbf{l},-\mathbf{l})\Gamma^{(1)}_{ss;s_4s_3}(\mathbf{l},-\mathbf{l};\mathbf{p},-\mathbf{p}) \tag{B.3.63}$$

with $j \geq 2$ standing for order of the perturbation theory. Since the scattering amplitudes depend on angles $\theta_{\mathbf{k}}$ and $\theta_{\mathbf{p}}$, they can be decomposed order by order into the Fourier series

$$\Gamma^{(j)}_{s_1s_2;s_3s_4}(\mathbf{k},-\mathbf{k};\mathbf{p},-\mathbf{p}) = \sum_{m,n=-\infty}^{\infty} \Gamma^{(j)\{m,n\}}_{s_1s_2;s_3s_4} e^{mi\theta_{\mathbf{p}}} e^{ni\theta_{\mathbf{k}}}, \tag{B.3.64}$$

where the coefficients in front of $e^{im\theta_{\mathbf{p}}}e^{in\theta_{\mathbf{k}}}$ are determined using the orthogonality property

$$\Gamma^{(j)\{m,n\}}_{s_1s_2;s_4s_3}(\mathbf{k},-\mathbf{k};\mathbf{p},-\mathbf{p}) = \int_0^{2\pi}\frac{d\theta_{\mathbf{k}}}{2\pi}\int_0^{2\pi}\frac{d\theta_{\mathbf{p}}}{2\pi}\Gamma^{(j)}_{s_1s_2;s_4s_3}(\mathbf{k},-\mathbf{k};\mathbf{p},-\mathbf{p})e^{-im\theta_{\mathbf{p}}}e^{-in\theta_{\mathbf{k}}}. \tag{B.3.65}$$

Resumming the coefficients of $e^{im\theta_{\mathbf{p}}}e^{in\theta_{\mathbf{k}}}$ to infinite order (with m and n being fixed)

$$\Gamma^{(\infty)\{m,n\}}_{s_1s_2;s_4s_3}(\mathbf{k},-\mathbf{k};\mathbf{p},-\mathbf{p}) = \sum_{j=1}^{\infty}\Gamma^{(j)\{m,n\}}_{s_1s_2;s_4s_3}(\mathbf{k},-\mathbf{k};\mathbf{p},-\mathbf{p}) \tag{B.3.66}$$

we can find the renormalized amplitudes. For each combination of partial harmonics, which occurs to second order in the magnetic field, we derive explicitly the scattering amplitudes up to seventh order in the Cooper channel renormalization parameter UL and then make a guess for general j-th order amplitude. The final result is obtained by resumming these amplitudes to infinite order and then substituted into the RG flow equations to check the correctness of our guess. In all cases, the guess turns out to be correct. All *nonzero* RG charges as well as their large L limits are listed below. We begin with the $n = m = 0$ and $n = m = 1$ harmonics, given by

$$U_{ss;ss}(L) = \frac{U}{2}\frac{1}{2+UL} + \frac{U}{8}\delta^2 = \frac{U}{8}\delta^2 + \mathcal{O}(\ln^{-1}T), \tag{B.3.67}$$

$$U_{ss;-s-s}(L) = \frac{U}{2}\frac{1}{2+UL} - \frac{U}{8}\delta^2 = -\frac{U}{8}\delta^2 + \mathcal{O}(\ln^{-1}T), \tag{B.3.68}$$

$$U_{s-s;-ss}(L) = \frac{U}{2}\frac{1}{2+UL} - \frac{U}{8}\frac{1}{1+UL}\delta^2 = \mathcal{O}(\ln^{-1}T), \tag{B.3.69}$$

$$U_{s-s;s-s}(L) = \frac{U}{2}\frac{1}{2+UL} + \frac{U}{8}\frac{1}{1+UL}\delta^2 = \mathcal{O}(\ln^{-1}T), \tag{B.3.70}$$

$$U_{\sigma(\pm\mp;\mp\mp)}(L) = \frac{U}{2}\frac{1}{2+UL} = \mathcal{O}(\ln^{-1}T), \tag{B.3.71}$$

$$V_{ss;ss}(L) = \frac{U}{2}\frac{1}{1+UL} - \frac{U}{4}\frac{1}{(1+UL)^2}\delta^2 = \mathcal{O}(\ln^{-1} T), \tag{B.3.72}$$

$$V_{ss;-s-s}(L) = -\frac{U}{2}\frac{1}{1+UL} + \frac{U}{4}\frac{1}{(1+UL)^2}\delta^2 = \mathcal{O}(\ln^{-1} T), \tag{B.3.73}$$

$$V_{s-s;-ss}(L) = -\frac{U}{2} + \frac{U}{4}(1+UL)\delta^2 = -\frac{U}{2} + \mathcal{O}(U^2), \tag{B.3.74}$$

$$V_{s-s;s-s}(L) = \frac{U}{2} - \frac{U}{4}(1+UL)\delta^2 = \frac{U}{2} + \mathcal{O}(U^2). \tag{B.3.75}$$

An important remark should be made at this point: in addition to amplitudes which flow either to zero or to finite values at low temperatures, there are also amplitudes which grow logarithmically at low temperatures, namely, the amplitudes in Equations(B.3.74) and (B.3.75). This peculiar feature, which occurs only in the presence of both the SOI and in-plane magnetic field, may indicate a phase transition below certain field-dependent temperature or it may be an artifact of the expansion to lowest order in δ^2. In the derivation of the spin susceptibility that follows in Appendix B.3.2, we assume that the electron gas is far above the temperature below which the instability becomes important, i.e., that $UL \ll 1/\delta^2$, so that the effect of the instability can be neglected but the nonperturbative regime of Cooper renormalization, where $1 \ll UL \ll 1/\delta^2$, can still be accessed.

The remaining harmonics are

$$W_{ss;ss}(L) = U_{ss;ss}(L), \tag{B.3.76}$$

$$W_{ss;-s-s}(L) = U_{ss;-s-s}(L), \tag{B.3.77}$$

$$W_{s-s;-ss}(L) = U_{s-s;-ss}(L), \tag{B.3.78}$$

$$W_{s-s;s-s}(L) = U_{s-s;s-s}(L), \tag{B.3.79}$$

$$W_{\sigma(\pm\mp;\mp\mp)}(L) = -U_{\sigma(\pm\mp;\mp\mp)}(L), \tag{B.3.80}$$

$$A_{ss;ss}(L) = -A_{ss;-s-s}(L) = \frac{U}{16}\frac{1}{1+UL}\delta^2 = \mathcal{O}(\ln^{-1} T), \tag{B.3.81}$$

$$A_{s-s;-ss}(L) = -A_{s-s;s-s}(L) = -\frac{U}{16}\delta^2 \tag{B.3.82}$$

$$B_{s_1 s_2; s_3 s_4}(L) = A_{s_1 s_2; s_3 s_4}(L). \tag{B.3.83}$$

$$F_{\pm\mp;\mp\mp}(L) = -\frac{U}{4}i\delta, \tag{B.3.84}$$

$$F_{\mp\pm;\mp\mp}(L) = \frac{U}{4}i\delta, \tag{B.3.85}$$

$$F_{\mp\mp;\pm\mp}(L) = -\frac{U}{4}\frac{1}{1+UL}i\delta = \mathcal{O}(\ln^{-1} T), \tag{B.3.86}$$

$$F_{\mp\mp;\mp\pm}(L) = \frac{U}{4}\frac{1}{1+UL}i\delta = \mathcal{O}(\ln^{-1} T), \tag{B.3.87}$$

$$G_{\pm\mp;\mp\mp}(L) = \frac{U}{4}\frac{1}{1+UL}i\delta = \mathcal{O}(\ln^{-1}T), \tag{B.3.88}$$

$$G_{\mp\pm;\mp\mp}(L) = -\frac{U}{4}\frac{1}{1+UL}i\delta = \mathcal{O}(\ln^{-1}T), \tag{B.3.89}$$

$$G_{\mp\mp;\pm\mp}(L) = \frac{U}{4}i\delta, \tag{B.3.90}$$

$$G_{\mp\mp;\mp\pm}(L) = -\frac{U}{4}i\delta, \tag{B.3.91}$$

$$H_{s_1s_2;s_3s_4}(L) = G_{s_1s_2;s_3s_4}(L) \tag{B.3.92}$$

$$J_{s_1s_2;s_3s_4}(L) = F_{s_1s_2;s_3s_4}(L) \tag{B.3.93}$$

$$L_{ss;ss}(L) = \frac{U}{2}\frac{1}{(2+UL)^2} + \frac{U}{8}\delta^2 = \frac{U}{8}\delta^2 + \mathcal{O}(\ln^{-1}T), \tag{B.3.94}$$

$$L_{ss;-s-s}(L) = \frac{U}{2}\frac{1}{(2+UL)^2} - \frac{U}{8}\delta^2 = -\frac{U}{8}\delta^2 + \mathcal{O}(\ln^{-1}T), \tag{B.3.95}$$

$$L_{s-s;-ss}(L) = \frac{U}{8}\frac{(4+3UL)UL}{(1+UL)(2+UL)^2}\delta^2 = \mathcal{O}(\ln^{-1}T), \tag{B.3.96}$$

$$L_{s-s;s-s}(L) = \frac{U}{8}\frac{8+12UL+5U^2L^2}{(1+UL)(2+UL)^2}\delta^2 = \mathcal{O}(\ln^{-1}T), \tag{B.3.97}$$

$$L_{\pm\mp;\mp\mp}(L) = L_{\mp\pm;\mp\mp}(L) = -\frac{U}{2}\frac{1+UL}{(2+UL)^2}\delta^2 = \mathcal{O}(\ln^{-1}T), \tag{B.3.98}$$

$$L_{\mp\mp;\pm\mp}(L) = L_{\mp\mp;\mp\pm}(L) = -\frac{U}{2}\frac{1}{(2+UL)^2}\delta^2 = \mathcal{O}(\ln^{-1}T). \tag{B.3.99}$$

$$M_{ss;ss}(L) = L_{ss;ss}(L), \tag{B.3.100}$$

$$M_{ss;-s-s}(L) = L_{ss;-s-s}(L), \tag{B.3.101}$$

$$M_{s-s;-ss}(L) = L_{s-s;-ss}(L), \tag{B.3.102}$$

$$M_{s-s;s-s}(L) = L_{s-s;s-s}(L), \tag{B.3.103}$$

$$M_{\pm\mp;\mp\mp}(L) = L_{\mp\pm;\mp\mp}(L) = -\frac{U}{2}\frac{1}{(2+UL)^2}\delta^2 = \mathcal{O}(\ln^{-1}T), \tag{B.3.104}$$

$$M_{\mp\mp;\pm\mp}(L) = L_{\mp\mp;\mp\pm}(L) = -\frac{U}{2}\frac{1+UL}{(2+UL)^2}\delta^2 = \mathcal{O}(\ln^{-1}T), \tag{B.3.105}$$

$$P_{s_1s_2;s_3s_4}(L) = Q_{s_1s_2;s_3s_4}(L) = -3A_{s_1s_2;s_3s_4}(L), \tag{B.3.106}$$

$$R_{ss;ss}(L) = R_{ss;-s-s}(L) = R_{s-s;-ss}(L) = R_{s-s;s-s}(L) = -\frac{U}{4}\frac{1}{2+UL}\delta^2 = \mathcal{O}(\ln^{-1}T), \tag{B.3.107}$$

$$R_{\sigma(\pm\mp;\mp\mp)}(L) = \frac{U}{4}\frac{1}{2+UL}\delta^2 = \mathcal{O}(\ln^{-1}T), \tag{B.3.108}$$

$$S_{s_1s_2;s_3s_4}(L) = R_{s_1s_2;s_3s_4}(L). \tag{B.3.109}$$

It can be readily verified that all the amplitudes satisfy RG equations (B.3.48)–(B.3.62) with initial conditions (B.3.32)–(B.3.46) up to $\mathcal{O}(\delta^3)$ accuracy.

Finally, the renormalized scattering amplitude is given by

$$\begin{aligned}\Gamma_{s_1s_2;s_3s_4}(\mathbf{k},-\mathbf{k};\mathbf{p},-\mathbf{p}) &= U_{s_1s_2;s_3s_4}(L) + V_{s_1s_2;s_3s_4}(L)e^{i\theta_{\mathbf{p}}}e^{-i\theta_{\mathbf{k}}} + W_{s_1s_2;s_3s_4}(L)e^{2i\theta_{\mathbf{p}}}e^{-2i\theta_{\mathbf{k}}} \\ &+ A_{s_1s_2;s_3s_4}(L)e^{i\theta_{\mathbf{p}}}e^{i\theta_{\mathbf{k}}} + B_{s_1s_2;s_3s_4}(L)e^{-i\theta_{\mathbf{p}}}e^{-i\theta_{\mathbf{k}}} + F_{s_1s_2;s_3s_4}(L)e^{2i\theta_{\mathbf{p}}}e^{-i\theta_{\mathbf{k}}} \\ &+ G_{s_1s_2;s_3s_4}(L)e^{i\theta_{\mathbf{p}}}e^{-2i\theta_{\mathbf{k}}} + H_{s_1s_2;s_3s_4}(L)e^{i\theta_{\mathbf{p}}} + J_{s_1s_2;s_3s_4}(L)e^{-i\theta_{\mathbf{k}}} + L_{s_1s_2;s_3s_4}(L)e^{2i\theta_{\mathbf{p}}} \\ &+ M_{s_1s_2;s_3s_4}(L)e^{-2i\theta_{\mathbf{k}}} + P_{s_1s_2;s_3s_4}(L)e^{3i\theta_{\mathbf{p}}}e^{-i\theta_{\mathbf{k}}} + Q_{s_1s_2;s_3s_4}(L)e^{i\theta_{\mathbf{p}}}e^{-3i\theta_{\mathbf{k}}} \\ &+ R_{s_1s_2;s_3s_4}(L)e^{4i\theta_{\mathbf{p}}}e^{-2i\theta_{\mathbf{k}}} + S_{s_1s_2;s_3s_4}(L)e^{2i\theta_{\mathbf{p}}}e^{-4i\theta_{\mathbf{k}}}.\end{aligned} \tag{B.3.110}$$

Renormalization of the in-plane component

As for the transverse-field case, the free energy for the in-plane magnetic field is found by replacing the bare interaction U in Equation (3.3.39) by the renormalized vertex Γ

$$\begin{aligned}\delta\Xi_{xx} = -\frac{1}{4}\int_0^{2\pi}\frac{d\theta_{\mathbf{k}}}{2\pi}T\sum_{\Omega}\sum_{\{s_i\}}\int_0^{\infty}\frac{qdq}{2\pi}\Gamma_{s_1s_4;s_3s_2}(\mathbf{k},-\mathbf{k};-\mathbf{k},\mathbf{k}) \\ \times\Gamma_{s_3s_2;s_1s_4}(-\mathbf{k},\mathbf{k};\mathbf{k},-\mathbf{k})\Pi_{s_1s_2}^{+\mathbf{k}_F}\Pi_{s_3s_4}^{-\mathbf{k}_F},\end{aligned} \tag{B.3.111}$$

where $\Pi_{ss'}^{\pm\mathbf{k}_F}$ given by Equation (3.3.40) depends on the direction of the electron momentum with respect to the magnetic field.

A general formula for $\delta\Xi_{xx}$ is very complicated; however, in the regime of strong Cooper renormalization, i.e. for $1 \ll UL \ll 1/\delta^2$, there are only a few partial amplitudes which survive the downward renormalization. Keeping only these partial amplitudes in Γ, we obtain for the thermodynamic potential

$$\begin{aligned}\delta\Xi_{xx} = &-\frac{U^2}{16}\int_0^{2\pi}\frac{d\theta_{\mathbf{k}}}{2\pi}T\sum_{\Omega}\int\frac{qdq}{2\pi}[(\Pi_{-+}^{+\mathbf{k}_F}\Pi_{-+}^{-\mathbf{k}_F} + \Pi_{+-}^{+\mathbf{k}_F}\Pi_{+-}^{-\mathbf{k}_F} - 2\Pi_0^2) + 4\Pi_0^2] \\ &-\frac{\Delta^2}{\alpha^2k_F^2}\frac{U^2}{8}T\sum_{\Omega}\int\frac{qdq}{2\pi}[\Pi_0(\Pi_{-+}+\Pi_{+-}-2\Pi_0)+\Pi_0^2],\end{aligned} \tag{B.3.112}$$

where the angular dependence of the polarization bubbles in the second line was neglected because of an overall factor Δ^2 originating from the scattering amplitudes, and the angular integral in those terms was readily performed. On the other hand, the field dependence in the first term is exclusively due to the bubbles, hence the angular integration has to be carried out last. The integrals over the momentum and frequency yield

$$\delta\Xi_{xx} = -\frac{T^3}{8\pi v_F^2}\left(\frac{mU}{4\pi}\right)^2\left[\int_0^{2\pi}\frac{d\theta_{\mathbf{k}}}{2\pi}\mathcal{F}\left(\frac{\bar{\Delta}_{\mathbf{k}_F}+\bar{\Delta}_{-\mathbf{k}_F}}{T}\right)+2\frac{\Delta^2}{\alpha^2k_F^2}\mathcal{F}\left(\frac{|\alpha|k_F}{T}\right)\right]. \tag{B.3.113}$$

Expanding $\mathcal{F}(x) \approx x^3/3$ for $x \gg 1$ and differentiating with respect to the field twice, we obtain for the nonanalytic part of the spin susceptibility

$$\delta\chi_{xx} = \frac{1}{3}\chi_0 \left(\frac{mU}{4\pi}\right)^2 \frac{|\alpha|k_F}{E_F}. \tag{B.3.114}$$

Somewhat unexpectedly, the fully renormalized result (B.3.114) coincides with the leading (first) term in the second-order result (3.3.55). The formally subleading but T-dependent $T/2E_F$ term in Equation (3.3.55) does not show up in the fully renormalized result, which implies that, at best, it is of order $T/UL \propto T/\ln T$ for large but finite UL. Hence follows the result for $\delta\chi_{xx}$ presented in the main text, Equation (3.4.39).

Appendix C

Appendix to 'Ferromagnetic order of nuclear spins coupled to conduction electrons: a combined effect of electron-electron and spin-orbit interactions'

C.1 Derivation of common integrals

In this Appendix, we derive explicit expressions for some integrals of the Green's function which occur throughout the paper.

C.1.1 "Quaternions" (I_{lmnr} and J_{lmnr}) and a "triad" (I_{lmn})

The first integral is a "quaternion"–a convolution of four Green's functions defined by Equation (4.2.7e). This convolution occurs in diagram 1, where it needs to be evaluated at small external and transferred momenta: $q, \tilde{q} \ll k_F$. To linear order in q and α, $\epsilon_{\mathbf{k}+\mathbf{q}} + s\alpha|\mathbf{k}+\mathbf{q}| = \epsilon_k + v_F q\cos\theta_{kq} + \alpha k_F + o(q^2, \alpha q)$ with $\theta_{kq} \equiv \angle(\mathbf{k}, \mathbf{q})$. The same approximation holds for $\tilde{\mathbf{q}}$ with $\theta_{k\tilde{q}} \equiv \angle(\mathbf{k}, \tilde{\mathbf{q}})$. Switching to polar coordinates and replacing kdk by $m^* d\epsilon_k$, we reduce the integral to

$$I_{lmnr}(\Omega, \theta_{k\tilde{q}}, q, \tilde{q}) = m^* \int \frac{d\theta_{kq}}{2\pi} \int \frac{d\omega_k}{2\pi} \int \frac{d\epsilon_k}{2\pi} \frac{1}{i\omega_k - \epsilon_k - v_F \tilde{q}\cos\theta_{k\tilde{q}} - l\alpha k_F} \times \frac{1}{i\omega_k a - \epsilon_k - m\alpha k_F} \frac{1}{i(\omega_k + \Omega) - \epsilon_k - v_F q\cos\theta_{kq} - n\alpha k_F} \frac{1}{i\omega_k - \epsilon_k - r\alpha k_F}. \tag{C.1.1}$$

Integrating first over ϵ_k and then over ω_k, we obtain

$$I_{lmnr}(\Omega,\theta_{k\tilde{q}},q,\tilde{q}) = \frac{im^*\Omega}{(2\pi)^2}\int d\theta_{kq}\frac{1}{i\Omega - v_F q\cos\theta_{kq} + (m-n)\alpha k_F} \times \frac{1}{i\Omega - v_F q\cos\theta_{kq} + (r-n)\alpha k_F}\frac{1}{i\Omega - v_F q\cos\theta_{kq} + v_F\tilde{q}\cos\theta_{k\tilde{q}} + (l-n)\alpha k_F}. \tag{C.1.2}$$

Finally, the integral over θ_{kq} gives

$$\begin{aligned} I_{lmnr}(\Omega,\theta_{k\tilde{q}},q,\tilde{q}) =& \frac{m^*|\Omega|}{2\pi}\frac{1}{(r-m)\alpha k_F[(l-m)\alpha k_F + v_F\tilde{q}\cos\theta_{k\tilde{q}}][(l-r)\alpha k_F + v_F\tilde{q}\cos\theta_{k\tilde{q}}]} \\ &\times\left[\frac{(l-r)\alpha k_F + v_F\tilde{q}\cos\theta_{k\tilde{q}}}{\sqrt{v_F^2q^2 + (\Omega + i(n-m)\alpha k_F)^2}} - \frac{(l-m)\alpha k_F + v_F\tilde{q}\cos\theta_{k\tilde{q}}}{\sqrt{v_F^2q^2 + (\Omega + i(n-r)\alpha k_F)^2}}\right. \\ &\left.\times + \frac{(r-m)\alpha k_F}{\sqrt{v_F^2q^2 + (\Omega - iv_F\tilde{q}\cos\theta_{k\tilde{q}} + i(n-l)\alpha k_F)^2}}\right]. \end{aligned} \tag{C.1.3}$$

Because to the overall term $(r-m)\alpha k_F$ in the denominator, the case $r = m$ has to be treated specially. Taking the limit $I_{lmnm}(\Omega,\theta_{k\tilde{q}},q,\tilde{q}) = \lim_{r\to m} I_{lmnr}(\Omega,\theta_{k\tilde{q}},q,\tilde{q})$, one obtains

$$\begin{aligned} I_{lmnm}(\Omega,\theta_{k\tilde{q}},q,\tilde{q}) =& \frac{m^*|\Omega|}{2\pi}\frac{1}{[(l-m)\alpha k_F + v_F\tilde{q}\cos\theta_{k\tilde{q}}]^2} \\ &\times\left[\frac{1}{\sqrt{v_F^2q^2 + (\Omega - iv_F\tilde{q}\cos\theta_{k\tilde{q}} + i(n-l)\alpha k_F)^2}}\right. \\ &\left. - \frac{v_F^2q^2 + [\Omega + i(n-m)\alpha k_F][\Omega + iv_F\tilde{q}\cos\theta_{k\tilde{q}} + i(l+n-2m)\alpha k_F]}{[v_F^2q^2 + (\Omega + i(n-m)\alpha k_F)^2]^{3/2}}\right]. \end{aligned} \tag{C.1.4}$$

Similarly, we obtain for another quaternion J_{lmnr}, defined by Equation (4.2.14c)

$$\begin{aligned} J_{lmnr}(\Omega,\theta_{k\tilde{q}},q,\tilde{q}) =& \frac{m^*|\Omega|}{2\pi}\frac{1}{\Omega - iv_F\tilde{q}\cos\theta_{k\tilde{q}} + i(n-m)\alpha k_F} \\ &\times\frac{1}{\Omega - iv_F\tilde{q}\cos\theta_{k\tilde{q}} + i(r-l)\alpha k_F}\left[\frac{1}{\sqrt{v_F^2q^2 + (\Omega - iv_F\tilde{q}\cos\theta_{k\tilde{q}} + i(r-m)\alpha k_F)^2}}\right. \\ &\left. + \frac{1}{\sqrt{v_F^2q^2 + (\Omega - iv_F\tilde{q}\cos\theta_{k\tilde{q}} + i(n-l)\alpha k_F)^2}}\right]. \end{aligned} \tag{C.1.5}$$

Finally, we obtain for a convolution of three Green's functions–a "triad"–defined by

Equation (4.2.14d)

$$I_{lmn}(\Omega,\theta_{k\tilde{q}},q,\tilde{q}) = \frac{m^*|\Omega|}{2\pi}\frac{1}{v_F\tilde{q}\cos\theta_{k\tilde{q}}+(l-m)\alpha k_F} \times\left[\frac{1}{\sqrt{v_F^2q^2+(\Omega+i(n-l)\alpha k_F-v_F\tilde{q}\cos\theta_{k\tilde{q}})^2}}-\frac{1}{\sqrt{v_F^2q^2+(\Omega+i(n-m)\alpha k_F)^2}}\right]. \tag{C.1.6}$$

C.1.2 Integrals over bosonic variables

There is a number of integrals over the bosonic frequency Ω and momentum $\mathbf{q}$ one encounters while calculating the spin susceptibility. The following strategy provides a convenient way of calculating all of them: (i) integrate over v_Fq for $x\in[0,\infty[$, (ii) integrate over Ω by introducing a cut-off Λ–the low-energy physics proves to be independent of the choice of the cut-off, (iii) perform angular integration, which is trivial for the out-of-plane spin susceptibility and, in that case, can be performed at the very beginning.

Again, it is convenient to treat the out-of-plane and in-plane components separately.

Out-of-plane components

As it was explained in the main text, the $\tilde{q}$ dependence of χ^{zz} for $\tilde{q}\ll q_\alpha$ can be calculated perturbatively, by expanding in $\tilde{q}/q_\alpha$, where $q_\alpha=2m^*|\alpha|$. In this section, we calculate only the leading term of this expansion obtained by setting $\tilde{q}=0$. Later, in Appendix C.2, we find the entire dependence of χ^{zz} on $\tilde{q}$ exactly, and show that this dependence is absent for $\tilde{q}\le q_\alpha$, which means that all terms of the expansion in $\tilde{q}/q_\alpha$ vanish. For now, we focus on the $\tilde{q}=0$ case and evaluate the integrals in Equations (4.2.8a) and (4.2.8b) for χ_1^{zz}

$$\begin{aligned}&\int\frac{d\Omega}{2\pi}\int\frac{d\theta_{k\tilde{q}}}{2\pi}\int\frac{qdq}{2\pi}(I_{+---}+I_{-+++})\Pi_0=\\&=\left(\frac{m}{8\pi^2v_F\alpha k_F}\right)^2\int_{-\infty}^{\infty}d\Omega\int_0^\infty xdx\,\frac{\Omega^2}{\sqrt{x^2+\Omega^2}}\left(\frac{1}{\sqrt{x^2+(\Omega+2i\alpha k_F)^2}}-\frac{1}{\sqrt{x^2+\Omega^2}}+\text{c.c.}\right)\\&=\left(\frac{m}{8\pi^2v_F\alpha k_F}\right)^2\int_{-\Lambda}^{\Lambda}d\Omega\Omega^2\ln\frac{\Omega^2}{\Omega^2+\alpha^2k_F^2}=\left(\frac{m}{4\pi v_F}\right)^2\frac{|\alpha|k_F}{6\pi}+\dots\end{aligned} \tag{C.1.7}$$

$$\int\frac{d\Omega}{2\pi}\int\frac{d\theta_{k\tilde{q}}}{2\pi}\int\frac{qdq}{2\pi}(I_{-+-+}\Pi_{-+}+I_{+-+-}\Pi_{+-})=$$
$$=\left(\frac{m}{8\pi^2 v_F\alpha k_F}\right)^2\int d\Omega\int xdx\left[\frac{1}{\sqrt{x^2+(\Omega+2i\alpha k_F)^2}}\right.$$
$$\left.\times\left(\frac{1}{\sqrt{x^2+\Omega^2}}-\frac{1}{\sqrt{x^2+(\Omega-2i\alpha k_F)^2}}+\frac{2i\alpha k_F(\Omega-2i\alpha k_F)}{[x^2+(\Omega-2i\alpha k_F)^2]^{3/2}}\right)+\text{c.c.}\right]$$
$$=\left(\frac{m}{8\pi^2 v_F\alpha k_F}\right)^2\int d\Omega\Omega^2\ln\frac{\Omega^2}{\Omega^2+\alpha^2k_F^2}=\left(\frac{m}{4\pi v_F}\right)^2\frac{|\alpha|k_F}{6\pi}+\ldots \qquad \text{(C.1.8)}$$

where ... stands for non-universal, Λ-dependent terms and c.c. denotes the complex conjugate of the preceding expression. Substituting these results back into Equations (4.2.8a) and (4.2.8b), we obtain Equations (4.2.9a) and (4.2.9b). Similarly, we obtain for the combination of triads in Equation (4.2.17) for χ_2^{zz}

$$2\int\frac{d\Omega}{2\pi}\int\frac{d\theta_{k\tilde{q}}}{2\pi}\int\frac{qdq}{2\pi}(I_{+--}I_{-++}+I_{+-+}I_{-+-})=$$
$$=-\left(\frac{m}{4\pi^2 v_F\alpha k_F}\right)^2\int d\Omega\int xdx\left|\frac{1}{\sqrt{x^2+(\Omega+2i\alpha k_F)^2}}-\frac{1}{\sqrt{x^2+\Omega^2}}\right|^2$$
$$=\left(\frac{m}{4\pi^2 v_F\alpha k_F}\right)^2\int d\Omega\Omega^2\ln\frac{\Omega^2}{\Omega^2+\alpha^2k_F^2}=\frac{2}{3\pi}\left(\frac{m}{4\pi v_F}\right)^2|\alpha|k_F+\ldots \qquad \text{(C.1.9)}$$

In-plane components

We start with χ_1^{xx} given by Equations (4.2.10a) and (4.2.10b). First, we notice that the quaternion structure of the first lines in Equations (4.2.10a) and (4.2.10b) is the same as in the first lines of Equations (4.2.8a) and (4.2.8b) for the out-of-plane component; the only difference is in the factor of $\sin^2\theta_{k\tilde{q}}$. Since these expressions contain α, they can be evaluated at $\tilde{q}=0$ in the same way as the corresponding expressions in χ_1^{zz} were evaluated. At $\tilde{q}=0$, the factor of $\sin^2\theta_{kq}$ just gives 1/2 of the corresponding contribution to χ_1^{zz}. Next, we calculate explicitly the integrals in the second line of Equation (4.2.10a) and in the third line of Equation (4.2.10b). These contributions contain an overall factor of $\tilde{q}^{-2}$ and, therefore, one has to calculate the full dependence on $\tilde{q}$ without expanding in $\tilde{q}/q_\alpha$. The part of the integrands that are odd in the angle drop out and, since $\int_0^{2\pi}d\theta f(i\cos\theta)=\int_0^{2\pi}d\theta[f(i\cos\theta)+f(-i\cos\theta)]/2$, all the formulas can be written in an explicitly real form. For the first of these two integrals we obtain

(for brevity, we relabel $\theta_{k\tilde{q}} \to \theta$)

$$\begin{aligned}
&\int \frac{d\Omega}{2\pi}\int \frac{d\theta}{2\pi}\int \frac{qdq}{2\pi}\cos^2\theta(I_{++++}+I_{----})\Pi_0 = \left(\frac{m}{4\pi^2 v_F^2\tilde{q}}\right)^2 \int_0^{2\pi}\frac{d\theta}{\pi}\int_{-\infty}^{\infty}d\Omega\int_0^{\infty}xdx \\
&\times \frac{\Omega^2}{\sqrt{x^2+\Omega^2}}\left(\frac{1}{\sqrt{x^2+(\Omega-iv_F\tilde{q}\cos\theta)^2}}-\frac{1}{\sqrt{x^2+\Omega^2}}\right)-\frac{i\Omega^3 v_F\tilde{q}\cos\theta}{(x^2+\Omega^2)^2} \\
&= \left(\frac{m}{4\pi^2 v_F^2\tilde{q}}\right)^2 \int_0^{2\pi}\frac{d\theta}{2\pi}\int_{-\infty}^{\infty}d\Omega\int_0^{\infty}xdx\frac{\Omega^2}{\sqrt{x^2+\Omega^2}}\left(\frac{1}{\sqrt{x^2+(\Omega+iv_F\tilde{q}\cos\theta)^2}}\right. \\
&\left.-\frac{1}{\sqrt{x^2+\Omega^2}}+\text{c.c.}\right) = -\left(\frac{m}{4\pi^2 v_F^2\tilde{q}}\right)^2 \int_{-\Lambda}^{\Lambda}d\Omega\int_0^{2\pi}\frac{d\theta}{2\pi}\Omega^2\ln\left(1+\frac{v_F^2\tilde{q}^2}{4\Omega^2}\cos\theta^2\right) \\
&= -2\left(\frac{m}{4\pi^2 v_F^2\tilde{q}}\right)^2 \int_{-\Lambda}^{\Lambda}d\Omega\Omega^2\ln\left[\frac{1}{2}\left(1+\sqrt{1+\frac{v_F^2\tilde{q}^2}{4\Omega^2}}\right)\right] = \left(\frac{m}{4\pi v_F}\right)^2\frac{v_F\tilde{q}}{9\pi^2}+\dots
\end{aligned} \tag{C.1.10}$$

where, as before, ... stands for non-universal, Λ-dependent terms. Notice that the SOI dropped out and, therefore, the equation above is valid for any ratio $\tilde{q}/q_\alpha$. The second integral reads as

$$\begin{aligned}
&\int \frac{d\Omega}{2\pi}\int \frac{d\theta_{k\tilde{q}}}{2\pi}\int \frac{qdq}{2\pi}\cos^2\theta(I_{++-+}\Pi_{-+}+I_{--+-}\Pi_{+-}) = \left(\frac{m}{4\pi^2 v_F^2\tilde{q}}\right)^2 \int \frac{d\theta}{\pi}\int d\Omega\int xdx \\
&\times\left\{\left[\frac{\Omega^2}{\sqrt{x^2+(\Omega+2i\alpha k_F)^2}}\left(\frac{1}{\sqrt{x^2+(\Omega-2i\alpha k_F-iv_F\tilde{q}\cos\theta)^2}}\right.\right.\right. \\
&\left.\left.\left.+\frac{1}{\sqrt{x^2+(\Omega-2i\alpha k_F+iv_F\tilde{q}\cos\theta)^2}}-\frac{2}{\sqrt{x^2+(\Omega-2i\alpha k_F)^2}}\right)+\text{c.c.}\right]\right. \\
&\left.-\frac{i\Omega^2 v_F\tilde{q}\cos\theta}{|x^2+(\Omega+2i\alpha k_F)^2|^2}\left[\frac{\Omega+2i\alpha k_F}{x^2+(\Omega+2i\alpha k_F)^2}+\text{c.c.}\right]\right\} \\
&= -\left(\frac{m}{4\pi^2 v_F^2\tilde{q}}\right)^2 \int_{-\Lambda}^{\Lambda}d\Omega\Omega^2\int\frac{d\theta}{2\pi}\ln\left(1+\frac{v_F^2\tilde{q}^2}{4\Omega^2}\cos^2\theta\right) = \left(\frac{m}{4\pi v_F}\right)^2\frac{v_F\tilde{q}}{9\pi^2}+\dots
\end{aligned} \tag{C.1.11}$$

which is the same result as in Equation (C.1.10). The second line in Equation (4.2.10b) gives the same result as the third one. Collecting all the results above, we arrive at Equations (4.2.11a) and (4.2.11b).

Finally, for the SOI-independent part of diagram 3, we find

$$\begin{aligned}
&\int\frac{d\Omega}{2\pi}\int\frac{d\theta_{k\tilde{q}}}{2\pi}\int\frac{qdq}{2\pi}\cos^2\theta[I_{+++}(\Omega,\theta_{k\tilde{q}},q,\tilde{q})I_{---}(\Omega,\theta_{k\tilde{q}},q,-\tilde{q})\\
&+I_{++-}(\Omega,\theta_{k\tilde{q}},q,\tilde{q})I_{--+}(\Omega,\theta_{k\tilde{q}},q,-\tilde{q})+(\tilde{q}\to-\tilde{q})]\\
&=-\left(\frac{m}{4\pi^2v_F^2\tilde{q}}\right)^2\int\frac{d\theta}{\pi}\int d\Omega\Omega^2\int xdx\left(\left|\frac{1}{\sqrt{x^2+(\Omega+iv_F\tilde{q}\cos\theta)^2}}-\frac{1}{\sqrt{x^2+\Omega^2}}\right|^2\right.\\
&\left.+\left|\frac{1}{\sqrt{x^2+(\Omega+2i\alpha k_F+iv_F\tilde{q}\cos\theta)^2}}-\frac{1}{\sqrt{x^2+(\Omega+2i\alpha k_F)^2}}\right|^2\right)\\
&=-2\left(\frac{m}{4\pi^2v_F^2\tilde{q}}\right)^2\int d\Omega\Omega^2\int\frac{d\theta}{\pi}\ln\left(1+\frac{v_F^2\tilde{q}^2\cos^2\theta}{\Omega^2}\right)\\
&=-2\left(\frac{m}{2\pi^2v_F^2\tilde{q}}\right)^2\int_{-\Lambda}^{\Lambda}d\Omega\Omega^2\ln\frac{1}{2}\left(1+\sqrt{1+\frac{v_F^2\tilde{q}^2}{4\Omega^2}}\right)=\left(\frac{m}{2\pi v_F}\right)^2\frac{v_F\tilde{q}}{9\pi^2}+\dots
\end{aligned}\tag{C.1.12}$$

C.2 Full $\tilde{q}$ dependence of the spin susceptibility

In the main text and preceding Appendices we found χ^{zz} at zero external momentum. Here, we show how the full dependence of χ^{zz} can be found using the $q=0$ part of diagram 1 in Figure 4.2 as an example.

We consider Equation (4.2.8a) at finite $\tilde{q}$. The integral over bosonic variables reads as reads

$$\begin{aligned}
&\int\frac{d\Omega}{2\pi}\int\frac{d\theta}{2\pi}\int\frac{qdq}{2\pi}\left[I_{+---}+I_{-+++}\right]\Pi_0(\Omega,q)\\
&=\left(\frac{m}{4\pi^2v_F}\right)^2\int_0^{2\pi}\frac{d\theta}{2\pi}\int_{-\infty}^{\infty}d\Omega\int_0^{\infty}xdx\frac{\Omega^2}{\sqrt{x^2+\Omega^2}}\left[\frac{1}{(2\alpha k_F+v_F\tilde{q}\cos\theta)^2}\right.\\
&\times\left(\frac{1}{\sqrt{x^2+(\Omega-2i\alpha k_F-iv_F\tilde{q}\cos\theta)^2}}-\frac{1}{\sqrt{x^2+\Omega^2}}-\frac{i\Omega(2\alpha+v_F\tilde{q}\cos\theta)}{(x^2+\Omega^2)^{3/2}}\right)\\
&\left.+(\alpha\to-\alpha)\right],
\end{aligned}\tag{C.2.1}$$

where $(\alpha\to-\alpha)$ stands for a preceding term with a reversed sign of α and, as before, we relabeled $\theta_{k\tilde{q}}\to\theta$. The last term in the parenthesis vanishes upon integration over either the angle (in the principal value sense) or the frequency (it is odd in Ω), whereas

the remainder yields

$$\int_0^{2\pi}\frac{d\theta}{2\pi}\int_{-\infty}^{\infty}d\Omega\int_0^{\infty}xdx\frac{\Omega^2}{\sqrt{x^2+\Omega^2}}\frac{1}{(2\alpha k_F+v_F\tilde{q}\cos\theta)^2}\left(\frac{1}{\sqrt{x^2+(\Omega+2i\alpha k_F+iv_F\tilde{q}\cos\theta)^2}}\right.$$
$$\left.-\frac{1}{\sqrt{x^2+\Omega^2}}+\text{c.c.}\right)=-\int_0^{2\pi}\frac{d\theta}{2\pi}\int_{-\Lambda}^{\Lambda}d\Omega\Omega^2\frac{\ln\left[1+(2\alpha k_F+v_F\tilde{q}\cos\theta)^2/4\Omega^2\right]}{(2\alpha k_F+v_F\tilde{q}\cos\theta)^2}$$
$$=\frac{1}{24}\int_0^{2\pi}d\theta|2\alpha k_F+v_F\tilde{q}\cos\theta|=\frac{v_F\tilde{q}}{6}\text{Re}\left[\sqrt{1-\left(\frac{q_\alpha}{\tilde{q}}\right)^2}+\frac{q_\alpha}{\tilde{q}}\left(\frac{\pi}{2}-\arccos\frac{q_\alpha}{\tilde{q}}\right)\right]$$
$$=\begin{cases}\pi v_F q_\alpha/12 & \text{for } \tilde{q}\le q_\alpha,\\ \frac{v_F\tilde{q}}{6}\left[1+\frac{1}{2}\left(\frac{q_\alpha}{\tilde{q}}\right)^2+\ldots\right] & \text{for } \tilde{q}\gg q_\alpha.\end{cases}\tag{C.2.2}$$

We see that while χ_1^{zz} is independent of $\tilde{q}$ for $\tilde{q}\le q_\alpha$, for $q_\alpha\gg q_\alpha$ it approaches the linear-in-$\tilde{q}$ form found in [Chubukov03] in the absence of the SOI.

Another integral of this type occurs in the in-plane component, e.g., in the first line of Equation (4.2.10a). The only difference compared to the out-of-plane part is an extra $\sin^2\theta$ factor. The q and Ω integrals are calculated in the same way while the angular integral is replaced by

$$\int\frac{d\Omega}{2\pi}\int\frac{d\theta}{2\pi}\int\frac{qdq}{2\pi}\sin^2\theta\left[I_{+---}+I_{-+++}\right]\Pi=\frac{1}{24}\int_0^{2\pi}d\theta\sin^2\theta|2\alpha k_F+v_F\tilde{q}\cos\theta|$$
$$=\frac{v_F\tilde{q}}{12}\,\text{Re}\left[\frac{1}{3}\sqrt{1-\left(\frac{q_\alpha}{\tilde{q}}\right)^2}\left\{2+\left(\frac{q_\alpha}{\tilde{q}}\right)^2\right\}+\frac{q_\alpha}{\tilde{q}}\left(\frac{\pi}{2}-\arccos\frac{q_\alpha}{\tilde{q}}\right)\right]$$
$$=\begin{cases}\pi v_F q_\alpha/24 & \text{for } \tilde{q}\le q_\alpha,\\ \frac{v_F\tilde{q}}{18}\left[1+\frac{3}{2}\left(\frac{q_\alpha}{\tilde{q}}\right)^2+\ldots\right] & \text{for } \tilde{q}\gg q_\alpha.\end{cases}\tag{C.2.3}$$

C.3 Logarithmic renormalization

In this Appendix, we analyze renormalization of the out-of-plane component of the spin susceptibility in the Cooper channel for $\tilde{q}\ll q_\alpha$. As an example, we consider diagram 1 at large momentum transfer to third order in the electron-electron interaction, see Figure C.1. The calculation is carried out most conveniently in the chiral basis as shown

below

$$\begin{aligned}\chi^{xx}_{1,q=2k_F} =& -2U^3 \int_Q \int_K \int \frac{d\omega_p}{2\pi} \int \frac{d\epsilon_k}{2\pi} \int_P \int_L \mathrm{Tr}[G(-K+Q)G(-P+Q)G(-L+Q)] \\ & \times \mathrm{Tr}[G(K+\tilde{Q})\sigma^x G(K)G(P)G(L)G(K)\sigma^x] \\ =& -4U^3 \int \frac{d\Omega}{2\pi} \int \frac{d\theta_{k\tilde{q}}}{2\pi} \int \frac{qdq}{2\pi} \int \frac{d\theta_l}{2\pi} \sum_{\{s_i\}} \Gamma_{tm;ns}(\theta_k,\theta_p)\Gamma_{ns;vu}(\theta_p,\theta_l)\Gamma_{vu;tr}(\theta_l,\theta_k) \\ & \times \sigma^x_{rl}(\theta_k)\sigma^x_{lm}(\theta_k) I_{lmnr}\Pi_{st}L_{uv}, \end{aligned} \tag{C.3.1}$$

where

$$\Gamma_{s_1s_2;s_4s_3}(\theta_k,\theta_p) \equiv U\langle \mathbf{p},s_3|\mathbf{k},s_1\rangle\langle \mathbf{p},s_4|\mathbf{k},s_2\rangle = \frac{U}{4}\left(1+s_1s_3e^{i(\theta_p-\theta_k)}\right)\left(1+s_2s_4e^{i(\theta_p-\theta_k)}\right) \tag{C.3.2}$$

is the scattering amplitude in the Cooper channel ($\mathbf{k}=-\mathbf{p}$) , $\sigma_{st}(\theta_k) \equiv \langle \mathbf{k},s|\,\sigma^x\,|\mathbf{k},t\rangle = -i(se^{i\theta_k}-te^{-i\theta_k})/2$, and

$$\begin{aligned} L_{uv} &= \frac{m}{2\pi}\int d\omega_l \int d\epsilon_l g_u(L) g_v(-L+Q) = \frac{m}{4\pi}\ln\frac{\Lambda^2}{(v_Fq\cos\theta_{lq}+(u-v)\alpha k_F)^2+\Omega^2} \\ &= \begin{cases} \frac{m}{4\pi}\ln\frac{\Lambda^2}{\alpha^2k_F^2} \equiv L(\alpha) & \text{for } u=v \\ \frac{m}{4\pi}\ln\frac{\Lambda^2}{v_F^2q^2\cos^2\theta_{lq}+\Omega^2} \equiv L(q) & \text{for } u=-v \end{cases} \end{aligned} \tag{C.3.3}$$

is the particle-particle (Cooper) propagator, evaluated on the Fermi surface at fixed direction of the fermionic momentum $\mathbf{l}$. An additional factor of 2 in Equation (C.3.1) is related to the possibility of extracting the logarithmic contribution from either the integral over P or that over L. Note that each scattering amplitude depends on the difference of two angles, i.e., $\theta_p-\theta_l=\theta_{pq}-\theta_{lq}$, such that the angle θ_{lq} is shared between the vertices and the function L_{uv}. Moreover, due to the correlation of momenta, we have $\theta_p=\theta_k+\pi$ and $\theta_k=\pi/2-\theta_{k\tilde{q}}$.

Upon summation over the Rashba indices, the integration over θ_{lq} is readily carried out in all $u=v$ terms, whereas the $u=-v$ terms require more a careful treatment. Due to the dependence of the scattering amplitudes on θ_{lq}, L_{uv} enters multiplied by a either constant, or by $\sin 2\theta_{lq}$, or else by $\cos 2\theta_{lq}$

$$\int_0^{2\pi}\frac{d\theta_{lq}}{2\pi}\begin{bmatrix}1\\ \sin 2\theta_{lq}\\ \cos 2\theta_{lq}\end{bmatrix} L(q) = \frac{m}{2\pi}\begin{bmatrix}\ln\frac{\Lambda}{|\Omega|+\sqrt{v_F^2q^2+\Omega^2}}\\ 0\\ -\frac{1}{2}-\frac{|\Omega|}{v_Fq}\left(|\Omega|-\sqrt{v_F^2q^2+\Omega^2}\right)\end{bmatrix}. \tag{C.3.4}$$

Obviously, only the first choice leads to logarithmic renormalizaton. Keeping only this

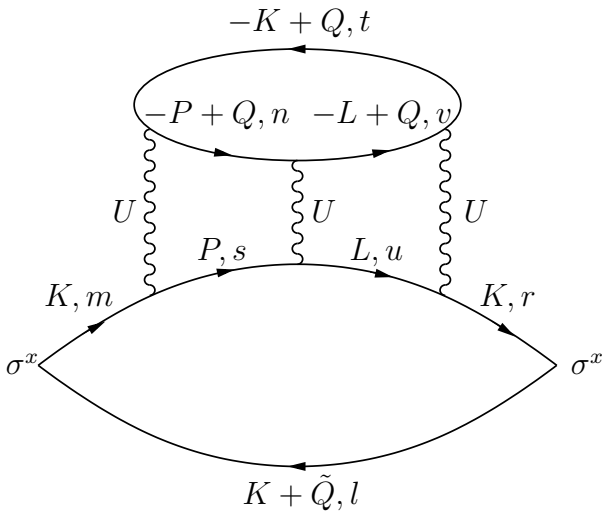

Figure C.1: Diagram 1 to third order in electron-electron interaction at large momentum transfer; here, the in-plane component is shown.

choice for $u=-v$, we obtain

$$\begin{aligned}\chi^{xx}_{1,q=2k_F} =& -U^3\frac{m}{2\pi}\int\frac{d\Omega}{2\pi}\int\frac{d\theta_{k\tilde{q}}}{2\pi}\int\frac{qdq}{2\pi}\Big\{\Big[3\sin^2\theta_{k\tilde{q}}(I_{+---}+I_{-+++})\Pi_0\\ &+3\cos^2\theta_{k\tilde{q}}(I_{++++}+I_{----})\Pi_0+\sin^2\theta_{k\tilde{q}}(I_{+-+-}\Pi_{+-}+I_{-+-+}\Pi_{-+})\\ &+\cos^2\theta_{k\tilde{q}}(I_{++-+}\Pi_{-+}+I_{--+-}\Pi_{+-})\Big]\ln\frac{\Lambda}{|\alpha|k_F}\\ &+\Big[\sin^2\theta_{k\tilde{q}}(I_{+---}+I_{-+++})\Pi_0+\cos^2\theta_{k\tilde{q}}(I_{++++}+I_{----})\Pi_0\\ &+3\sin^2\theta_{k\tilde{q}}(I_{+-+-}\Pi_{+-}+I_{-+-+}\Pi_{-+})+3\cos^2\theta_{k\tilde{q}}(I_{++-+}\Pi_{-+}+I_{--+-}\Pi_{+-})\\ &\times\ln\frac{\Lambda}{|\Omega|+\sqrt{v_F^2q^2+\Omega^2}}\Big]\Big\}. \end{aligned}\tag{C.3.5}$$

The first two lines in Equation (C.3.5) contain an Ω and q-independent logarithmic factor. Integrations over q, $\theta_{k\tilde{q}}$, and Ω in these lines produce terms which scale either as $\tilde{q}$ or as $|\alpha|$, thus these two lines generate terms of the type $\tilde{q}\ln|\alpha|$ and $|\alpha|\ln|\alpha|$. Next, we note that some combinations of quaternions and polarizations bubbles in these two lines,when integrated over q, $\theta_{k\tilde{q}}$, and Ω, produce a $\tilde{q}$ term while others produce an $|\alpha|$ term. Namely, combinations $(I_{++++}+I_{----})\Pi_0$ and $I_{++-+}\Pi_{-+}+I_{--+-}\Pi_{+-}$ produce $\tilde{q}$, while $(I_{+---}+I_{-+++})\Pi_0$ and $I_{+-+-}\Pi_{+-}+I_{-+-+}\Pi_{-+}$ produce $|\alpha|$. To extract the leading logarithmic dependence, we split the Ω and q-dependent logarithmic factor into two parts as $\ln\frac{v_F\tilde{q}}{|\Omega|+\sqrt{v_F^2q^2+\Omega^2}}+\ln\frac{\Lambda}{v_F\tilde{q}}$, when it multiplies the combinations of the first type, and as $\ln\frac{k_F|\alpha|}{|\Omega|+\sqrt{v_F^2q^2+\Omega^2}}+\ln\frac{\Lambda}{k_F|\alpha|}$, when it multiples the combinations of the second type. The Ω- and q-dependent remainders do not produce main logarithms because the

internal scales of Ω and q are set either by $\tilde{q}$ or by $|\alpha|$ for the first and second types, correspondingly. Therefore, the only main logarithmis we have are either $\ln \frac{\Lambda}{v_F \tilde{q}}$ or $\ln \frac{\Lambda}{k_F |\alpha|}$. Collecting all the contributions, we finally obtain

$$\begin{aligned}\chi^{xx}_{1,q=2k_F} &= -u^3 \frac{2\chi_0}{3}\left[\frac{|\alpha|k_F}{E_F}\ln\frac{\Lambda}{|\alpha|k_F} + \frac{2}{3\pi}\frac{v_F\tilde{q}}{E_F}\left(\ln\frac{\Lambda}{|\alpha|k_F} + \ln\frac{\Lambda}{v_F\tilde{q}}\right)\right] \\ &\approx -u^3\frac{2\chi_0}{3}\left[\frac{|\alpha|k_F}{E_F}\ln\frac{\Lambda}{|\alpha|k_F} + \frac{2}{3\pi}\frac{v_F\tilde{q}}{E_F}\ln\frac{\Lambda}{v_F\tilde{q}}\right], \end{aligned} \tag{C.3.6}$$

where in the last line we retained only leading logarithms renormalizing each of the two terms in of the second-order result. Thus we see that each energy scale, i.e., $v_F\tilde{q}$ and $v_F q_\alpha$, is renormalized by itself.

C.4 Nonanalytic dependence of the free energy as a function of SOI

In a number of recent papers [Agarwal11, Chesi11b, Chesi11a], the properties of interacting helical Fermi liquids were analyzed from a general point of view. In particular, Chesi and Giuliani [Chesi11b] have shown that an equilibrium value of helical imbalance

$$\delta N \equiv \frac{N_+ - N_-}{N_+ + N_-}, \tag{C.4.1}$$

where $N_\pm$ is the number of electrons in the $\pm$ Rashba subbands, is not affected to any order in the electron-electron interaction and to first order in Rashba SOI. Mathematically, this statement is equivalent to the notion that, for small δN and α, the ground state energy of the system $\mathcal{F}$ can be written as $\mathcal{E} = A(\delta N - 2m\alpha/k_F)^2$, so that the minimum value of $\mathcal{F}$ corresponds to the non-interacting value of δN. The analysis of [Chesi11b] was based on the assumption that $\mathcal{F}$ is an analytic function of α, at least to order α^2. In a related paper, Chesi and Giuliani [Chesi11a] analyzed the dependence of $\mathcal{F}$ on δN within the Random-Phase Approximation (RPA) for a Coulomb interaction and found a non-analytic $\delta N^4 \ln|\delta N|$ term.

In this Appendix, we analyze the non-analytic dependence of $\mathcal{F}$ on α by going beyond the RPA. [For small α, there is no need to consider the dependences of $\mathcal{F}$ on α and δN separately, as the shift in the equilibrium value of δN due to the electron-electron interaction can be found perturbatively.] To this end, we derive the free energy at $\tilde{q} = T = 0$ –equal, therefore, to the ground state energy–following the method of [Żak10a] which includes renormalization in the Cooper channel to all orders in the interaction.

The free energy is given by the skeleton diagram in Figure C.2

$$\mathcal{F}_{zz} = -\frac{1}{4}\int_q \tilde{\Gamma}_{s_1 s_4; s_3 s_2}(\mathbf{k_F}, -\mathbf{k_F}; -\mathbf{k_F}, \mathbf{k_F})\tilde{\Gamma}_{s_3 s_2; s_1 s_4}(-\mathbf{k_F}, \mathbf{k_F}; \mathbf{k_F}, -\mathbf{k_F})\Pi_{s_1 s_2}\Pi_{s_3 s_4}, \tag{C.4.2}$$

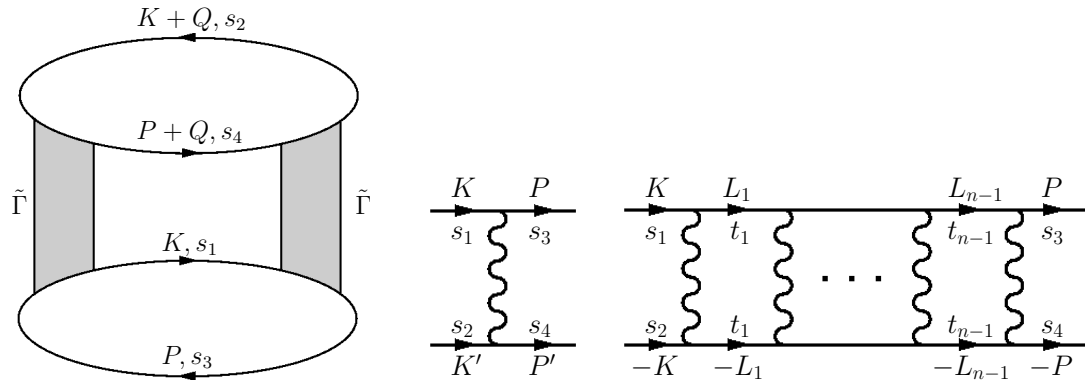

Figure C.2: Left: A skeleton diagram for the free energy in the presence of the Cooper renormalization; $\tilde{\Gamma}$ is a renormalized Cooper vertex. Middle: The effective scattering amplitude $\Gamma^{(1)}_{s_1s_2;s_3s_4}(\mathbf{k},\mathbf{k}';\mathbf{p},\mathbf{p}')$ in the chiral basis. Right: A generic n-th order ladder diagram in the Cooper channel, $\Gamma^{(n)}_{s_1s_2;s_3s_4}(\mathbf{k},-\mathbf{k};\mathbf{p},-\mathbf{p})$.

where a particle-hole bubble is given by Equation (4.2.7f) and $\tilde{\Gamma}_{s_1s_2;s_3s_4}(\mathbf{k_F},-\mathbf{k_F};-\mathbf{k_F},\mathbf{k_F})$ is a scattering amplitude renormalized in the Cooper channel. To first order in electron-electron interaction U, $\tilde{\Gamma}_{s_1s_2;s_3s_4}$ is given by Equation (C.3.2).

It is convenient to decompose the renormalized amplitude into s, p, and d channels as

$$\Gamma^{(1)}_{s_1s_2;s_3s_4}(\mathbf{k},-\mathbf{k};\mathbf{p},-\mathbf{p})(L) = U_{s_1s_2;s_3s_4}(L) + V_{s_1s_2;s_3s_4}(L)e^{i(\theta_{\mathbf{p}}-\theta_{\mathbf{k}})} + W_{s_1s_2;s_3s_4}(L)e^{2i(\theta_{\mathbf{p}}-\theta_{\mathbf{k}})}, \tag{C.4.3}$$

where the bare values of the corresponding harmonics are $U_{s_1s_2;s_3s_4}(0) = u_{2k_F}/2$, $V_{s_1s_2;s_3s_4}(0) = u_{2k_F}(s_1s_3+s_2s_4)/2$, and $W_{s_1s_2;s_3s_4}(0) = u_{2k_F}s_1s_2s_3s_4/2$. The s,p,d harmonics of $\tilde{\Gamma}$ were shown in [Żak10a] to obey a system of decoupled Renormalization Group (RG) equations:

$$-\frac{d}{dL}U_{s_1s_2;s_3s_4}(L) = \sum_s U_{s_1s_2;s-s}(L)U_{s-s;s_3s_4}(L), \tag{C.4.4}$$

$$-\frac{d}{dL}V_{s_1s_2;s_3s_4}(L) = \sum_s V_{s_1s_2;s-s}(L)V_{s-s;s_3s_4}(L), \tag{C.4.5}$$

$$-\frac{d}{dL}W_{s_1s_2;s_3s_4}(L) = \sum_s W_{s_1s_2;s-s}(L)W_{s-s;s_3s_4}(L), \tag{C.4.6}$$

where the RG variable is defined as

$$L \equiv L_{ss} = \frac{m}{2\pi}\ln\frac{\Lambda}{|\alpha|k_F}. \tag{C.4.7}$$

and the initial conditions were specified above. Solving these equations, we obtain $U_{s_1s_2;s_3s_4}(L) = u/[2(1+uL)]$, $V_{ss;\pm s\pm s}(L) = \pm u$, $V_{s_1s_2s_3s_4}(L) = u(s_1s_3+s_2s_4)/(1+2uL)$ for

the remaining s_i's, and $W_{s_1 s_2; s_3 s_4}(L) = u s_1 s_2 s_3 s_4/[2(1+uL)]$, with $u \equiv u_{2k_F}$. Combining the solution in the Cooper channel, we find

$$\tilde{\Gamma}_{s\pm s;\pm ss}(\mathbf{k_F}, -\mathbf{k_F}; -\mathbf{k_F}, \mathbf{k_F}) = \frac{u}{1+uL} \mp u, \tag{C.4.8}$$

$$\tilde{\Gamma}_{s-s;\pm s\mp s}(\mathbf{k_F}, -\mathbf{k_F}; -\mathbf{k_F}, \mathbf{k_F}) = \frac{u}{1+uL} \mp \frac{u}{1+2uL}, \tag{C.4.9}$$

and zero for the remaining cases.

Substituting the RG amplitudes into Equation (C.4.2) and summing over the Rashba indices, we arrive at

$$\begin{aligned}\mathcal{F} = &- u^2 \int \frac{d\Omega}{2\pi} \int \frac{d\theta_{k\tilde{q}}}{2\pi} \int \frac{qdq}{2\pi} \Bigg\{ \left(\frac{1}{1+uL} - \frac{1}{1+2uL} \right)^2 \left(\Pi_{-+}^2 + \Pi_{+-}^2 - 2\Pi_0^2 \right) \\ &+ 2\left(\frac{1}{1+uL} + 1 \right)^2 \left(\Pi_{-+}\Pi_{+-} - \Pi_0^2 \right) + 2 \Bigg[\left(\frac{1}{1+uL} - 1 \right)^2 \\ &+ \left(\frac{1}{1+uL} + \frac{1}{1+2uL} \right)^2 + \left(\frac{1}{1+uL} - \frac{1}{1+2uL} \right)^2 + \left(\frac{1}{1+uL} + 1 \right)^2 \Bigg] \Pi_0^2 \Bigg\}.\end{aligned} \tag{C.4.10}$$

The terms proportional to Π_0^2 are divergent and scale with the upper cut-off Λ, thus they can be dropped as we are interested only in the low energy sector. Making use of the following integrals $\int qdq(\Pi_{+-}\Pi_{-+} - \Pi_0^2) = 0$ and

$$\int d\Omega \Omega^2 \int dqq(\Pi_{+-}^2 + \Pi_{-+}^2 - 2\Pi_0^2) = \int d\Omega \frac{\Omega^2}{v_F^2} \ln \frac{\Omega^2}{\Omega^2 + 4\alpha^2 k_F^2} = \frac{16\pi}{3v_F^2} |\alpha|^3 k_F^3 + \mathcal{O}(\Lambda), \tag{C.4.11}$$

we obtain the final result

$$\mathcal{F} = -u^2 \chi_0 \left[\frac{1}{1 + u \ln \frac{\Lambda}{|\alpha| k_F}} - \frac{1}{1 + 2u \ln \frac{\Lambda}{|\alpha| k_F}} \right]^2 \frac{|\alpha|^3 k_F^3}{2E_F}. \tag{C.4.12}$$

Note that $\mathcal{F}$ is non-zero starting only from the fourth order in u:

$$\mathcal{F}^{(4)} = -u^4 \chi_0 \frac{|\alpha|^3 k_F^3}{2E_F} \ln^2 \left(\frac{|\alpha| k_F}{\Lambda} \right). \tag{C.4.13}$$

Apart from the logarithmic factor, a cubic dependence of $\mathcal{F}$ on $|\alpha|$ is in line with a general power-counting argument [Maslov06, Maslov09] which states that the non-analytic dependence of the free energy in 2D is cubic in the relevant energy scale. A cubic dependence of $\mathcal{F}$ on α implies that the shift in δN scales as $\alpha^2 \mathcal{C}(L)$, where $\mathcal{C}(L)$ is a function describing logarithmic renormalization in Equation (C.4.12). This is to be contrasted with an $\alpha^3 \ln \alpha$ scaling predicted within the RPA [Chesi11a].

Bibliography

[Agarwal11] A. Agarwal, S. Chesi, T. Jungwirth, J. Sinova, G. Vignale and M. Polini. *Plasmon mass and Drude weight in strongly spin-orbit-coupled two-dimensional electron gases*. Phys. Rev. B **83**, 115135 (2011).

[Aleiner06] I. L. Aleiner and K. B. Efetov. *Supersymmetric low-energy theory and renormalization group for a clean Fermi gas with a repulsion in arbitrary dimensions*. Phys. Rev. B **74**, 075102 (2006).

[Amasha08] S. Amasha, K. MacLean, I. P. Radu, D. M. Zumbühl, M. A. Kastner, M. P. Hanson and A. C. Gossard. *Electrical Control of Spin Relaxation in a Quantum Dot*. Phys. Rev. Lett. **100**, 046803 (2008).

[Ando82] T. Ando, A. B. Fowler and F. Stern. *Electronic properties of two-dimensional systems*. Rev. Mod. Phys. **54**, 437 (1982).

[Ashcroft76] N. W. Ashcroft and N. D. Mermin. *Solid State Physics* (Saunders College, Philadelphia, 1976).

[Ashrafi] A. Ashrafi and D. L. Maslov. Unpublished.

[Aspect82] A. Aspect, P. Grangier and G. Roger. *Experimental Realization of Einstein-Podolsky-Rosen-Bohm Gedankenexperiment: A New Violation of Bell's Inequalities*. Phys. Rev. Lett. **49**, 91 (1982).

[Atatüre06] M. Atatüre, J. Dreiser, A. Badolato, A. Högele, K. Karrai and A. Imamoglu. *Quantum-Dot Spin-State Preparation with Near-Unity Fidelity*. Science **312**, 551 (2006).

[Badalyan10] S. M. Badalyan, A. Matos-Abiague, G. Vignale and J. Fabian. *Beating of Friedel oscillations induced by spin-orbit interaction*. Phys. Rev. B **81**, 205314 (2010).

[Baranov93] M. A. Baranov, M. Y. Kagam and M. S. Mar'enko. *Singularity in the quasiparticle interaction function in 2D Fermi gas.* JETP Lett. **58**, 709 (1993).

[Belitz97] D. Belitz, T. R. Kirkpatrick and T. Vojta. *Nonanalytic behavior of the spin susceptibility in clean Fermi systems.* Phys. Rev. B **55**, 9452 (1997).

[Belitz05] D. Belitz, T. R. Kirkpatrick and T. Vojta. *How generic scale invariance influences quantum and classical phase transitions.* Rev. Mod. Phys. **77**, 579 (2005).

[Betouras05] J. Betouras, D. Efremov and A. Chubukov. *Thermodynamics of a Fermi liquid in a magnetic field.* Phys. Rev. B **72**, 115112 (2005).

[Bluhm04] H. Bluhm, S. Foletti, I. Neder, M. Rudner, D. Mahalu, V. Umansky and A. Yacoby. *Dephasing time of GaAs electron-spin qubits coupled to a nuclear bath exceeding 200μs.* Nature Phys. **7**, 109 (2004).

[Bonesteel01] N. E. Bonesteel, D. Stepanenko and D. P. DiVincenzo. *Anisotropic Spin Exchange in Pulsed Quantum Gates.* Phys. Rev. Lett. **87**, 207901 (2001).

[Bracker05] A. S. Bracker, E. A. Stinaff, D. Gammon, M. E. Ware, J. G. Tischler, A. Shabaev, A. L. Efros, D. Park, D. Gershoni, V. L. Korenev and I. A. Merkulov. *Optical Pumping of the Electronic and Nuclear Spin of Single Charge-Tunable Quantum Dots.* Phys. Rev. Lett. **94**, 047402 (2005).

[Burkard99] G. Burkard, D. Loss and D. P. DiVincenzo. *Coupled quantum dots as quantum gates.* Phys. Rev. B **59**, 2070 (1999).

[Burkard02] G. Burkard and D. Loss. *Cancellation of Spin-Orbit Effects in Quantum Gates Based on the Exchange Coupling in Quantum Dots.* Phys. Rev. Lett. **88**, 047903 (2002).

[Bychkov84a] Y. A. Bychkov and E. I. Rashba. *Oscillatory effects and the magnetic susceptibility of carriers in inversion layers.* J. Phys. C: Solid State Phys. **17**, 6039 (1984).

[Bychkov84b] Y. A. Bychkov and E. I. Rashba. *Properties of a 2D electron gas with lifted spectral degeneracy.* JETP Lett. **39**, 78 (1984).

[Caride83a] A. O. Caride, C. Tsallis and S. I. Zanette. *Criticality of the Anisotropic Quantum Heisenberg Model on a Self-Dual Hierarchical Lattice.* Phys. Rev. Lett. **51**, 145 (1983).

[Caride83b] A. O. Caride, C. Tsallis and S. I. Zanette. *Criticality of the Anisotropic Quantum Heisenberg Model on a Self-Dual Hierarchical Lattice.* Phys. Rev. Lett. **51**, 616 (1983).

[Carneiro77] G. M. Carneiro and C. J. Pethick. *Finite-temperature contributions to the magnetic susceptibility of a normal Fermi liquid.* Phys. Rev. B **16**, 1933 (1977).

[Casey03] A. Casey, H. Patel, J. Nyéki, B. P. Cowan and J. Saunders. *Evidence for a Mott-Hubbard Transition in a Two-Dimensional ^3He Fluid Monolayer.* Phys. Rev. Lett. **90**, 115301 (2003).

[Chen99] G.-H. Chen and M. E. Raikh. *Small-q anomaly in the dielectric function and high-temperature oscillations of the screening potential in a two-dimensional electron gas with spin-orbit coupling.* Phys. Rev. B **59**, 5090 (1999).

[Chesi07] S. Chesi. *Effects of structural spin-orbit coupling in two dimensional electron and hole liquids.* Ph.D. thesis, Purdue University (2007).

[Chesi09] S. Chesi, R. A. Żak, P. Simon and D. Loss. *Momentum dependence of the spin susceptibility in two dimensions: Nonanalytic corrections in the Cooper channel.* Phys. Rev. B **79**, 115445 (2009).

[Chesi11a] S. Chesi and G. F. Giuliani. *High-density limit of the two-dimensional electron liquid with Rashba spin-orbit coupling.* Phys. Rev. B **83**, 235309 (2011).

[Chesi11b] S. Chesi and G. F. Giuliani. *Two exact properties of the perturbative expansion for the two-dimensional electron liquid with Rashba or Dresselhaus spin-orbit coupling.* Phys. Rev. B **83**, 235308 (2011).

[Chitov01a] G. Y. Chitov and A. J. Millis. *First temperature corrections to the Fermi-liquid fixed point in two dimensions.* Phys. Rev. B **64**, 054414 (2001).

[Chitov01b] G. Y. Chitov and A. J. Millis. *Leading Temperature Corrections to Fermi-Liquid Theory in Two Dimensions.* Phys. Rev. Lett. **86**, 5337 (2001).

[Chubukov93] A. V. Chubukov. *Kohn-Luttinger effect and the instability of a two-dimensional repulsive Fermi liquid at T=0.* Phys. Rev. B **48**, 1097 (1993).

[Chubukov03] A. V. Chubukov and D. L. Maslov. *Nonanalytic corrections to the Fermi-liquid behavior.* Phys. Rev. B **68**, 155113 (2003).

[Chubukov04a] A. V. Chubukov and D. L. Maslov. *Singular corrections to the Fermi-liquid theory.* Phys. Rev. B **69**, 121102 (2004).

[Chubukov04b] A. V. Chubukov, C. Pépin and J. Rech. *Instability of the Quantum-Critical Point of Itinerant Ferromagnets.* Phys. Rev. Lett. **92**, 147003 (2004).

[Chubukov05a] A. V. Chubukov, D. L. Maslov, S. Gangadharaiah and L. I. Glazman. *Singular perturbation theory for interacting fermions in two dimensions.* Phys. Rev. B **71**, 205112 (2005).

[Chubukov05b] A. V. Chubukov, D. L. Maslov, S. Gangadharaiah and L. I. Glazman. *Thermodynamics of a Fermi Liquid beyond the Low-Energy Limit.* Phys. Rev. Lett. **95**, 026402 (2005).

[Chubukov06] A. V. Chubukov, D. L. Maslov and A. J. Millis. *Nonanalytic corrections to the specific heat of a three-dimensional Fermi liquid.* Phys. Rev. B **73**, 045128 (2006).

[Chubukov07] A. V. Chubukov and D. L. Maslov. *Cooper channel and the singularities in the thermodynamics of a Fermi liquid.* Phys. Rev. B **76**, 165111 (2007).

[Chutia06] S. Chutia, M. Friesen and R. Joynt. *Detection and measurement of the Dzyaloshinskii-Moriya interaction in double quantum dot systems.* Phys. Rev. B **73**, 241304 (2006).

[Clark10] A. C. Clark, K. K. Schwarzwälder, T. Bandi, D. Maradan and D. M. Zumbühl. *Method for cooling nanostructures to microkelvin temperatures.* Rev. Sci. Instrum. **81**, 103904 (2010).

[Coffey93] D. Coffey and K. S. Bedell. *Nonanalytic contributions to the self-energy and the thermodynamics of two-dimensional Fermi liquids.* Phys. Rev. Lett. **71**, 1043 (1993).

[Coish04] W. A. Coish and D. Loss. *Hyperfine interaction in a quantum dot: Non-Markovian electron spin dynamics.* Phys. Rev. B **70**, 195340 (2004).

[Coish05] W. A. Coish and D. Loss. *Singlet-triplet decoherence due to nuclear spins in a double quantum dot.* Phys. Rev. B **72**, 125337 (2005).

[Coish07] W. A. Coish and D. Loss. *Handbook of Magnetism and Advanced Materials*, volume 5, 2895 (Wiley, 2007).

[Conduit09] G. J. Conduit, A. G. Green and B. D. Simons. *Inhomogeneous Phase Formation on the Border of Itinerant Ferromagnetism.* Phys. Rev. Lett. **103**, 207201 (2009).

[Cortez02] S. Cortez, O. Krebs, S. Laurent, M. Senes, X. Marie, P. Voisin, R. Ferreira, G. Bastard, J.-M. Gérard and T. Amand. *Optically Driven Spin Memory in n-Doped InAs-GaAs Quantum Dots.* Phys. Rev. Lett. **89**, 207401 (2002).

[Deutsch85] D. Deutsch. *Quantum Theory, the Church-Turing Principle and the Universal Quantum Computer.* Proc. R. Soc. London, Ser. A **400**, 97 (1985).

[DiVincenzo99] D. P. DiVincenzo. *Quantum computing and single-qubit measurements using the spin-filter effect.* Jour. Appl. Phys. **85**, 4785 (1999).

[DiVincenzo00] D. P. DiVincenzo. *The Physical Implementation of Quantum Computation.* Fortschritte der Physik **48**, 771 (2000).

[Dresselhaus55] G. Dresselhaus. *Spin-Orbit Coupling Effects in Zinc Blende Structures.* Phys. Rev. **100**, 580 (1955).

[Efremov08] D. V. Efremov, J. J. Betouras and A. Chubukov. *Nonanalytic behavior of two-dimensional itinerant ferromagnets.* Phys. Rev. B **77**, 220401 (2008).

[Einstein35] A. Einstein, B. Podolsky and N. Rosen. *Can Quantum-Mechanical Description of Physical Reality Be Considered Complete?* Phys. Rev. **47**, 777 (1935).

[Elzerman04] J. M. Elzerman, R. Hanson, L. H. Willems van Beveren, B. Witkamp, L. M. K. Vandersypen and L. P. Kouwenhoven. *Single-shot read-out of an individual electron spin in a quantum dot.* Nature **430**, 431 (2004).

[Feynman82] R. P. Feynman. *Simulating physics with computers.* Int. J. Theor. Phys. **21**, 467 (1982).

[Feynman86] R. P. Feynman. *Quantum mechanical computers.* Found. Phys. **16**, 507 (1986).

[Fiederling99] K. M. R. G. O. W. S. G. W. A. Fiederling, R. and L. W. Molenkamp. *Injection and detection of a spin-polarized current in a light-emitting diode.* Nature **402**, 787 (1999).

[Galitski03] V. M. Galitski and S. Das Sarma. *Kohn-Luttinger pseudopairing in a two-dimensional Fermi liquid.* Phys. Rev. B **67**, 144520 (2003).

[Gangadharaiah05] S. Gangadharaiah, D. L. Maslov, A. V. Chubukov and L. I. Glazman. *Interacting Fermions in Two Dimensions: Beyond the Perturbation Theory*. Phys. Rev. Lett. **94**, 156407 (2005).

[Giuliani05] G. F. Giuliani and G. Vignale. *Quantum Theory of the Electron Liquid* (Cambridge University Press, Cambridge, 2005).

[Gor'kov01] L. P. Gor'kov and E. I. Rashba. *Superconducting 2D System with Lifted Spin Degeneracy: Mixed Singlet-Triplet State*. Phys. Rev. Lett. **87**, 037004 (2001).

[Greywall83] D. S. Greywall. *Specific heat of normal liquid ^3He*. Phys. Rev. B **27**, 2747 (1983).

[Gywat04] O. Gywat, H.-A. Engel, D. Loss, R. J. Epstein, F. M. Mendoza and D. D. Awschalom. *Optical detection of single-electron spin decoherence in a quantum dot*. Phys. Rev. B **69**, 205303 (2004).

[Hanson07] R. Hanson, L. P. Kouwenhoven, J. R. Petta, S. Tarucha and L. M. K. Vandersypen. *Spins in few-electron quantum dots*. Rev. Mod. Phys. **79**, 1217 (2007).

[Hirashima98] D. S. Hirashima and H. Takahashi. *Correlation Effects on the Spin Susceptibility in Two Dimensional Fermion Systems*. J. Phys. Soc. Jpn. **67**, 3816 (1998).

[Imamoḡlu03] A. Imamoḡlu, E. Knill, L. Tian and P. Zoller. *Optical Pumping of Quantum-Dot Nuclear Spins*. Phys. Rev. Lett. **91**, 017402 (2003).

[Johnson05] A. C. Johnson, J. R. Petta, J. M. Taylor, M. D. Lukin, C. M. Marcus, M. P. Hanson and A. C. Gossard. *Triplet-singlet spin relaxation via nuclei in a double quantum dot*. Nature **435**, 925 (2005).

[Kaufman84] M. Kaufman and M. Kardar. *Comment on "Criticality of the Anisotropic Quantum Heisenberg Model on a Self-Dual Hierarchical Lattice"*. Phys. Rev. Lett. **52**, 483 (1984).

[Khaetskii02] A. V. Khaetskii, D. Loss and L. Glazman. *Electron Spin Decoherence in Quantum Dots due to Interaction with Nuclei*. Phys. Rev. Lett. **88**, 186802 (2002).

[Khaetskii03] A. Khaetskii, D. Loss and L. Glazman. *Electron spin evolution induced by interaction with nuclei in a quantum dot*. Phys. Rev. B **67**, 195329 (2003).

[Khalil02] I. G. Khalil, M. Teter and N. W. Ashcroft. *Singular structure and enhanced Friedel oscillations in the two-dimensional electron gas.* Phys. Rev. B **65**, 195309 (2002).

[Kittel87] C. Kittel. *Quantum theory of Solids* (Wiley & Sons, New York, 1987).

[Klauser06] D. Klauser, W. A. Coish and D. Loss. *Nuclear spin state narrowing via gate-controlled Rabi oscillations in a double quantum dot.* Phys. Rev. B **73**, 205302 (2006).

[Kohn65] W. Kohn and J. M. Luttinger. *New Mechanism for Superconductivity.* Phys. Rev. Lett. **15**, 524 (1965).

[Koppens08] F. H. L. Koppens, K. C. Nowack and L. M. K. Vandersypen. *Spin Echo of a Single Electron Spin in a Quantum Dot.* Phys. Rev. Lett. **100**, 236802 (2008).

[Kroutvar04] M. Kroutvar, Y. Ducommun, D. Heiss, M. Bichler, D. Schuh, G. Abstreiter and J. J. Finley. *Optically programmable electron spin memory using semiconductor quantum dots.* Nature **432**, 81 (2004).

[Laird06] E. A. Laird, J. R. Petta, A. C. Johnson, C. M. Marcus, A. Yacoby, M. P. Hanson and A. C. Gossard. *Effect of Exchange Interaction on Spin Dephasing in a Double Quantum Dot.* Phys. Rev. Lett. **97**, 056801 (2006).

[Landau57] L. D. Landau. *The Theory of a Fermi Liquid.* Sov. Phys. JETP **3**, 920 (1957).

[Landau59] L. D. Landau. *On the Theory of the Fermi Liquid.* Sov. Phys. JETP **8**, 70 (1959).

[Lidar01] D. A. Lidar and L.-A. Wu. *Reducing Constraints on Quantum Computer Design by Encoded Selective Recoupling.* Phys. Rev. Lett. **88**, 017905 (2001).

[Löhneysen07] H. v. Löhneysen, A. Rosch, M. Vojta and P. Wölfle. *Fermi-liquid instabilities at magnetic quantum phase transitions.* Rev. Mod. Phys. **79**, 1015 (2007).

[Loss98] D. Loss and D. P. DiVincenzo. *Quantum computation with quantum dots.* Phys. Rev. A **57**, 120 (1998).

[Loss11] D. Loss, F. L. Pedrocchi and A. J. Leggett. *Absence of Spontaneous Magnetic Order of Lattice Spins Coupled to Itinerant Interacting Electrons in One and Two Dimensions.* Phys. Rev. Lett. **107**, 107201 (2011).

[Mahan00] G. D. Mahan. *Many-Particle Physics* (Plenum Press, New York, 2000).

[Maslov06] D. L. Maslov, A. V. Chubukov and R. Saha. *Nonanalytic magnetic response of Fermi and non-Fermi liquids.* Phys. Rev. B **74**, 220402 (2006).

[Maslov09] D. L. Maslov and A. V. Chubukov. *Nonanalytic paramagnetic response of itinerant fermions away and near a ferromagnetic quantum phase transition.* Phys. Rev. B **79**, 075112 (2009).

[Mermin66] N. D. Mermin and H. Wagner. *Absence of Ferromagnetism or Antiferromagnetism in One- or Two-Dimensional Isotropic Heisenberg Models.* Phys. Rev. Lett. **17**, 1133 (1966).

[Misawa99] S. Misawa. *Temperature-Squared Term in the Heat Capacity of a Two-Dimensional Fermi Liquid.* Journal of the Physical Society of Japan **68**, 2172 (1999).

[Mishchenko] E. Mishchenko. Unpublished.

[Myers05] R. C. Myers, K. C. Ku, X. Li, N. Samarth and D. D. Awschalom. *Optoelectronic control of spin dynamics at near-terahertz frequencies in magnetically doped quantum wells.* Phys. Rev. B **72**, 041302 (2005).

[Ohno99] Y. Ohno, D. K. Young, B. Beschoten, F. Matsukara, H. Ohno and D. D. Awschalom. *Electrical spin injection in a ferromagnetic semiconductor heterostructure.* Nature **402**, 790 (1999).

[Pethick73] C. J. Pethick and G. M. Carneiro. *Specific Heat of a Normal Fermi Liquid. I. Landau-Theory Approach.* Phys. Rev. A **7**, 304 (1973).

[Petta05] J. R. Petta, A. C. Johnson, J. M. Taylor, E. A. Laird, A. Yacoby, M. D. Lukin, C. M. Marcus, M. P. Hanson and A. C. Gossard. *Coherent Manipulation of Coupled Electron Spins in Semiconductor Quantum Dots.* Science **309**, 2180 (2005).

[Petta06] J. R. Petta, A. C. Johnson, J. M. Taylor, E. A. Laird, A. Yacoby, M. D. Lukin, C. M. Marcus, M. P. Hanson and A. C. Gossard. *Coherent Manipulation of Coupled Electron Spins in Semiconductor Quantum Dots.* Science **309**, 2180 (2006).

[Petta08] J. R. Petta, J. M. Taylor, A. C. Johnson, A. Yacoby, M. D. Lukin, C. M. Marcus, M. P. Hanson and A. C. Gossard. *Dynamic Nuclear Polarization with Single Electron Spins.* Phys. Rev. Lett. **100**, 067601 (2008).

[Pines66] D. Pines and P. Noziéres. *The Theory of Quantum Liquids* (W. A. Benjamin, Inc., New York, 1966).

[Pletyukhov06] M. Pletyukhov and V. Gritsev. *Screening in the two-dimensional electron gas with spin-orbit coupling.* Phys. Rev. B **74**, 045307 (2006).

[Pletyukhov07] M. Pletyukhov and S. Konschuh. *Charge and spin density response functions of the clean two-dimensional electron gas with Rashba spin-orbit coupling at finite momenta and frequencies.* Eur. Phys. J. B **60**, 29 (2007).

[Prinz95] G. A. Prinz and K. Hathaway. *Magnetoelectronics.* Physics Today **4**, 24 (1995).

[Prus03] O. Prus, Y. Yaish, M. Reznikov, U. Sivan and V. Pudalov. *Thermodynamic spin magnetization of strongly correlated two-dimensional electrons in a silicon inversion layer.* Phys. Rev. B **67**, 205407 (2003).

[Rashba] E. I. Rashba. Private communication.

[Rashba05] E. I. Rashba. *Spin Dynamics and Spin Transport.* J. Supercond. **18**, 137 (2005).

[Rech06] J. Rech, C. Pépin and A. V. Chubukov. *Quantum critical behavior in itinerant electron systems: Eliashberg theory and instability of a ferromagnetic quantum critical point.* Phys. Rev. B **74**, 195126 (2006).

[Recher00] P. Recher, E. V. Sukhorukov and D. Loss. *Quantum Dot as Spin Filter and Spin Memory.* Phys. Rev. Lett. **85**, 1962 (2000).

[Requist05] R. Requist, J. Schliemann, A. G. Abanov and D. Loss. *Double occupancy errors in quantum computing operations: Corrections to adiabaticity.* Phys. Rev. B **71**, 115315 (2005).

[Salis01] K. Y. E. K. D. D. C. G. A. C. Salis, G. and D. D. Awschalom. *Electrical control of spin coherence in semiconductor nanostructures.* Nature **414**, 619 (2001).

[Saraga05] D. S. Saraga, B. L. Altshuler, D. Loss and R. M. Westervelt. *Coulomb scattering cross section in a two-dimensional electron gas and production of entangled electrons.* Phys. Rev. B **71**, 045338 (2005).

[Schliemann10] J. Schliemann. *Spins coupled to a spin bath: From integrability to chaos.* Phys. Rev. B **81**, 081301 (2010).

[Schrödinger35] E. Schrödinger. *Die gegenwrtige Situation in der Quantenmechanik.* Naturwissenschaften **23**, 823 (1935).

[Schwiete06] G. Schwiete and K. B. Efetov. *Temperature dependence of the spin susceptibility of a clean Fermi gas with repulsion.* Phys. Rev. B **74**, 165108 (2006).

[Shabaev03] A. Shabaev, A. L. Efros, D. Gammon and I. A. Merkulov. *Optical readout and initialization of an electron spin in a single quantum dot.* Phys. Rev. B **68**, 201305 (2003).

[Shankar94] R. Shankar. *Renormalization-group approach to interacting fermions.* Rev. Mod. Phys. **66**, 129 (1994).

[Shekhter06a] A. Shekhter and A. M. Finkel'stein. *Branch-cut singularities in thermodynamics of Fermi liquid systems.* Proc. Natl. Acad. Sci. U.S.A. **103**, 15765 (2006).

[Shekhter06b] A. Shekhter and A. M. Finkel'stein. *Temperature dependence of spin susceptibility in two-dimensional Fermi liquid systems.* Phys. Rev. B **74**, 205122 (2006).

[Simon07] P. Simon and D. Loss. *Nuclear Spin Ferromagnetic Phase Transition in an Interacting Two Dimensional Electron Gas.* Phys. Rev. Lett. **98**, 156401 (2007).

[Simon08] P. Simon, B. Braunecker and D. Loss. *Magnetic ordering of nuclear spins in an interacting two-dimensional electron gas.* Phys. Rev. B **77**, 045108 (2008).

[Stepanenko03] D. Stepanenko, N. E. Bonesteel, D. P. DiVincenzo, G. Burkard and D. Loss. *Spin-orbit coupling and time-reversal symmetry in quantum gates.* Phys. Rev. B **68**, 115306 (2003).

[Stepanenko04] D. Stepanenko and N. E. Bonesteel. *Universal Quantum Computation through Control of Spin-Orbit Coupling.* Phys. Rev. Lett. **93**, 140501 (2004).

[Stepanenko06] D. Stepanenko, G. Burkard, G. Giedke and A. Imamoglu. *Enhancement of Electron Spin Coherence by Optical Preparation of Nuclear Spins.* Phys. Rev. Lett. **96**, 136401 (2006).

[Taylor07] J. M. Taylor, J. R. Petta, A. C. Johnson, A. Yacoby, C. M. Marcus and M. D. Lukin. *Relaxation, dephasing, and quantum control of electron spins in double quantum dots.* Phys. Rev. B **76**, 035315 (2007).

[Żak] R. A. Żak, D. L. Maslov and D. Loss. Unpublished.

[Żak10a] R. A. Żak, D. L. Maslov and D. Loss. *Spin susceptibility of interacting two-dimensional electrons in the presence of spin-orbit coupling.* Phys. Rev. B **82**, 115415 (2010).

[Żak10b] R. A. Żak, B. Röthlisberger, S. Chesi and D. Loss. *Quantum computing with electron spins in quantum dots.* La Rivista del Nuovo Cimento **33**, 7 (2010).

[Zhou10] L. Zhou, J. Wiebe, S. Lounis, E. Vedmedenko, F. Meier, S. Blügel, P. H. Dederichs and R. Wiesendanger. *Strength and directionality of surface RudermanKittelKasuyaYosida interaction mapped on the atomic scale.* Nature Phys. **6**, 187 (2010).

List of Publications

(∗) Publication covered in this thesis

(∗) R. A. Żak, D. Maslov, and D. Loss. *Ferromagnetic order of nuclear spins coupled to conduction electrons: a combined effect of the electron-electron and spin-orbit interactions*. Phys. Rev. B **85**, 115424 (2012).

(∗) R. A. Żak, D. Maslov, and D. Loss. *Spin susceptibility of interacting two-dimensional electrons in the presence of spin-orbit coupling*. Phys. Rev. B **82**, 115415 (2010).

R. A. Żak, B. Röthlisberger, S. Chesi, and D. Loss. *Quantum computing with electron spins in quantum dots*. La Rivista del Nuovo Cimento **33**, 7 (2010).

(∗) S. Chesi, R. A. Żak, P. Simon, and D. Loss. *Momentum dependence of the spin susceptibility in two dimensions: nonanalytic corrections in the Cooper channel*. Phys. Rev. B **79**, 115445 (2009).

R. A. Żak and K. Flensberg. *Coulomb blockade of a three-terminal quantum dot*. Phys. Rev. B **77**, 045329 (2008).

Acknowledgments

Writing this thesis would not have been possible without the support from many people.

I would like to thank my supervisor Daniel Loss and my collaborators Dmitrii Maslov, Stefano Chesi, and Bernd Braunecker for lively discussions, motivation, help and trust.

I would also like to thank all members and visitors of the condensed matter theory group – Samuel Aldana, Ali Ashrafi, Dan Bohr, Massoud Borhani, Bernd Braunecker, Christoph Bruder, Martin Brühlmann, Denis Bulaev, Guido Burkard, Oleg Chalaev, Stefano Chesi, Bill Coish, Charles Doiron, Mathias Duckheim, Carlos Egues, Gerson Ferreira, Jan Fischer, Suhas Gangadharaiah, Stefanie Garni, Marco Hachiya, Rahel Heule, Kevin van Hoogdalem, Philippe Jacquod, Jelena Klinovaja, Daniel Klauser, Verena Koerting, Christoph Klöffel, Franz Knuth, Jörg Lehmann, Andriy Lyakhov, Franziska Maier, Dimitrii Maslov, Fabio Pedrocchi, Felipe Penha, Poliana Penteado, Diego Rainis, Maximilian Rinck, Beat Röthlisberger, Manuel Schmidt, Thomas Schmidt, Pascal Simon, Dimitrije Stepanenko, Vladimir Stojanovic, Grégory Strübi, Björn Trauzettel, Mircea Trif, Luka Trifunovic, Yaroslav Tserkovnyak, Oleksandr Tsyplyatyev, Mihajlo Vanevic, Andreas Wagner, Ying-Dan Wang, Richard Warburton, Robert Zielke, Oded Zilberberg, and Dominik Zumbühl – for a wonderful time we spent together in Basel.